Hydrochemistry of ice-covered lakes and ponds in the Untersee Oasis (Queen Maud Land, Antarctica)

Benoit Faucher

Thesis submitted to the University of Ottawa
in partial Fulfillment of the requirements for the
Doctorate of Philosophy in Geography

Department of Geography, Environment, and Geomatics
Faculty of Arts
University of Ottawa

© Benoit Faucher, Ottawa, Canada, 2021

ABSTRACT

Several thousand coastal perennially ice-covered oligotrophic lakes and ponds have been identified on the Antarctic continent. To date, most hydrochemical studies on Antarctica's ice-covered lakes have been undertaken in the McMurdo Dry Valleys (more than 20 lakes/ponds studied since 1957) because of their proximity to the McMurdo research station and the New Zealand station Scott Base. Yet, little attention has been given to coastal ice-covered lakes situated in Antarctica's central Queen Maud Land region, and more specifically in the Untersee Oasis: a polar Oasis that encompasses two large perennially ice-covered lakes (Lake Untersee & Lake Obersee), and numerous small ice-covered morainic ponds. Consequently, this PhD research project aims to describe and understand the distribution, ice cover phenology, and contemporary hydrochemistry of perennially ice-covered lakes and ponds located in the Untersee Oasis and their effect on the activity of the benthic microbial ecosystem.

Lake Untersee, the largest freshwater coastal lake in central Queen Maud Land, was the main focus of this study. Its energy and water mass balance was initially investigated to understand its current equilibrium and how this perennially well-sealed ice-covered lake may evolve under changing climate conditions. Results suggest that Lake Untersee's mass balance was in equilibrium between the late 1990s and 2018, and the lake is mainly fed by subglacial meltwater (55-60%) and by subaqueous melting of glacier ice (40-45%). A recursive stable water isotope (δD-$\delta^{18}O$) evolution model for well-sealed perennial ice-covered lakes that takes into account the effect of changing chemistry in residual waters on δD-$\delta^{18}O$ values was then developed and determined that Lake Untersee is in isotopic steady-state. Modeling results also showed that Untersee most likely did not receive additional inputs from surface streams during the last 300–500 years at the time of sampling, in November-December 2017. However, in mid-January 2019, Untersee experienced a glacial lake outburst flood (GLOF) that increased the water level by 2 m (contributing 1.75×10^7 m^3 of water), modifying its water chemistry and inorganic carbon load. High-resolution grain size and carbon isotope analyses of the benthic microbial mats suggest that GLOFs occurred periodically over the Holocene and that those events sporadically increased the primary productivity of its benthic microbial ecosystem. Finally, ice-covered ponds in the Oasis were identified and sampled to compare their morphometric properties, hydrochemical properties, and microbial mat activity with Lake Untersee. It was discovered that the Untersee Oasis ponds offer the full spectrum of ice cover types (i.e., perennial well-sealed, perennial and moat forming,

and seasonally ice-covered) and that their hydrochemical properties depend on ice cover type. Empirical pond data was used to determine how Lake Untersee and the ponds themselves will evolve as they transition under a warming climate from well-sealed to moat forming and from moat forming to seasonally ice-covered.

RÉSUMÉ

Plusieurs milliers de lacs et étangs côtiers recouverts de glace ont été identifiés en Antarctique. Jusqu'à présent, la plupart des études hydrochimiques sur les lacs couverts de glace de l'Antarctique ont été entreprises dans les vallées sèches de McMurdo (plus de 20 lacs/étangs étudiés depuis 1957) en raison de leur proximité avec la station de recherche de McMurdo (américaine) et la base Scott (néo-zélandaise). Cependant, peu d'attention a été accordée aux lacs côtiers couverts de glace situés dans la région centrale de la Terre de la Reine Maud, en Antarctique, et plus particulièrement dans l'Oasis Untersee : une oasis polaire qui comprend deux grands lacs couverts de glace pérenne (le lac Untersee et le lac Obersee), et de nombreux petits étangs morainiques couverts de glace. Par conséquent, l'objectif de ce projet de recherche doctorale est de décrire et comprendre la distribution, la phénologie de la couverture de glace et l'hydrochimie contemporaine des lacs et des étangs couverts de glace pérenne situés dans l'oasis d'Untersee, ainsi que leur effet sur l'activité primaire de leur écosystème microbien benthique.

Le lac Untersee, le plus grand lac côtier d'eau douce de la partie centrale de la Terre de la Reine Maud, a été le sujet principal de cette étude. Le bilan de masse énergétique et hydrologique de ce dernier a été étudié dans un premier temps afin de comprendre son équilibre actuel et la manière dont ce lac recouvert de glace bien scellée pourrait évoluer dans le contexte de changements climatiques globaux. Les résultats suggèrent que le bilan de masse hydrologique du lac Untersee était en équilibre entre la fin des années 1990 et 2018, et que le lac est principalement alimenté par les eaux de fonte sous-glaciaires (55-60%), et par la fonte subaquatique de glaciers (40-45%). Un modèle récursif d'évolution des isotopes stables de l'eau (δD-$\delta^{18}O$) pour les lacs couverts de glace pérenne qui sont bien scellés et qui tient compte de l'effet de l'évolution de la chimie des eaux résiduelles sur les valeurs δD-$\delta^{18}O$ a ensuite été développé et a permis de déterminer que le lac Untersee est en équilibre isotopique. Les résultats de la modélisation ont également montré que le lac Untersee n'a fort probablement pas reçu d'apport supplémentaire d'eaux de surface au cours des 300 à 500 dernières années, au moment de l'échantillonnage (en novembre-décembre 2017). Cependant, à la mi-janvier 2019, le lac Untersee a été affecté par une inondation glaciaire qui a augmenté le niveau d'eau de 2 m (apportant $1{,}75\times10^{7}$ m^3 d'eau) modifiant son hydrochimie ainsi que sa charge en carbone inorganique dissous. Des analyses à haute résolution de la taille des grains et des isotopes du carbone de carottes prélevées sur des stromatolites benthiques suggèrent que de telles inondations se sont produites périodiquement au

cours de l'Holocène, et que ces événements ont sporadiquement augmenté la productivité primaire de son écosystème microbien benthique. Enfin, des étangs couverts de glace dans l'Oasis ont été identifiés et échantillonnés afin de comparer leurs propriétés morphométriques et hydrochimiques, ainsi que leur activité microbienne, avec le lac Untersee. Il fut découvert que les étangs de l'Oasis Untersee offrent tous les types de couvertures de glace (c.-à-d., couvertures de glace pérennes bien scellées, pérennes et formant des douves, et couvertures saisonnières) et qu'ils présentent des propriétés hydrochimiques variées qui dépendent du type de couverture de glace. Ainsi, les données sur les étangs ont été utilisées pour déterminer comment le lac Untersee et les étangs eux-mêmes évolueront, alors qu'ils entameront une transition, sous l'effet d'un réchauffement climatique, de type de couverture de glace.

REMERCIEMENTS

J’aimerais débuter par remercier le professeur Denis Lacelle d’avoir agi en tant que superviseur de thèse et mentor pour ce projet de recherche doctorale. Merci Denis de m’avoir inclus dans le projet de recherche du Lac Untersee et de m’avoir guidé à travers mes études supérieures durant les six dernières années. Merci aussi de m’avoir avoir encouragé à élargir mes horizons de carrière, que ce soit par l’entremise de conférences à travers le monde, de campagnes de travail de terrain dans l’Arctique avec d’autres étudiant(e)s, d’expériences d’enseignement à l’Université d’Ottawa et en Chine, ou d’expériences de travail au sein de la fonction publique. Ta passion pour la recherche est contagieuse. Je crois aussi que chacun(e) de tes étudiant(e)s diplômés peux s’accorder pour dire que tu tiens réellement à notre succès, donc merci énormément aussi pour ceci. Bref, merci pour tout ! J’espère pouvoir continuer de collaborer avec toi dans le futur, dans le cadre d’autres projets.

J’aimerais aussi remercier Dale T. Andersen, l’investigateur principal du projet de recherche du lac Untersee, qui m’a permis d’aller faire du travail de terrain en Antarctique à trois reprises avec celui-ci. Dale, merci d’avoir transmis toutes ces connaissances en lien avec la limnologie polaire. Merci aussi pour ta confiance envers moi lorsque nous étions sur le terrain et désolé encore pour les pièces de motoneige cassées. Ce fut toujours divertissant de t’entendre parler, lors de nos soupers sur le terrain, de tes expéditions antérieures effectuées dans l’Arctique et en Antarctique. J’espère aussi pouvoir continuer à collaborer avec toi dans d’autres projets futurs.

Merci aussi au professeur émérite Bernard Lauriol d’avoir agi en tant que mentor durant les huit dernières années. C’est réellement en ayant fait un mémoire de baccalauréat sous votre supervision en 2014 que j’ai développé cette passion pour la recherche. Je n’aurais jamais complété des études supérieures n’eut été de cette merveilleuse expérience. Au plaisir de continuer à travailler avec vous dans les années à suivre !

Je tiens aussi à offrir des remerciements aux membres du comité d’évaluation pour cette thèse, les professeurs Ian D. Clark, Antoni Lewkowicz, Luke Copland et Warwick F. Vincent. Merci pour votre support tout au long de mon doctorat et pour vos commentaires/suggestions en lien avec les manuscrits présentés dans cette thèse.

Merci aussi à Jean Bjornson pour son support à travers mes études supérieures. Ce fut un plaisir d’échanger avec toi sur mes projets de recherche et d’obtenir d’excellents conseils de ta part

sur de potentielles approches méthodologiques. J'ai particulièrement beaucoup apprécié être ton assistant d'enseignement pour le cours de terrain en Gaspésie ainsi que dans le cours de géomorphologie; on faisait une bonne équipe !

Merci aussi à David A. Fisher pour son aide avec le développement des modèles numériques utilisés dans la cadre de ce projet de recherche. Ton aide avec ceci m'a permis d'en apprendre beaucoup sur la modélisation hydro- et géo-chimique. Je suis certain que ces acquis me seront utiles dans le futur.

J'aimerais aussi remercier mes collègues de bureau (Hugo Crites, Roxanne Frappier, Marjolaine Verret, Kethra Campbell-Heaton et Nicolas Comerford) ainsi que les étudiant(e)s diplômé(e)s du département de Géographie, Environnement, et Géomatique) pour leur amitié et support tout au long de mon doctorat.

Cette recherche aurait aussi été impossible sans le support financier et logistique de l'Université d'Ottawa (bourse d'admission), du Conseil de Recherche en Sciences Naturelles et Génie du Canada (bourse d'études supérieures du Canada Alexander-Graham-Bell), de la fondation TAWANI, de la fondation de la famille Trottier, du programme Russe de recherche sur l'Arctique et l'Antarctique, et de la compagnie Antarctic Logistics Centre International.

Finalement, j'aimerais remercier ma famille pour leur support tout au long de mes études. Merci à ma mère et mon père, Johanne et François, de m'avoir encouragé à poursuivre des études supérieures et à avoir tenu à en savoir toujours plus sur mes recherches. Pour terminer, merci infiniment à mes deux plus grandes fans, Caroline et notre petite perle, Alice. Les filles, merci d'avoir endurer mon horaire de travail atypique et d'avoir offert votre support et amour inconditionnel pendant les hauts et les bas de mon doctorat.

TABLE OF CONTENTS

LIST OF TABLES

LIST OF FIGURES

CHAPTER 1: INTRODUCTION

1.1 Introduction

Lacustrine basins are good indicators of climate change because of their physical, chemical, and biological responsiveness to changes in local environmental conditions (Paquette et al., 2015; Adrian et al., 2009; Williamson et al., 2009). Some of the most understudied and enigmatic types of lakes (for logistical reasons) are those found in the ice-free and desertic sectors of polar regions that are perennially ice-covered (Vincent et al., 2008). Controls exerted by ice-walls (when proglacially damned) and ice-covers in such lacustrine environments (which themselves exhibit spatial heterogeneity at a variety of temporal and spatial scales) have the potential to change the physical structure of their water column and can ultimately shape their biological communities and ecosystem processes (Simmons et al., 1993; MacIntyre & Melack, 1995; Kratz et al., 2005). Studying the physical and hydrochemical properties of their water and ice cover can provide valuable paleoenvironmental information (e.g., the timing of formation, filling, and desiccating events), insights into their paleolimnological characteristics (Doran et al., 2002; Wilson, 1964; Lyons et al., 1985), and can inform on the potential hydrochemical modifications they may go through in response to local climate variations, which is especially important in the current context of climate change.

It is expected that the percentage of ice-free regions on the Antarctic continent will increase by 25 % by the end of the present century due to global increases in air temperature (Lee et al., 2017). In central Queen Maud Land, the Mean Annual Air Temperature (MAAT) increased at a rate of 1.1±0.7°C decade^{-1} between 1998 and 2016 (Medley et al., 2018) and in Victoria Land's McMurdo Dry Valleys (MDV), the MAAT has increased since 2006 (Obryk et al., 2019). It is predicted that these climatic regime shifts will significantly impact the mass balance, ecology, and ice cover phenology (Obryk et al., 2019) of lakes covered by an annually persistent ice-cover implying a need to monitor these peculiarly sensitive lacustrine environments.

To date, most physicochemical investigations on Antarctica's ice-covered lakes have been undertaken in the MDV. These studies have shown that their ice cover dynamics significantly influence the rate and nature of physicochemical and biological processes in these lacustrine basins (Wharton et al., 1993a; Fritsen and Priscu, 1999). They've also recently shown that increases in MAAT had significant impacts on their ice cover thickness (e.g., Obryk et al., 2019) and that the

primary source of water for these lakes is englacial meltwater and that water loss mainly occurs through ablation of the ice cover (i.e., sublimation and/or surface melt) (Dugan et al., 2013).

However, very little work has been done to constrain the chemical properties (including input source) and water/energy mass balance of ice-covered lentic bodies located in Queen Maud Land's Untersee Oasis. This information limits understanding on how their ice-cover, water-column, and benthic ecosystem will evolve under the polar amplification of climate warming. Thus, this thesis's primary goal was to conduct laboratory work and numerical modeling analyses of samples gathered during the 2016-2019 Untersee Oasis field seasons to fill these knowledge gaps.

1.2 Background literature

1.2.1 Perennially ice-covered lakes

High latitude regions host a broad range of inland water reservoirs (i.e., surface, subglacial, and groundwater systems) which range from being perennially to seasonally ice-covered and that have very contrasting hydrochemical conditions (Vincent et al., 2008). Perennially ice-covered lakes are common freshwater lacustrine features in ice-free polar desert regions of the Arctic and the Antarctic, at high elevations where winter air temperatures are below 0°C, and where the summer air temperature is low enough and/or cooling associated with the latent heat of sublimation is sufficient to allow an ice cover to persist throughout the summer months (Doran et al., 2004; Vincent et al., 2008; Faucher et al., 2019). They differ from subglacial lakes because their ice cover is derived exclusively from accreted lake water ice, and is generally thinner than 20 m. They are usually found in coastal regions, whereas subglacial lakes are typically found inland and are capped by a combination of several hundred meters of accreted lacustrine and glacier ice (Priscu & Foreman, 2009).

Although subglacial lakes have been extensively studied and cataloged in the Arctic (e.g., Greenland, Devon Ice Cap) and Antarctic (especially in East Antarctica) regions (Livingstone et al., 2013; Rutishauser et al., 2018; Wright & Siegert, 2012), there is no inventory of perennially ice-covered surface lakes in polar regions.

Most of the work in the high Arctic that has been undertaken on such lacustrine basins focused on ten lakes: 1) Anguissaq Lake (Greenland); 2) Rundfjeld pond (Ellesmere Island, Canada); 3) Ziegler island lake (Franz Joseph land); 4) Lake A (Ellesmere Island, Canada); 5)

Lake B (Ellesmere Island, Canada); 6) Lake C1 (Ellesmere Island, Canada); 7) Lake C2 (Ellesmere Island, Canada); 8) Lake C3 (Ellesmere Island, Canada); 9) Lake E (Ellesmere Island, Canada); and 10) Ward Hunt Lake (Ward Hunt Island) (Doran et al., 2004; Van Hove et al., 2006).

Chinn (1993) classified coastal Antarctic perennially ice-covered lakes into two categories: 1) wet-based lakes (lakes that do not freeze to the bottom during the wintertime); and 2) dry-based lakes (shallow lakes that freeze to the bottom during the austral winter). The most studied perennial ice-covered lakes in the Antarctic have been those of the MDV (more than 20 lakes/ponds investigated since 1957) because of their proximity to the American McMurdo station, and the New Zealand station Scott Base (Doran et al., 1994). Amongst other Antarctic regions where perennially ice-covered have been investigated are: 1) the Vestfold hills, out of which a few are monitored year-round (Ferris et al., 1988); 2) the Larsemann hills, which encompass more than 150 ponds and lakes (Vincent et al., 2008); 3) the central Queen Maud Land lakes of the Schirmacher and Untersee Oases (Bormann & Fritszche, 1995); 4) the Bunger hills, which encompasses around 100 freshwater and saline lakes; and 5) the Syowa Oasis where freshwater, saline, and hypersaline ponds and lakes are found (Vincent et al., 2008). The earth's oldest permanently ice-covered lacustrine basins (aside from subglacial lakes) are likely found in Antarctica's MDVs; these valleys have been ice-free and are suspected of hosting such ice-capped water reservoirs for at least 2.7 Ma (Armstrong et al., 1968).

1.2.2 Ice cover mass balance & dynamics

Early investigations into the thermodynamics of ice-covered lakes in Antarctica's MDVs revealed that the thickness of the ice cover is primarily controlled by the balance between the conduction of energy out of the ice and the release of latent heat during freezing at the ice-water interface (Wilson et al., 1962; McKay et al., 1985). It is also significantly impacted by heat upwelling from the lake's water column and by geothermal fluxes, enhancing subaqueous ice melt at the ice cover/water interface (Vincent et al., 2008; Obryk et al., 2016a, 2016b). To maintain the energy balance in a steady-state condition, the rate of winter water freezing (i.e., ice accretion) at the bottom of the ice cover must equal the summer ablation rate (i.e., sublimation, evaporation, and melting) at the ice surface. The bulk turnover rate of the ice cover can be deduced from the annual difference between summer ablation (estimated to be between 0.47 to 0.89 m/yr^{-1} in the MDV) and winter ice formation (estimated from *in situ* measurements of ablation ropes and/or via

spectral analysis of the ice's $\delta^{18}O$ ratios and bubble content) (e.g., Dugan et al., 2013; Faucher et al., 2019).

Fluctuations in climatic conditions, especially air temperature, have significant impacts on lake ice thickness and seasonal variations (i.e., phenology) in polar regions where local anthropogenic influences are virtually absent; this explains why perennially ice-covered lakes are powerful climate change barometers (Vincent et al., 2008; William & Stefan, 2006). In the high Arctic, Mueller et al. (2009) and Paquette et al. (2015) showed through Synthetic Aperture Radar (SAR) analyses that the ice cover on small Ellesmere Island and Ward Hunt Island lakes had hit a climatic threshold due to increased air temperatures and thawing degree days (TDD). This led to their progressive transition from perennial to seasonal ice-covered lakes. This trend is expected to continue in the near future when ice cover and snow cover thickness on most Arctic lakes will have, respectively, hypothetically decreased and increased (Brown & Duguay, 2011). In Antarctica, it has been observed in the MDV lakes that ice cover and lake level respond rapidly to local climatic variations (Doran et al., 2008). In fact, the ice cover thickness of wet based perennially ice-covered lakes in the MDV (ranging from 3 to 6 m) has waxed and waned during the last few decades as a direct result of fluctuations in local air temperatures (Doran et al., 2002; Wharton et al., 1992; Chinn, 1993; Clow et al., 1988; Doran et al., 2008; Dugan et al., 2013). The volume of meltwater received in the lakes was found to be proportional to the degree-days above freezing (Dugan et al., 2013; Gooseff et al., 2017) and Obryk et al. (2019) demonstrated through modeling that the ice cover on MDV lakes should become seasonal by the end of the present century due to increased solar radiation and associated air temperatures. The impacts of climate change on the ice cover of ice-covered lakes located elsewhere in coastal Antarctica have yet to be assessed.

The annually persistent thick ice cover of these lakes influences several limnological parameters (Wharton et al., 1989). Consequently, a reduction in ice cover thickness and a shift from a perennial ice cover to a seasonal one for high latitude lakes as predicted for the future decades has several important implications. First, a reduction in the thickness and temporal persistence of the ice cover favors the penetration of incoming solar radiation (usually limited by the presence of a thick and persistent ice cover), leading to an increase in water column heat storage which, in return, acts as a positive feedback mechanism (similar to the sea ice-albedo feedback) for the progressively enhanced melting of the ice cover (Palmisano & Simmons, 1987; Obryk et

al., 2016). Moreover, additional incoming solar radiation inputs increase ephemeral rates of primary production of benthic organisms (shielded from harsh winter air temperatures, which permits their viability) but could significantly halt the growth of phytoplankton (Doran et al., 1994; Gooseff et al., 2017; Obryk et al., 2016; Dore & Priscu, 2001). The seal between the water column and the atmosphere created by the perennial ice cover prevents exchanges of gases (Wharton et al., 1986, 1987) and leads to the supersaturation of various dissolved gases in the water columns (e.g., Andersen et al., 1998). The formation of moats during the austral summer can lead to the water column's degassing and destabilization of the water's pH due to the dissolution of more dissolved inorganic carbon (DIC). The perennial ice cover also prevents wind enhanced mixing of the lake's water (Hawes, 1983; Ragotzkie & Likens, 1964), and during its seasonal partial absence, changes in the water column's circulation and stratification via wind-driven mixing could transform previously meromictic lakes into holomictic lakes (e.g., Mueller et al., 2009).

1.2.3 Ice cover segregation

Preferential segregation of salts in the liquid water phase during freezing has been thoroughly studied (e.g., Clayton et al., 1990; Killawee et al., 1998). Such investigations demonstrated that the concentration of various water-soluble ions (i.e., inorganic impurities) in the remaining water should increase linearly (assuming that almost no salts are included during ice formation) and that this partitioning is influenced by the initial solute concentration in the water reservoir and by diffusional and convective processes. The effective segregation coefficient (K_{eff}) has been used to describe the segregation of ions in the water phase during such freezing processes (e.g., Killawee et al., 1998; Garandet et al., 1994; Santibáñez et al., 2019) and can be expressed as follows:

$$[\textbf{EQ. 1-1}]\ K_{eff} = \frac{C_{ice(i)}}{C_{bw(i)}}$$

where:

K_{eff} is the effective segregation coefficient;

$C_{ice(i)}$ is the concentration of soluble ions in the ice (at time i);

$C_{bw(i)}$ is the concentration of water-soluble ions in the liquid phase (at time i).

Segregation of gases during winter accretion also occurs in the ice cover of these lakes: the abundance of gas bubbles occluded in the ice cover should vary as freezing progresses and excess dissolved air develops in the water (Lipp et al., 1987; Killawee et al., 1998). Besides, Santibáñez et al. (2019) recently discovered that, unlike inorganic impurities, organic material (i.e., bacteria) were preferentially incorporated in the ice during experimental freezing of waters sampled from Antarctic perennially ice-covered lakes and Alaskan (near Barrow) thermokarst ponds. Priscu et al. (1998) also showed that liquid water pockets within these lakes' ice cover were small oases for many microorganisms (fed by cryoconite nutrients). Together, these results demonstrated that bacteria could survive (preferentially) within the ice cover of these lakes: a critical implication for searching for life in cold/icy planetary bodies in our solar system.

1.2.4 Physical limnology and hydrochemistry of lake waters

The polar and high elevation region's perennially ice-covered lakes are often annually physicochemically stratified (i.e., amictic) because their permanent ice cover prevents wind enhanced mixing of their waters (Parker et al., 1982). Because of their geographic location, their water temperature tends to be close to 0°C (Table 1-1) but can also be lower due to freezing point depression by highly concentrated water-soluble ions (e.g., Spigel & Priscu, 1996; Angino et al. 1964). These generally amictic lakes also frequently exhibit cold water thermal stratification, with waters at the ice-water interface at ~ 0°C and the denser hypolimnion close to ~ 4°C (Parker et al., 1982). The only permanently ice sealed lakes that have a permanently mixed water column are those which are subaqueously proglacially damned (e.g., Dronning Maud Land's Lake Untersee): their water is cooled down by the glacier's ice wall and moved upwards due to buoyancy-driven convection inducing mixing of the water column (Steel et al., 2015). Some of these lakes, such as the ones found in the MDV's Taylor Valley (e.g., East Lake Bonney & West Lake Bonney), and others situated on Ellesmere Island (e.g., Van Hove et al., 2006) can also be dichothermic: their highest water temperature is in the mid-point of the water column (Parker et al., 1982) because of solar radiation coupled with the salt-dependent stability of their water columns (Spigel et al., 1990; Heywood 1984).

Table 1-1: Summary table of the mean ($\bar{X}$), maximum (Max) and minimum (Min) measured values and corresponding depth for the physical and chemical limnology characteristics of seven McMurdo Dry Valley perennially ice-covered lakes (data taken from the McMurdo Dry Valley's Long Term Ecological Research Project website; http://mcm.lternet.edu/).

Lake	Approximative Depth	Temperature (ºC)	pH	DOC (mg/L^{-1})	DIC ($mg\ C/L^{-1}$)	Conductivity (mS/cm^{-1})	TDS (g/L^{-1})
East Bonney (2010)	40 m	$\bar{X}$ = 2.65 Max = 4.81 (16.08 m) Min = -1.33 (40.51 m)	$\bar{X}$ = 7.48 Max = 9.02 (6 m) Min = 5.99 (25 m)	$\bar{X}$ = 10.36 Max = 36.32 (37 m) Min = 0.46 (6 m)	$\bar{X}$ = 79.02 Max = 225.3 (22 m) Min = 14.4 (4 m)	$\bar{X}$ = 58.10 Max = 114.56 (27.98 m) Min = 1.23 (0.30 m)	$\bar{X}$ = 83.21 Max = 266.36 (37 m) Min = 0.93 (4 m)
West Bonney (2016)	45 m	$\bar{X}$ = -1.01 Max = 2.89 (7.72 m) Min = -4.25 (43.13 m)	X = 6.95 Max = 9.12 (5 m) Min = 5.66 (35 m)	$\bar{X}$ = 5.77 Max = 24.46 (42 m) Min = 0.46 (6 m)	$\bar{X}$ = 301.80 Max = 862.3 (42 m) Min = 9.2 (5 m)	$\bar{X}$ = 47.84 Max = 80.12 (35.38) Min = 0.82 (1.52 m)	$\bar{X}$ = 53.36 Max = 152.29 (43 m) Min = 0.54 (4 m)
Fryxell (2017)	20 m	$\bar{X}$ = 1.75 Max = 2.71 (10.45 m) Min = -0.02 (4 m)	$\bar{X}$ = 7.64 Max = 10.91 (5 m) Min = 5.42 (7 m)	$\bar{X}$ = 9.35 Max = 22.4 (17.3 m) Min = 4.1 (5 m)	$\bar{X}$ = 255.74 Max = 647 (20 m) Min = 55.2 (6 m)	$\bar{X}$ = 3.75 Max = 8.53 (18.64 m) Min = 0.08 (0.83 m)	$\bar{X}$ = 2.93 Max = 7.23 (18 m) Min = 1.10 (6 m)
Hoare (2012)	34 m	$\bar{X}$ = 0.29 Max = 0.64 (5 m) Min = 0.02 (3 m)	$\bar{X}$ = 8.09 Max = 8.96 (6 m) Min = 7.39 (30 m)	$\bar{X}$ = 1.81 Max = 2.51 (30 m) Min = 0.51 (5 m)	$\bar{X}$ = 44.02 Max = 85.4 (30 m) Min = 2 (4 m)	$\bar{X}$ = 0.56 Max = 0.82 (30 m) Min = 0.01 (2.5 m)	$\bar{X}$ = 0.38 Max = 0.61 (30 m) Min = 0.01 (4 m)
Joyce (2003)	38 m	$\bar{X}$ = 0.16 Max = 0.31 (13 m) Min = -0.06 (38 m)	$\bar{X}$ = 8.54 Max = 9.7 (12 m) Min = 7.2 (33 m)	$\bar{X}$ = 2.45 Max = 3.77 (33 m) Min = 0.58 (7 m)	$\bar{X}$ = 39.53 Max = 98.7 (33 m) Min = 3 (7 m)	$\bar{X}$ = 1.65 Max = 3.50 (37.84 m) Min = 0.12 (5 m)	$\bar{X}$ = 1.89 Max = 3.86 (33 m) Min = 0.15 (6m
Miers (2017)	21 m	$\bar{X}$ = 3.29 Max = 4.99 (16 m) Min = 0.001 (3 m)	$\bar{X}$ = 8.38 Max = 9.16 (9 m) Min = 7.73 (19 m)	$\bar{X}$ = 0.47 Max = 0.63 (18 m) Min = 0.38 (4.5 m)	$\bar{X}$ = 18.64 Max = 33.6 (19 m) Min = 6.4 (5 m)	$\bar{X}$ = 0.09 Max = 0.15 (16.5 m) Min = 0.01 (1 m)	$\bar{X}$ = 51.60 Max = 63.52 (19 m) Min = 39.12 (7 m)
Vanda (2007)	75 m	$\bar{X}$ = 8.05 Max = 21.54 (70 m) Min = 0.41 (0.5 m)	$\bar{X}$ = 7.25 Max = 8.51 (45 m) Min = 5.32 (73.5 m)	$\bar{X}$ = 6.13 Max = 40.88 (73.5) Min = 0.20 (4 m)	$\bar{X}$ = 34.36 Max = 109.7 (73.5 m) Min = 7.6 (4 m)	$\bar{X}$ = 13.89 Max = 112.17 (70 m) Min = 0.25 (2 m)	$\bar{X}$ = 28.92 Max = 118.61 (73.5 m) Min = 0.29 (4 m)

The pH values in these lacustrine environments depend primarily on their water column and atmospheric gases. In the MDV, those lakes have pH values ranging from ~ 10.9 to 5.32, and the pH is typically highly negatively correlated with DIC concentrations. DIC in the form of bicarbonate (HCO_3^-) controls their alkalinity and usually keeps these lakes slightly acidic to circumneutral (Parker et al., 1982). In the absence of an annual interaction with the atmosphere (due to the lack of moats) coupled with the consumption of any available DIC by benthic microbial mats, their pH can evolve to very alkaline values (e.g., pH of ~ 11 at Lake Untersee; Andersen et al., 2011).

The saturation level of dissolved O_2 (DO) in such Antarctic water basins tends to be abnormally high (i.e., supersaturation) in many instances because of the photosynthetic activity of benthic microbial mats releasing substantial quantities of oxygen and also because of gas bubble inputs from glacial meltwater which accumulate over time because of the combined action of: 1) the seal created by their ice cover preventing venting of the water column (e.g., Wharton et al., 1986; Wand et al., 1997); and 2) the expulsion of gases during winter freezing (Bari & Hallett, 1974). Other dissolved gases such as N_2 are also often found in supersaturated states in those lakes' water column because of the latter phenomenon (e.g., Wharton et al., 1987). Oxygen levels can still be deficient in some instances, creating an anoxylimnion in their bottom waters, where methanogenesis (i.e., production of CH_4 via H_2 and CO_2 reduction) becomes the preferred biochemical pathway (e.g., Wand et al., 2006). The highest concentrations of methane in aquatic ecosystems have been measured in the anoxic waters of Antarctica's perennially ice-covered Lake Untersee (21.8±1.4 mmol L^{-1}; Wand et al., 2006). Also, the ratios between O_2, N_2, and Ar have been used in limnological studies (e.g., Andersen et al., 1998; Craig et al., 1992) to determine the origin of the water column's dissolved air (e.g., dissolved atmospheric air originating from glacier ice should present atmospheric air ratios) and can therefore inform on the relative contributions of biological activity and physical contributions to the concentration of these dissolved water column gases.

As most Antarctic perennially ice-covered lakes are fed by ephemeral glacial meltwater streams and lack outlet surface streams, their water-soluble ionic content and associated conductivity tend to depend on the age of their basin, where the younger and older are respectively generally less and more saline due to the progressive increase in salinity from one year to the next because of salt segregation during the freezing of the ice cover. In the MDV, the concentration of

total dissolved solids (TDS) in these meromictic lakes varies from 0.28 to 266 g/L^{-1} (i.e., freshwater to extremely saline brine), and the maximum concentrations are typically obviously found at their bottom (Spigel & Priscu, 1998). Their dissolved ions species which vary greatly from one lake to another, originate from 1) marine aerosols; 2) subaqueous *in situ* weathering; and 3) salts carried by local glacial melt streams (Doran et al., 1994). In central Queen Maud Land, the freshwaters' hydrochemical facies in Lakes Untersee and Obersee are of Na–Ca–Cl–SO4 type; their TDS concentration is respectively 0.31 and 0.05 g/L^{-1} (Haendel et al., 2011).

The analysis of stable water isotope ratios (SWI; δD-$\delta^{18}O$) of the Antarctic perennially ice-covered lakes has shown that $\delta^{18}O$ and δD ratios (Fig. 1-1) tend to be highly depleted with regards to the Vienna Standard Mean Ocean Water (VSMOW) standard due to the positive correlation between air temperatures and SWI ratios (e.g., Dansgaard, 1964). Analysis of SWI ratios has proven to be a reliable tool to trace back the origin (including the source of moisture) and subsequent fractionation of water inputs to these high latitude lakes and has also been helpful for hydrological mass balance calculations (e.g., Jeffries et al., 1984; Gooseff et al., 2006). For instance, in the high Arctic, Jeffries et al. (1984) combined the analysis of $\delta^{18}O$ ratios and other stable isotopes (e.g., $\delta^{34}S$-SO_4, $\delta^{13}C$-HCO_3) of Ellesmere Island's Lake A to conclude that evaporation had fractionated the seawater that first infilled the lake's basin (and that now composes the hypolimnion) soon after the post-Wisconsin glaciation isostatic rebound. The δD-$\delta^{18}O$ ratios of waters in permanently ice-capped polar lakes will typically plot below the Global Meteoric Water Line (GMWL) when kinetic fractionation affects their water via evaporation (Clark et al., 2015) during the summer months (e.g., Gooseff et al., 2006). However, in some rare instances, the δD-$\delta^{18}O$ of well-sealed ice-covered lakes can also plot above the GMWL. This happens if interactions between the water column and the atmosphere are very limited or nonexistent (e.g., Haendel et al., 2001; Matsubaya et al., 1979) and/or if their input is derived from subglacial meltwater, where freeze concentration causes progressive δD-$\delta^{18}O$ depletion of the lake waters due to the progressive inclusion of heavier oxygen and hydrogen atoms in the ice cover during the accretion period. The interpretation of the δD-$\delta^{18}O$ ratios in these lakes depends on: 1) the initial δD-$\delta^{18}O$ values of the water input (i.e., where it plots with regards to a local meteoric water line) which controls their fractionation factor during freezing (Souchez & Jouzel, 1984); and on 2) the proportion of ice annually accreted above the water reservoir which controls the rate a which freeze-concentration will deplete the δD-$\delta^{18}O$ values of the remaining liquid (Lacelle, 2011).

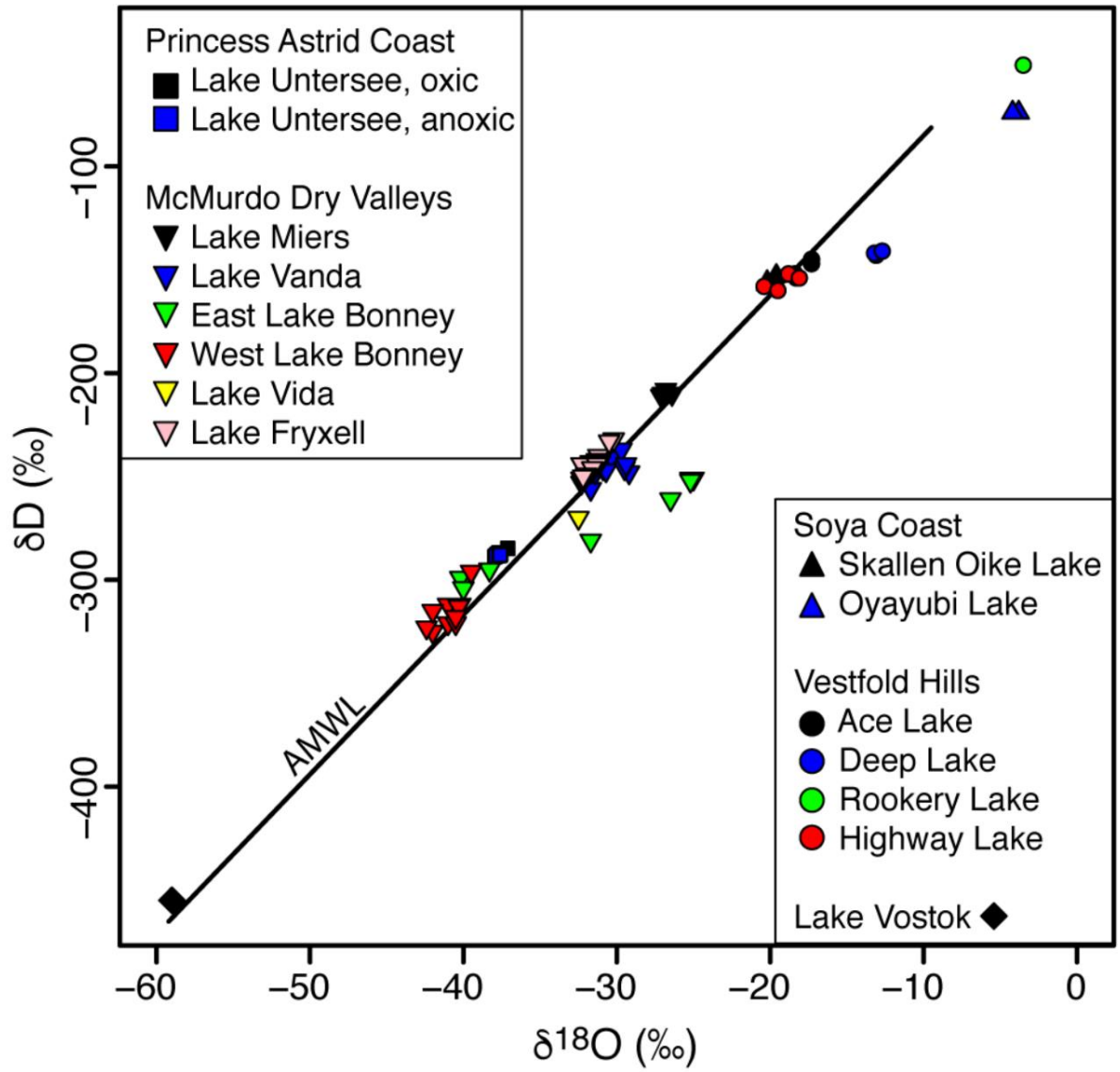

Figure 1-1: Stable water isotope (δD-$\delta^{18}O$) ratios of perennially ice-covered lakes found in Antarctica's Princess Astrid Coast (i.e., Lake Untersee; Hermichen, 1985), Southern Vicotria land region (i.e., Lake Miers, Lake Vanda, Lake Bonney, Lake Fryxell, Lake Vida; Matsubaya et al., 1979; Miller & Asken, 1996; Dugan et al., 2015) and Soya Coast (i.e., Skallen Oike, Oike; Matsubaya et al., 1979). The black line indicates the Antarctic Meteoric Water Line ($8*\delta^{18}O + 10$). The 2016 Lake Untersee data is unpublished (personal notes of B. Faucher). δD-$\delta^{18}O$ data of Lake Vostok's water column is included for comparison.

1.2.5 Antarctica's groundwater and subglacial meltwater systems

The occurrence and connectivity of groundwater systems in coastal Antarctica is still poorly constrained. Nevertheless, the existence of multiple subglacial lakes beneath the thick East Antarctic Ice Sheet is a direct indication of subglacially running liquid water systems (Wingham et al., 2006). Several of those lakes are interconnected by subsurface channels and allow for the rapid migration of liquid water from one basin to another. Those are ultimately discharged into the surrounding Antarctic Ocean as submarine groundwater discharges (SGD) (Siegert et al., 2016; Siegert et al., 2007; Sawagaki & Hirakawa, 2002; Wingham et al., 2006). Foley et al. (2019) recently estimated that about 65 km^3 of water is annually melted below the Antarctic continent and that about 1.5 % (1 km^3) is discharged annually as hypersaline groundwaters to the Antarctic Ocean.

The first area where SGDs have been measured in the Antarctic was near Lutzow-Holm Bay (Uemura et al., 2011), indicating that this Queen Maud Land region's coastal sector was likely hydraulically supplied by deep underground water systems. In the Victoria Land region, Mikucki et al.'s (2015) conducted the first airborne transient electromagnetic sensor survey in the MDV, which led to the detection of a deep briny groundwater system (Fig. 1-2A): the first empirically based evidence confirming such a water network driven by local hydrological gradients in Eastern Antarctica (Foley et al., 2019). This finding was corroborated by Toner et al.'s (2017) investigation on Taylor Valley's Don Juan Pond, which indicated that its water input is derived from a regional, flow-through briny groundwater system. To this day, the only other coastal ice-free region of East Antarctica suspected of harboring a groundwater system is in the Untersee Oasis region, where a water mass balance analysis of Lake Untersee indicated that groundwaters are expected to recharge Lake Untersee at an apparent rate of ~ 8.8 x 10^{-2} m^3 sec^{-1} which is a reasonable estimate given the reported range of subglacial water flux in the region (Faucher et al., 2019). The discharge of subglacial and submarine groundwater has also been measured and constrained in the western part of the continent (peninsula region) by Null et al. (2019). The only known surface expression of subglacial meltwater discharges on the Antarctic continent discovered thus far is the Taylor Valley's Blood Falls, a Fe (II) enriched hypersaline brine exiting the Taylor glacier's snout (Foley et al., 2019; Mikucki et al., 2009).

Basal melting conditions below the WAIS and the EAIS are expected to be quite different (Fig. 1-2B). Foley et al. (2019) predict that there is much more melting occurring below the WAIS than there is below the EAIS, and that subglacial and/or groundwaters below the latter become cryoconcentrated because of their long residence time (and a lower discharge rate than below the WAIS) before they are expulsed from the continent via SGDs.

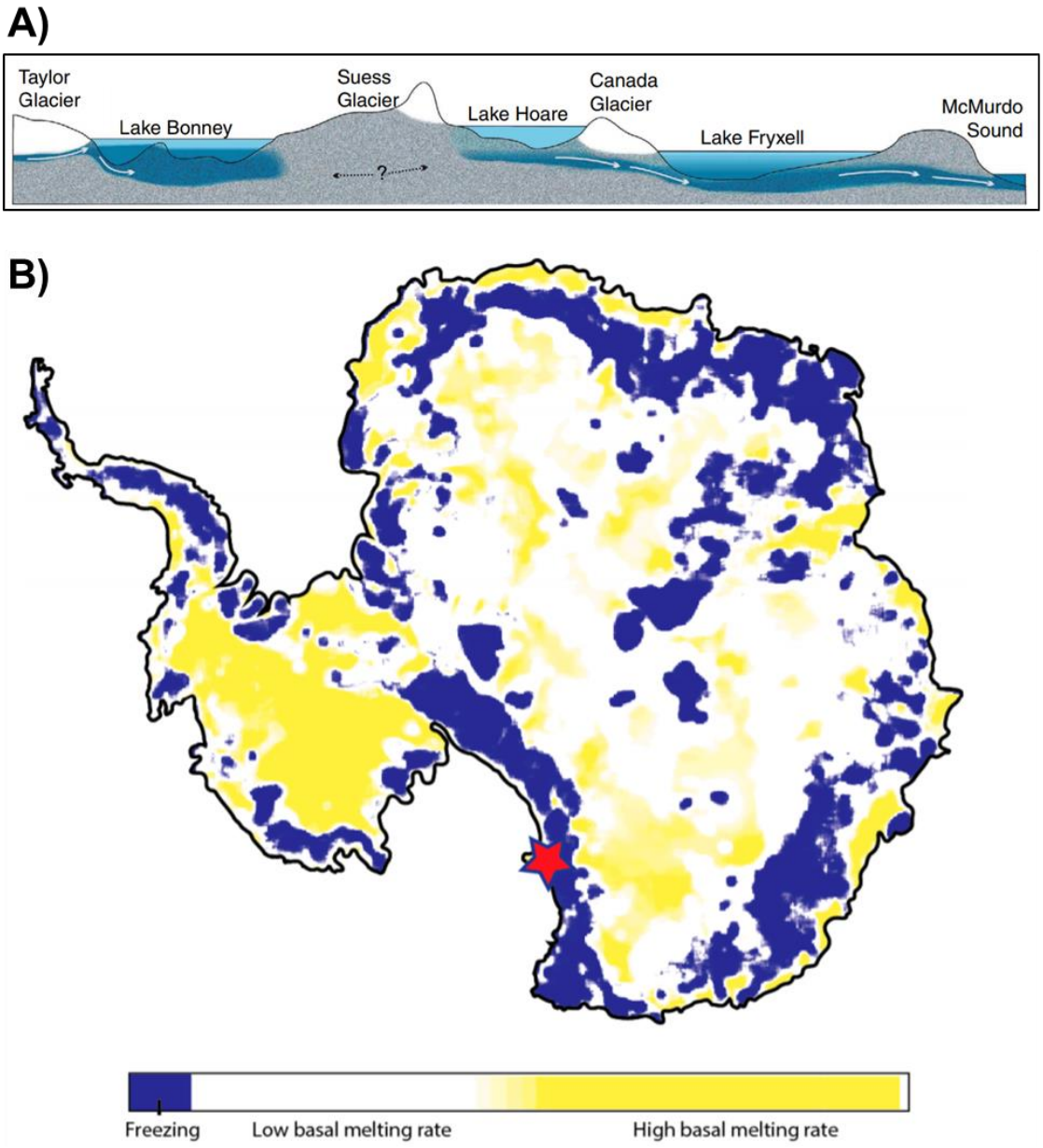

Figure 1-2: Cross-section and map showing: A) the predicted groundwater system connectivity in the MDV (from Mikucki et al., 2015); and B) basal melting conditions below the WAIS and the EAIS (from Foley et al., 2019 and Pattyn, 2010). The red star indicates the study site (MDV) of Foley et al. (2019).

1.2.6 Biogeochemistry of microbial benthic organisms

The benthic zone of Antarctica's perennially ice-covered lakes is composed mainly of microbial mats populated by heterotrophic bacteria, cyanobacteria, and eukaryotic algae (i.e., diatoms) (Doran et al., 1994), but it also commonly hosts fungi and protozoans (Baublis et al., 1991; Cathey et al., 1981). These organisms' matrix is mainly formed of the filamentous cyanobacterium *Phormydium frigidum* and *Lyngbya martensiana* Menegh, which are often low-light adapted with the red photosynthetic pigment phycoerythrin (Wharton et al., 1983; Allnutt et al., 1981; Doran et al., 1994).

The stable carbon and nitrogen isotopes (i.e., ^{13}C & ^{15}N) of these peculiar organisms can provide details on the source of their organic matter uptake and on their photosynthetic and respiration rates (Georicke et al., 1994; Tanabe et al., 2019). These isotopic ratios have been well documented in the MDV (e.g., Wharton et al., 1993b; Lawson et al., 2004). The primary source of carbon being fixed by benthic phototrophic cyanobacteria in these environments is derived from DIC. These organisms will preferentially assimilate the lightest form of carbon (^{12}C) if the system is not carbon-deprived (e.g., Marsh et al., 2020). Their $\delta^{13}C$ ratios should therefore be depleted with regards to the water column's $\delta^{13}C_{DIC}$. However, inorganic carbon used for photosynthesis might also be partially derived from respired CO_2 from heterotrophic activity in underlying mat layers (e.g., Marsh et al., 2020). The resulting $\delta^{13}C$ ratio of the benthic organisms will also depend on the $\delta^{13}C$ of the heterotrophs' initial carbon source. The $\delta^{15}N$ ratios of these benthic organisms, on the other hand, will be indicative of the trophic level of the nitrogen source (e.g., NO_3, NH_4) where enriched ratios indicate a high trophic level for the nutrient source and vice-versa and will provide details on the subsequent transformation and uptake of this nutrient (e.g., Han et al., 2010).

In the MDV, the $\delta^{13}C$ of the benthic mats varies from ~ -30 to 0 ‰, and their $\delta^{15}N$ fluctuates from ~ -20 to 10 ‰ (Fig. 1-3). In Central Queen Maud Land, these same ratios for benthic microbial mats fluctuate from -12 to -6 ‰ and from 10 to 30 ‰: their $\delta^{15}N$ ratios are much higher than those for the microbial mats in the MDV, possibly indicating their nutrient is from a higher trophic level.

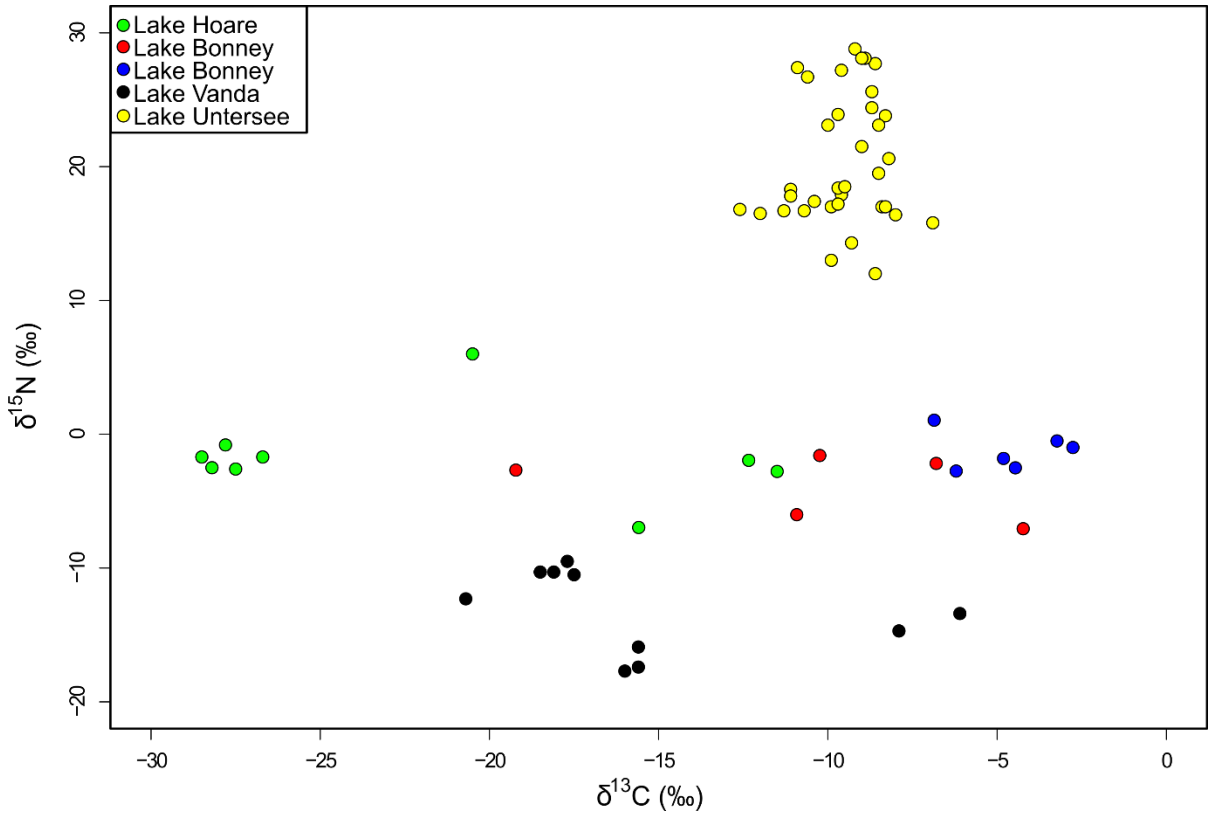

Figure 1-3: Stable carbon and nitrogen isotope ratios of benthic microbial mats in the MDV (Lakes Hoare, Bonney, Fryxell & Vanda) and Central Queen Maud Land (Lake Untersee). MDV data from: Wharton et al. (1993b); Lawson et al. (2004); Wada et al. (2012). Lake Untersee data from Marsh et al. (2020).

1.2.7 Perennially ice-covered lakes as planetary analogs

The fossil record suggests that laminated structures of phototrophic bacterial mats in the form of conical stromatolites are the oldest recorded marine organisms that lived on earth, and in general that microbial organisms flourishing under subaqueous conditions were the dominant species on our planet during the first 2.5 Ga of life (Knoll, 2003). It has been shown that the benthic zone of Antarctica's perennially ice-covered lakes (especially in the MDV) hosts primitive microbial lifeforms and that planktonic organisms solely populate their pelagic zone (e.g., Parker et al., 1982); no high trophic level species populate these lakes. Therefore, these lacustrine ecosystems have been considered by many as relevant analog sites for early life on planet earth (e.g., Mckay et al., 2017; McKay, 1986; Wharton et al., 1989).

Antarctic perennially ice-covered lakes have also been recognized as relevant analogs for icy and/or cold planetary bodies in our solar system because they consist of reservoirs of life in frigid and dry environments (McKay, 1986). The two prime candidates where traces of a second

genesis of life in our solar system might be found and where Antarctic ice-covered lakes might inform on the biological pathways that such organisms could employ to survive are Mars and Enceladus (McKay et al., 2017).

Sedimentological and geomorphological studies showed that Mars had a vast reservoir of liquid water running on its surface (500 m in thickness) about 3.8 Ga BP (late heavy bombardment period), when the red planet was much warmer/wetter (Clifford, 1993) and when life started evolving on planet Earth (Knoll, 2003). It has been hypothesized that ice-covered lakes (similar to those found in the ice-free regions of Antarctica) could have occupied some of Mars' craters (e.g., Gale Crater; Kling et al., 2019) for a relatively short period (thousands to million years; Fassett & Head, 2008), before atmospheric temperatures and pressures began dropping due to the CO_2 enriched atmosphere being progressively stripped away by solar winds. It is plausible that primitive lifeforms (i.e., microbes) similar to those presently thriving in ice sealed Antarctic lakes could have adapted to the extreme ecosystemic conditions that these Martian lacustrine basins offered (McKay, 1986; McKay & Stocker, 1989) and that their potential biosignature (if they ever existed) might be preserved in the crater lake's sedimentary rocks (e.g., Onstott et al., 2019).

Geochemical measurements from NASA's Cassini spacecraft in 2005 have shown that Enceladus, the sixth-largest icy moon of Saturn, hosts a vast anaerobic and habitable ocean beneath its thick surface ice cover (Porco et al., 2006). On earth, one of the few regions where O_2 depleted lakes are sealed by permanent ice covers is on the frigid Antarctic continent. Queen Maud Land's Lake Untersee and its anoxic sub-basin presents itself as the best-known model for biochemical processes potentially taking place in Enceladus' oceans because they are both unlit, anoxic, and contain high dissolved concentrations of CH_4 (McKay et al., 2017).

1.3 Study area

1.3.1 Antarctica's Queen Maud Land region

Antarctica (Fig. 1-4), "the last known frontier", hosts the South Pole and, as such, is the earth's southernmost land/ice mass. It is the only continent that is not inhabited by native communities and the only one that is simultaneously governed by multiple countries (through the Antarctic treaty) (Campbell & Claridge, 1987; Hanessian, 1960). Glaciated areas occupy a staggering 99.8 % of the continent (Burton-Johnson et al., 2016; Hrbáček et al., 2018). Cold climate conditions have persisted in the Antarctic for at least the last ~ 23 Ma and were initiated

by the Drake Passage's opening at the southern tip of South America. Formation of the Antarctic circumpolar current ensued and isolated the continent from warm ocean waters, which allowed for the *in situ* growth of the world's two biggest ice sheets, on the planet's 5th biggest continent (Priscu & Foreman, 2009; Souchez, 1988; Campbell & Claridge, 1987).

The westernmost portion of this landmass (the peninsula region) is occupied by the West Antarctic Ice Sheet (WAIS): a marine ice sheet (most of the ice in this part of the continent is grounded below sea level) with a surface area of 1,970,000 km^2 that spans from the Weddell to the Ross ice shelves. The world's largest (10,350,000 km^2) ice sheet, the East Antarctic Ice Sheet (EAIS), is found in Antarctica's easternmost section. The bedrock below the EAIS is respectively grounded above and below sea levels between 20°W-90°E and between 90°-155°E. These two ice sheets are separated by the 3,500 km long Transantarctic mountains, reaching 4528 m above sea level (a.s.l.) (Souchez, 1988).

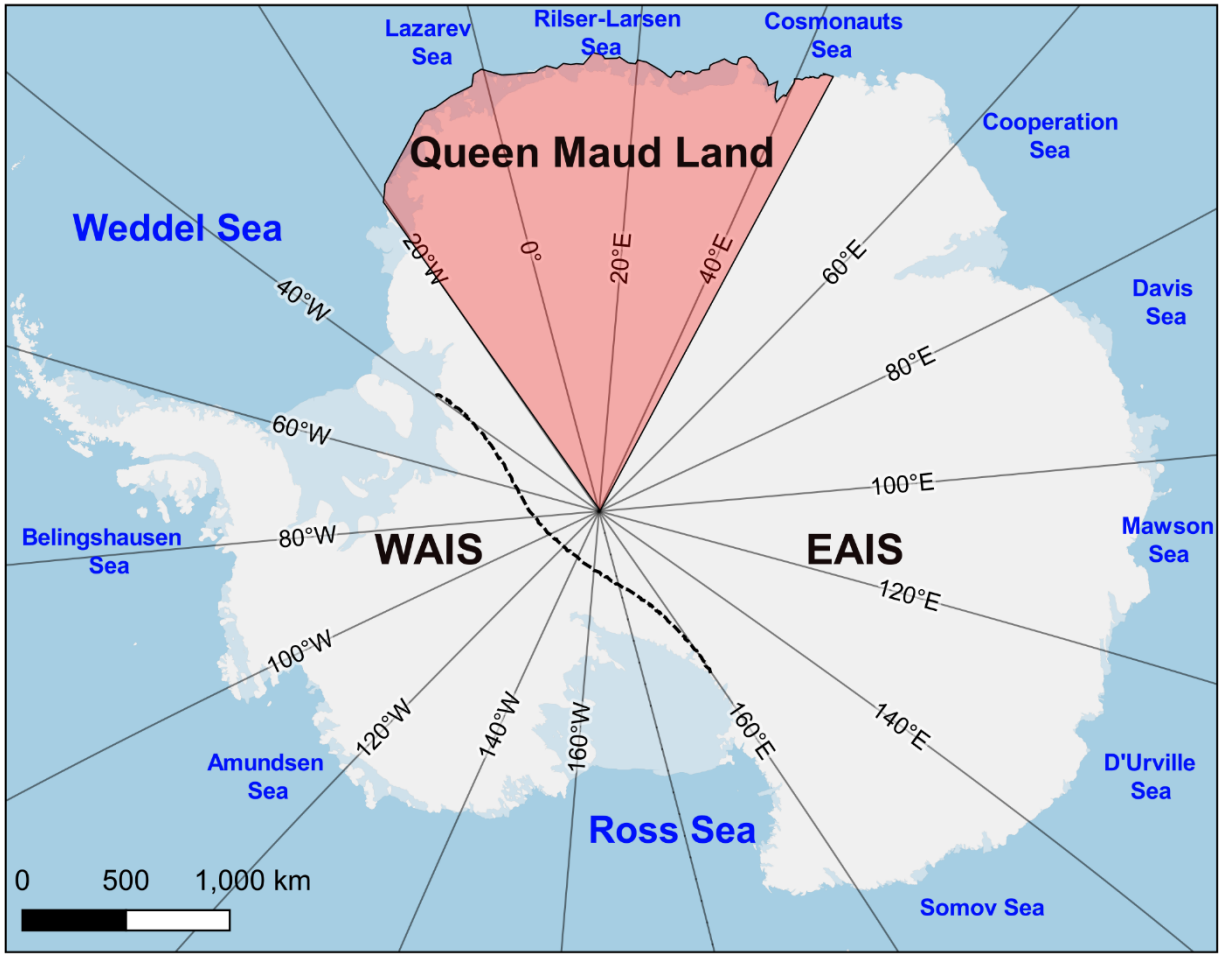

Figure 1-4: Location of the West Antarctic Ice Sheet (WAIS), East Antarctic Ice Sheet (EAIS), and Queen Maud Land (in pink) regions of Antarctica. The dotted line indicates the approximate location of the Transantarctic mountains.

Queen Maud Land (Dronning Maud Land), the second-largest Antarctic territory, was claimed by Norway in 1939 (De Blij, 1978) and is located in the EAIS region, between 20°W and 45°E (Fig. 1-4). It covers 2.7 million km^2 of the continent, and elevations range from sea level to 3,148 m a.s.l. Most of the region is occupied by ice. Still, its coastal areas include multiple nunataks, small groups of mountains (especially in its northern section), as well as polar desert oases (e.g., Schirmacher Oasis, Untersee Oasis, Bunger Oasis, Larsemann Hills) (Campbell and Claridge, 1987).

1.3.2 The Untersee Oasis

The area of interest for this PhD dissertation is the Untersee Oasis. It is located in the Gruber mountains of the Princess Astrid Coast section of Queen Maud Land (~ 200 km south of the Lazarev Sea and ~ 100 km south-east of the Schirmacher Oasis), between 71.40-71.26°S and 13.20-13.80°E (Fig. 1-5).

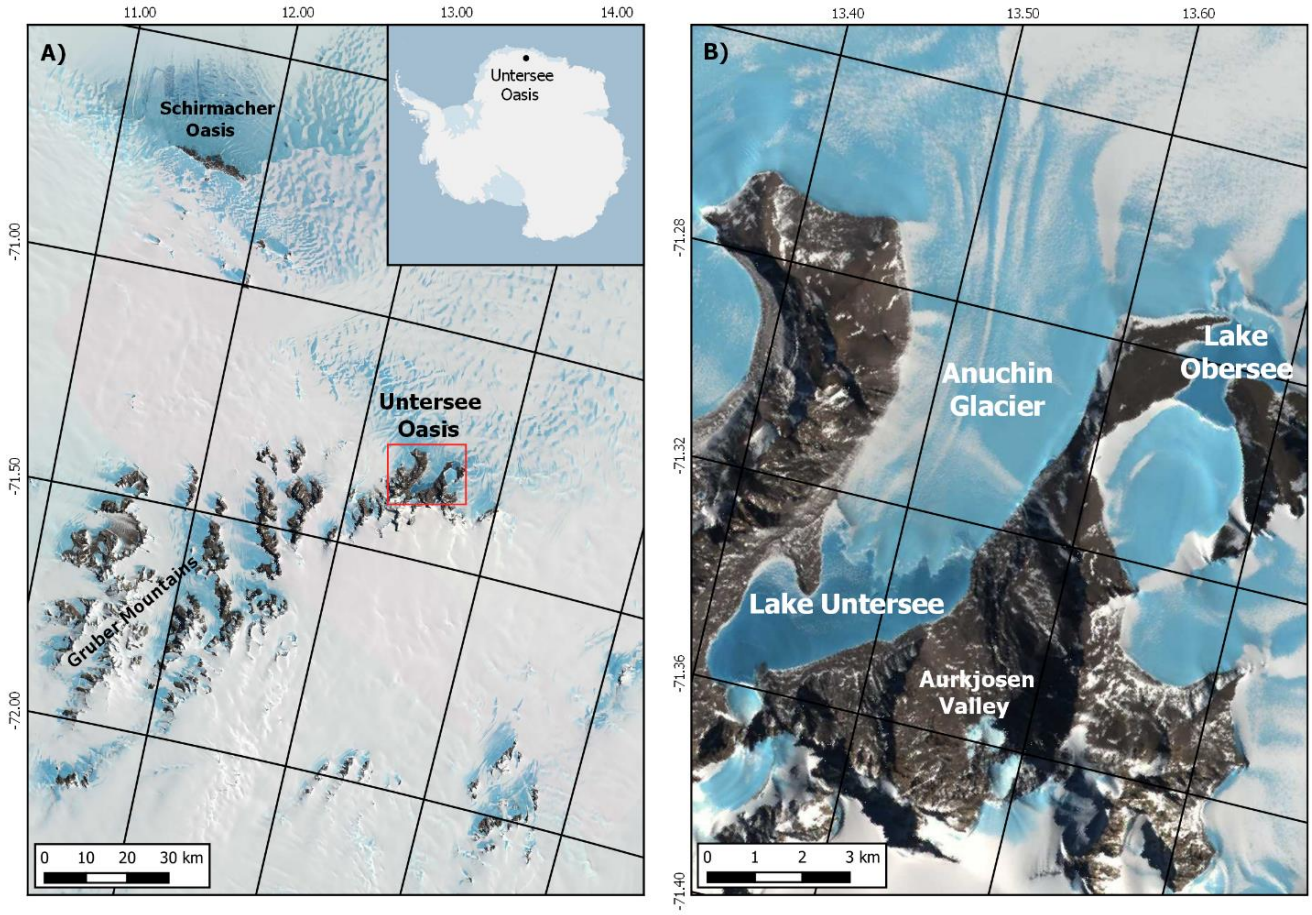

Figure 1-5: Maps showing A) the location of the Untersee Oasis in the Queen Maud Land region (overlaid on the LIMA Landsat high-resolution virtual mosaic; Bindschadler et al., 2008); and B) the Untersee oasis and its contemporary (Untersee & Obersee) and ancient (Aurkjosen Valley) perennially ice-covered lakes (overlaid on a December 2017th WorldView satellite image).

1.3.3.1 Physiography

The Untersee Oasis encompasses two perennially ice-covered lakes (Lake Untersee & Lake Obersee), a dried-up paleo-lacustrine basin (Aurkjosen Valley), and numerous small ice-covered ponds located on the western and eastern lateral moraines of the Anuchin Glacier (Bormann & Fritzsche, 1985; Schwab, 1998). Mountains with elevations ranging from 600 to 2790 m bound the oasis on its western, eastern, and southern ends. The oasis receives ice flowing from a local ice

field (elevation of ~ 800m) connected to the EAIS (Schwab, 1998; Hiller et al., 1988). NASA's *MEaSUREs Annual Antarctic Ice Velocity Maps* (2011-2017) indicate that the Anuchin Glacier flows at an average velocity of ~ 8-9 m yr^{-1} with nearby ice streams to the east and west of the Untersee Oasis flowing at an average speed of ~ 70-100 m yr^{-1} (Mouginot et al., 2017).

Lake Untersee (71.34°S, 13.45°E) is located in the closed-basin Lake Untersee Valley, at ~ 610 m a.s.l. and is dammed at its northern end by the Anuchin Glacier where a pressure-ridge forms at the lake-glacier interface (Fig. 1-6).

Figure 1-6: Aerial shot of the Lake Untersee Valley (Nov. 20th 2016) showing the Anuchin Glacier and the perennially ice-covered Lake Untersee. The approximate location of the pressure ridge at the lake-glacier interface is indicated with a black line. Photo credit: Dale T. Andersen.

The lake is 2.5 km wide and 6.5 km long, making it the largest freshwater lake in central Queen Maud Land (Hermichen et al., 1985). Except for a boulder field at the southern end of the lake and other large boulders scattered across the lake, the ice cover's surface on Lake Untersee is smooth and free of any fine sediments. The lake has two sub-basins: 1) a large basin occupies the northern and central section to a maximum observed depth of 169 m; and 2) a shallower basin occupies its southern section to a depth of 100 m. The two basins are separated by a sill that cuts across the lake at 50 m depth (Wand et al., 1997). The water in the larger and deeper basin, as well as that above the sill in the shallower basin, is well-mixed, has a temperature near 0.5°C, pH near 10.6, dissolved oxygen near 150%, and specific conductivity of about 505 µS/cm^{-1} (Wand et al., 1997, 2006, Andersen et al., 2011). The ice-wall presence at the lake-glacier interface results in buoyancy-driven convection allowing effective mixing throughout most of the lake at time scales of one month (Steel et al., 2015). However, in the southern basin, the water below the sill (60-100 m) is stratified with temperature ranging between 0°C at the ice-water interface to a maximum of 5°C, with lower pH (~ 7), higher specific conductivity (1100-1300 µS/cm^{-1}) and dissolved oxygen levels near 0%. This anoxic water in the hypolimnion does not mix with the overlying oxic epilimnion water due to its higher density (Bevington et al., 2018). Photosynthetic microbial mats cover the floor of the oxic basin in Lake Untersee with the lake ice's transparency to photosynthetically active radiation (PAR) being 4.9±0.9% (Andersen et al., 2011).

Lake Obersee (71.28°S, 13.65°E) is a smaller perennially ice-covered lake that sits at ~ 750 m a.s.l. and is located at the N-E extremity of the oasis. It is damned on its N-E and S-W ends by EAIS ice flows and is separated from the rest of the oasis by the Sjøneset Spur. The lake is 2.7 km long, 2.6 km wide and has a surface area of 3.43 km^2. No fine sediments or large boulders are found on its smooth ice cover (Schwab, 1998). Bathymetric maps of the lake (Schwab, 1998) indicate that its sole basin's depth increases in an SW-NE direction to a maximum of ~ 85 m. The water column is not well mixed, and the temperature rises slightly with depth from 0.2 to 0.45°C. The dissolved oxygen, pH, and conductivity decrease respectively with depth from ~ 200 to 170%, from 10 to 9.75, and from 93 to 85 µS/cm^{-1}. The floor of this lake is also covered in benthic photosynthetic cyanobacterial mats.

The Aurkjosen Valley (Fig. 1-7) is a ~ 1.5 km long and ~ 0.8 km wide ice-free valley located to the east of Lake Untersee, which has preserved evidence of a former lake in the form of strandlines. In January 2016, organic mats similar in appearance to those on the bottom of Lake

Untersee were discovered by D. Lacelle and D.T. Andersen in some of the strandlines in this Valley, providing clues that the paleo-lacustrine basin ~ 50 m deep hosted a microbial ecosystem similar to that existing in Lake Untersee. No studies on the various physical, chemical, and biological aspects (e.g., sedimentology, microbial geochemistry, quaternary history) of the valley have been published.

Figure 1-7: Panoramic view of the Aurkjosen valley (Nov. 2015th). Photo credit: Denis Lacelle.

A series of small ice-covered morainic lakes are located on the west (n=24) and east (n=7) lateral moraines of the Anuchin Glacier, on the terminal moraine (n=5) of the Lake Untersee Valley, and on the eastern shore of Lake Untersee itself (n=3). The ponds' mean surface area is 2190±4536 m^2 (60 to 21,771 m^2) and based on Landsat and Digital Globe imagery, they have maintained a similar extent for the past two decades. Some of the ponds on the lateral moraines (Fig. 1-8) are seemingly connected by creek beds ≤1 m wide and ≤ 0.5 m deep, indicating that water likely cascaded from one lake to another during warmer periods (Kaup et al., 1998). The biggest frozen lake on the west lateral moraine, Lake Burevestniksee, is 80 m long 50 m wide and was last studied by Kaup et al. (1988) during the 1980s. It sits at an elevation of 631 m, has an ice

cover ~ 4 m thick, and a 3 m deep water column below which benthic microbial mats are also thriving (Kaup et al., 1988).

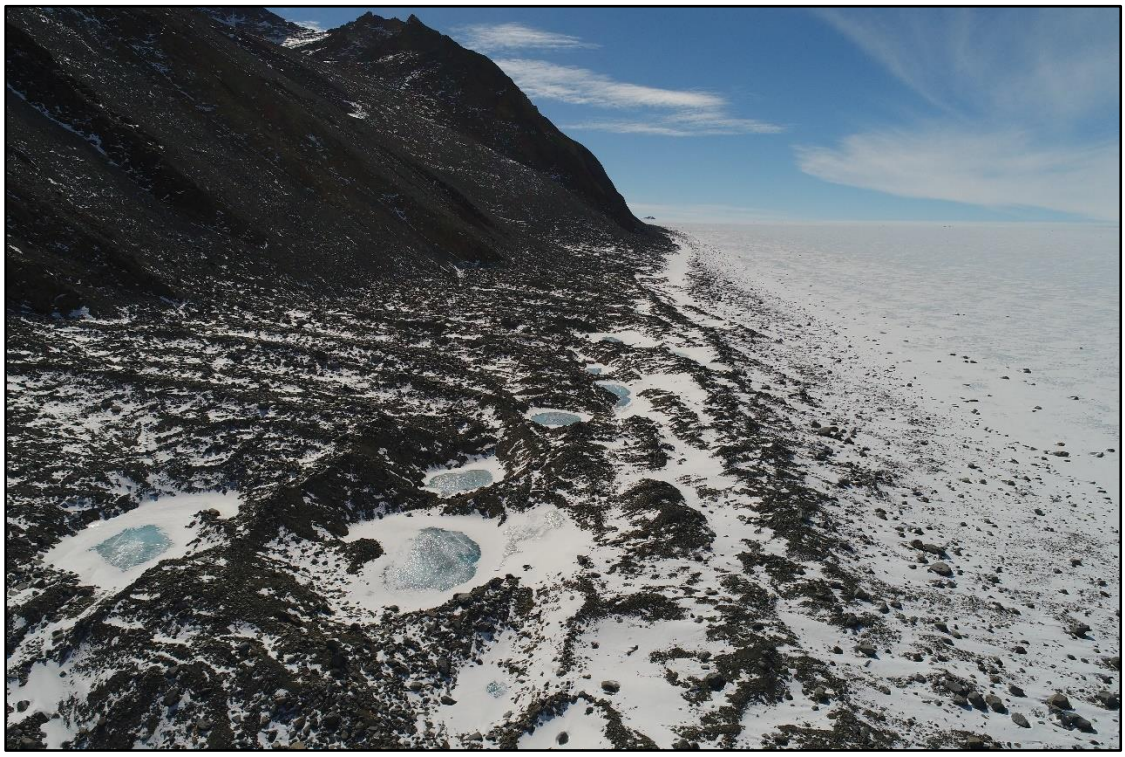

Figure 1-8: A series of small frozen lakes (n=24) located on the west lateral moraine of the Anuchin Glacier (photo taken on Nov. 7th 2017th). Diameter of the leftmost pond is ~10m.

Some of these small lentic basins are host to ice cover blisters. Those are likely the result of closed-system hydrostatic pressures (e.g., Guglielmin et al., 2009), suggesting that they are perhaps almost frozen to their bottom. Their input source has not been determined but probably originates from either: 1) the *in situ* melting of the ice-rich moraine; 2) snow meltwater contributions from ephemeral slope streaks running on the sides of the adjacent mountains; or 3) a mix of both input sources.

1.3.3.2 Climate

Ice cores have been the most reliable tools to reconstruct climate changes in Antarctica because of the lack of accessibility to other climate proxies that are as well constrained as the latter (Ingolfsson, 2004). The oldest climate record for Central Queen Maud Land comes from the nearby Dome Fuji ice cores (DF1 & DF2), dating back to ~ 750 kyr BP. Uemura et al.'s (2018)

analysis of the core's stable water isotope ratios shows that there has been a 100 kyr glacial cyclicity (dominated by orbital eccentricity) since the Mid-Pleistocene Transition (MPT) and associated local temperature fluctuations during that timeframe (Fig. 1-9). Their results suggest that the most significant local positive and negative temperature deviations from the normal (i.e., an average of the past two kyr) had respectively occurred in Antarctica during the Marine Isotope Stage (MIS) 9.3 (~ +2.3°C above normal) and during the MIS 12.2 (~ -7°C below normal).

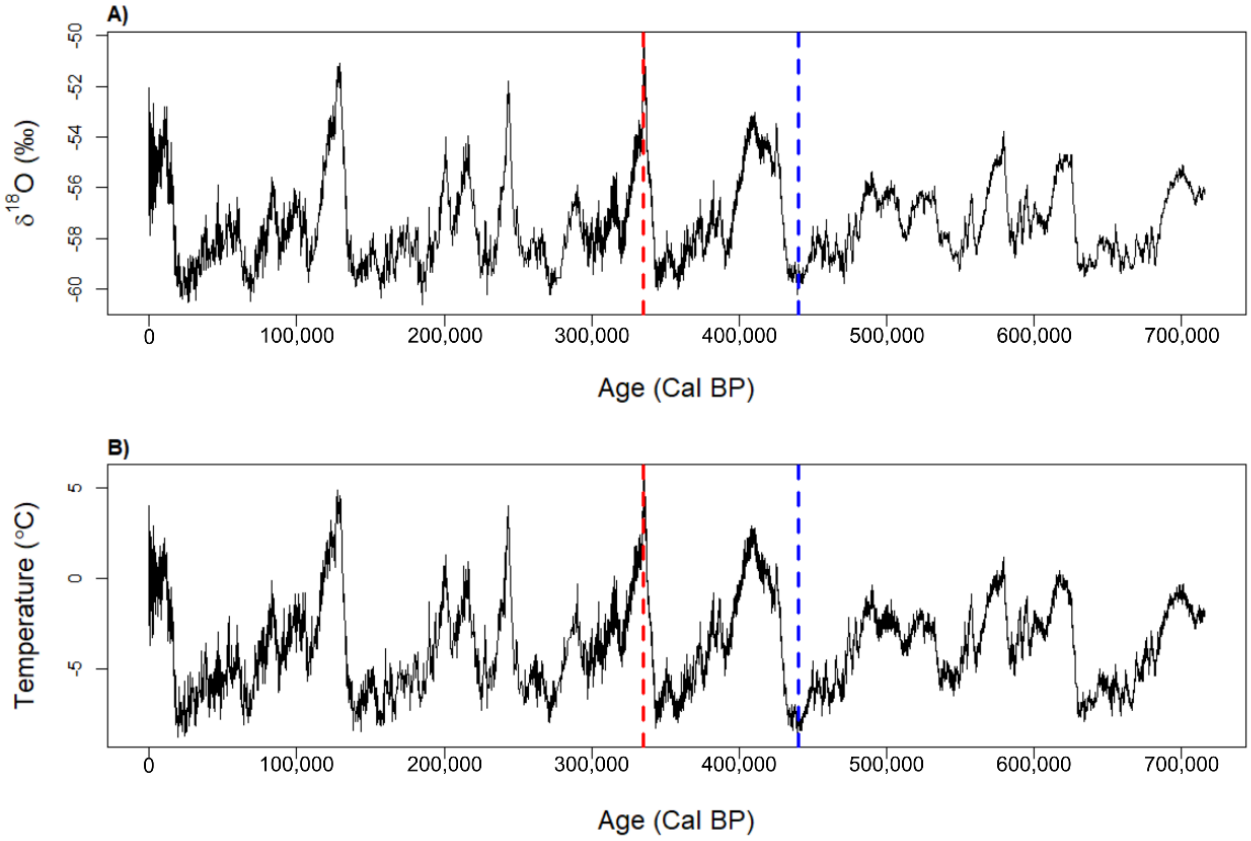

Figure 1-9: 720 kyr Dome Fuji ice core data showing: A) stable water isotope ratios ($\delta^{18}O$); and B) temperature deviations from the normal (i.e., the average of the past two kyr). Red and blue dotted lines respectively indicate the warmest interglacial (MIS 9.3) and coldest glacial period (MIS 12.2) during the last 800 kyr BP (data taken from Uemura et al., 2018).

Analysis of normalized (for an elevation of 500 m) late Pleistocene $\delta^{18}O$ data from the Dronning Maud Land (DML), Dome C, and Dome Fuji ice cores (Fig. 1-10) demonstrates that Antarctic air temperatures steadily rose from the last glacial maximum (~ 18 kyr BP) until ~ 14.5 kyr BP when they went into the two millennia-long Antarctic cold reversal period (EPICA community members, 2006; Uemura et al., 2018; Stenni et al., 2003). This cooling event was likely caused by a meltwater pulse (i.e., 1A) originating from the Laurentide or Antarctic ice sheets that potentially disrupted global thermohaline circulations at that time (Weber et al., 2014). The Antarctic cold reversal period was the southern hemisphere's equivalent of the northern hemisphere's Younger Dryas but occurred before the latter because of the bipolar seesaw phenomenon (Putnam et al., 2010). Air temperatures continued rising until the Holocene Climate Optimum (~ 11-9 kyr BP), when temperatures were 1-2°C higher than the present. The remainder of the Holocene was punctuated by short temperature fluctuations such as anomalously warm and cold periods at ~ 4.5 kyr BP (i.e., mid-Holocene Climatic Optimum) and ~ 2 kyr BP (Ciais et al., 1994).

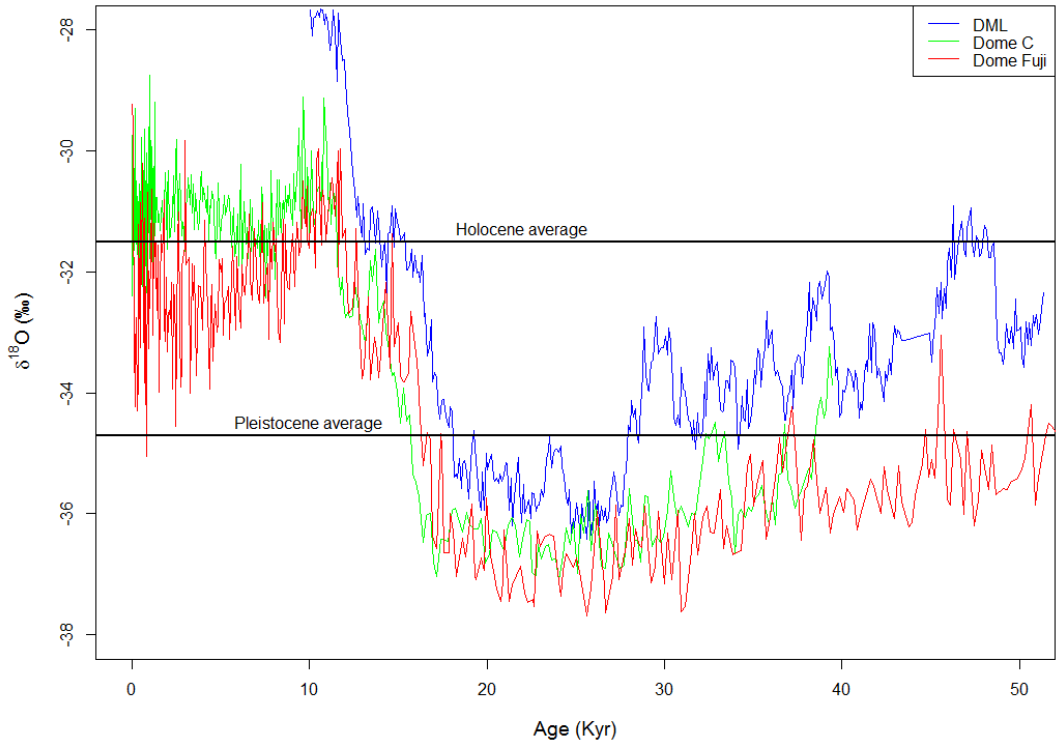

Figure 1-10: $\delta^{18}O$ values for the Dronning Maud Land (DML), Dome C, and Dome Fuji ice cores during the last 50 kyr BP. Values normalized for an elevation of 500 m (i.e., the elevation of the DML ice core sampling site). Average Holocene and late Pleistocene values are shown with labeled horizontal lines.

Untersee Oasis climate data was collected during the 2008-2019 period by an automated *Data Garrison* weather station along the western shore of Lake Untersee (71.34°S, 13.45°E, 612 m a.s.l.) (Table 1-2). It showed that between 2008 and 2019, this polar desert region had experienced: 1) mean summer insolation of 99±7 Wm^{-2}; 2) MAAT of –10.6 ± 0.7°C; 3) TDD ranging from 7 to 51 degree-days; 4) and a mean relative humidity (R.H.) of 42±5% (Faucher et al., 2019). The MAAT showed little to no change over the past decade. The average wind speed was 5.4 m s^{-1}, with strong southern winds descending the polar plateau and sweeping across the southern section of the lake and also strong east wind descending from the Aurkjosen Valley and flowing across the snout of the Anuchin Glacier. Despite having a relatively warm MAAT for Antarctica, the oasis climate is dominated by intense evaporation and sublimation, limiting the surface melt of its perennially ice-covered lakes due to cooling associated with the latent heat of sublimation (e.g., Hoffman et al., 2008).

Table 1-2: Interannual summer comparison of climatic data in the Untersee Oasis during the 2008-2019 period (taken from Faucher et al., 2019).

Summer	Average DJF temperature (ºC)	Maximum DJF temperature (ºC)	Minimum DJF temperature (ºC)	Summer thawing index (ºC-days)	Light (Wm^{-2})
2008/09	-3.5	+5.3	-13.8	9.7	55.4[1]
2009/10	-1.9	+7.6	-12.8	37.7	99.3
2010/11	-2.2	+5.7	-12.9	22.4	99.9
2011/12	-3.6[2]	+4.4	-13.5	7.0	98.8
2012/13	-1.9[2]	+9.0	-12.1	51.3[3]	98.6
2013/14	-3.0	+10.6[4]	-11.1	16.3	94.6
2014/15	-3.2	+6.3	-13.4	8.1	99.7
2015/16	-3.0	+3.9	-10.3	11.5	98.0
2016/17	-1.9	+6.6	-13.9	29.7	n/a[5]
2017/18[6]	-2.3	+8.4	-12.8	32.6	n/a[5]
2018/19	-2.0	+6.4	-10.8	26.8	n/a

[1]Starting after 8 Dec 2008.
[2]Correct here (cf. Andersen et al. 2015 incorrect in Table 1, correct monthly averages in Table 2)
[3]48.8ºC-days, excluding Nov 2012 (cf. Andersen et al. 2015).
[4]High temperatures corrected for the loss of solar shield (11 Sep 2013 to 9 Dec 2014)
[5]Not available due to winter battery failure.
[6]Data from Hobo Garrison Station

1.3.3.3 Quaternary history

The Untersee Oasis was partially glaciated during the Late Pleistocene; however, the region's terminal and recessional moraines have poorly constrained ages (Bormann & Fritezsche, 1995). Based on Altmaier et al.'s (2010) cosmogenic exposure dating (^{10}Be) of quartz-rich nunataks in central Queen Maud Land, it is presumed that elevations in this oasis that are above 1400 m a.s.l. were not covered in ice during at least the last 200 kyr. Indirect evidence of ice sheet

thickness changes in the area was also obtained from radiocarbon dating of snow petrel stomach oils (mumiyo) from nesting sites in the mountain slopes surrounding Lake Untersee. Based on these ^{14}C ages, the regional elevation of the ice sheet was below 950 m a.s.l. at 33,900 ^{14}C yr BP and was below 700 m a.s.l. by 8020 ^{14}C yr BP (Hillier et al., 1988; 1995). Also, Schwab (1998) suggested, based on optically stimulated luminescence (OSL) dating of some of the oasis's morainic material, that the oasis was glaciated until ~ 13 kyr and that Lake Untersee likely formed between 13 and 11 kyr BP when the Anuchin Glacier started to retreat northwards (Fig. 1-11). The dried-up lacustrine basin in the Aurkjosen valley would have ceased to receive its glacial water input at ~7 kyr. This coarse glacial chronology will be updated based on OSL and thermoluminescence (TL) dating of anorthosite rich moraines and paleo-strandlines in the coming years, by uOttawa PhD Candidate Timothy Christian Roy. The latter results will be compared with ages yielded by ^{14}C dating of microbial mats buried in the moraines and paleo-strandlines, which are expected to reflect a carbon reservoir effect (i.e., to provide an older age than OSL and TL because of their consumption of older glacially entrapped CO_2 during photosynthesis and/or heterotrophy).

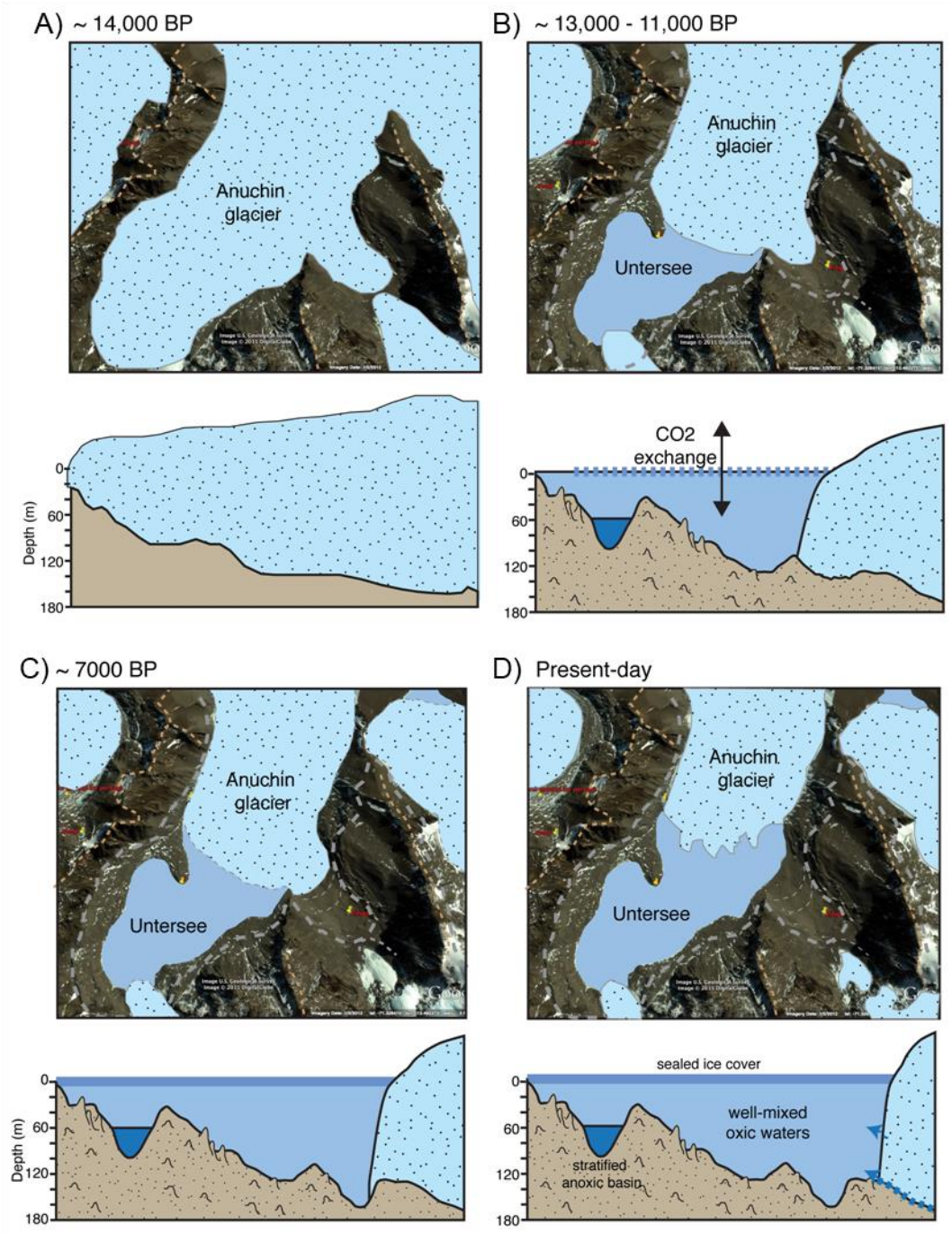

Figure 1-11: Late Pleistocene Untersee Oasis glacial chronology. A) Ice-covered oasis at ~ 14 kyr (absence of a subglacial lacustrine basin); B) Northward retreat of the Anuchin Glacier and formation of Lake Untersee (possible CO_2 exchanges with the atmosphere through seasonal moats); C) Retreat of the Anuchin Glacier from the Aurkjosen valley; and D) the present-day extent of the Anuchin Glacier and Lake Untersee. Sketch adapted from Schwab (1998). Dotted grey lines indicate the maximum extent of the Anuchin Glacier during the late Pleistocene/early Holocene period.

1.3.3.4 Geology and surface deposits

The study area is located in the geological region of the Eliseev massif: one of Antarctica's biggest (~ 1500 km^2) mafic intrusive geological units composed of Precambrian aged norite, anorthosite, and anorthosite-norite alternation (Fig. 1-12) (Kampf & Stackebrandt, 1985; Bormann et al., 1986; Borman & Fritzsche, 1995; Swoboda & Gallagher, 1991).

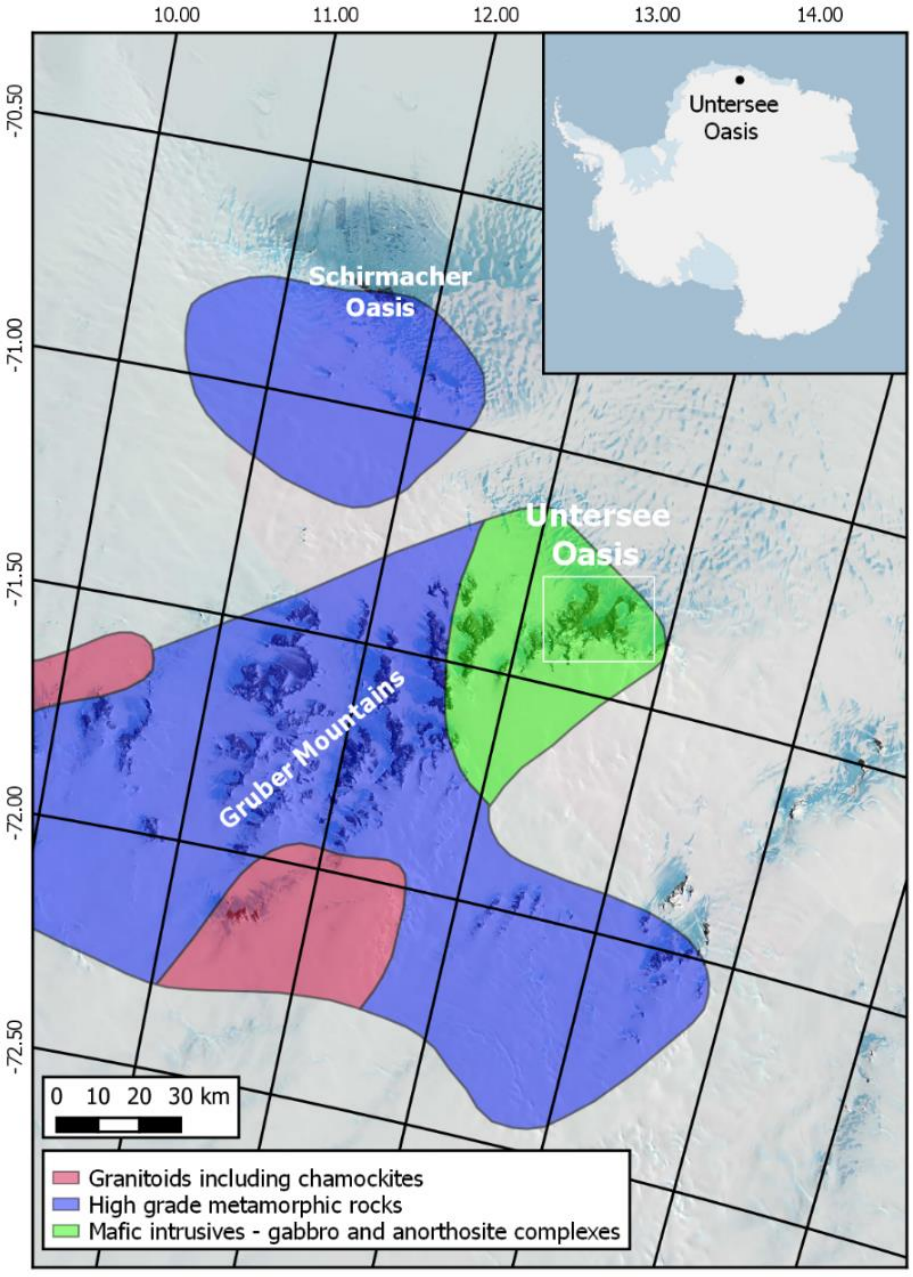

Figure 1-12: Geological map of the Untersee Oasis and surrounding mountains (data taken from Swoboda & Gallagher, 1991).

Surface deposits consist exclusively of glacial diamicton (i.e., till) rich in anorthosite plagioclases laid down by the Anuchin Glacier's retreat during the late Pleistocene/early Holocene period (Schwab, 1998). The glacial till is distributed in the form of various moraine types throughout the oasis. A ground moraine occupies its flat areas, and ice-cored lateral moraines are located on each side (i.e., east and west) of the Anuchin Glacier. Push moraines occupy the oasis's peninsula region, indicative of the Anuchin Glacier's waxing and waning during the late Pleistocene/early Holocene period. A terminal moraine is located in the southernmost portion of the oasis. Ice-rich debris indicated by a steep slope is also found at the base of the mountains surrounding the oasis. There are distinctive differences in the mineralogy of the glacial tills located in the eastern and western areas of the Untersee Oasis: 1) there are more Rare Earth Elements (REE) in the oasis' western glacial deposits than in the eastern ones; 2) the west moraines are more enriched in Pb, Be, Ba, K and Li; and 3) the eastern moraines are enriched in Na, Ca and Sr (Bormann & Fritszche, 1995). Strong winds have removed most of the interlocked fines between the till's coarser grains and have generated a desert pavement throughout the oasis.

1.3.3.5 Flora and Fauna

Low summer air temperatures on the Antarctic continent are a limiting factor for the growth of vascular plants. Only two species have managed to colonize the warmest ice/snow-free maritime regions of the continent: 1) the hair grass *Deschampsia antarctica* (Poaceae); and 2) the pearlwort *Colobanthus quitensis* (Caryophyllaceae) (Cavieres et al., 2016). Air temperatures and liquid water accessibility are too low in the Untersee Oasis to allow for either species' growth. However, a few moss species have been found to grow in some of the oasis' seasonally wet areas. At least half a dozen species of hypolothic lichen communities have also been identified on boulders in the oasis (Andreev & Andersen, in preparation).

Snow petrels are one of the few animal species inhabiting the oasis. They make their nests in the surrounding mountains' cliffs and feed on Antarctic Ocean krill (~ 100 km north of the oasis). Radiocarbon dating of their mumiyo (i.e., stomach oils) indicates that they have inhabited the Queen Maud Land region for at least 37 kyr (Thor & Low, 2011). Skuas are also present in the oasis; they make frequent visits to the oasis to feed on snow petrel chicks.

Thus far, phytoplankton production has only been measured for Lake Untersee and is one of the lowest on record for Antarctic lacustrine systems (Simonov and al., 1985; Kaup et al., 1988;

Haendel et al., 1995; Wand et al., 1997). Microbial communities are ubiquitous in the benthic zones of permanently ice-capped lakes in the Untersee Oasis. Andersen et al. (2011) identified two main benthic microbial mat macrostructures in Lake Untersee: 1) pinnacle mats (few cm in height) dominated by *Leptolyngbya* species; and 2) conical stromatolites (up to 0.5 m in height) dominated by *Phormidium* species (an analogue to archean stromatolites). The dominant bacteria (based on microbial 16S rRNA amplicon sequencing) in Lake Untersee, the Anuchin Glacier's cryoconite holes, and surrounding till are affiliated with Actinobacteria, Bacteroidetes, Cyanobacteria, Firmicutes, and Proteobacteria (Weisleitner et al., 2019). The cyanobacterial mats populating the benthic zone of Lake Obersee and the Anuchin Glacier's lateral moraine ponds have still not been characterized.

1.3.3.6 Permafrost

The thermal state and ground ice content of the soil found in the Untersee Oasis remain largely unknown. The closest ground thermal dataset available is for the permafrost at the Novolazarevskaya station (90 km northwest of the Untersee Oasis), which had a temperature of -8.3°C at the top of the permafrost (TTOP) between 2007-2009. Continuous permafrost should be present in the Untersee Oasis, however, because 1) the MAAT is well below the -8°C isotherm (MAAT of -10.6°C); and 2) as a consequence of high winds (and associated high sublimation rates), little to no snow accumulation stays on the ground; and 3) vascular plants are absent (Bockheim, 1995). Modeling of the Temperature of the Top of the Permafrost (TTOP) for ice-free Antarctic regions shows in fact that the Untersee Oasis' regolith should have a TTOP in the range of -12 to -10 °C (similar to the MAAT; Table 2) (Obu et al., 2019) because the region is mainly devoid of vegetation and snow (e.g., Lacelle et al., 2016).

1.3.3.7 Hydrology

There are no rivers or ephemeral springs in the Untersee Oasis nor supraglacial streams on the Anuchin Glacier. There are, however, a few slope streaks that form on talus slopes during the austral summer (originating from the melting of snowpacks that accumulate on surrounding mountain peaks). Many have proposed that the main source of water for Lake Untersee originates from the subaqueous melting of the Anuchin Glacier's terminus ice (e.g., Hermichen et al., 1985; Bevington et al., 2018; Andersen et al., 2015; Steel et al., 2015; Wand & Perlt, 1999) at the glacial ice-water interface and from subglacial/groundwater contributions (e.g., Faucher et al., 2019);

there has been speculation that a similar input mechanism might apply to the smaller Lake Obersee. There are also no surface melt channels connecting Obersee and Untersee but are presumed to exist (Simonov et al., 1985). Unlike the lakes in the MDV, there are no visible surface inflows of water to the lakes that would carry sensible heat energy to either Lake Untersee or Obersee's water column. Therefore, the subaqueous melting of terminus ice must be accomplished by solar energy that penetrates the ice cover (e.g., McKay et al., 1985).

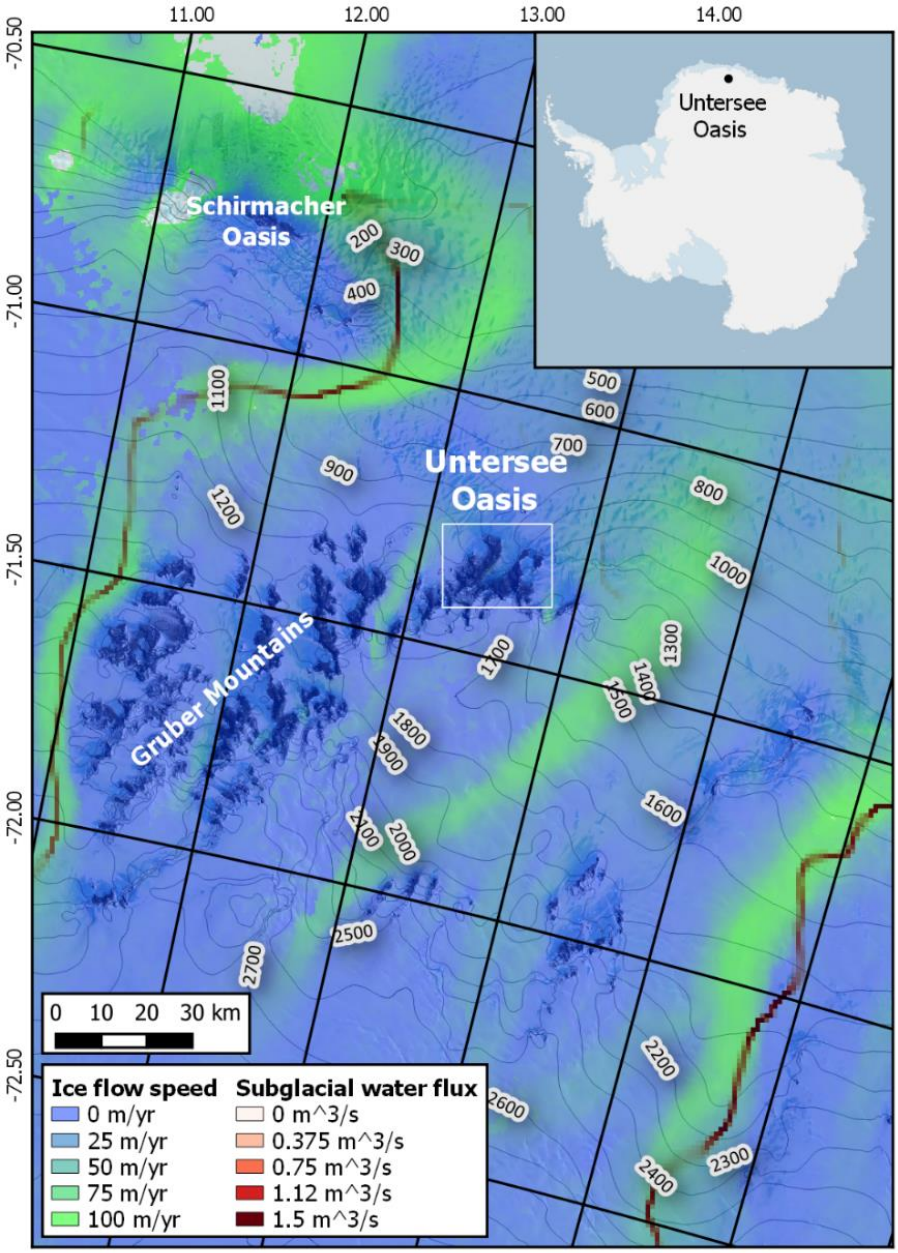

Figure 1-13: Ice flow speed (m/yr^{-1}) (from Rignot et al., 2017) and subglacial meltwater fluxes (m^3/s^{-1}) (from Le Brocq et al., 2013) in the Princess Astrid region of Queen Maud Land. Elevation contours are displayed in meters.

1.4 Thesis organization and research objectives

This doctoral thesis is written in an article format. Each of the following chapters addresses current knowledge gaps related to the hydrochemistry of ice-covered lakes in Antarctica's Untersee Oasis (Queen Maud Land region). Chapters 2 & 3 were published in peer-reviewed journals. Chapters 4 & 5 are respectively under review in the *Scientific Reports* and *Antarctic Science* journals. Chapter 6 presents conclusions concerning the findings showcased in Chapters 2, 3, 4 & 5. References are separately provided at the end of each chapter. Below are the specific objectives addressed in each manuscript.

Objective 1: *Assess the energy and water mass balance of Lake Untersee and its ice cover*

Chapter 2 is an analysis of the hydrological and energetic mass balance of Lake Untersee. Thus far, studies of Lake Untersee have focused primarily on physical and chemical limnology (e.g., Hermichen et al., 1985; Wand et al., 1997, 2006; Steel et al., 2015; Bevington et al., 2018) and microbial ecology (Wand et al., 2006; Andersen et al., 2011; Koo et al., 2017; Greco et al., 2020). Further, it had been suggested by past studies that Lake Untersee was recharged from subaqueous melting of the ice damming Anuchin Glacier (Hermichen et al., 1985; Wand et al., 1997), yet the specifics on the thermodynamics of the ice cover and the hydrological balance of the lake remained largely unconstrained.

It is hypothesized that: 1) the lake is recharged by subaqueous melting of terminus ice and perhaps by subglacial meltwaters; 2) in addition to solar radiation, wind affects the ablation rate of the lake's ice cover; 3) the amount of solar radiation that penetrates the ice cover controls the subaqueous melting of the Anuchin Glacier; 4) spectral analysis of ice cover δD-$\delta^{18}O$ ratios and bubble content can inform on the annual accretion rate of the ice cover. These predictions are tested by analyzing empirical lake ice cover (i.e., thickness, δD-$\delta^{18}O$ ratios, and bubble content) and pro-glacial velocity data collected by colleagues and myself between 2011 and 2017. Findings are then used to inform on the relative contributions of water input sources. Chapter 2 was published in the *Antarctic Science* journal.

Faucher, B., Lacelle, D., Fisher, D. A., Andersen, D. T. & McKay, C. P. (2019). Energy and water mass balance of Lake Untersee and its perennial ice cover, east Antarctica. *Antarct. Sci.* 31(5), 271 – 285.

Objective 2: *Develop a model of δD- δ18O evolution of well-sealed perennial ice-covered lakes that accounts for changing chemistry in the residual water and annual recharge that mixes with residual water*

Chapter 3 presents a newly developed recursive hydrochemical model (*FREEZCH9*) used to investigate the δD-$\delta^{18}O$ steady-state of well-sealed perennially ice-covered lakes (e.g., Lake Untersee), to constrain their recharge source, and to estimate their residence time. Ice cover freezing imparts ionic segregation, annually increasing the solute content in the residual water of ice-covered lakes (Killawee et al., 1998; Terwilliger and Dizio, 1970). In return, this affects the ice-water D/H and $^{18}O/^{16}O$ water-ice fractionation factors, as freezing changes the salinity of the residual water and recursive recharge that mixes with the residual lake water. However, lake water salinity's influence on the evolution of stable water isotopes in well-sealed ice-covered lakes remains to be included in currently accessible δD-$\delta^{18}O$ steady-state predictive models (e.g., Royston-Bishop, 2004; Souchez et al., 2004). We alleviate this problem by modifying the isotope-augmented *FREEZCH5* model (Fisher et al., 2020) and making it recursive and sensible to solute load concentration.

We hypothesize that: 1) *FREEZCH9* can serve to test the effects of input water with differing isotopic signatures (i.e., evaporated water, meteoric water, cryo-freezing water) on the distribution of lake water isotopic composition in a δD-$\delta^{18}O$ diagram; 2) Lake Vostok and Lake Untersee are in isotopic steady-state; and 3) the average δD-$\delta^{18}O$ composition of waters that have fed Lake Untersee during the last few hundred years can be determined using *FREEZCH9*. Our assumptions are tested by conducting *FREEZCH9* simulations with datasets from Lake Vostok and Lake Untersee. The results are presented in terms of residence times of water with different mixing scenarios, which allow applying the findings to other well-sealed perennial ice-covered lakes or subglacial lakes. Chapter 3 was published in the *Frontiers in Earth Science* journal.

Faucher, B., Lacelle, D., Fisher, D. A., Weisleitner, K. & Andersen, D. T. (2020). Modeling δD-$\delta^{18}O$ Steady-State of Well-Sealed Perennially Ice-Covered Lakes and Their Recharge Source: Examples From Lake Untersee and Lake Vostok, Antarctica. *Front. Earth Sci.* 8, 220.

Objective 3: *Describe the effect of a glacial lake outburst flood on the water column and benthic ecosystem of Lake Untersee*

In mid-January 2019, Lake Untersee experienced a glacial lake outburst flood (GLOF) that increased the water column's depth by 2m (1.75×10^7 m^3). In recent years, GLOFs in polar regions have increased in frequency. These disturbances affect the water chemistry and biological productivity of freshwater and marine ecosystems (Bastidas Navarro et al., 2018; Meerhoff et al., 2019). In remote Antarctica, GLOFs are rarely observed, but some have been described in the Larsemann Hills region in recent years, where ice-dammed perennially ice-covered lakes drained catastrophically (Pryakhina et al., 2020); however, their impacts on water chemistry and benthic microbial ecosystems were not described. Chapter 4 examines if and how the 2019 GLOF event altered Lake Untersee's water column's hydrochemistry and nutrient load and, in return, how this may have affected the lake's benthic microbial ecosystem.

The following hypotheses are put forward: 1) the nutrient load in the previously well-sealed and subaqueously fed Lake Untersee increased following the GLOF event providing a biological stimulus to its benthic ecosystem; 2) similar events may have affected the benthic ecosystem of the lake in the past, and this may be recorded in the biogeochemical signature of the microbial mats. These hypotheses are tested by investigating the water column's hydrochemical properties before and after the GLOF event and evaluating its carbon mass balance through numerical modeling. Chapter 4 is under review in the *Antarctic Science* journal.

Faucher, B., Marsh, N.B., Jasperse, L., Clark, I.D., Andersen, D.T. & Lacelle, D. (in review): Glacial lake outburst floods sustain microbial ecosystem in Lake Untersee, Antarctica. *Antarctic Science*.

Objective 4: *Determine the distribution and chemical composition of ice-covered ponds in the Lake Untersee Valley*

Climate change should alter the Antarctic surface lakes' ice cover stability in the coming decades, and this could lead to a shift from a perennial to a seasonal ice coverage for some of those (Obryk et al., 2019; Echeverria et al., 2019). It has also been suggested that the chemical and biological properties of the water column and the primary productivity of the benthic microbial ecosystem of Antarctic surface ice-covered lakes are strongly associated with the fate of their ice cover (Fountain et al., 2016; Gooseff et al., 2016; Badgeley et al., 2017; Lawrence et al., 2020).

However, predictions on how this ice cover phenology shift will affect their hydrochemistry and ecosystem processes for these lentic Antarctic bodies are not based on *in situ* empirical data but on studies done on high Arctic lakes. Chapter 5 aims at addressing these knowledge gaps by conducting a hydrochemical investigation on the Untersee oasis ponds, which offer the full spectrum of ice cover types (i.e., perennially to seasonally ice-covered). Thus, a comparison of hydrochemical properties between basins with different ice coverages can yield insight into their water column and microbial activity response to a warming climate in this particular polar desert oasis.

The hypotheses associated with chapter 5 are that: 1) ice cover type mainly controls the hydrochemistry of the ponds' water column; 2) the amount of incoming solar radiation received by the ponds influence the formation of moats; and 3) a decrease in ice cover extent, as a consequence of climate change, will increase interactions with the atmosphere (i.e., uptake of CO_2), and this will significantly alter their geochemistry regardless of their current ice cover phenology. These are tested by describing the distribution and morphometry of the Untersee Oasis ponds and by proceeding with various hydrochemical analyses of their surface waters. Chapter 5 is under review in the *Scientific Report* journal.

Faucher, B., Lacelle, D., Marsh, N.B., Fisher, D.A & Andersen, D.T. (in review): Ice-covered ponds in Untersee Oasis (East Antarctica): distribution, hydrochemistry, microbial activity, and trajectory under a warming climate. *Scientific Report.*

1.5 Authorship and co-authorship contributions

I have first-authored the four manuscripts presented in this PhD dissertation (i.e., Chapters 2,3,4 & 5). Research objectives, field data collection methods, and data analysis approaches were defined in consultation with my thesis advisor, Dr. Denis Lacelle. Field data was collected by myself, by Dr. Denis Lacelle, and by colleagues during the 2016-2019 period. The contributions showcased in Chapters 2-5 originate from novel ideas put forward by myself and Dr. Denis Lacelle (a co-author of each of those manuscripts). Financial and logistical support for this Antarctic research project was made possible by Dr. Dale T. Andersen (SETI Institute).

The authors of Chapter 2 are Benoit Faucher, Dr. Denis Lacelle, Dr. David A. Fisher, Dr. Dale T. Andersen, and Dr. Chris McKay. BF wrote the manuscript with contributions from DL. BF conducted data analyses and laboratory work. DAF provided hydrochemical modeling

expertise and insights for some of the data analyses. CM provided expertise in ice cover thermodynamics modeling. All authors, except DAF, collected the field data showcased in this publication.

The authors of Chapter 3 are Benoit Faucher, Dr. Denis Lacelle, Dr. David A. Fisher, Dr. Klemens Weisleitner, and Dr. Dale T. Andersen. BF wrote the paper with contributions from DL. DAF provided hydrochemical modeling expertise. DTA provided financial, logistical, and field support. All authors, except DAF, conducted field data collection.

The authors of Chapter 4 are Benoit Faucher, Nicole B. Marsh, Liam Jasperse, Dr. Ian D. Clark, Dr. Dale T. Andersen, and Dr. Denis Lacelle. BF wrote the manuscript with contributions from NBM and DL. Field data collection was done by BF, NBM, DTA, and DL. BF, NBM, and LJ conducted laboratory work and data analyses. IDC provided funding for laboratory analyses.

The authors of Chapter 5 are Benoit Faucher, Dr. Denis Lacelle, Nicole B. Marsh, Dr. David A. Fisher, and Dr. Dale T. Andersen. BF wrote the manuscript with contributions from DL and NBM. BF and NBM did laboratory work and data analysis. DAF provided expertise in hydrochemical modeling. All authors, except DAF, conducted field data collection.

1.6 References

Adrian, R., O'Reilly, C. M., Zagarese, H., Baines, S. B., Hessen, D. O., Keller, W., Livingstone, D. M., Sommaruga, R., Straile, D., Van Donk, E., Weyhenmeyer, G. A. & Winder, M. (2009). Lakes as sentinels of climate change. *Limnol. Oceanogr.* 54, 2283–2297.

Allnutt, F. T. C., Parker, B. C., Seaburg, K.G. & Simmons G. M. Jr. (1981). In situ nitrogen (C_2H_2)-fixation in lakes of Southern Victoria Land, Antarctica. *Hydrobiol. Bull*. 51, 99-109.

Altmaier, M., Herpers, U., Delisle, G., Merchel, S., Ott, U., (2010). Glaciation history of Queen Maud Land (Antarctica) reconstructed from in situ produced cosmogenic ^{10}Be, ^{26}Al and ^{21}Ne. *Polar Sci.* 4, 42-61.

Andersen, D. T., Mckay, C. P. & Wharton, R. A. Jr (1998). Dissolved gases in perennially ice-covered lakes of the McMurdo Dry Valleys, Antarctica. *Antarc. Sci.* 10, 124–133.

Andersen, D. T., Sumner, D. Y., Hawes, I., Webster-Brown, J. & McKay, C. P. (2011). Discovery of large conical stromatolites in Lake Untersee, Antarctica. *Geobiology* 9, 280–293.

Andersen, D. T., McKay, C. P. & Lagun, V. (2015). Climate Conditions at Perennially Ice-covered Lake Untersee, East Antarctica. *JAMC* 54(7), 1393–412.

Andreev, M. & Andersen, D. T. (in preparation). Phytological description and distribution of mosses and lichen in the Untersee Oasis.

Angino, E. E., Armitage, K. B. & Tash, J. C. (1964). Physicochemical limnology of Lake Bonney, Antarctica, *Limnol. Oceanogr*, 9, 207-217.

Armstrong, R. L., Hamilton, W. & Denton, G. H. (1968). Glaciation in Taylor Valley. Antarctica, older than 2.7 million years. *Science* 159, 187-9.

Bari, S. A. & Hallett, J. (1974). Nucleation and growth of bubbles at an ice-water interface. *J. Glaciol*. 13, 4892520.

Baublis, J. A., Wharton R. A. Jr. & Volz, E. A. (1991). Diversity of micro-fungi isolated in an Antarctic dry valley. J. *Basic Microbiol.* 31, 10-20.

Bevington, J., McKay, C. P., Davila, A., Hawes, I., Tanabe, Y., & Andersen, D. T. (2018). The thermal structure of the anoxic trough in Lake Untersee, Antarctica. *Antarct. Sci. 30*(6), 333-344.

Bindschadler, R., Vornberger, P., Fleming, A., Fox, A., Mullins, J., Binnie, D., Paulsen, S. J., Granneman, B. & Gorodetzky. D. (2008). The Landsat image mosaic of Antarctica, *Rem. Sens. Environ.* 112, 4214-4226.

Bockheim, J. G. (1995). Permafrost distribution in the southern circumpolar region and its relation to the environment: a review and recommendations for further research. *Permafr. Periglac. Process* 6, 27–45.

Bormann, P., Bankwitz, P., Bankwitz, E., Damm, V., Hurtig, E., Kampf, H., Menning, M., Paech, H. J., Schafer, V. & Stackebrandt, W. (1986). Structure and development of the passive continental margin across the Princess Astrid Coast, East Antarctica. *J. Geodyn*. 6, 347-373.

Bormann, P., & Fritzsche P., editors. (1995). The Schirmacher Oasis, Queen Maud Land, East Antarctica, and its surroundings. Justus Perthes Verlag, Gotha, Germany.

Brown, L. & Duguay, C. R. (2011). The fate of lake ice in the North American Arctic. *The Cryosphere* 5(4),1775–1834.

Burton-Johnson, A., Black, M., Fretwell, P. T. & Kaluza-Gilbert, J. (2016). An automated methodology for differentiating rock from snow, clouds and sea in Antarctica from Landsat 8 imagery: a new rock outcrop map and area estimation for the entire Antarctic continent, *The Cryosphere* 10(4), 1665–1677.

Campbell, I. B. & Claridge, G. G. C. (1987). Antarctic Soils, Weathering Processes and Environments, 368, Amsterdam, The Netherlands: Elsevier.

Cathey, D. D., Parker, B. C., Simmons, G. M. Jr., Yongue, W. H. & Van Brunt, M. R. (1981). The microfauna of algal mats and artificial substrates in Southern Victoria Land lakes of Antarctica. *Hydrobiologia* 85, 3-15.

Cavieres, L. A., Sáez, P., Sanhueza, C., Sierra-Almeida, A., Rabert, C., Corcuera, L. J. & Bravo, L. A. (2016). Ecophysiological traits of Antarctic vascular plants: their importance in the responses to climate change. *Plant Ecol.* 217, 343–358.

Chinn, T. J. H. (1993). Physical hydrology of the dry valley lakes. In W. Green & E. I. Friedmann (eds), Physical and Biogechemical Processes in Antarctic Lakes. *Ant. Res. Series.* AGU, 59, 1-52.

Ciais, P., Jouzel, J., Petit, J. R., Lipenkov, V. & White, J. W. C. (1994). Holocene temperature variations interred from six Antarctic ice cores, *Ann. Glaciol.* 20, 427-436.

Clark, I. D. (2015). Groundwater Geochemistry and Isotopes, pp. 247–302, CRC Press, Boca Raton, Fla.

Clayton, J. R. Jr., Reimnitz, E., Payne, J. R. & Kempema, E. W. (1990). Effects of advancing freeze fronts on distributions of fine-grained sediment particles in seawater-and freshwater-slush ice slurries. *J. Sediment. Res. 60*(1), 145–151.

Clifford, S. M. (1993). A model for the hydrologic and climatic behavior of water on Mars, *J. Geophys. Res.* 98(10), 973-11.

Clow, G. D., McKay, C. P., Simmons, G. M. Jr & Wharton, R. A. Jr. (1988). Climatological observations and predicted sublimation rates at Lake Hoare, Antarctica. *J. Clim.* 1, 715-728.

Craig, H., Wharton, R. A. & McKay, C. P. (1992). Oxygen supersaturation in ice-covered Antarctic Lakes: Biological versus physical contributions, *Science* 255, 318–321.

De Blij, H. (1978). A Regional Geography of Antarctica and the Southern Ocean, 33 U. MIAMI L. REV. 299, 299.

Dansgaard, W. (1964). Stable isotopes in precipitation. *Tellus* 16, 436-468.

Doran, P. T., Wharton, R. A. Jr & Lyons, W. B. (1994). Paleolimnology of the McMurdo Dry Valleys, Antarctica. *J. Paleolimnol.* 10, 85-114.

Doran, P. T., Wharton R. A. Jr., Des Marais, D. J. & McKay, C. P. (1998). Antarctic paleolake sediments and the search for extinct life on Mars, *J. Geophys. Res.* 103(E12), 28481-28493.

Doran, P. T., McKay, C. P., Clow, G. D., Dana, G. L., Fountain, A. G., Nylen, T. *et al.* (2002). Valley floor climate observations from the McMurdo Dry Valleys, Antarctica, 1986–2000. *J. Geophys. Res. Atmos.* 107(D24), ACL 13-1-ACL 13-12.

Doran, P. T., Priscu, J. C., Lyons, W. B., Powell, R., Andersen, D. & Poreda, R., (2004): Paleolimnology of extreme cold terrestrial and extraterrestrial environments. In Pienitz, R., Douglas, M. S. V., and Smol, J. P. (eds.), Long-Term Environmental Change in Arctic and Antarctic Lakes. Dordrecht, The Netherlands: Kluwer Academic Publishers, 475–507.

Doran, P. T., McKay, C. P., Fountain, A. G., Nylen, T., McKnight, D. M., Jaros, C. & Barrett, J. E. (2008). Hydrologic response to extreme warm and cold summers in the McMurdo Dry Valleys, East Antarctica. *Antarc. Sci. 20*(5), 499-509.

Dore, J. E. & Priscu, J. C. (2001). Phytoplankton phosphorus deficiency and alkaline phosphatase activity in the McMurdo Dry Valley lakes, Antarctica. *Limnol. Oceanogr.* 46(6), 1331–1346.

Dugan, H. A., Obryk, M. K. & Doran, P. T. (2013). Lake ice ablation rates from permanently ice-covered Antarctic lakes. *J. Glaciol.* 59(215), 491–498.

Dugan, H. A., Doran, P. T., Wagner, B., Kenig, F., Fritsen, C. H., Arcone, S. A., Kuhn, E., Ostrom, N. E., Warnock, J. P. & Murray, A. E. (2015). Stratigraphy of Lake Vida, Antarctica: hydrologic implications of 27 m of ice. *The Cryosphere* 9, 439–450.

EPICA Community Members (2006): One-to-one coupling of glacial climate variability in Greenland and Antarctica, *Nature* 444, 195 – 198.

Fassett, C. I. & Head, J. W. (2008). Valley network-fed, open-basin lakes on Mars: distribution and implications for Noachian surface and subsurface hydrology. *Icarus* 198, 37–56.

Faucher, B., Lacelle, D., Fisher, D. A., Andersen, D. T. & McKay, C. P. (2019). Energy and water mass balance of Lake Untersee and its perennial ice cover, east Antarctica. *Antarct. Sci.* 31(5), 271 – 285.

Ferris, J. M., Burton, H. R., Johnstone, G. W. & Bayly, I. A. E. (1988). Biology of the Vestfold Hills. *Hydrobiologia,* 165.

Foley, N., Tulaczyk, M. S., Grombacher, D., Doran, P. T., Mikucki, J., Myers, F. K., Foged, N., Dugan, H., Auken, E. & Ross, V. (2019). Evidence for Pathways of Concentrated Submarine Groundwater Discharge in East Antarctica from Helicopter-Borne Electrical Resistivity Measurements. *Hydrology* 6(2), 54.

Fritsen, C. H. & Priscu, J. C. (1999). Seasonal change in the optical properties of the permanent ice cover on Lake Bonney, Antarctica: consequences for lake productivity and dynamics. *Limnol. Oceanogr.* 44, 447–454.

Garandet, J. P., Favier, J. J. & Camel, D. (1994). Segregation phenomena in crystal growth from the melt. In *Handbook of Crystal Growth* (Vol. 2). Amsterdam. Elsevier Science Publishers., 659-705.

Georicke, R., Montoya, J. O. & Fry, B. (1994). Physiology and isotopic fractionation in algae and cyanobacteria, Stable Isotopes in Ecology and Environmental Science, Ed. by K. Kajtah and R. H. Michener. Blackwell, Oxford, 187–221.

Gooseff, M. N., Lyons, W. B., McKnight, D. M., Vaughn, B. H., Fountain, A. G. & Dowling, C. (2006). A stable isotopic investigation of a polar desert hydrologic system, McMurdo Dry Valleys, Antarctica. *Arct. Antarct. Alp. Res.* 38, 60–71.

Gooseff, M. N., Barrett, J. E., Adams, B. J., Doran, P. T., Fountain, A. G., Lyons, W. B. et al. (2017). Decadal ecosystem response to an anomalous melt season in a polar desert in Antarctica. *Ecol. Evol.* 1, 1334–1338.

Guglielmin, M., Lewkowicz, A., French, H. & Strini, A. (2009). Lake-ice blisters, Terra Nova Bay Area, Northern Victoria Land, Antarctica. *Geogr. Ann. A.* 91, 99–111.

Haendel, D., Kaup, E., Loopmann, A. & Wand, U. (1995). Physical and hydrochemical properties of water bodies in the Schirmacher Oasis, Queen Maud Land, East Antarctica, and its Surroundings (eds Bormann P, Fritzsche D). 289, Perthes, Gotha, pp. 259–319.

Haendel, D., Hermichen, W. D., Höfling, R. & Kowski, P. (2011). Hydrology of the lakes in Central Wohlthat Massif, East Antarctica: new results, *Isotopes Environ Health Stud*. 47(4), 402-406.

Han, S., Yan, S., Chen, K., Zhang, Z., Zed, R., Zhang, J., Song, W. & Liu, H. (2010). ^{15}N isotope fractionation in an aquatic food chain: Bellamya aeruginosa (Reeve) as an algal control agent. *J. Environ. Sci. (China)*, 22, 242–247.

Hanessian, J. (1960). The Antarctic Treaty 1959. *ICLQ 9*(3), 436-480.

Hawes, I. (1983). Nutrients and their effects on phytoplankton in populations in lakes on Signy Island, Antarctica. *Polar Biol.* 2, 115-126.

Heywood, R. B. (1984). Inland waters. p. 279-344. In R.M. Laws [ed.], Antarctic Ecology. Academic Press. New York.

Hrbáček, F., Vieira, G., Oliva, M., Balks, M., Guglielmin, M., Pablo, M. Á. de, Molina, A., Ramos, M., Goyanes, G., Meiklejohn, I., Abramov, A., Demidov, N., Fedorov-Davydov, D., Lupachev, A., Rivkina, E., Láska, K., Kňažková, M., Nývlt, D., Raffi, R., Strelin, J., Sone, T., Fukui, K., Dolgikh, A., Zazovskaya, E., Mergelov, N., Osokin, N. & Miamin, V. (2018). Active layer monitoring in Antarctica: an overview of results from 2006 to 2015, *Polar Geogr.* 0(0), 1–16.

Hermichen, D., Kowski, P. & Wand, U. (1985). Lake Untersee-the first isotope study of the largest fresh-water lake in the interior of East Antarctica. *Nature* 315, 131-133.

Hiller, A., Wand, U., Kämpf, H. & Stackebrandt, W. (1988). Occupation of the Antarctic continent by petrels during the past 35,000 years: inferences from a 14C study of stomach oil deposits. *Polar Biol.* 9, 69-77.

Hiller, A., Hermichen, W. D. & Wand, U. (1995). Radiocarbon-dated subfossil, stomach oil deposits from petrel nesting sites: novel paleoenvironmental records from continental

Antarctica. In: Cook GT, Harkness DD, Miller BF, Scott EM (eds) *Proc 15th Int 14C Conf Radiocarbon* 37, 171–180.

Hoffman, M. J., Fountain, A. G. & Liston, G. E. (2008). Surface energy balance and melt thresholds over 11 years at Taylor Glacier, Antarctica. *J. Geophys. Res.* 113, F04014.

Ingolfsson, Ó. (2004). Quaternary glacial and climate history of Antarctica. In: Ehlers J, Gibbard PL (eds), Quaternary Glaciations - Extent and Chronology, Part III, Elsevier, 3-43.

Jeffries, M. O., Krouse, H. R., Shakur, M. A. & Harris, S. A. (1984). Isotope geochemistry of stratified Lake A, Ellesmere Island, N.W.T., Canada. Can. *J. Earth Sci.* 21, 1008–1017.

Jouzel, J. & Souchez, R.A. (1982). Melting-refreezing at the glacier sole and the isotopic composition of the ice. *J. Glaciol.* 28(98), 35-42.

Kampf, H. & Stackebrandt, W. (1985). Crustal evolution of the Eastern Antarctic craton, Gerlands Beitr. *Geophys*. 94, 251-258.

Kaup, E., Loopman, A., Klokov, V., Simonov, I. & Haendel, D. (1988): Limnological investigations in the Untersee Oasis during the summer season 1983 ⁄ 84. In Limnological Studies in Queen Maud Land (ed. Martin J). Academy of Sciences of Estonia, Tallinn, pp. 43–56.

Killawee, J. A., Fairchild, I. J., Tison, J. -L., Janssens, L. & Lorrain, R. (1998). Segregation of solutes and gases in experimental freezing of dilute solutions: implications for natural glacial systems. *Geochim. Cosmochim. Acta* 62, 3637-3655.

Knoll, A. H. (2003). Life on a Young Planet (Princeton Univ Press, Princeton, NJ).

Kratz, T. K., MacIntyre, S. & Webster, K. W. (2005). Causes and consequences of spatial heterogeneity in lakes, p.329–347. In G. M. Lovett, C. G. Jones, M. G. Turner, and K. C. Weathers [eds.], *Ecosystem function in heterogeneous landscapes.* Springer Verlag.

Lacelle, D. (2011). On the $\delta^{18}O$, δD and D-excess relation in meteoric precipitation and during equilibrium freezing: theoretical approach and field examples. *Permafr. Periglac. Process*. 22, 13–25.

Lacelle, D., Lapalme, C., Davila, A. F., Pollard, W., Marinova, M., Heldmann, J. & McKay, C. P. (2016). Solar radiation and air and ground temperature relations in the cold and hyper-arid Quartermain Mountains, McMurdo Dry Valleys of Antarctica. *Permafr. Periglac. Process*. 27(2), 163-176.

Lawson, J., Doran, P. T., Kenig, F., Des Marais, D. J. & Priscu, J. C. (2004). Stable carbon and nitrogen isotope composition of benthic and pelagic organic matter in lakes of the McMurdo Dry Valleys, Antarctica. *Aquat. Geochem.* 10, 269–301.

Le Brocq, A. M., Ross, N., Griggs, J. A., Bingham, R. G., Corr, H. F. J., Ferraccioli, F., Jenkins, A., Jordan, T. A., Payne, A. J., Rippin, D. M. & Siegert, M. J. (2013). Evidence from ice shelves for channelized meltwater flow beneath the Antarctic Ice Sheet. *Nat. Geosci*. 6, 945–948.

Lee, J. R., Raymond, B., Bracegirdle, T. J., Chadès, I., Fuller, R. A., Shaw, J. D., et al. (2017). Climate change drives expansion of Antarctic ice-free habitat. *Nature* 547, 49–54.

Lipp, G., Korber, C., Englich, S., Hartmann, U. & Rau, G. (1987). Investigation of the behavior of dissolved gases during freezing. *Cryobiology* 24, 489-503.

Livingstone, S. J., Clark, C. D., Woodward, J. & Kingslake, J. (2013). Potential subglacial lake locations and meltwater drainage pathways beneath the Antarctic and Greenland ice sheets. *Cryosphere* 7(6), 1721–1740.

Lyons, W. B., Mayewski, P. A., Donahue, P. & Cassidy, D. (1985). A preliminary study of the sedimentary history of Lake Vanda, Antarctica: climatic implications. N.Z. *J. Mar. Freshwat.Res.* 19, 253-260.

Lyons, W. B., Laybourn-Parry, J., Welch, K. A. & Priscu, J. C. (2006). Antarctic Lake Systems and Climate Change. In: Bergstrom D.M., Convey P., Huiskes A.H.L. (eds) *Trends in Antarctic Terrestrial and Limnetic Ecosystems.* Springer, Dordrecht.

Mackay, R. (1963). The Mackenzie Delta area, N.WT.: Canada Dept. of Mines and Tech. Services, Geographical Branch, Memoir 8.

MacIntyre, S. & Melack, J. M. (1995). Vertical and horizontal transport in lakes: Linking littoral, benthic and pelagic habitats. *J. North Am Benthol Soc*. 14, 599–615.

Marsh, N. B., Lacelle, D., Faucher, B., Cotroneo, S., Jasperse, L., Clark, I. D. & Andersen, D. T. (2020). Sources of solutes and carbon cycling in perennially ice-covered Lake Untersee, Antarctica. *Sci. Rep*. *10*(1), 12290, 1–12.

Matsubaya, O., Sakai, H., Torii, T., Burton, H. & Knowles, K. (1979). Antarctic saline lakes stable isotopic ratios, chemical compositions and evolution. *Geochim. Cosmochim. Acta* 43, 7–25.

McKay, C. P., Clow, G., Wharton, R. A. Jr. & Squyres, S. W. (1985). Thickness of ice on perennially frozen lakes. *Nature* 313, 561-562.

McKay, C. P. (1986). Exobiology and future Mars missions: The search for Mars' earliest biosphere, *Adv. Space Res*. 6, 269-285.

McKay, C. P. & Stoker, C. R. (1989). The early environment and its evolution on Mars: Implications for life. *Reu. Geophys.* 27, 189-214.

McKay, C. P., Andersen, D. T. & Davila, A. (2017). Antarctic environments as models of planetary habitats: University Valley as a model for modern Mars and Lake Untersee as a model for Enceladus and ancient Mars, *Polar J.* 7(2), 303-318.

Mikucki, J. A., Pearson, A., Johnston, D. T., Turchyn, A. V., Farquhar, J., Schrag, D. P., Anbar, A. D., Priscu, J. C. & Lee, P. A (2009). A Contemporary Microbially Maintained Subglacial Ferrous “Ocean”. *Science* 324, 397–400.

Mikucki, G., Auken, E., Tulaczyk, S., Virginia, R. A., Schamper, C., Sørensen, K. I., Doran, P. T., Dugan, H. & Foley, N. (2015). Deep groundwater and potential subsurface habitats beneath an Antarctic Dry Valley. *Nat Commun.*, 6, 6831.

Miller, L. G. & Aiken, G. R. (1996). Effects of glacial meltwater inflows and moat freezing on mixing in an ice-covered Antarctic lake as interpreted from stable isotope and tritium distribution, *Limnol. Oceanography* 1, 966-976.

Mouginot, J., Rignot, E., Scheuchl, B. & Millan, R. (2017). Comprehensive annual ice sheet velocity mapping using Landsat-8, Sentinel-1, and RADARSAT-2 data. *Remote Sens.* 9(4), 364.

Mueller, D. R., Van Hove, P., Antoniades, D., Jeffries, M. O. & Vincent, W. F. (2009). High Arctic lakes as sentinel ecosystems: Cascading regime shifts in climate, ice cover, and mixing. *Limnol. Oceanography* 54(6part2), 2371–2385.

Obu, J., Westermann, S., Vieira, G., Abramov, A., Balks, M., Bartsch, A., Hrbáček, F., Kääb, A. & Ramos, M. (2019). Pan-Antarctic map of near-surface permafrost temperatures at 1 km^2 scale. *The Cryosphere.* 14(2), 497–519.

Obryk, M. K., Doran, P. T., Friedlaender, A. S., Gooseff, M. N., Li, W., Morgan-Kiss, R. M., et al. (2016). Responses of Antarctic marine and freshwater ecosystems to changing ice conditions. *Bioscience* 66(10), 864–879.

Obryk, M. K., Doran, P. T., Hicks, J. A., McKay, C. P. & Priscu, J. C. (2016). Modeling the thickness of perennial ice covers on stratified lakes of the Taylor Valley, Antarctica. *J. Glaciol.* 62(235), 825–834.

Obryk, M. K., Doran, P. T. & Priscu, J. C. (2019). Prediction of ice-free conditions for a perennially ice-covered Antarctic lake. *JGR Earth Surface* 124(2), 686-694.

Onstott, T. C., Ehlmann, B. L., Sapers, H., Coleman, M., Ivarsson, M., Marlow, J. J., Neubeck, A. & Niles, P. (2019). Paleo-Rock-Hosted Life on Earth and the Search on Mars: A Review and Strategy for Exploration. *Astrobiology* 19(10), 1230-1262.

Palmisano, A. C. & Simmons, G. M. Jr. (1987). Spectral down-welling irradiance in an Antarctic lake. *Polar Biol*. 7, 145-151.

Parker, B. C., Simmons, G. M. Jr., Seaburg, K. G., Cathey, D. D. & Allnutt, F. T. C. (1982). Comparative ecology of plankton communities in seven Antarctic oasis lakes. *J. Plankton Res.* 4, 271-286.

Pattyn, F. (2010). Antarctic subglacial conditions inferred from a hybrid ice sheet/ice stream model. Earth *Planet. Sci. Lett.* 295, 451–461.

Paquette, M., Fortier, D., Mueller, D. R., Sarrazin, D. & Vincent, W. F. (2015). Rapid disappearance of perennial ice on Canada's most northern lake. *Geophys. Res. Lett.* 42, 1433–1440.

Porco, C. C., Helfenstein, P., Thomas, P. C., Ingersoll, A. P., Wisdom, J., West, R., Neukum, G., Denk, T., Wagner, R., Roatsch, T., Kieffer, S., Turtle, E., McEwen, A., Johnson, T. V., Rathbun, J., Veverka, J., Wilson, D., Perry, J., Spitale, J., Brahic, A., Burns, J.A., DelGenio, A.D., Dones, L., Murray, C. D. & Squyres, S. (2006). Cassini observes the active south pole of Enceladus. *Science* 311(5766), 1393–1401.

Priscu, J. C., Fritsen, C. H., Adams, E. E.,Giovanni, S. J., Paerl, H. W., McKay, C. P., Doran, P. T., Gordon, D. A., Lan-oil, B. D. & Pinckney, J. L. (1998). Perennial Antarctic lake ice: an oasis for life in a polar desert. *Science* 280, 2095–2098.

Priscu, J. C. & Foreman, C. M. (2009). Lakes of Antarctica. In: Gene E. Likens, (Editor) *Encyclopedia of Inland Waters.* volume 2, pp. 555-566 Oxford: Elsevier.

Putnam, A. E., Denton, G. H., Schaefer, J. M., Barrell, D. J. A., Andersen, B. G., Finkel, R. C., Schwartz, R., Doughty, A. M., Kaplan, M. C. & Schluechter, C. (2010). Glacier advance in southern middle-latitudes during the Antarctic Cold Reversal, *Nat. Geosci.* 3(10), 700–704.

Ragotzkie, R. A. & Likens, G. E. (1964). The heat balance of two Antarctic lakes. *Limnol. Oceanogr.* 9, 412-425.

Rignot, E., Mouginot, J. & Scheuchl, B. (2017). MEaSUREs InSAR-Based Antarctica Ice Velocity Map, Version 2. [Indicate subset used]. Boulder, Colorado USA. NASA National Snow and Ice Data Center Distributed Active Archive Center. [Accessed on Feb. 15th 2019].

Rutishauser, A., Blankenship, D. D., Sharp, M., Skidmore, M. L., Greenbaum, J. S., Grima, C., Schroeder, D. M., Dowdeswell, J. A. & Young, D. A. (2018). Discovery of a hypersaline subglacial lake complex beneath Devon Ice Cap, Canadian Arctic. *Sci. Adv*. 4(4), eaar4353.

Santibáñez, P. A., Michaud, A. B., Vick-Majors, T. J., D'Andrilli, J., Chiuchiolo, A., Hand, K. P. & Priscu, J. C. (2019). Differential incorporation of bacteria, organic matter, and inorganic ions into lake ice during ice formation. *JGR: Biogeosciences* 124, 585– 600.

Sawagaki, T. & Hirakawa, K. (2002). Hydrostatic investigations on glacial meltwater: implications for the formation of streamlined bedforms and subglacial lakes, East Antarctica, *Polar Geosci.* 15, 123–147.

Schwab, M. J. (1998). Rekonstruktion der spatquartaren Klima und Umweltgeschichte der Schirmacher Oase und des Wohlthat Massivs (Ostantarktika). Ber. *Polarforschung* 293, 1–128.

Simmons, G. M. Jr., Vestal, J. R. & Wharton, R. A. Jr. (1993). Environmental regulators of microbial activity in continental antarctic lakes. In W. Green & E. I. Friedmann (eds), Physical and Biogechemical Processes in Antarctic Lakes. *Ant. Res. Series.* AGU. 59, 165-195.

Simonov, I. M., Stackebrandt, W., Haendel, D., Kaup, E., Kämpf, H. & Loopmann, A. (1985). Report on scientific investigations at the Untersee and Obersee Lakes, Central Dronning-Maud- Land (east Antarctica). Geodätische und Geophysikalische Veröffentlichungen I (12), 8–26.

Siegert, M. J., Ross, N. & Le Brocq, A. M. (2016). Recent advances in understanding Antarctic subglacial lakes and hydrology. Phil. Trans. R. Soc. A. 374, 20140306.

Siegert, M. J., Le Brock, A. & Payne, A. J. (2007). Hydrological connections between Antarctic subglacial lakes, the flow of water beneath the East Antarctic Ice Sheet and implications of sedimentary processes. In Hambrey, M.J., P. Christoffersen, N.F. Glasser and B. Hubbard, eds. Glacial sedimentary processes and products. *Oxford, Blackwell Publishing 39, 3-10.*

Souchez, R. A. & Jouzel, J. (1984). On the isotopic composition in delta D and delta18O of water and ice during freezing: *J. Glaciol.* 30, 369–372.

Souchez, R. A. (1988). Les glaces polaires. *Editions de l'Université de Bruxelles*, 156 pp.

Spigel, R. H., Sheppard, I. V. & Priscu, J.C. (1990). Temperature and conductivity finestructure from Lake Bonney. *Antarct. J*. 25, 228.

Spigel, R. H. & J. C. Priscu. (1996). Evolution of temperature and salt structure of Lake Bonney, a chemically stratified Antarctic lake. *Hydrobiology* 321, 177–190.

Steel, H. C. B., McKay, C. P. & Andersen, D. T. (2015). Modeling Circulation and Seasonal Fluctuations in Perennially Ice-covered and Ice-walled Lake Untersee, Antarctica. *Limnol. Oceanogr.* 60(4), 1139–1155.

Stenni, B., Jouzel, J., Masson-Delmotte, V., Rothlisberger, R., Castellano, E., Cattani, O., Falourd, S., Johnsen, S. J., Longinelli, A., Sachs, J. P., Selmo, E., Souchez, R., Steffensen, J. P. & Udisti, R. (2003). A late-glacial high-resolution site and source temperature record derived from the EPICA Dome C isotope records (East Antarctica). *Earth Planet. Sci. Lett.* 217, 183-195.

Swoboda, R. & Gallagher, J. (1991). 1:10 million scale Continent-wide surface schematic geological units and ages, compiled in 1985-1986 Australian Bureau of Mineral Resources. Schematic Geological Map of Antarctica. First Edition. 1:10 000 000. Hobart, Australia: Mercury-Walch.

Tanabe, Y., Hori, M., Mizuno, A. N., Osono, T., Uchida, M., Kudoh, S. & Yamamuro, M. (2019). Light quality determines primary production in nutrient-poor small lakes. *Sci. Rep.* 9, 4639.

Thor, G. & Low, M. (2011). The persistence of the snow petrel (Pagodroma nivea) in Dronning Maud Land (Antarctica) for over 37,000 years. *Polar Biol.* 34, 609-613.

Toner, J. D., Catling, D. C. & Sletten, R. S. (2017). The geochemistry of Don Juan Pond: evidence for a deep groundwater flow system in Wright Valley, Antarctica. *Earth Planet Sci Lett*. 474, 190–197.

Uemura, T., Taniguchi, M. & Shibuya, K. (2011). Submarine groundwater discharge in Lutzow-Holm Bay, Antarctica. *Geophys. Res. Lett.* 38, L08402.

Uemura, R., Motoyama, H., Masson-Delmotte, V., Jouzel, J., Kawamura, K., Goto-Azuma, K., et al. (2018). Asynchrony between Antarctic temperature and CO2 associated with obliquity over the past 720,000 years. *Nat. Commun.* 9(1), 961.

Van Hove, P., Belzile, C., Gibson, J. A. E. & Vincent, W. F. (2006). Coupled landscape-lake evolution in High Arctic Canada. *Can. J. Earth Sci.* 43, 533–546.

Vincent, W. F., Hobbie, J. E. & Laybourn-Parry, J. (2008). Introduction to the limnology of high-latitude lake and river ecosystems. In Vincent, W.F. and J. Laybourn-Parry, eds. Polar lakes and rivers: limnology of Arctic and Antarctic aquatic ecosystems. Oxford, UK., *Oxford University Press*, 1–23.

Wada, E., Ohki, K., Yoshikawa, S., Parker, P.L., Baalen, C. V., Matsumoto, G. I., et al. (2012). Ecological aspects of carbon and nitrogen isotope ratios of cyanobacteria. *Plankton Benthos Res*. 135–145.

Wand, U., Schwarz, G., Brüggemann, E. & Bräuer, K. (1997). Evidence for physical and chemical stratification in Lake Untersee (central Dronning Maud Land, East Antarctica). *Antarc. Sci*. 9, 43–45.

Wand, U., Samarkin, V. A., Nitzsche, H. -M. & Hubberten, H. -W. (2006). Biogeochemistry of methane in the permanently ice-covered Lake Untersee, central Dronning Maud Land, East *Antarctica. Limnol. Oceanogr*. 51, 1180–1194.

Wand, U. & Perlt, J. (1999). Glacial boulders 'floating' on the ice cover of Lake Untersee, East Antarctica. *Antarc. Sci.* 11, 256–260.

Weber, M. E., Clark, P. U., Kuhn, G., Timmermann, A., Sprenk, D., Gladstone, R., Zhang, X., Lohmann, G., Menviel, L., Chikamoto, M. O., Friedrich, T. & Ohlwein, C. (2014). Millennial-scale variability in Antarctic ice-sheet discharge during the last deglaciation, *Nature* 510, 134–138.

Weisleitner, K., Perras, A., Moissl-Eichinger, C., Andersen, D. T. & Sattler, B. (2019). Source Environments of the Microbiome in Perennially Ice-Covered Lake Untersee, Antarctica. *Front. Microbiol.* 10, 1019.

Wharton, R. A. Jr., Parker, B. C. & Simmons, G. M. Jr. (1983). Distribution, species composition, and morphology of algal mats in Antarctic dry valley lakes. *Phycologia* 22, 355-365.

Wharton, R. A., Jr., McKay, C. P., Simmons, G. M. Jr. & Parker, B. C. (1986). Oxygen budget of a perennially ice-covered Antarctic dry valley lake, *Limnol. Oceanogr.* 31, 437-443.

Wharton, R. A. Jr., McKay, C.P., Mancinelli, R.L. & Simmons, G.M. Jr. (1987). Perennial N^2 supersaturation in an Antarctic lake. *Nature* 325, 343-345.

Wharton, R. A., Jr, Simmons, G. M., Jr & McKay, C. P. (1989). Perennially ice-covered Lake Hoare, Antarctica: physical environment, biology and sedimentation. *Hydrobiol*. 172, 305-320.

Wharton, R. A. Jr., McKay, C. P., Clow, G. D., Andersen, D. T., Simmons, G. M. Jr. & Love, F. G. (1992). Changes in ice cover thickness and lake level of Lake Hoare, Antarctica: Implications for local climate change. *J. Geophys. Res*. 97, 3503-3513.

Wharton, R. A., McKay, C. P., Clow, G. D. & Andersen, D. T. (1993a). Perennial ice covers and their influence on Antarctic lake ecosystems. *Antarct. Res. Ser*. ANTSA, 4, 53–70.

Wharton, R. A. Jr., Lyons, W. B. & Des Marais, D. J. (1993b). Stable isotopic biogeochemistry of carbon and nitrogen in a perennially ice-covered Antarctic lake. *Chem. Geol.* 102, 159-172.

Williamson, C. E., Saros, J. E., Vincent, W. F. & Smol, J. P. (2009). Lakes and reservoirs as sentinels, integrators, and regulators of climate change. *Limnol. Oceanogr*. 54, 2273–2282.

Wilson, A. T. & Wellman, H. W. (1962). Lake Vanda: An Antarctic Lake: Lake Vanda as a Solar Energy Trap. *Nature* 196, 1171–1173.

Wilson, A. T. (1964). Evidence from chemical diffusion of a climatic change in the McMurdo Dry Valleys 1200 years ago. *Nature* 201, 176-177.

Wingham, D. J., Siegert, M. J., Shepherd, A. & Muir, A. S. (2006). Rapid discharge connects Antarctic subglacial lakes. *Nature* 440(7087), 1033–1036.

Wright, A. & Siegert, M. A. (2012). Fourth inventory of Antarctic subglacial lakes. *Antarc. Sci.* 24, 659–664.

CHAPTER 2: ENERGY AND WATER MASS BALANCE OF LAKE UNTERSEE AND ITS PERENNIAL ICE COVER, EAST ANTARCTICA

Abstract

Lake Untersee is one of the largest perennially ice-covered lakes in Dronning Maud Land. We investigated the energy and water mass balance of Lake Untersee to predict its fate under changing climate conditions. The thickness of the ice cover shows a strong relation with sublimation rates. Variations in sublimation rates across the ice cover are primarily determined by turbulent heat fluxes and the number of snow-covered days. Lake extent and water level have remained stable for the past 20 years, indicating that the water mass balance is in equilibrium. The Anuchin Glacier damns the lake, and mass balance calculations suggest that englacial meltwater contributes 44-50% of the annual water budget; since there is no evidence of streams flowing into the lake, the lake must be connected to a groundwater system to maintain the lake budget in balance. The groundwater likely flows at a rate of ~ 6.8×10^{-2} m^3 s^{-1}, a reasonable estimate given the reported range of subglacial water flux in the region. The fate of well-sealed ice cover is likely tied to changes in wind regime, whereas changes in water budget are more closely linked to the response of surrounding glaciers to climate change.

2.1 Introduction

Perennially ice-covered lakes are prominent features in ice-free coastal Antarctica (Laybourne-Parry & Wadham, 2014). Early investigations into the thermodynamics of ice-covered lakes in the McMurdo Dry Valleys (MDV) revealed that the thickness of the ice cover is primarily controlled by the balance between the conduction of energy out of the ice and the release of latent heat during freezing at the ice-water interface (Wilson et al., 1962; McKay et al., 1985). To maintain the energy balance in a steady-state condition, the water freezing rate at the bottom of the ice cover must equal the ice surface's ablation rate (sum of melting, evaporation, and sublimation). It has been observed in the MDV lakes that ice cover and lake level respond rapidly to local climate variations (Doran et al., 2002; Lyons et al., 2006). In the MDVs, lake levels have risen several meters over the past two decades due to increased glacial meltwater inflow from ephemeral streams (e.g., Hawes et al., 2011; Castendyk et al., 2016), and lake ice thickness on the various lakes has waxed and waned (Clow et al., 1988; Wharton et al., 1992; Doran et al., 2002; Dugan et al., 2013). The amount of meltwater received in the lakes was found to be proportional to the degree-days above freezing, and with the predicted increase in summer warming, lake levels are expected to continue to increase, thereby affecting ecological systems (Wharton et al., 1992; Doran et al., 2008; Dugan et al., 2013; Fountain et al., 2016; Gooseff et al., 2017; Obryk et al., 2016).

In central Queen Maud Land, the Untersee Oasis contains two large perennially ice-covered lakes – Untersee and Obersee (Bormann & Fritzsche, 1995; Schwab, 1998). Lake Untersee has characteristics that differentiate it from the lakes in the MDV and elsewhere around the continent. Untersee is a closed-basin lake damned at the north end by the Anuchin Glacier and resides in a region with a climate dominated by intense evaporation and sublimation. Interestingly, Untersee does not develop a moat during the summer when air temperatures rise above freezing, and there is little evidence of surface streams flowing into the lake (Andersen et al., 2015). It has been suggested that Lake Untersee is recharged from the Anuchin Glacier's melting (Hermichen et al., 1985; Richter & Bormann, 1995; Wand et al., 1997). Thus far, studies of Untersee have focused primarily on physical and chemical limnology (Hermichen et al., 1985; Wand et al., 1997, 2006; Steel et al., 2015; Bevington et al., 2018) and microbial ecology (Wand et al., 2006; Andersen et al., 2011; Koo et al., 2017; Weisleitner et al., 2019). Detailed studies have yet to investigate the thermodynamics of the ice cover and the lake's hydrological balance. Therefore, this study examines the energy and water mass balance of Lake Untersee and its ice cover to predict

its fate under changing climate conditions. This objective was achieved by determining: 1) the ice thickness and density across the lake; 2) ablation and freezing rates of the ice; and 3) contemporary changes in lake level and relative contribution of inflows and outflows of water to the lake water balance. Based on the results, we assess the energy balance of Lake Untersee and its ice cover and discuss its fate under changing climate and how it may affect its unique microbial ecology.

2.2 Study area

The Untersee Oasis is located in the Gruber Mountains of central Dronning Maud Land, approximately 90 km southeast of the Schirmacher Oasis (Fig. 2-1). Elevations in the oasis range from 600 to 2790 m and local geology consists of norite, anorthosite, and anorthosite-norite alternation of the Eliseev anorthosite massif (Bormann et al., 1986). The oasis was glaciated during the Late Pleistocene and continues to receive ice flowing from a local ice field (elevation of ~ 800m) connected to the East Antarctic ice sheet (Schwab, 1998; Hiller et al., 1988). NASA's *MEaSUREs Annual Antarctic Ice Velocity Maps* (2011-2017) indicate that the Anuchin Glacier flows at an average velocity of ~ 8-9 m yr^{-1} with nearby ice streams to the east and west of Untersee Oasis flowing at an average velocity of ~ 70-100 m yr^{-1} (Mouginot et al., 2017; Fig. 2-1). In addition to lakes Untersee and Obersee, numerous small ice-covered ponds reside on the western and eastern lateral moraines of the Anuchin Glacier. Schwab (1998) suggested that Lake Untersee likely formed between 12 and 10 kyr BP when the Anuchin Glacier retreated to near its present location.

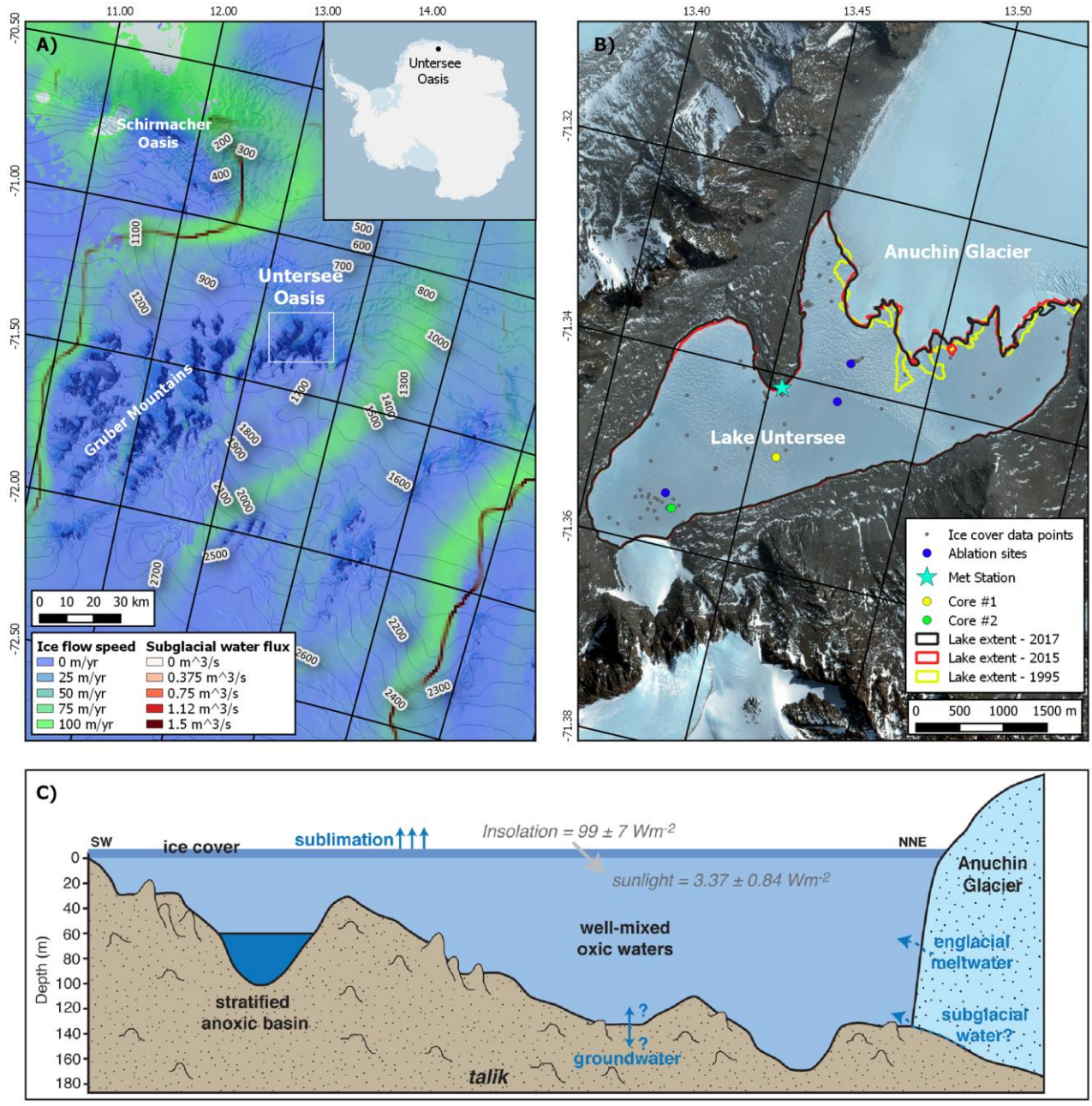

Figure 2-1: Maps and cross-section showing: A) the location of the Untersee Oasis, adjacent regional ice stream velocities (from Rignot et al., 2017), and regional subglacial water fluxes (from Le Brocq et al., 2013); B) location of sampling points on Lake Untersee's ice cover; and C) Lake Untersee's bathymetry, ice cover solar radiation transmissivity and proposed sources of inputs and outputs to the lake.

Lake Untersee is located in a closed-basin at ~ 610 m a.s.l. and is dammed at its northern end by the Anuchin Glacier, where a pressure ridge forms at the lake-glacier interface (Fig. 2-1). The lake is 2.5 km wide and 6.5 km long, making it the largest freshwater lake in central Queen Maud Land (Hermichen et al., 1985). Except for a boulder field at the south end of the lake and other large boulders scattered across the lake, the ice cover's surface on Lake Untersee is smooth and free of any fine sediments. The lake has two sub-basins: 1) a large basin occupies the northern and central sections to a maximum observed depth of 169 m; and 2) a shallower basin occupies its southern section to a depth of 100 m. The two basins are separated by a sill that cuts across the lake at 50 m depth (Wand et al., 1997). The water in the larger and deeper basin, as well as that above the sill in the shallower basin is well-mixed, has a temperature near 0.5°C, pH near 10.6, dissolved oxygen near 150%, and a specific conductivity near 505 µS/cm^{-1} (Wand et al., 1997; 2006; Andersen et al., 2011). The ice-wall presence at the lake-glacier interface results in buoyancy-driven convection allowing effective mixing throughout most of the lake with time scales of one month (Steel et al., 2015). However, in the southern basin, the water below the sill (60-100 m) is stratified with temperature ranging between 0°C at the ice-water interface to a maximum of 5°C, with lower pH (~ 7), higher specific conductivity (1100-1300 µS/cm^{-1}) and dissolved oxygen levels near 0%. This anoxic water does not mix with the overlying oxic water due to its higher density (Bevington et al., 2018). Photosynthetic microbial mats cover the floor of the oxic basin in Lake Untersee, with the transparency of the lake ice to photosynthetically active radiation (PAR) being 4.9±0.9% (Andersen et al., 2011).

The climate in the Untersee Oasis is part of a polar desert regime. Ten years of climate data (2008-2017) collected by an automated weather station along the shore of Lake Untersee (71.34°S, 13.45°E, 612 m a.s.l.) shows a mean summer insolation of 99±7 Wm^{-2}, mean annual air temperature (MAAT) of –9.5±0.7°C, thawing degree-days ranging from 7 to 51 degree-days, and a mean relative humidity of 42±5% (Andersen et al., 2015). The mean annual air temperature showed little to no change over the past decade. The average wind speed was 5.4 m s^{-1}, with strong south wind speed descending the polar plateau and sweeping across the southern section of the lake and also strong east wind descending from the Aurkjosen Cirque and flowing across the snout of the Anuchin Glacier. Despite having a relatively warm MAAT for Antarctica, the climate in the oasis is dominated by intense evaporation and sublimation, which limits surface melt features due to cooling associated with the latent heat of sublimation (e.g., Hoffman et al., 2008).

2.3 Methods

2.3.1 Ice thickness and density of ice cover

During each expedition to Lake Untersee since 2008, holes were drilled through the ice cover using a 10-inch Jiffy drill. The ice thickness and freeboard (the difference between the height of the ice and water surface in the borehole) were determined using a 4 m pole graduated at 1 cm. From these two parameters, the ice cover density (in kg m^{-3}) was calculated from **EQ. 2-1**:

[**EQ. 2-1**] $\rho_{ice} = \left(1 - \frac{Fb_i}{H_i}\right) \times 1000$

where:

Fbi = freeboard (in cm);

Hi = thickness of ice cover (in cm).

Given the lake's dimension, the location of most drill holes was randomly selected, with one repeat location to verify if ice thickness changes over time. The location of each drill hole (n = 84) was recorded with a handheld *Garmin GPSMAP 64s* GPS with an accuracy of ±3 m, and the ice thickness and density data were added as points to ArcMap. The values were interpolated with ordinary spherical kriging where parameters (number of lags: 12 points; sector type: 8 sectors; maximum and minimum neighbors: 5 and 2) were set to obtain the lowest root-mean-square error possible. The interpolated results were displayed on a common scale and overlaid on a *World View* satellite image (acquisition date: Dec. 7th, 2017).

2.3.2 Ice cover ablation rates

Wand et al. (1996) reported the first ablation measurements at Lake Untersee based on measurement of three wooden ablation stakes in the ice cover; each was 4.5 cm in diameter and 4 meters long and covered with white reflective tape. They reported upward movement of the ice over 12 days in February 1995 by 1 cm at the north end of the lake, 3 cm at the south end of the lake, and 2.5 cm midway. No detailed descriptions of the ablation stakes observed the following year were published.

On Dec. 7th, 2008, we inserted ablation ropes (~ 10 m lengths of braided 5 mm diameter white polyester) into seven holes drilled through the ice on a north-south transect, similar to that used by Wand et al. (1996), as well as five holes in the NE and NW corners of the lake (Fig. 2-1).

Holes were backfilled with snow and ice to ensure the lines froze into the 15 cm diameter drill holes. Three years later, we recovered some, but not all, of the ablation lines; extensive snow cover on the lake that year made finding and recovery of the ropes difficult.

2.3.3 Ice cover freezing rates

An approach to quantify the amount of ice freezing at the ice-water interface has yet been developed for ice-covered lakes, but it can likely be derived from measurements of parameters in the ice cover that are affected by freezing. The morphology of gas bubbles occluded in the ice cover should vary as freezing progresses and excess dissolved air develops in the water (Lipp et al., 1987; Killawee et al., 1998). The stable isotopes of water (δD-$\delta^{18}O$) will also evolve during closed-system freezing, such as in Lake Untersee (i.e., Lacelle, 2011). Given that freezing at the ice-water interface largely occurs in winters (i.e., Clow et al., 1988; Dugan et al., 2013), the bubble morphology and δD-$\delta^{18}O$ values in the ice cover should reflect seasonal freezing of the water and preserve the conditions under which freezing occurred.

The ice cover of Lake Untersee was sampled at its central and southern sectors in December 2017 to verify if the bubble morphology and δD-$\delta^{18}O$ values in the ice cover can preserve information related to freezing rates (Fig. 2-1). The ice was sampled using a CRREL coring kit to a depth of ~ 2 m to prevent mixing with lake water. The ice cores were first photographed in the field under a light table using a Nikon D850 camera (focal length of 35 mm and exposure time of 1/20 second). The ice cores were then sliced at 2-cm, allowed to melt in sealed Ziploc bags, transferred in HDPE bottles, and shipped in coolers to the University of Ottawa and where they were stored at 4°C until analyses.

The distribution and morphology of air bubbles in the ice cover were extracted from the ice cores' photographs using the *ImageJ* software. The photos were first converted to 8-bit grayscale format and classified following thresholding as: 1) area occupied by bubbles; and 2) bubble-free area. The size, distribution, and sphericity of the bubbles were extracted at 1-cm slices using the *analyze particles* tool (e.g., Kinnard et al., 2008).

The $^{18}O/^{16}O$ and D/H ratios were determined using a Los Gatos Research liquid water analyzer coupled to a CTC LC-PAL autosampler for simultaneous $^{18}O/^{16}O$ and D/H ratios measurements of H_2O and verified for spectral interference contamination. The results are presented using the δ-notation ($\delta^{18}O$ and δD), where δ represents the parts per thousand differences

for $^{18}O/^{16}O$ or D/H in a sample with respect to Vienna Standard Mean Ocean Water (VSMOW). Analytical reproducibility for $\delta^{18}O$ and δD was ±0.3‰ and ±1‰, respectively. Deuterium excess (*d*) was then calculated using **EQ. 2-2** (Dansgaard, 1964):

[**EQ. 2-*2***] $d = \delta D - 8 * \delta^{18}O$

The periodicity of bubble content (%) and the distribution of δ18O values were extracted via spectral analysis (Fourier transformation) using the R software's Spectrum tool (Stats built-in package). Significant amplitude spectrum peaks indicate the periodicity of freezing events. The frequencies were converted to annual ice accretion using **EQ. 2-3** (Blackman & Tuckey, 1958):

[EQ. 2-3]: *Annual ice accretion* = $\frac{1}{x} \times SI$

where:

x = peak frequency

SI = sampling interval (here, 2 cm)

2.3.4 Water mass balance of Lake Untersee

Lake Untersee is a closed-basin lake dammed at its northern end by the Anuchin Glacier. As such, the water mass balance of the lake can be determined from **EQ. 2-4**:

[**EQ. 2-4**] $\Delta S = P + I_S + I_e + I_g - O_S - O_g$

where:

ΔS = change in the volume of water;

P is total annual precipitation;

Is, Ie and Ig are the inflows of surface water, englacial meltwater, and groundwater (basal meltwater or other sources);

Os and Og are the outflows of surface and groundwater.

The water volume in Lake Untersee was determined from the bathymetry map of Wand et al. (2006), which was digitized and georeferenced in the *ArcMap* software. Since water levels have not been historically monitored at the lake, the relations between water volume versus surface elevation and surface area versus surface elevation were determined with the digitized bathymetry map. Changes in lake surface area between 1995 and 2017 were then determined using the Geomaud 1995 air photographs, which were digitized and georeferenced in *ArcMap*, and with the use of 2015 and 2017 *World View* satellite images (acquisition dates: December 7^{th,} 2015; December 7th, 2017; image resolution 50 cm). The lake extent in 1995, 2015, and 2017 was traced in ArcMap (WGS 1984; UTM Zone 33S), and the surface area was computed from the derived polygons.

The sealed nature of Lake Untersee is such that direct precipitation (P) is likely not contributing to its water mass balance. The amount of englacial meltwater contribution from the Anuchin Glacier (Ie) was determined from its average annual velocity, the cross-sectional area at the ice-water interface, and from changes in the position of the glacial ice tongues at the contact with the lake. The Anuchin Glacier velocity was obtained by tracking the displacement of a target on its surface over ten years (2008-2017). The target's position was recorded with a handheld *Garmin GPSMAP 64s* GPS with an accuracy of ±3 m. The target velocity data was compared to the 2011-2017 NASA MEaSUREs Antarctic ice velocity (Mouginot et al., 2017). The outflow of surface water (Os) was determined from our calculation of ice cover loss by ablation.

2.4 Results

2.4.1 Thickness and density of the ice cover

Ice thickness measurements taken at the same location between 2011 and 2017 provided near identical results (3.78±0.07 m; n = 4), indicating that measurements obtained over ten years should have little effect on estimating ice thickness. The measurements of the ice cover thickness range from 1.96 to 3.96 m, with a bi-modal distribution (median = 2.52 m; average = 2.76±0.59 m; n = 89). Based on geostatistical kriging interpolation, the average lake ice thickness is 2.77±0.25 m. Ice thickness shows a general north-south trend, with thicker ice cover in the northwest and thinner ice in the southern and northeast sectors (Fig. 2-2). The ice cover density ranges from 764 to 916 kg m^{-3}, with an average of 902±47 kg m^{-3}. Geostatistical interpolation

indicates an average ice density of 891±5 kg m^{-3}. Under-dense ice (< 850 kg m^{-3}) is found in the central section of the lake, due east of the moraine.

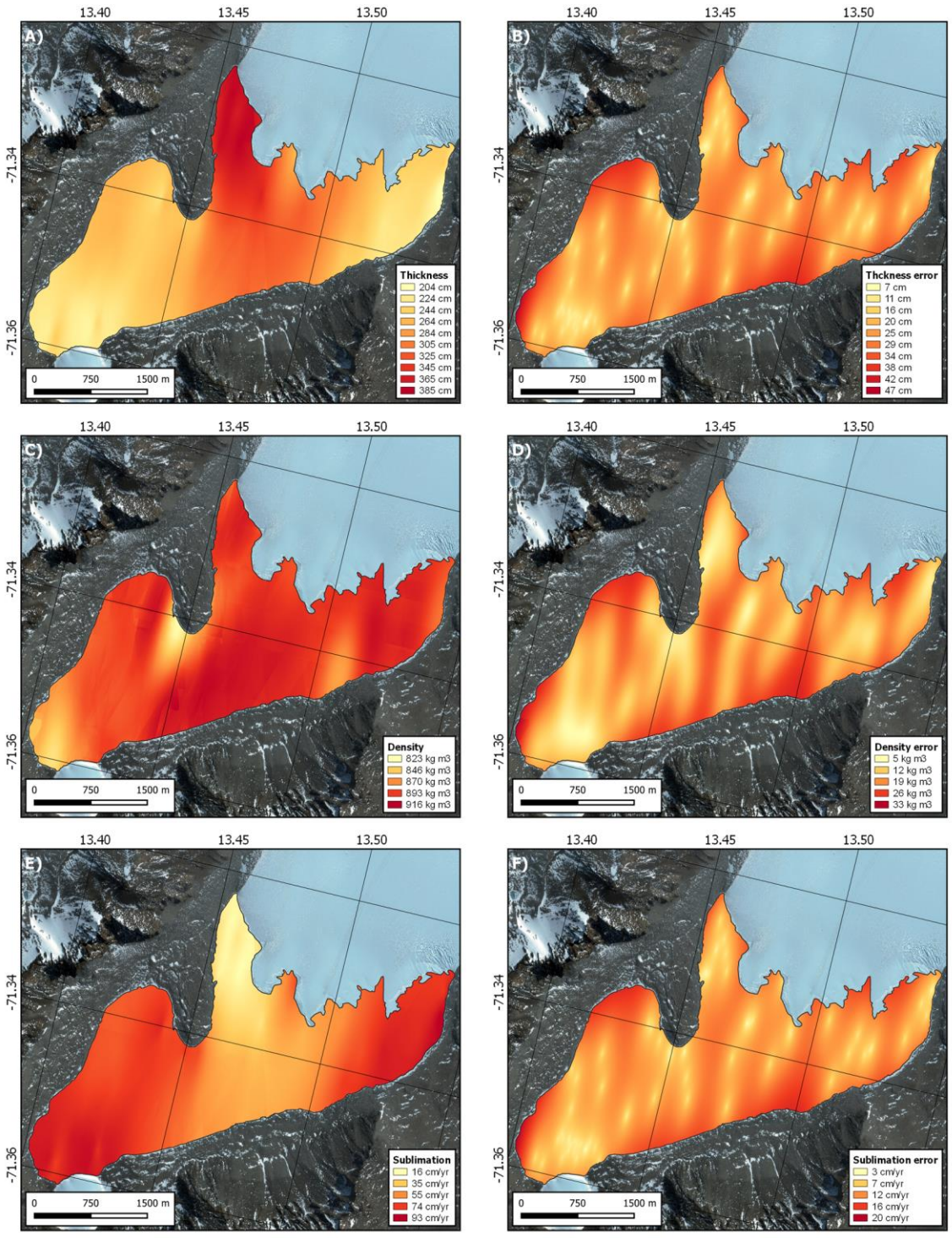

Figure 2-2: World view image (Dec. 7th, 2017) of Lake Untersee showing: A) interpolated ice cover thickness; B) interpolated ice cover thickness errors; C) interpolated ice cover density; D) interpolated ice cover density errors; E) interpolated annual ice cover sublimation rate; and F) interpolated annual ice cover sublimation rate errors.

2.4.2 Ablation rates from ablation ropes

On November 17th, 2011, two ablation ropes at the southern end of the lake indicated a net upward ice movement of 230 and 213 cm over three years. On December 18th, 2011, an additional 7 cm of ablation was measured. These results indicate an annual average ablation rate of 78 and 72 cm yr^{-1} at the two sites. Three ablation ropes due east of the meteorological station (central area of the lake) indicated a net upward ice movement of 116, 117, and 122 cm, corresponding to annual average ablation rates of 39, 41, 39 cm yr^{-1}. We infer that the yearly ablation rate is ~ 40 cm yr^{-1} in the central portion of the lake, and it increases to ~ 75 cm yr^{-1} in the southern end of the lake, where some of the thinnest ice is also observed.

2.4.3 Freezing rates from bubble morphology and δD-$\delta^{18}O$ composition of ice cover

The ice cover of Lake Untersee contains a range of bubble sizes and shapes (Fig. 2-3). In both ice cores, the form of the bubbles was either spherical, oval, dendritic, or tubular. The ice cover in the central sector had a bubble content ranging from 2 to 50%, with higher bubble content and variability in the uppermost 75 cm (peak of 50% at 54 cm depth) (Fig. 2-4). Bubble content was more constant below 100 cm, where it varied between 2 and 18%. The $\delta^{18}O$ values in the ice cover ranged from –35.5 to –34.2‰, whereas D-excess values ranged from –1.31 to 6.9‰. The $\delta^{18}O$ and D-excess values showed progressive decreasing and increasing trends with depth, respectively.

The ice cover in the southern sector had bubble content ranging from 0.3 to 46%, with higher bubble content in the uppermost 150 cm. No particular trend was observed for the bubble content, but three impressive peaks were identified at depths of 18, 85, and 135 cm. The $\delta^{18}O$ values in the ice fluctuated from –36.2 to –35.6‰, with D-excess varying from –8.8 to 11.4‰. Variations in $\delta^{18}O$ and D-excess values were negatively correlated in the uppermost 50 cm; this was reflected to a lesser degree in the lower portion of the core where $\delta^{18}O$ and D-excess values were much more stable.

The spectral power for bubble distribution and $\delta^{18}O$ showed peaks at ~ 67 cm and ~ 80 cm for the cores retrieved from the lake's central and southern sectors, respectively (Fig. 2-5). The cross-correlation between these two parameters also showed coherence and low phase differences. This suggests that the freezing rate is 67 cm yr^{-1} at the central section and 80 cm yr^{-1} at the lake's southern section.

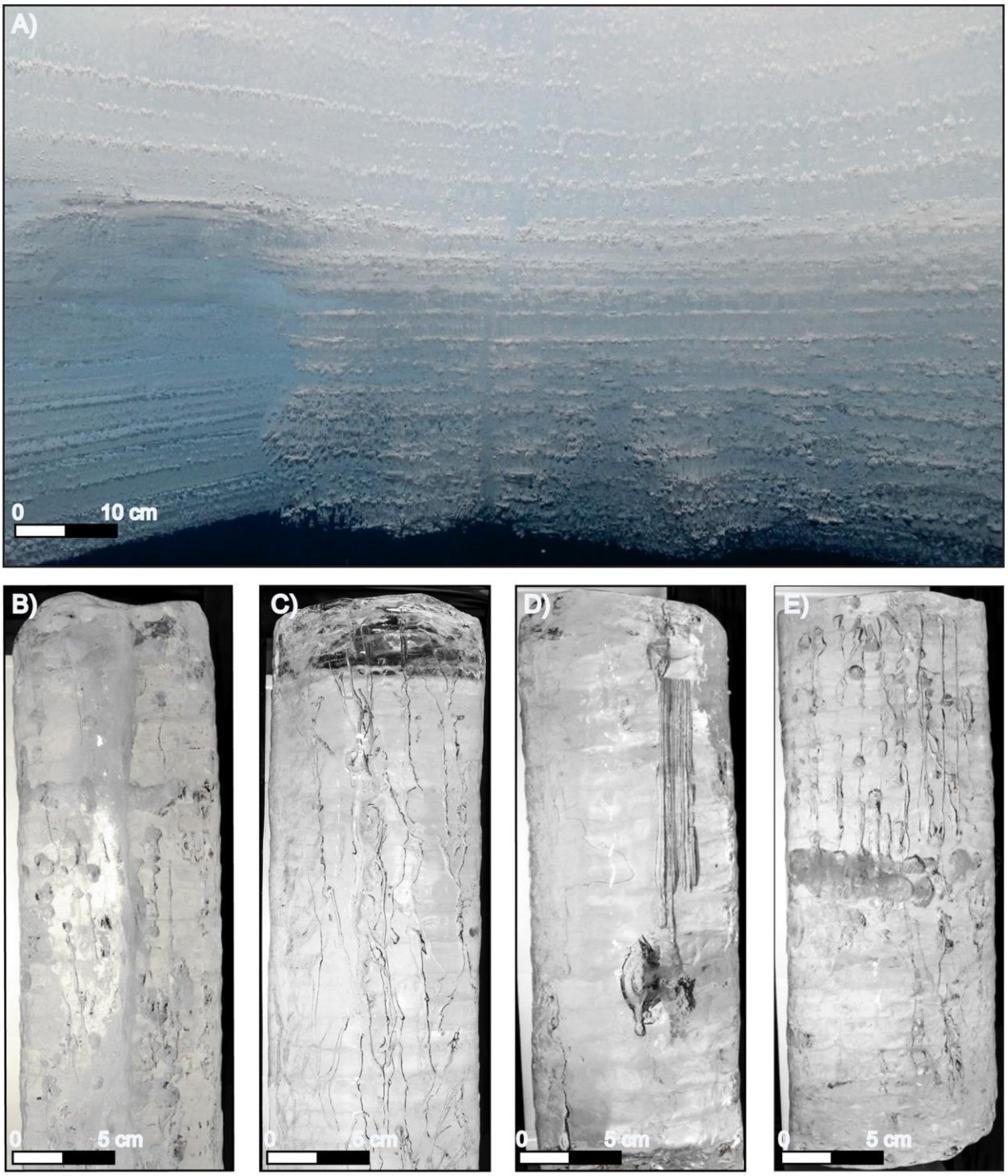

Figure 2-3: Ice cover bubble abundance and morphology. A) underwater view of bubbles in the lower portion of the ice cover; B-E) examples of different morphology of bubbles observed in ice cover: B) spherical bubbles in core #1; C) dendritic bubbles in core #1; D) tubular and oval bubbles in core #2; and E) tubular and spherical bubbles in core #2.

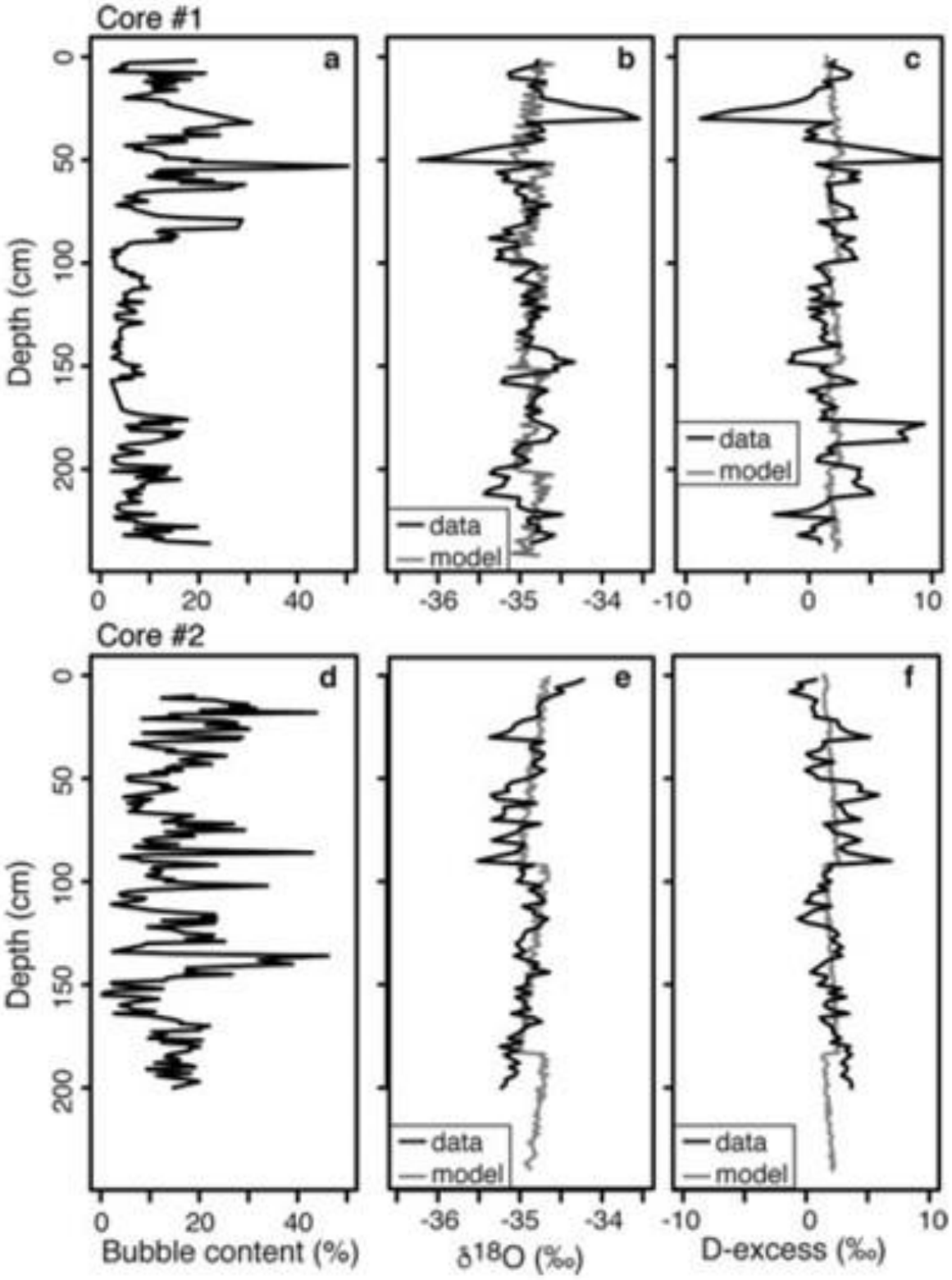

Figure 2-4: Depth profiles of bubble content (%), $\delta^{18}O$ and D-excess measurements in a.–c. core #1, and d.–f. core #2. Modelled annual ice-cover coevolution of $\delta^{18}O$ ratios and D-excess is shown in grey.

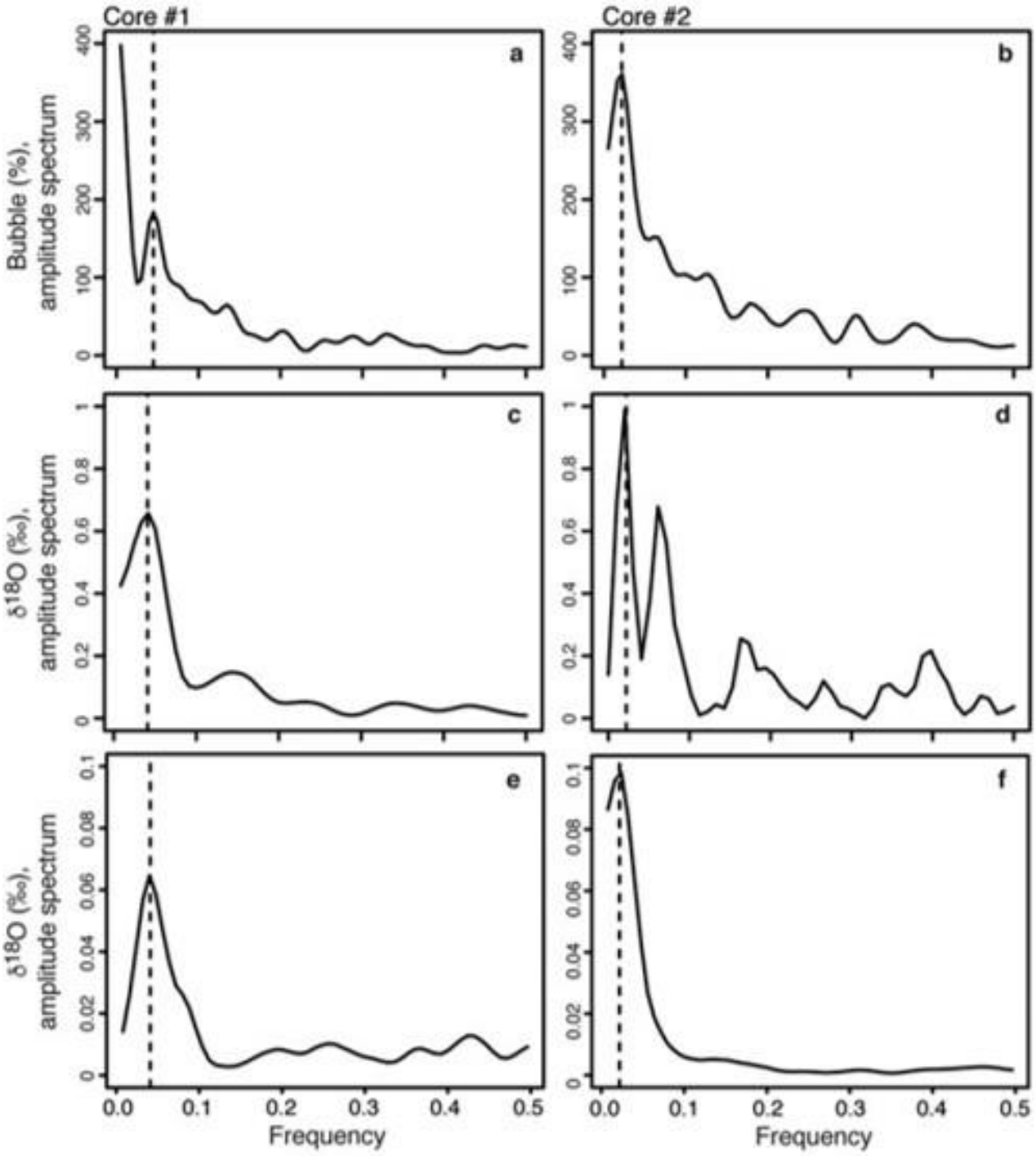

Figure 2-5: Amplitude spectra in radians for $\delta^{18}O$ and bubble content (%) in (a. & c.) core #1, and (b. & d.) core #2. Frequencies can be converted to annual ice accretion ($1/X \times 2$), where X is the peak frequency. The dotted lines indicate the peak of the spectral signal frequencies for core #1 (c. 0.041 = 49 cm) and for core #2 (c. 0.022 = 91 cm). Amplitude spectra for modelled seasonal ice-cover freezing rates (using a simple Rayleigh-type fractionation of the residual water) of 49 cm (core #1) and 91 cm (core #2) are shown in e. and f., respectively.

2.4.4 Water mass balance of Lake Untersee

Analysis of the bathymetry of Lake Untersee with the *Surface Volume* tool in *3D analyst* (*ArcGIS 10* software) demonstrates that lake surface area and lake water-level are positively correlated; it is only when lake-level is below 520 m that a further lowering of lake-level results in small changes in surface area (Fig. 2-6). Based on the digitized bathymetry, Lake Untersee has a water volume of 5.21 x 10^8 m^3. In 2017 and 2015, Lake Untersee had surface areas of 8.73 km^2 and 8.72 km^2, values slightly higher than what was measured in 1995 (8.45 km^2). The surface area difference is caused by two of the Anuchin Glacier's ice tongues that retreated by 420 and 480 m, between 1995 and 2017 (Fig. 2-1B). Visual comparison of oblique air photographs from 1939 also shows slight variations in the extent of Lake Untersee, which implies that its extent has been relatively stable for the past 80 years. The ice cover where the ice tongues had receded is composed of both lake ice and patches of white glacier ice that have been smoothly ablated to the same elevation of the lake ice (Fig. 2-1B). Unlike the lake ice that is sediment-free, the patches of glacier ice contain cryoconite holes.

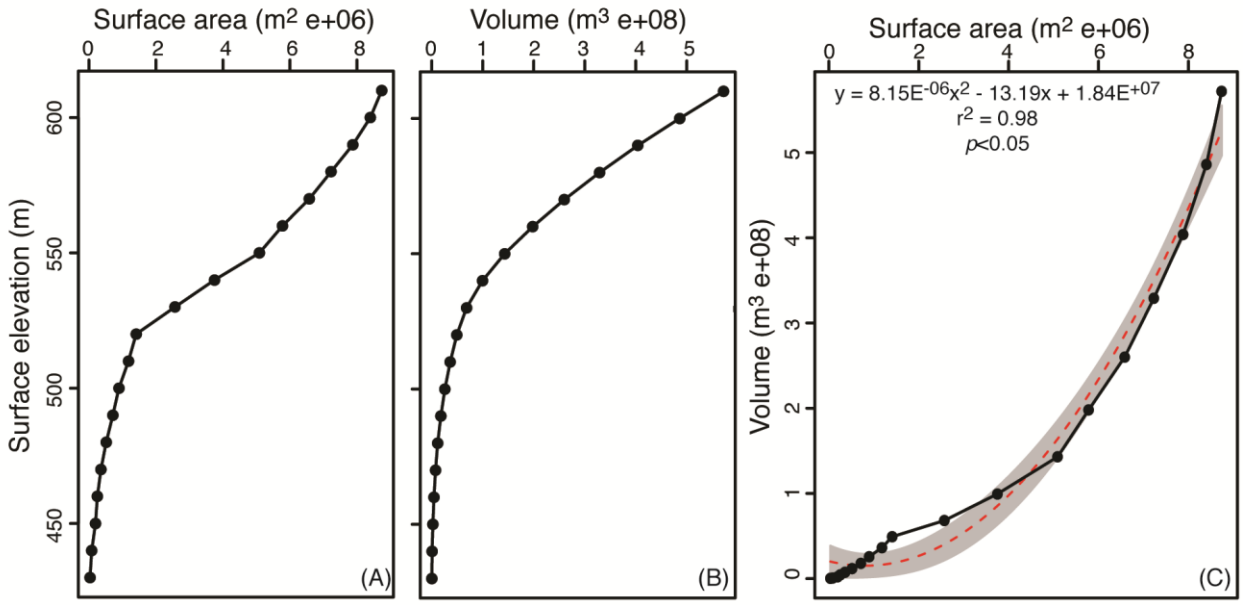

Figure 2-6: Relation between lake surface elevation and surface area (A), and water volume (B). C) Relation between surface area and water volume. The dashed line is the best fit polynomial line. Analysis derived from bathymetry from Wand et al. (2006).

The amount of direct precipitation (P) and inflow of surface water (Is) contributing to the water mass balance of Lake Untersee can be ignored because: 1) the lake does not develop a moat in summer; 2) no ephemeral streams feeding into the lake were historically observed; and 3) any snow that falls on the ice cover quickly sublimates. The amount of englacial meltwater contribution from the Anuchin Glacier (Ie) was estimated from the velocity of the glacier, its cross-sectional area along the ice-water interface, and changes in the location of the glacial ice tongues. A target placed on the surface of the Anuchin Glacier has moved by 76 m at an azimuth of 183° between 2008 and 2017, which corresponds to a mean annual ice velocity of 8.4 m yr^{-1}: this is in the range of that reported by MEaSUREs annual Antarctic ice velocity (~ 8-9 m yr^{-1} on average between 2011 and 2017; Fig. 2-1). Based on the bathymetry along the lake-glacier interface and the glacier's width along the lake, the ice wall's cross-sectional area is estimated to be 0.27 km^2. Considering that the glacier advances at a rate of 8-9 m yr^{-1}, this means that the Anuchin Glacier contributes annually 2.16 to 2.43 x 10^6 m^3 of englacial meltwater to the lake. The amount of surface water (Os) loss was determined from our calculation of the amount of ice loss by ablation, which ranges between ~ 40 cm yr^{-1} in the central portion of the lake and increases to ~ 80 cm yr^{-1} in the southern end of the lake. The range rate of annual ablation translates into annual surface water loss in the order of 3.22 to 6.43 x 10^6 m^3.

2.5 Discussion

2.5.1 Spatial variations in ice cover thickness and ablation/freezing rates

The thickness of the ice cover of the 6.5 km long Lake Untersee shows a general north-south trend, with thicker ice cover in the north-west sector (~ 3.5 to 3.96 m) and thinner ice in the southern and north-east sectors (~ 1.96 to 2.5 m). The ice cover is thinner than most of the ice-covered lakes in the MDV, where they range from 3 to 6 m, despite considerable variations in depth, temperature, and salinity between the lakes (Parker et al., 1982; Doran et al., 2002).

It is inferred that the ice cover of Lake Untersee is in steady-steady because its thickness at the same location did not change between 2011 and 2017 (3.78±0.07 m; n = 4). This means that the ice cover's freezing and ablation rates must be near equal (i.e., McKay et al., 1985). Our measurements from *in situ* ablation ropes provided ablation rates of ~ 40 cm yr^{-1} and ~ 75 cm yr^{-1} in the northern and southern sectors. The freezing rates derived from the frequency distribution of the bubbles and $\delta^{18}O$ vertical profiles in the ice cover yielded values of 67 cm yr^{-1} in the central

sector and 80 cm yr^{-1} at the southern sector of the lake, similar to the nearby ablation rates. It thus appears that the frequency distribution of bubble content in the ice cover preserves information about thickness of annual freezing at the bottom of the ice cover. Lipp et al. (1987) observed, although at a smaller scale, dendritic breakdown of the planar ice-water interface due to gas enrichment and bubbles nucleated in interdendritic spaces under closed-system freezing experiment of highly saturated gas solutions. The nucleation and growth of gas bubbles was seen to be a periodic process under certain circumstances, which was explained by the continuous buildup and reduction of the concentration of gases in the remaining solution. The δD-$\delta^{18}O$ measurements also allow for the determination of freezing events, and because in closed-system equilibrium freezing, a progressive depletion in $\delta^{18}O$ and δD values in the residual water (and forming ice) occurs following Rayleigh-type fractionation (Clark, 2015). In ice-covered lakes, where repeated annual freezing occurs at the bottom of the ice cover, an isotopic discontinuity should separate the individual freezing episodes in the ice cover, and this is should be reflected in the frequency distribution of $\delta^{18}O$ profile.

A significant negative relationship exists between the ice thickness and ablation/freezing rates (Fig. 2-7). The relationship was used to derive the ablation rate across the entire lake using geostatistical interpolation, which averaged 61±11 cm yr^{-1} (median = 71 cm yr^{-1}). Like the systematic increase in ice thickness from the north to the south in the lake, the ablation rates increase along this same direction. This suggests that ablation has a substantial control on ice thickness; considering little change over the past decade in insolation, MAAT, thawing degree-days and relative humidity, the spatial variations in ablation rate across the ice cover is likely due to the persistent strong south winds descending the Sjobotnen Cirque and sweeping across the southern section of the lake (summer 2011 average of 4.9 m s^{-1}) and also the strong east wind descending from the Aurkjosen Cirque (summer 2011 average of 6.2 m s^{-1}) and flowing across the snout of the Anuchin Glacier. The lake's central area where the thicker ice is found is sheltered from the strong winds (summer 2011 average of 4.2 m s^{-1}), as evidence of the snow-shadow on the lake ice (Fig. 2-1b).

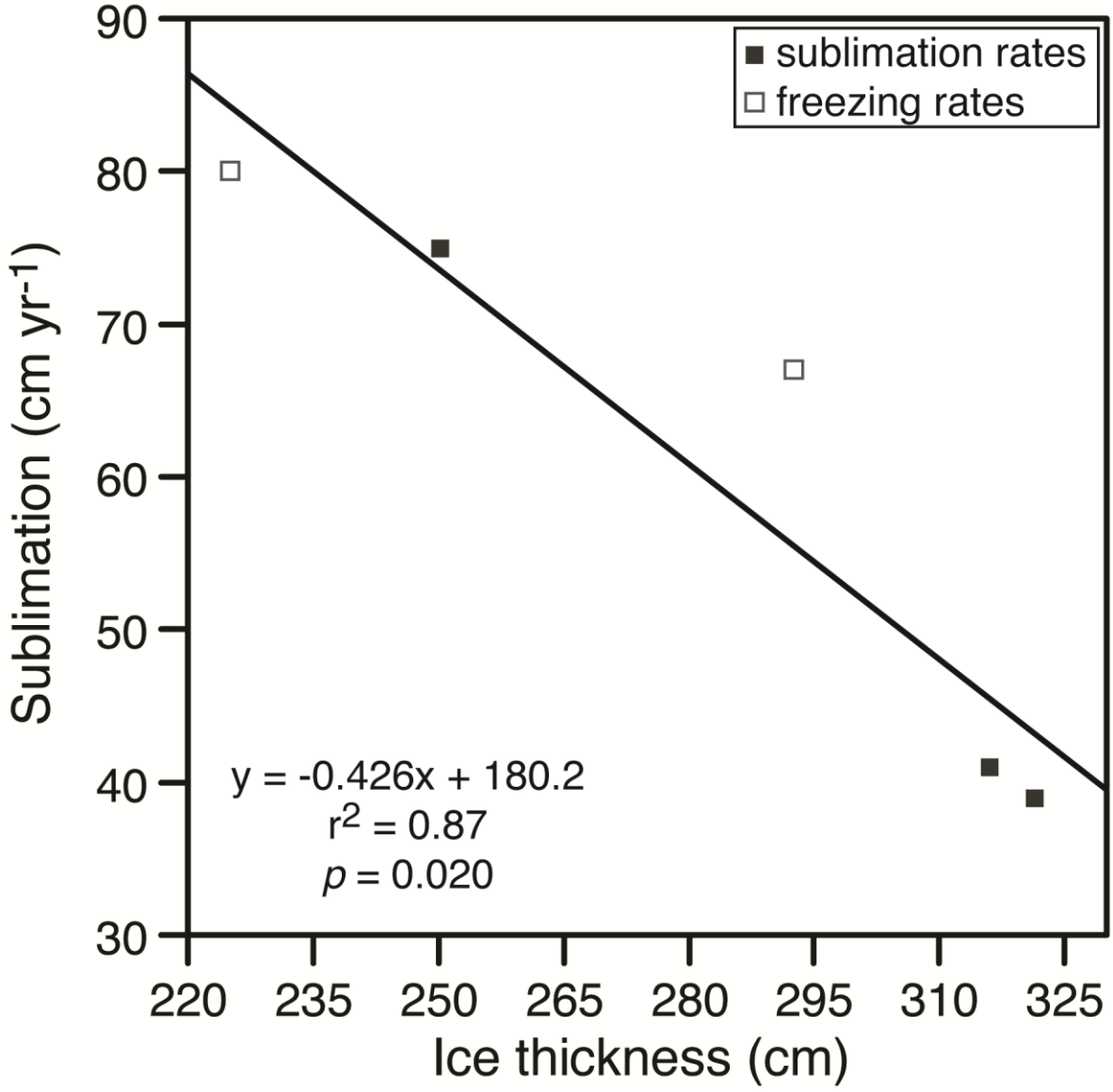

Figure 2-7: Relation between the ice cover thickness and ablation/freezing rates. White and black squares indicate freezing rates inferred from the spectral analysis of ice cover cores and measured ice cover sublimation rates, respectively.

2.5.2 Heat energy model of the ice cover

Clow et al. (1988) developed a climate-based model that incorporated non-steady molecular diffusion into Kolmogorov-scale eddies to derive the average sublimation rate of the ice cover of lakes in the MDV (~ 30 cm yr^{-1}). Given that the MAAT at Lake Untersee is about 7°C warmer than that used by Clow et al. (1988), the sublimation rate at Lake Untersee is expected to be ~ 1.8x higher, a factor given by the ratio of the vapor pressure of ice at –9.5ºC and –17°C. This

first-order scaling would predict an average sublimation rate at Lake Untersee of 60 cm yr^{-1}, similar to the average ablation rate of 61±11 cm yr^{-1}. However, the thickness of the ice cover of lake Untersee has a strong spatial variation that appears to be associated with the wind regime across the lake. To test for the effect of wind on sublimation rates, we assume that the energy required to sublimate the ice comes from turbulent heat fluxes caused by the wind blowing over the ice surface (i.e., Paterson, 2010). We used a standard turbulent heat flux equation for smooth-surface ice cover to calculate the amount of ice that can sublimate from variable wind speeds (SR, in m yr^{-1}) using **EQ. 2-5**:

$$[\textbf{EQ. 2-5}]\ SR = \frac{22.2\ A\ u\ (e_s - e)t}{L_v \rho_{ice}}$$

where:

A = 0.002 (the transfer coefficient for air moving over smooth ice with temperatures in the -10 to 0°C range; Ambach & Kirchlechner, 1986);

u is the wind speed (m s^{-1}) at screen height (1 m);

e_s is the saturation water vapor pressure over ice (at the ice surface temperature in Pa;

a value that is ~ 600 Pa for ice near 0°C);

e is the water vapor pressure at screen height (relative humidity = 42%, so e ~ 252 Pa;

t is the number of seconds in a year (3.153 x 10^7);

Lv is latent heat of vaporization (3.1335 x 10^6J kg^{-1});

ρ_{ice} is density of ice (917 kg m^{-3}).

The theoretical amount of sublimating ice due to turbulent heat flux shows a positive relationship with wind speed blowing over the ice surface (Fig. 2-8). Our measured summer 2011 average wind speeds and sublimation rates offer a good fit with the theoretical line. The lake locations with slightly lower sublimation rates than that predicted are attributed to the presence of snow on the ice surface, which would decrease the amount of time sublimation is occurring (i.e., would reduce the value of t in **EQ. 2-5** to less than one year). Therefore, variations in sublimation

rates on the ice cover appear to be primarily influenced by wind and its associated turbulent heat fluxes and the number of snow-covered days (which reduces the sublimation of the ice cover).

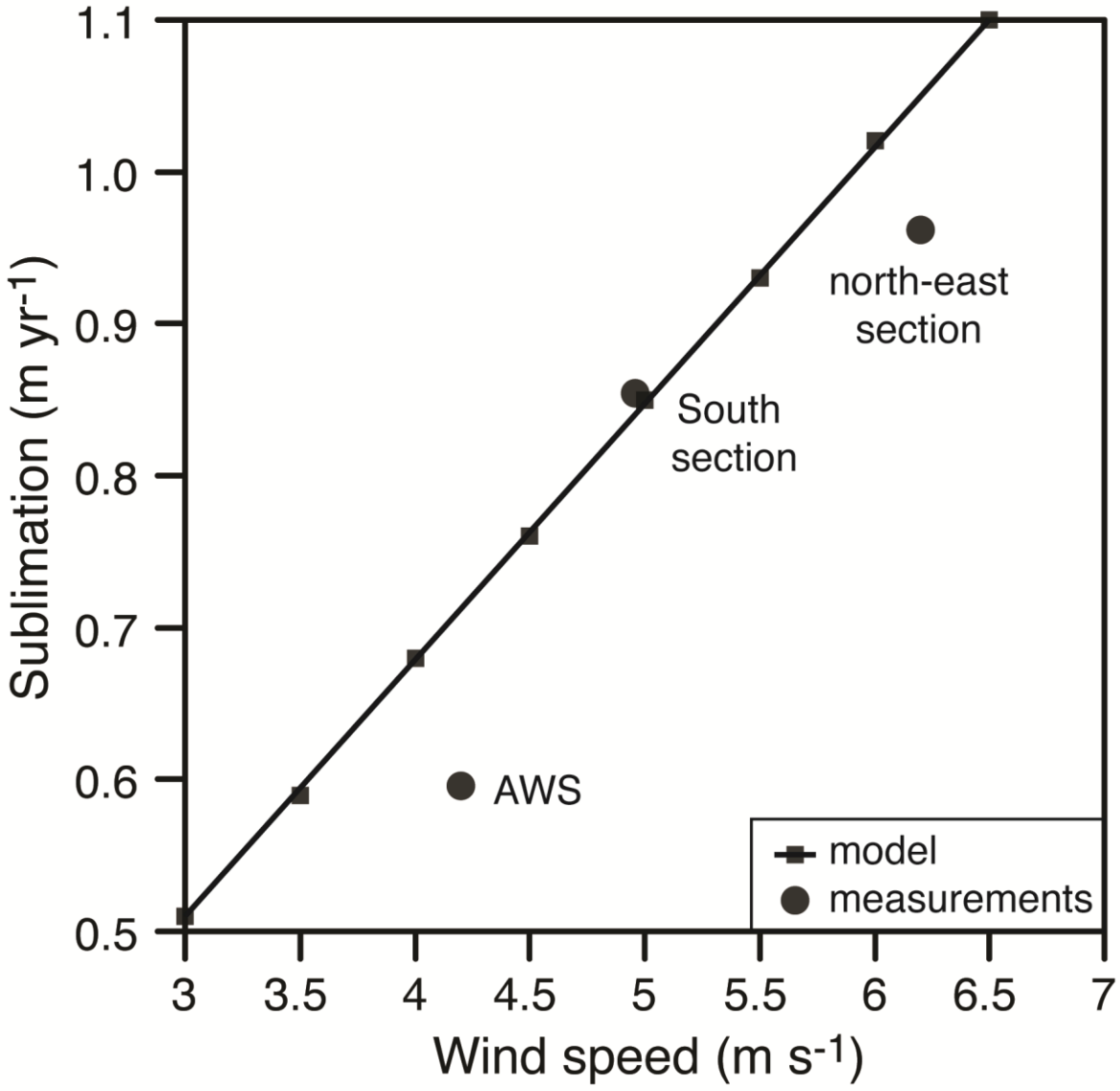

Figure 2-8: Relation between wind speeds and sublimation rates at three locations on the ice cover. See Fig. 2-1 for the location of sites.

2.5.3 Water mass balance and heat energy model of Lake Untersee

Lake Untersee has a water volume of 5.21 x 10^8 m^3 and has remained stable since at least 1995 and was most likely stable for the past 80 years. With a surface area of 8.73 km^2 and an average sublimation rate of 61±11 cm yr^{-1}, Lake Untersee is losing annually 4.90±0.8 x 10^6 m^3 of water (0.94±0.17% of total lake water volume). Assuming that the ice cover sublimation is the only output of water for the lake, the lake must receive an equal amount of inflow to maintain the water budget in equilibrium. There are no visible inflows of surface water to the lake, and although the lake's surface receives snowfall, none (or very little) makes it way to the water column due to its sealed nature. This means that direct precipitation does not contribute to the lake water. Hence, *P* can be taken out of the hydrological mass balance equation. Hermichen et al. (1985) inferred that the Anuchin Glacier's melting was recharging the lake with no distinction between englacial and basal meltwaters or other potential groundwater sources. The Anuchin Glacier advances toward Lake Untersee at a velocity of 8 to 9 m yr^{-1}. Since the ice tongues at the glacier-lake interface remained at the same location for at least the past 30 years, englacial meltwater contributes 2.16 to 2.43 x 10^6 m^3 to the lake annually (44-50% of annual lake water volume; Fig. 2-9A). Water additions from the small stagnant ice patch at the southern of the Untersee Oasis, which is sourced from avalanches falling down from a hanging glacier, have not been considered in this hydrological mass balance calculation since: 1) it is not in direct contact with the Lake (i.e., no subaqueous melting of terminus ice and/or subglacial contributions); and 2) surface runoff on the latter have also not been observed.

Overall, our calculations suggest that approximately 2.47 to 2.74 x 10^6 m^3 (50-56% of yearly lake water volume) must be contributed annually from basal meltwater and/or a groundwater source. This amounts to a groundwater discharge of ~ 6.8 x 10^{-2} m^3 sec^{-1}, a reasonable flux given the reported range of subglacial water flux in the region (Fig. 2-1A). Given the lake's surface area and depth, a through talik is present beneath it (i.e., Mackay, 1963), allowing groundwaters to recharge the lake. Therefore, Lake Untersee is hydrologically connected to a regional groundwater system, as inferred for Lake Bonney in the McMurdo Dry Valleys from airborne transient electromagnetic sensor (i.e., Mikucki et al., 2015).

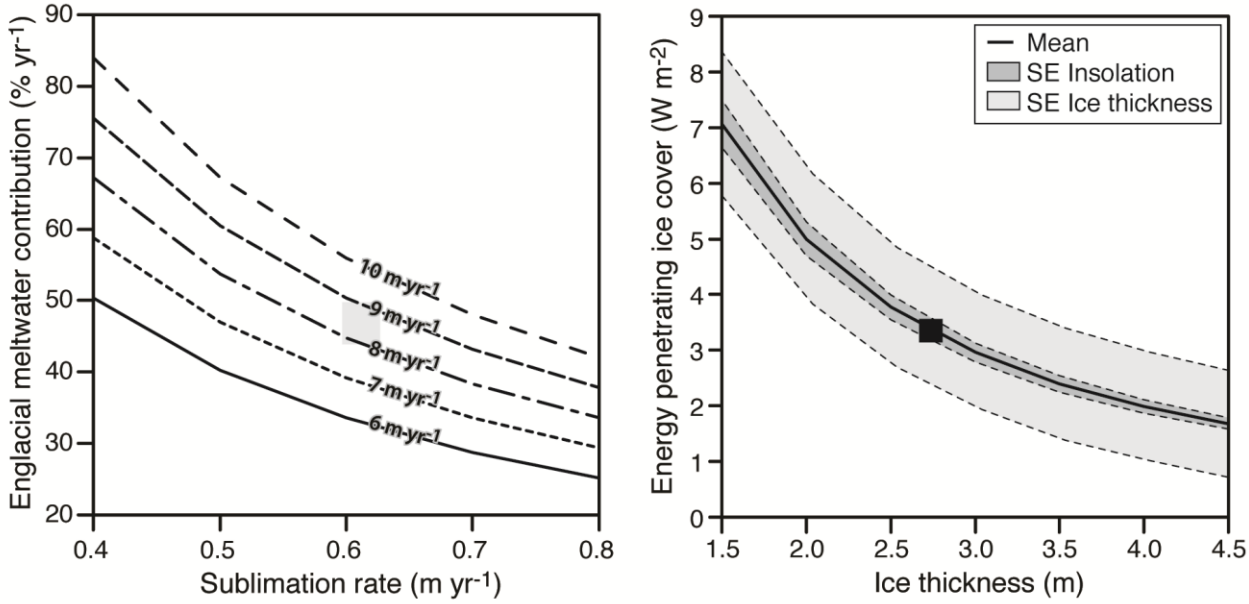

Figure 2-9: A) Annual englacial meltwater contributions to Lake Untersee's volume as a function of various ice cover sublimation rates and glacial velocities. B) Transmissivity of the ice cover to visible light (based on PAR measurements) as a function of ice thickness.

Unlike the lakes in the MDV, there are no visible surface inflows of water to the lake, bringing sensible heat energy to the lake water. Therefore, the englacial melting of the Anuchin Glacier must be accomplished by sunlight energy that penetrates the ice cover. To test if enough sunlight reaches the water column to melt annually 2.16 to 2.43 x 10^6 m^3 of englacial ice, we undertook an energy mass balance calculation. Previous studies (e.g., McKay et al., 1985; Palmisano & Simmons, 1987; Lizotte & Priscu, 1992) have been using a simple Beer's law, exp(-z/H) to estimate the amount of light that penetrates the ice cover and fitted scale height (H) to PAR measurements. This is incorrect in two ways: 1) in ice cover, scattering dominates over absorption, and Beer's law is for absorption only; and 2) the properties of the ice are not uniform over the PAR measurements. Here we use a simple scattering model for the lake ice cover that: 1) assumes uniform optical properties with depth, consistent with observations (absorption by very clean ice and scattering by large bubbles; Fig. 2-3); 2) uses the absorption coefficient in ice as a function of wavelength from the latest compilation (i.e., Warren & Brandt, 2008); and 3) uses a two-stream scattering model that includes absorption (i.e., **EQ. 3** to **EQ. 7** in Sagan & Pollack, 1967). This model has two key parameters: the total scattering optical depth and the scattering asymmetry factor. Given that ice is transparent mainly to the visible portion of the spectrum, we did a

wavelength resolved analysis from 350 to 800 nm and treated 800-3200 nm as black body. Using our two measurements beneath the ice cover (PAR albedo = 0.66 and PAR transmission = 0.049; Andersen et al., 2011) and assuming isotropic scattering by the bubbles in the ice cover to derive a fit to PAR measurements, we obtain a scattering optical depth of 9 m.

Based on the measured surface radiation (99±0.7 Wm^{-2}), the spectral transmission of ice (38.6%), the transmissivity of the ice cover to visible light from PAR measurements (4.9±1%), and the range of the thickness of the ice cover (1.96 to 3.96 m), 3.37±0.84 Wm^{-2} enters the water column; an amount sensitive to ice thickness (Fig. 2-9B). A first-order calculation of the amount ice that can melt can be estimated from **EQ. 2-6**:

[**EQ. 2-6**]: $h = \frac{\alpha \Delta T_1 t}{\rho L + c \Delta T_2}$ (Tomirdiaro,1972; Are, 1980, 1985):

where:

h is the thickness of melted ice (m);

α *is the heat-exchange coefficient between water and ice (W/* m^{-2} *K);*

ΔT_1 *(K) is the temperature difference between water and the melting ice (1K; Andersen et al., 2011);*

t is time (s):

ρ*(kg* m^{-3}*) is the ice density;*

L is the latent heat of fusion (334,000 J kg^{-1}*);*

c (J/kg K) is the volumetric specific heat of ice;

ΔT_2 *(K) is the difference between initial ice temperature and ice melting point (0K).*

The 3.37±0.84 Wm^{-2} that enters the water column can melt 34.70 cm yr^{-1}. With a lake surface area of 8.73 km^2, there is enough energy to melt an equivalent of 3.33 x 10^6 m^3, which is more than enough to sustain the annual contribution of englacial meltwater (2.16 to 2.43 x 10^6 m^3). Considering that the annual contribution of englacial melting is dependent on the velocity of the Anuchin Glacier, there is enough sunlight energy entering the water column to sustain englacial melting for contributions up to 65%, an equivalent in glacier velocity up to 12 m yr^{-1}.

2.5.4 Lake Untersee and changing climate

Lakes are good indicators of climate change because of their physical, chemical, and biological responsivity to environmental conditions changes (Adrian et al., 2009; Williamson et al., 2009). Ten-year measurements of ice cover thickness of Lake Untersee showed little change; this contrast to lakes in the MDV which experienced an ice thickness decrease by over 2 m between 1999-2016 (Obryk et al., 2019). The Untersee Oasis has a relatively warm MAAT for Antarctica; in fact, about 7°C warmer than in the coastal zone in the MDV (i.e., Clow et al., 1988; Doran et al., 2002). Our climate measurements indicate that the MAAT in the Untersee Oasis has been relatively stable during the past decade (2008-2018). This contrast with the rest of the Queen Maud Land region where MAAT has increased at a rate of 1.1±0.7°C decade^{-1} between 1998 and 2016 (Medley et al., 2018) and with the MDV where air temperature has increased since 2006 with no distinct trend (Obryk et al., 2019). Compared to the MDV ice-covered lakes, Lake Untersee should be developing a moat in summer given the similar range in thaw-degree days (7 to 51) and higher MAAT; however, no moat develops around Lake Untersee, even during summers with a high number of thawing degree-days. A minor increase in summer air temperature is not expected to alter this condition as the region is dominated by intense evaporation and sublimation, which limits surface melt features and prevents summer moats from developing around the edges of the lake due to cooling associated with the latent heat of sublimation (e.g., Hoffman et al., 2008). However, a change in wind regime should significantly impact the lake ice dynamic as it largely drives the sublimation and controls the thickness of the ice cover and, consequently, the amount of sunlight that reaches the water column.

A more direct impact of climate change on the hydrology of Lake Untersee would be its effect on the surrounding glaciers, namely the Anuchin Glacier. Currently, the Anuchin has a velocity of 8-9 m yr^{-1} and given that the position of the glacier-lake interface has not changed over the past 10 years, we assume that the amount the Anuchin Glacier advances all melts and contributes ~ 50% of the annual the lake water volume input. However, under current ice thickness configuration, only ~ 3.37 Wm^{-2} of sunlight reaches the water column, which provides enough energy to melt a maximum of 2.9 x 10^{-3} km^3 of englacial ice along the ice wall. This amount would be exceeded if the Anuchin Glacier's velocity exceeds 12 m yr^{-1}; in that case, the lake water level would rise since the glacier would act like a piston and force the water level to increase. On the other hand, a receding Anuchin Glacier would lower the water level by ~ 9% of the receding

distance (difference in density between ice and water). The response of other potential water sources to climate change is also uncertain. Currently, no surface streams are feeding into Lake Untersee; however, it is possible that under a warming scenario that the lake could receive surface runoff from ephemeral streams and supraglacial runoff contributions. In that case, the lake would receive sensible and latent heat, which would drastically alter the hydrochemical conditions (i.e., allowing for interactions with the atmosphere) of the lake waters may cause severe shifts in benthic biochemical regimes. If this happens, Lake Untersee would become more similar to lakes in the coastal MDV.

2.6 Conclusion

This study investigated the thermodynamics and the hydrological balance of Lake Untersee, one of the largest freshwater lakes in East Antarctica. Based on the results, the following conclusions can be reached:

1. $\delta^{18}O$ and abundance of bubble trends in the ice cover can identify the annual thickness of ice accretion. As such, when combined with ablation rate measurements, the steady-state condition of perennially ice-covered lakes can properly be determined.
2. Ten-year measurements at the same location showed that the ice cover had near-identical thickness, indicating that the ice cover is in a steady-state.
3. The sublimation rate of Lake Untersee, and its control on ice cover thickness, is primarily influenced by wind and its associated turbulent heat fluxes and the number of snow-covered days. With an annual average ablation rate of 61±11 cm yr^{-1}, the ice cover has a 3-6 years turnover rate.
4. Lake Untersee has a water volume of 5.21 x 10^8 m^{-3} and is losing annually 0.94±0.17% of total lake water volume. The Anuchin Glacier advances toward Lake Untersee at a velocity of 8 to 9 m $yr^{-1,}$ and englacial meltwater contributes 44-50% of annual lake water volume; the remaining volume must be contributed annually from basal meltwater and/or a groundwater source likely flowing at a rate of ~ 6.8 x 10^{-2} m^3 sec^{-1} into Lake Untersee. This provides one of the first direct evidence of groundwater recharging lakes in an ice-free Antarctic region.
5. Based on a simple scattering model for the lake ice cover, 3.37± 0.84 Wm^{-2} enters the water column and provides enough energy to melt the englacial ice contribution to the lake, up to a velocity of 12m yr^{-1}.

2.7 References

Adrian, R., O'Reilly, C. M., Zagarese, H., Baines, S. B., Hessen, D. O., Keller, W., Livingstone, D. M., Sommaruga, R., Straile, D., Van Donk, E., Weyhenmeyer, G. A. & Winder, M. (2009). Lakes as sentinels of climate change. *Limnol. Oceanogr.* 54, 2283–2297.

Ambach, W. & Kirchlechner, P. (1986). Nomographs for the determination of the meltwater from ice and snow surfaces by sensible and latent heat flux. *Wetter Leben* 38, 181–189.

Andersen, D. T., Sumner, D. Y., Hawes, I., Webster-Brown, J. & McKay, C. P. (2011). Discovery of large conical stromatolites in Lake Untersee, Antarctica. *Geobiology* 9, 280–293.

Andersen, D. T., McKay, C. P. & Lagun, V. (2015). Climate Conditions at Perennially Ice-covered Lake Untersee, East Antarctica. *J. Appl. Meteorol. Climatology* 54(7), 1393–412.

Are, F. E. (1980). Thermo-abrasion of Sea Shores. Nauka: Novosibirsk (in Russian).

Are, F. E. (1985). Principles of Shore Thermo-abrasion Forecast. Nauka: Novosibirsk (In Russian).

Bevington, J., McKay, C. P., Davila, A., Hawes, I., Tanabe, Y. & Andersen, D. T. (2018). The thermal structure of the anoxic trough in Lake Untersee, Antarctica. *Antarc. Sci. 30*(6), 333-344.

Bormann, P. & Fritzsche P., editors. (1995). The Schirmacher Oasis, Queen Maud Land, east Antarctica, and its surroundings. Justus Perthes Verlag, Gotha, Germany.

Bormann, P., Bankwitz, P., Bankwitz, E., Damm, V., Hurtig, E., Kampf, H., Menning, M., Paech, H. J., Schafer, V. & Stackebrandt, W. (1986). Structure and development of the passive continental margin across the Princess Astrid Coast, East Antarctica. *J. Geodyn*. 6, 347-373.

Castendyk, D. N., Obryk, M. K., Leidman, S. Z., Gooseff, M. & Hawes, I. (2016). Lake Vanda: a sentinel for climate change in the McMurdo Sound Region of Antarctica. *Glob Planet Change* 144, 213–227.

Clark, I. D. (2015): Groundwater Geochemistry and Isotopes. *CRC Press, Taylor and Francis Group: Boca Ratón*, FL.

Clow, G. D., McKay, C. P., Simmons, G. M. Jr & Wharton, R. A. Jr. (1988). Climatological observations and predicted sublimation rates at Lake Hoare, Antarctica. *J. Clim.* 1, 715-728.

Dansgaard, W. (1964). Stable isotopes in precipitation. *Tellus* 16, 436–468.

Doran, P. T., Priscu, J. C., Lyons, W. B., Walsh, J. E., Fountain, A. G., McKnight, D. M., Moorhead, D. L., Virginia, R. A., Wall, D. H., Clow, G. D., Fritsen, C. H., McKay, C. P. & Parsons, A. N. (2002). Antarctic climate cooling and terrestrial ecosystem response. *Nature* 415(6871), 517–520.

Doran, P. T., McKay, C. P., Fountain, A. G., Nylen, T., McKnight, D. M., Jaros, C. & Barrett, J. E. (2008). Hydrologic response to extreme warm and cold summers in the McMurdo Dry Valleys, East Antarctica. *Antarc. Sci.* 20, 499–509.

Dugan, H. A., Obryk, M. K. & Doran, P. T. (2013). Lake ice ablation rates from permanently ice-covered Antarctic lakes. *J. Glaciol*, 59(215), 491–498.

Fountain, A. G., Saba, G., Adams, B., Doran, P., Fraser, W., Gooseff, M., Obryk, M., Priscu, J. C., Stammerjohn, S. & Virginia R. A. (2016). The impact of a large-scale climate event on Antarctic ecosystem processes. *Bioscience* 66(10), 848–863.

Gooseff, M. N., Barrett, J. E., Adams, B. J., Doran, P. T., Fountain, A. G., Lyons, W. B., McKnight, D. M., Priscu, J. C., Sokol, E. R., Takacs-Vesbach, C., Vandegehuchte, M. L., Virginia, R. A. & Wall, D. H. (2017). Decadal ecosystem response to an anomalous melt season in a polar desert in Antarctica. *Ecol. Evol.* 1(9), 1334–1338.

Hawes, I., Sumner, D. Y., Andersen, D. T. & Mackey, T. J. (2011). Legacies of recent environmental change in the benthic communities of Lake Joyce, a perennially ice-covered Antarctic lake, *Geobiology 9*(5), 394-410.

Hermichen, D., Kowski, P. & Wand, U. (1985). Lake Untersee- the first isotope study of the largest fresh-water lake in the interior of East Antarctica. *Nature* 315, 131-133.

Hiller, A., Wand, U., Kampf, H. & Stackebrandt, W. (1988). Occupation of the Antarctic continent of by petrels during the past 35000 years e inferences from a ^{14}C study of stomach oil deposits. *Polar Biol.* 9, 69-77.

Hoffman, M. J., Fountain, A. G. & Liston, G. E. (2008). Surface energy balance and melt thresholds over 11 years at Taylor Glacier, Antarctica. *JGR Earth Surface* 113(F4).

Killawee, J. A., Fairchild, I. J., Tison, J. -L., Janssens, L. & Lorrain, R. (1998). Segregation of solutes and gases in experimental freezing of dilute solutions: implications for natural glacial systems. *Geochim. Cosmochim. Acta* 62, 3637-3655.

Kinnard, C., Koerner, R. M., Zdanowicz, C. M., Fisher, D. A., Zheng, J., Sharp, M. J., Nicholson, L. & Lauriol, B. (2008). Stratigraphic analysis of an ice core from the Prince of Wales Icefield, Ellesmere Island, Arctic Canada, using digital image analysis: high-resolution density, past summer warmth reconstruction, and melt effect on ice core solid conductivity. *JGR Atmoshpere* 113(D24).

Koo, H., Mojib, N., Hakim, J. A., Hawes, I., Tanabe, Y., Andersen, D. T. & Bej, A. K. (2017). Microbial communities and their predicted metabolic functions in growth laminae of a unique large conical mat from Lake Untersee, East Antarctica. *Front. Microbiol.* 8, 1347.

Lacelle, D. (2011). On the $\delta^{18}O$, δD and D-excess relation in meteoric precipitation and during equilibrium freezing: theoretical approach and field examples. *Permafr. Periglac. Process.* 22(1): 13–25.

Laybourn-Parry, J. & Wadham, J. L. (2014). Antarctic Lakes. *Oxford: Oxford University Press.* 256 p.

Le Brocq, A. M., Ross, N., Griggs, J. A., Bingham, R. G., Corr, H. F. J., Ferraccioli, F., Jenkins, A., Jordan, T. A., Payne, A. J., Rippin, D. M. & Siegert, M. J. (2013). Evidence from ice shelves for channelized meltwater flow beneath the Antarctic Ice Sheet. *Nat. Geosci*. 6, 945–948.

Lipp, G., Korber, C., Englich, S., Hartmann, U. & Rau, G. (1987). Investigation of the behavior of dissolved gases during freezing. *Cryobiology* 24, 489-503.

Lizotte, M. P. & Priscu, J. C. (1992). Spectral irradiance and biooptical properties in perennially ice-covered lakes of the dry valleys (McMurdo Sound, Antarctica), in Contributions to Antarctic Research III, *AntarcS. Res. Set.*, vol. 57, edited by D.H. Eliot, pp. 1-14, AGU, Washington, D.C.

Lyons, W. B., Laybourn-Parry, J., Welch, K. A. & Priscu, J. C. (2006). Antarctic Lake Systems and Climate Change, in *Trends in Antarctic Terrestrial and Limnetic Ecosystems: Antarctica as a Global Indicator*, edited by D. M. Bergstrom, P. Convey and A. H. L. Huiskes, pp. 273-295, Springer Netherlands, Dordrecht.

MacKay, R. (1963): The Mackenzie delta area N.WT.: Canada Dept. of Mines and Tech. Services, Geographical Branch, Memoir 8.

McKay, C. P., Clow, G., Wharton, R. A. Jr. & Squyres, S. W. (1985). Thickness of ice on perennially frozen lakes. *Nature* 313, 561-562.

Medley, B., McConnell, J. R., Neumann, T. A., Reijmer, C. H., Chellman, N., Sigl, M. & Kipfstuhl, S. (2018). Temperature and snowfall in western Queen Maud Land increasing faster than climate model projections, *Geophys. Res. Lett*. 45, 1472–1480.

Mikucki, G., Auken, E., Tulaczyk, S., Virginia, R.A., Schamper, C., Sørensen, K. I., Doran, P. T., Dugan, H. & Foley, N. (2015). Deep groundwater and potential subsurface habitats beneath an Antarctic Dry Valley. *Nat. Comm.* 6, 6831.

Mouginot, J., Rignot, E., Scheuchl, B. & Millan, R. (2017). Comprehensive annual ice sheet velocity mapping using Landsat-8, Sentinel-1, and RADARSAT-2 data. *Remote Sens*. 9(4), 364.

Obryk, M. K., Doran, P. T., Hicks, J. A., McKay, C. P. & Priscu, J. C. (2016). Modeling the thickness of perennial ice covers on stratified lakes of the Taylor Valley, Antarctica. *J. Glaciol*. 62(235), 825–834.

Obryk, M. K., Doran, P. T. & Priscu, J. C. (2019). Prediction of ice-free conditions for a perennially ice-covered Antarctic lake. *JGR Earth Surface* 124(2), 686-694.

Palmisano, A. C. & Simmons, G. M. Jr. (1987). Spectral down- welling irradiance in an Antarctic lake, *Polar Biol*. 7, 145-151.

Parker, B. C., Simmons, G. M. Jr., Seaburg, K. G., Cathey, D. D. & Allnutt, F. T. C. (1982). Comparative ecology of plankton communities in seven Antarctic oasis lakes, *J. Plankton Res.* 4, 271-286.

Paterson, W. S. B. (2010). The Physics of Glaciers, 4th ed.; Academic Press: Cambridge, MA, USA, 2010; p. 496.

Richter, W. & Bormann, P. (1995). Weather and climate. In: Bormann, P. & Fritzsche, D., (eds.): The Schirmacher Oasis, Queen Maud Land, East Antarctica, and its Surroundings: *Gotha*, 207-220.

Rignot, E., Mouginot, J. & Scheuchl, B. (2017). MEaSUREs InSAR-Based Antarctica Ice Velocity Map, Version 2. [Indicate subset used]. Boulder, Colorado USA. NASA National Snow and

Ice Data Center Distributed Active Archive Center. doi: http://dx.doi.org/10.5067/D7GK8F5J8M8R. [Accessed on Feb. 15th 2019].

Rintoul, S. R., Chown, S. L., DeConto, R. M., England, M. H., Fricker, H. A., Masson-Delmotte, V., Naish, T. R., Siegert, M. J. & Xavier, J. C. (2018). Choosing the future of Antarctica. *Nature* 558, 233–241.

Sagan, C. & Pollack, J. B. (1967). Anisotropic nonconservative scattering and the clouds of Venus. *JGR* 72(2), 469-477.

Schwab, M. J. (1998). Rekonstruktion der spatquartaren Klima und Umweltgeschichte der Schirmacher Oase und des Wohlthat Massivs (Ostantarktika). Ber. *Polarforschung* 293, 1–128.

Steel, H. C. B., McKay, C. P. & Andersen, D. T. (2015). Modeling Circulation and Seasonal Fluctuations in Perennially Ice-covered and Ice-walled Lake Untersee, Antarctica. *Limnol. Oceanogr.* 60(4), 1139–1155.

Tomirdiaro, S. V. (1972). Permafrost and Development of Mountain and Lowland Areas. Magadan Publishing House: Magadan (In Russian).

Wand, U., Samarkin, V. A., Nitzsche, H. -M. & Hubberten, H. -W. (2006). Biogeochemistry of methane in the permanently ice-covered Lake Untersee, central Dronning Maud Land, East *Antarctica. Limnol. Oceanogr.* 51, 1180–1194.

Wand, U., Schwarz, G., Brüggemann, E. & Bräuer, K. (1997). Evidence for physical and chemical stratification in Lake Untersee (central Dronning Maud Land, East Antarctica). *Antarc. Sci*. 9, 43–45.

Warren, S. G. & Brandt, R. E. (2008). Optical constants of ice from the ultraviolet to the microwave: A revised compilation. *JGR Atmospheres* 113(D14).

Weisleitner, K., Perras, A. K., Moissl-Eichinger, C., Andersen, D. T. & Sattler, B. (2019). Source environments of the microbiome in perennially ice-covered Lake Untersee. *Front. Microbiol.* 10, 1019.

Wharton, R. A., McKay, C. P., Clow, G. D., Andersen, D. T., Simmons, G. M. Jr. & Gordon Love, F. (1992). Changes in ice cover thickness and lake level of Lake Hoare, Antarctica: implications for local climatic change. *JGR* 97, 3503-3513.

Williamson, C. E., Saros, J. E., Vincent, W. F. & Smol, J. P. (2009). Lakes and reservoirs as sentinels, integrators, and regulators of climate change. *Limnol. Oceanogr.* 54, 2273–2282.

Wilson, A. T. & Wellman, H. W. (1962). Lake Vanda: An Antarctic Lake: Lake Vanda as a Solar Energy Trap. *Nature* 196, 1171–1173.

CHAPTER 3: MODELING δD-δ^{18}O STEADY-STATE OF WELL-SEALED PERENNIALLY ICE-COVERED LAKES AND THEIR RECHARGE SOURCE: EXAMPLES FROM LAKES UNTERSEE AND LAKE VOSTOK, ANTARCTICA

Abstract

We developed a recursive version of the *FREEZCH5* model (called *FREEZCH9*) to determine the δD-δ^{18}O steady-state of well-sealed perennially ice covered-lakes and their recharge source. *FREEZCH9* takes the evolved chemistry and δD-δ^{18}O composition of the residual water of well-sealed perennially ice-covered lakes after a specified amount of freezing and then adds as new input the volume of water that was frozen (to remain in hydrological equilibrium) with fixed chemistry and δD-δ^{18}O composition that mixes with the residual water to produce new input chemistry and δD-δ^{18}O for the next loop. Our model is tested against Lake Vostok datasets and is used to assess the δD-δ^{18}O mass balance of Lake Untersee and evaluate if it is in an isotopic steady-state. Our simulations using *FREEZCH9* fit well the predicted δD-δ^{18}O ratios for the upper layer of Lake Vostok's water column, near the ice-water interface and the measured overlying accreted ice δD-δ^{18}O values. Simulations with *FREEZCH9* also suggest that Lake Untersee is in an isotopic steady-state. Its two input sources (i.e., subaqueous terminus melting of the Anuchin Glacier and subglacial/groundwater contributions) are of Holocene age and have similar δD-δ^{18}O ratios. We also propose that *FREEZCH9* might help determine if subglacial lakes fully or partially recharge the hypothetical groundwater systems of the McMurdo Dry Valleys.

3.1 Introduction

In Antarctica, several hundred lakes have been identified and classified according to their ice cover regime (Fig. 3-1a; Morgan et al., 2007; Vincent et al., 2008). Seasonally ice-covered lakes are found along the Antarctic Peninsula and other coastal regions where climate conditions are warm enough to ablate the ice cover in austral summer fully. These lakes are typically recharged by a combination of local precipitation and glacial meltwater (e.g., Gibson, 1999; Lyons et al., 2013). Perennially ice-covered lakes are found in polar desert regions where the climate is colder and drier. There exist two main types of perennially ice-covered lakes: 1) those that develop moats in austral summer and are fed by glacial melt streams; and 2) those that are tightly sealed from the atmosphere and solely fed by sub-aqueous glacial melt and groundwater (e.g., Priscu, 1998; Faucher et al., 2019). Further, many subglacial lakes are found beneath the Antarctic ice sheet (e.g., Priscu & Foreman, 2009; Wright & Siegert, 2012). These subglacial lakes are recharged by a combination of subglacial and englacial waters (e.g., Wingham et al., 2006).

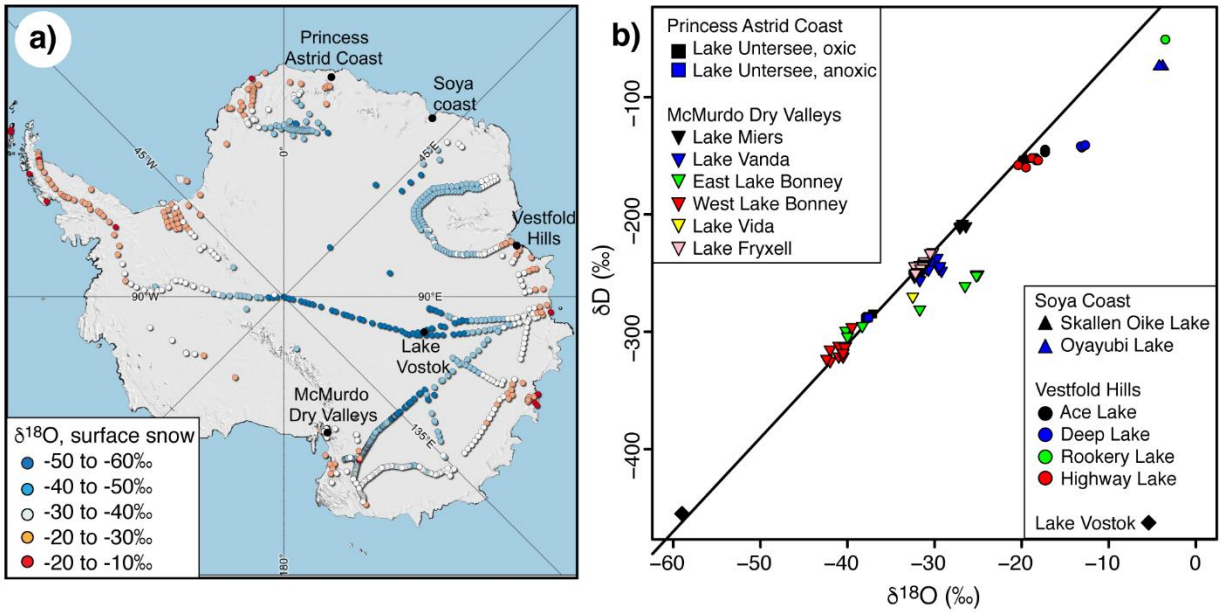

Figure 3-1: (a) Distribution of surface snow δ18O values across the Antarctic continent (data from Touzeau et al., 2016). (b) Stable water isotope (δD-δ18O) ratios of perennially ice-covered lakes found in Antarctica's Princess Astrid Coast (i.e., Lake Untersee), Southern Vicotria land region (i.e., Lake Miers, Lake Vanda, Lake Bonney, Lake Fryxell, Lake Vida) (Matsubaya et al., 1979; Miller and Aiken, 1996; Dugan et al., 2015) and Soya Coast (i.e., Skallen Oike) (Matsubaya et al., 1979). The black line indicates the Global Meteoric Water Line ($8*\delta^{18}O + 10$).

Depending on Antarctic lake type, the source of water recharging the various types of Antarctic lakes and its evolution can influence key physicochemical conditions and the composition of microbial communities and biogeochemical cycling (e.g., Lyons & Finlay, 2008; Wand et al., 2006). The analysis of the δD-$\delta^{18}O$ composition of polar lakes has been proven as a reliable tool to determine the source of water, the process that evolved the lake chemistry, and water balance parameters, such as the amount of evaporation (Jeffries et al., 1984; Gibson, 1999; Gooseff et al., 2006; Horita, 2009). In Antarctica, the $\delta^{18}O$ values of lakes range from *c*. 0 to –60‰ (Fig. 3-1b), a range that reflects the primary source of water recharging the lakes. Lakes with $\delta^{18}O$ values near 0‰ are a heritage of isostatic rebound, and their formation is attributed to the freezing of trapped seawater following a decrease in sea level (Bird et al., 1991). Considering that the $\delta^{18}O$ of precipitation along the coast is near –25 to –20‰, the source of waters in lakes with $\delta^{18}O$ values near –15 to –10‰ have been attributed to mixing of seawater and local coastal precipitation (Matsubaya et al., 1979; Richter & Strauch, 1983; Bird et al., 1991). Finally, lakes with $\delta^{18}O$ values <–25‰ are recharged mainly from glacial meltwater, with those with very depleted $\delta^{18}O$ composition likely receiving input from late Pleistocene meltwater (Matsubaya et al., 1979; Richter & Strauch, 1983; Bird et al., 1991). The lake's ice cover regime (i.e., seasonally or perennially ice-covered) determines whether the evaporation or freezing process drives the evolution of the lake isotope chemistry (Miller & Aiken, 1996). Both seasonally ice-covered lakes and perennially ice-covered lakes with a summer moat have lake waters with δD-$\delta^{18}O$ composition plotting below the Global Meteoric Water Line (GMWL) (Fig. 3-1b). These lakes' isotopic behavior is strongly influenced by the evaporation process that enriches the residual water and distributes it along an evaporative line with a lower slope than the GMWL. The $\delta^{18}O$ composition of evaporative lakes is determined by atmospheric parameters such as humidity and isotopic composition of the water vapor and the evolving salinity in the water column, and isotopic mass-balance models have been developed to estimate the lakes' δD-$\delta^{18}O$ steady-state (i.e., Gibson, 1999; Horita, 2009).

Three Antarctic lakes share a unique δD-$\delta^{18}O$ signature that has not yet been described elsewhere within the continent. Perennially ice-covered Lake Untersee and Lake Bonney (bottom waters in west lobe) and subglacial Lake Vostok have lake water with the lowest $\delta^{18}O$ composition (*c*. –59 to –38‰) and with δD-$\delta^{18}O$ values plotting above the GMWL (Fig. 3-1b). Lake Untersee is a well-sealed perennially ice-covered lake and Lake Vostok is a subglacial lake beneath the East

Antarctic Ice Sheet; consequently, the water column of these lakes does not interact with the atmosphere (i.e., no kinetic fractionation due to evaporation) and the δD-δ^{18}O evolution of their water column is controlled by recharge and the freezing process at the bottom of the ice cover. Despite an understanding of the recharge water source and the freezing process in Lake Vostok and its isotopic steady-state (e.g., Souchez et al., 2004; Royston-Bishop et al., 2004; Ekaykin et al., 2010), the isotopic mass-balance of Lake Untersee remains unknown. Also, unlike evaporative lakes, no studies have yet developed a model capable of predicting the δD-δ^{18}O steady-state of the water column that includes the evolution of the ice-water isotope fractionation factor as freezing changes the salinity of the residual water and recursive recharge that mixes with the residual lake water.

This study aims to develop a model of δD-δ^{18}O evolution of well-sealed perennial ice-covered lakes that accounts for changing chemistry in the residual water and annual recharge that mixes with residual water. This objective was achieved by using *FREEZCH5*, an isotope-augmented version of the *FREZCHEM* low-temperature geochemistry model (Marion et al., 2010; Fisher et al. 2019), and making the model recursive. The model is tested against Lake Vostok datasets and is used to assess the δD-δ^{18}O mass balance of Lake Untersee and evaluate if it is in an isotopic steady-state. The results are presented in terms of residence times of water in context with different mixing scenarios, which allow for application of the findings to other well-sealed perennial ice-covered lakes or subglacial lakes.

3.2 Materials and methods

3.2.1 Background on water-ice fractionation during freezing

The freezing of water under equilibrium condition follows a Rayleigh-type fractionation (**EQ. 3-1**):

[**EQ. 3-1**] $$R = R_0 f^{(\alpha i - w - 1)} + (a_{i-w} - 1)$$

where:

R is the isotope ratio of $^{18}O/^{16}O$ or D/H;

$\alpha_{i\text{-}w}$ is the water-ice fractionation factor with two distinct sets of $\alpha_{i\text{-}w}$ for $^{18}O/^{16}O$ and D/H reported in the literature: 1.0031 and 1.0193, respectively (O'Neil, 1968); 1.0028 and 1.0206, respectively (Suzuoki & Kimura, 1973).

The forming ice becomes ^{18}O enriched during freezing, but the residual water is progressively depleted and evolves above the GMWL because the freezing line has a lower slope (Lacelle, 2011; Horita, 2009). The freezing of water also imparts ionic segregation, increasing the residual water's solute content (Killawee et al., 1998; Terwilliger & Dizio, 1970). Because freezing reduces the water activity, a correction to the D/H and $^{18}O/^{16}O$ water-ice fractionation factors should be applied, especially at higher salinities where solutes may bind water molecules in hydration spheres around the cations and following the precipitation of hydrated salts (i.e., $NaCl{\cdot}2H_2O$, $MgCl_2{\cdot}12H_2O$, $CaCl_2{\cdot}6H_2O$). The theory of changing ice-water isotope fractionation under changing water salinities was described in Sofer & Gat (1972; 1975), and in Stewart & Friedman (1975), and they showed that the isotopic salt effect is linearly correlated for different salt solutions at varying concentrations.

In addition to the evolving isotope salt effect, Jouzel & Souchez (1982) observed that the water's initial isotope composition also affects the isotope composition of ice during freezing. Consequently, Souchez & Jouzel (1984) suggested that the influence of the initial isotope composition of water on the water-ice fractionation factor ($\alpha_{\delta O}$) could be estimated from **EQ. 3-2**:

[**EQ. 3-2**] $$\alpha_{\delta O} = (\alpha_{i-w} - 1)(1000 + \delta_O)/1000 + 1$$

where:

δ_O *is the initial isotope composition of water;*

$\alpha_{i\text{-}w}$ *is the equilibrium fractionation factor.*

EQ. 3-2 shows that $\alpha_{\delta O}$ is reduced with decreasing initial isotope composition of water; for most waters, this correction can be ignored, but it exceeds the analytical error when $\delta^{18}O \leq 40‰$.

Finally, the water-ice isotope fractionation during freezing depends on the reaction's kinetics, including the freezing rate, boundary layer thickness, and isotope diffusion at the ice-water interface. The kinetic water-ice isotope fractionation factor (α_{FR}) can be approximated by a modified version of Burton et al.'s (1953) equation for solute segregation (**EQ. 3-3**):

[**EQ. 3-3**] $$\alpha_{FR} = \left(\frac{\alpha_{i-w}}{\alpha_{i-w} - (\alpha_{i-w} - 1) e^{\frac{-h\nu}{D*}}} \right)$$

where:

h is the thickness of the boundary layer (cm);

v is the freezing rate (cm s^{-1});

D is the diffusion coefficient in water. At 0C, D* values for $H_2{}^{18}O$ and HDO are 1.1 x 10^{-5} cm^2 s^{-1} and 1.33 x 10^{-5} cm^2 s^{-1}, respectively (Wang et al., 1953).*

When the freezing rate is slower than the diffusion coefficient, α_{FR} approximates the equilibrium fractionation factor, but under increasing freezing rate, α_{FR} is reduced towards unity (i.e., Lacelle, 2011).

3.2.2 Description of FREEZCH5 (isotope-augmented *FREZCHEM*)

The core of the *FREEZCH5* model is *FREZCHEM(*v15), an equilibrium chemical thermodynamic model over the temperature range of –73 to 25°C (Fisher et al., 2019; Marion & Kargel, 2008). *FREZCHEM* simulates the freezing of water by decreasing the temperature in fixed steps and determines residual water presence if the water activity calculated from the Pitzer equations is less than the equilibrium constant for water-ice. At each decreasing temperature step ("i"), the model provides: 1) the amount of residual water (in g; WAT_{LIQ}); 2) the amount of ice formed (in g; Δ_{ICE}); 3) the molalities of the major cations (Na^+, Ca^{2+}, Mg^{2+} and K^+) and anions (Cl^-, NO_3^- and SO_4^{2-}); 4) the amount of hydrated salts that precipitate (in g; ΔWATNa, ΔWATMg, and ΔWATCa); and 5) the total ionic strength of the solution (proportional to conductivity and salinity of the residual water). *FREZCHEM* completely segregates the solutes in the residual water. None are incorporated as inclusions in the ice lattice or along grain boundaries and likely over-estimates the salinity in the residual water (i.e., Killawee et al., 1998; Petrenko & Whitworth, 1999). However, properly accounting for ionic segregation in equilibrium modeling is challenging as it was found that the concentration factor (or the segregation coefficient) is dependent on initial water chemistry and freezing rates (Santibáñez et al., 2019).

The evolution of $\delta^{18}O$ of the residual water ($\delta^{18}Orw$) and for the incremental ice that forms at each decreasing temperature step was added to *FREZCHEM* in a routine called *FREEZCH5*, where the initial $\delta^{18}O$ composition of the water and the $\alpha_{i\text{-}w}$ is specified by the user (**EQ. 3-4; EQ. 3-5**):

[**EQ. 3-4**] $\delta^{18}O_{rw}(i) = \delta^{18}O_{rw}(i\text{-}1) + \Delta\delta^{18}O_{rw}$

where:

$\Delta\delta^{18}O_{rw}$ *is given by* ***EQ. 3-5:***

[**EQ. 3-5**] $\Delta\delta^{18}O_{rw} = -(1000 + \delta^{18}O_{rw}\,(i\text{-}1))[(\alpha_{18O\text{-}i\text{-}w}\text{-}1)\Delta ICE/WATLIQ + (\alpha_{18O\text{-}w\text{-}Naprecip}\text{-}1)\Delta WATNa/WATLIQ + (\alpha_{18O\text{-}w\text{-}Mgprecip}\text{-}1)\Delta WATMg/WATLIQ + (\alpha_{18O\text{-}w\text{-}Caprecip}\text{-}1)\Delta WATCa/WATLIQ]$

where:

$\alpha_{18O\text{-}i\text{-}w}$ *is the ice-water fractionation factor (corrected for initial isotopic composition using equation 1);*

$\alpha^{18}O_{w\text{-}Naprecip}$ *is the water-*$NaCl{\cdot}2H_2O$ *precipitate fractionation coefficient;*

$\alpha^{18}O_{w\text{-}Mgprecip}$ *is that for water-*$MgCl_2{\cdot}12H_2O$*;*

$\alpha^{18}O_{w\text{-}Caprecip}$ *is* $CaCl_2{\cdot}6H_2O$*.*

**Note that* $\delta^{18}O_{rw}$ *is the isotopic composition for the total water in the solution (free water and the water attached to the hydration spheres around the positive ions).*

The various hydrated salts do not have reported water-precipitate fractionation coefficients and assume that they are unity or as defined by Sofer & Gat (1972; 1975) for the cations-hydration spheres within the liquid solution. Since *FREZCHEM* is an equilibrium model, the effect of freezing rates on water-ice fractionation factors is not included. Still, these should have little impact on the freezing of perennially ice-covered lakes where freezing takes place near 0°C at the ice-water boundary.

With $\delta^{18}O_{rw}$, we can use the Sofer & Gat (1972; 1975) isotope salt effects correction to determine the $\delta^{18}O$ offset between the $\delta^{18}O$ total water (free and hydration sphere waters) and $\delta^{18}O$ free water only (i.e., water activity), a correction that depends on the molality of each cation (Na^+, Ca^{2+}, Mg^{2+} and K^+) (**EQ. 3-6**):

[**EQ. 3-6**]: $(\delta^{18}O_{rw} - \delta^{18}O_{activty}) = \Delta\delta^{18}O_{Na+} + \Delta\delta^{18}O_{Mg2+} + \Delta\delta^{18}O_{Ca2+} + \Delta\delta^{18}O_{K+}$

where:

$\Delta\delta^{18}$Ocations are functions of the remaining liquid water molality, which are calculated at each temperature step. The FREEZCH5 model is described in detail in Appendix A of Fisher et al. (2019).

3.2.3 Description of *FREEZCH9* (a recursive *FREEZCH5*)

For perennially ice-covered lakes under steady-state hydrological conditions, the annual rate of water freezing at the bottom of the ice cover must equal the annual ablation rate at the ice surface (Mckay et al., 1985; Wilson & Wellman, 1962). This implies that to maintain the lake water volume constant ($\Delta V = 0$), the lake must be recharged by the same volume of water lost by ablation. We developed a looping version of *FREEZCH5* (called *FREEZCH9*) that takes the evolved chemistry and δD-$\delta^{18}O$ composition of the residual water after a specified amount of freezing and then to maintain $\Delta V = 0$, add as new input the volume of water that was frozen with fixed chemistry and δD-$\delta^{18}O$ composition that mixes with the residual water to produce a new input chemistry and δD-$\delta^{18}O$ for the next loop. The hydrated precipitates that may form are accumulated in the series.

3.2.3 Field Sampling and Laboratory Analysis

Water in the oxic basin of Lake Untersee was sampled in December 2016 at a 10-m depth interval using a 2.2-L acrylic Kemmerer bottle content, and samples were stored in sealed 20 ml HDPE bottles. In 2017, the ice cover was sampled at two locations (central and southern section; core #1 and core #2) with a *Cold Regions Research and Engineering Laboratory* coring kit to a depth of c. 2m to prevent mixing with lake water. Surface samples from the Anuchin Glacier were collected with a *Kovacs* ice corer powered by a Bosch Hammer GBH 36V-LI PLUS electric drill to a depth of 50 cm (e.g., Weisleitner et al., 2019). Samples from the Anuchin Glacier and Lake Untersee ice cover (sliced at 2 cm intervals) were left to melt in sealed Ziploc bags, transferred in high-density polyethylene bottles, and shipped in coolers to the University of Ottawa, where they were stored at 4°C alongside lake water samples until stable water isotope analysis.

The $^{18}O/^{16}O$ and D/H ratios of lake water and melted ice cover samples were analyzed using a Los Gatos Research liquid water analyzer coupled to a CTC LC-PAL autosampler and verified for spectral interference contamination. The results are presented using the δ-notation ($\delta^{18}O$ and δD), where δ represents the parts per thousand differences for $^{18}O/^{16}O$ or D/H in a sample

with respect to Vienna Standard Mean Ocean Water (VSMOW). Analytical reproducibility for $\delta^{18}O$ and δD was ±0.3‰ and ±1‰, respectively. Deuterium excess (d) was then calculated using EQ. 3-7 (Dansgaard, 1964):

[**EQ. 3-7**] $d = \delta D - 8 * \delta^{18}O$

3.3 Results

3.3.1 Modeling the freezing of low to high salinity waters

The freezing point of water is determined by the chemical composition of the solutions and ranges from 0°C for pure water to –2.3°C for seawater (Fig. 3-2a). Freezing under equilibrium conditions progressively decreases the amount of residual water while increasing the concentration of solutes in the residual water. This cryo-concentration of solutes on decreasing residual water depends on the initial chemical composition of the solution, where for nearly pure water, the bulk of the water is frozen over the 0 to –4°C range for more saline waters, c. 15-20% of residual water may occur over the –5 to –20°C range (Fig. 3-2a). For brackish to saline waters, hydrated salts can precipitate ($NaCl{\cdot}2H_2O$ at -23°C, $MgCl_2{\cdot}12H_20$ at –36°C), and the formation of these precipitates further reduces the amount of residual water (Fig. 3-2a).

The dependence of the initial chemical composition of the solutions on the amount of residual water is reflected in the $\delta^{18}O$ of the residual water (Fig 3-2b). For nearly pure water, the $\delta^{18}O$ of the residual water rapidly decreases as most of the water freezes over a narrow temperature range. For example, the freezing of nearly pure water with an initial $\delta^{18}O$ composition of –35‰ over the temperature range of 0 to –4°C will cause the $\delta^{18}O$ of the residual water to rapidly decrease to a value of –45‰ (a point when the residual water content is 0.05). In contrast, the freezing seawater with the same initial $\delta^{18}O$ composition over the temperature range of 0 to –4°C will cause the $\delta^{18}O$ of the residual water to decrease to –37‰ (a point when the residual water content is 0.85). A value of –45‰ in the residual water of sea water would only be reached following the precipitation of $NaCl{\cdot}2H_20$.

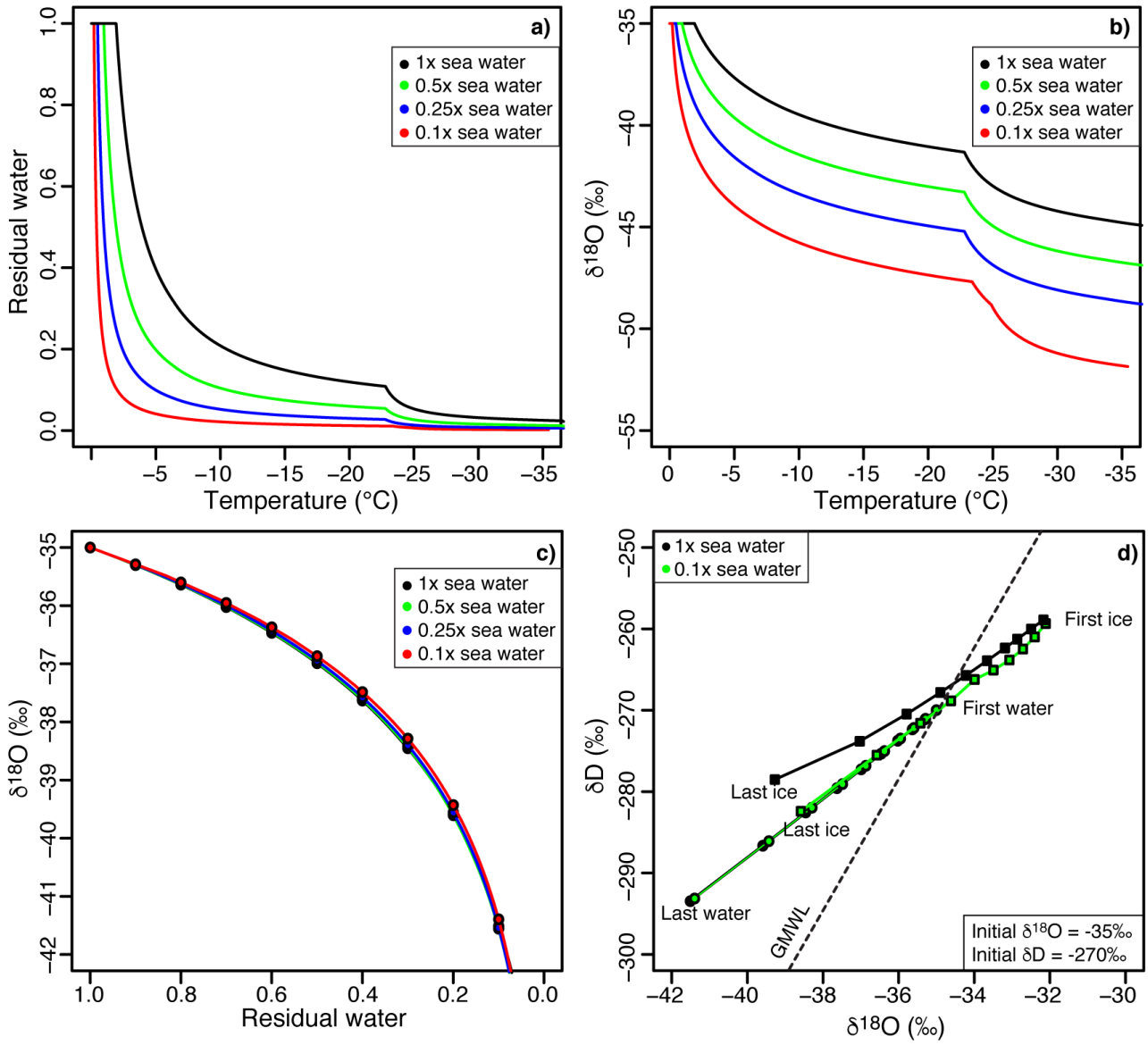

Figure 3-2: (a) Evolution of residual waters during freezing as a function of varied salinities; (b) Evolution of $\delta^{18}O$ during freezing, as a function of varied salinities; (c) Comparison of $\delta^{18}O$ and residual water values with varied salinities; and (d) δD-$\delta^{18}O$ evolution of water and ice during freezing, with 100% and 10% seawater salinity solutions.

These numerical simulations allow exploration of the effect of temperature on residual water content and its $\delta^{18}O$ composition during equilibrium freezing of solutions with varied salinities. However, exploring the evolution of $\delta^{18}O$ of residual water as a function of decreasing fractions of residual water revealed no significant differences between varying salinities solutions (Fig. 3-2c). As such, a Rayleigh-type isotope fractionation during equilibrium freezing of liquid

water with varied salinities using *FREEZCH5* shows that as freezing begins, the first ice to form will be enriched in $\delta^{18}O$ by about 3% (and about 20% in δD). Still, as freezing continues, the $\delta^{18}O$ composition of the ice formed progressively becomes depleted as the $\delta^{18}O$ composition of the residual water trends toward a lower value. The extent of $\delta^{18}O$ depletion of the residual water during freezing is constrained by the evolving eutectic temperature of the residual water and the ice-water interface temperature. Despite minor differences in the evolving δD-$\delta^{18}O$ of residual waters of varied salinities, a difference is observed in the δD-$\delta^{18}O$ composition of the forming ice following the precipitation of hydrated minerals (Fig. 3-2d).

The evolution of $\delta^{18}O$ in lake water and ice during equilibrium freezing was explored with *FREEZCH9* for various mixing scenarios (Fig. 3-3). The results are expressed in terms of residence times instead of annual loops to facilitate comparison. The results show that isotopic equilibrium (steady-state) in the lake water and ice is reached after more than three residence times for all mixing scenarios. However, the difference between the $\delta^{18}O$ of input water and that of isotopic equilibrium decreases under increasing mixing scenarios. For mixing scenarios < ~ 5%, the $\Delta\delta^{18}O$ input, and equilibrium approaches $\ln(\alpha^{18}O_{i\text{-}w})$; however, as the amount of annual mixing approaches 99%, the $\Delta\delta^{18}O$ input and equilibrium approaches 0.

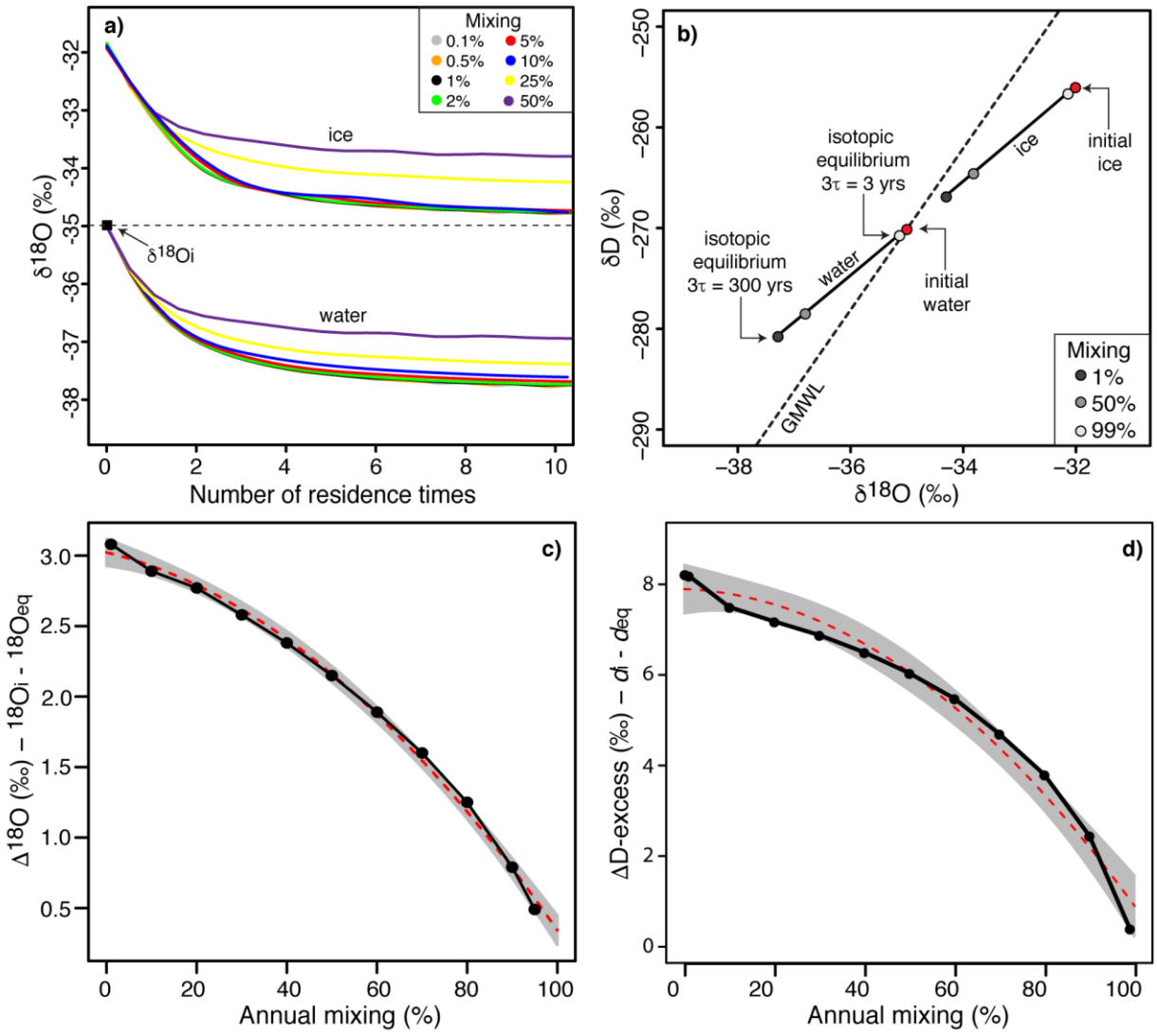

Figure 3-3: (a) $\delta^{18}O$ evolution of residual waters and forming ice for various mixing scenarios (initial δD-$\delta^{18}O$ values are respectively -270 and -35‰); (b) Final δD-$\delta^{18}O$ values of residual waters and ice as a function of the annual mixing rates of well-perennially sealed lacustrine basins; (c) Difference between the initial and steady-state $\delta^{18}O$ values of waters in a well-sealed perennially ice-covered lake as a function of the annual mixing rate of the latter; and (d) Difference between the initial and steady-state D-excess values of waters in a well-sealed perennially ice-covered lake as a function of the annual mixing rate of the latter.

3.3.2 Testing *FREEZCH9* with Lake Vostok, East Antarctic plateau

Lake Vostok is a sizeable subglacial lake located beneath c. 4 km of ice on the East Antarctic plateau (Lyons et al., 2016). The lake is roughly 250 km long and 80 km wide, has a surface area of ~ 13,000 km^2 and a water volume of 4658 to 6350 km^3 depending on the estimation method (e.g., Studinger et al., 2004; Siegert et al., 2011; Li et al., 2019). Lake Vostok is recharged from the melting of the overlying East Antarctic Ice Sheet in the northern basin (incoming rate of c. 4 cm yr^{-1}) and loses ice via ice accretion at the ice-water interface in the southern and central basins (freezing rate of c. 2 cm yr^{-1}) (Siegert et al., 2000; Studinger et al., 2004; Bell et al., 2002). The annual water input is estimated at 0.19 km^3 yr^{-1}, which translates to a residence time of waters equivalent to *c.* 28,000 years or a yearly mixing rate of *c.* 0.0037% (Royston-Bishop et al., 2004).

Based on the average of $\delta^{18}O$ time-series during the last four glacial cycles in the Dome B record, Royston-Bishop et al. (2004) first estimated the δD-$\delta^{18}O$ of input water to Lake Vostok to be –442.2 and –56.7‰, respectively. The δD-$\delta^{18}O$ of Lake Vostok was later estimated from water frozen in the borehole following drilling to the water column and from the δD- $\delta^{18}O$ composition of the overlying accreted ice (δD = –442.4‰, $\delta^{18}O$ = –56.2‰, D-excess = 7.2‰) (Ekaykin et al., 2016). Based on a closed-system isotopic equilibrium model, Ekaykin et al. (2016) estimated the average δD and $\delta^{18}O$ composition of the water column to be –455±1‰ and –59.0±0.3‰, respectively (D-excess of 17±1‰).

FREEZCH9 was used with input parameters defined as 0.0037% annual mixing (e.g., Royston-Bishop et al., 2004), the average major ions concentrations in the Vostok ice core which extends to 160 kyr BP (Legrand et al., 1988), and the equilibrium factors ($\alpha_{i\text{-}w}$) of O'Neil (1968) and Suzuoki & Kimura (1973) also corrected for initial isotope composition of water. When using the δD-$\delta^{18}O$ of the input water estimated by Royston-Bishop et al. (2004) (–442.2 and –56.7‰, respectively), the model does not perfectly match the measurements in the accreted ice (Fig. 3-4). However, if we used the $\alpha_{i\text{-}w}$ corrected for initial isotope composition of water and adjusting the δD-$\delta^{18}O$ of input water to match the measurements in the accreted ice, we find that input values for δD-$\delta^{18}O$ of –443.5 and –56.4‰, respectively. With 0.0037% annual mixing, the time for the water column to reach isotopic equilibrium is in the order of *c.* 2-3 residence times and the δD-$\delta^{18}O$ of Lake Vostok is estimated to be –453.5 and –59.1‰, nearly identical to the values reported by Ekaykin et al. (2016) (–455±1‰ and –59.0±0.3‰).

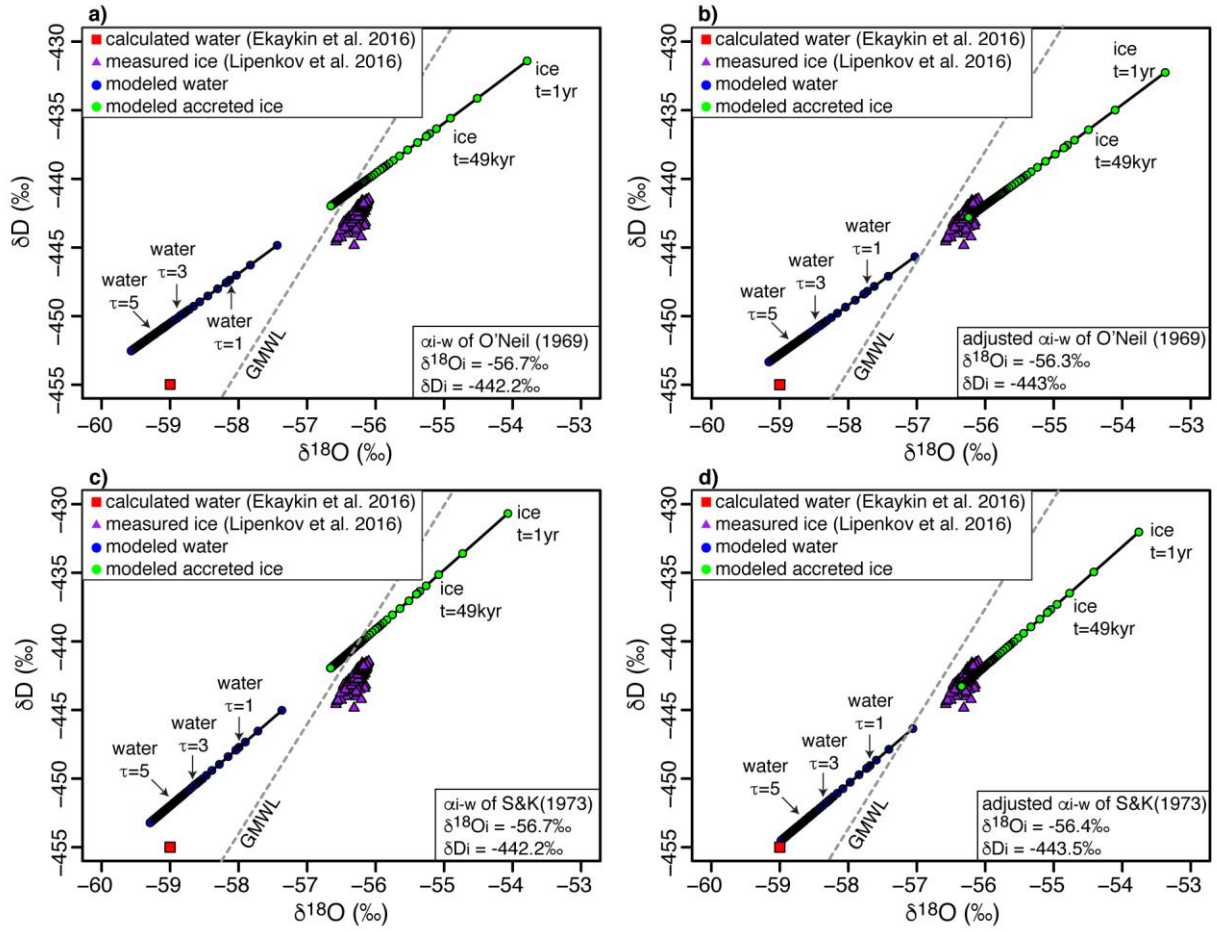

Figure 3-4: Modeled stable water isotope evolution of Lake Vostok's water and forming ice using (a) the initial δD-$\delta^{18}O$ input values employed by Royston-Bishop et al. (2004) with O'Neil's (1968) and (c) Suzuoki & Kimura's (1973) fractionation factors. (b) and (d) respectively show the modeled stable water isotope evolution of Lake Vostok water and forming ice using O'Neil's (1968) and Suzuoki & Kimura's (1973) fractionation factors based on adjusted δD-^{18}O inputs (to fit accreted lake ice values measured by Lipenkov et al. (2016)).

3.3.3 *FREEZCH9* and Lake Untersee, Dronning Maud Land, Antarctica

Lake Untersee is a perennially ice-covered lake located in the Gruber Mountains of central Dronning Maud Land, approximately 90 km southeast of the Schirmacher Oasis. The 6.5 km long and 1.5 km wide lake (surface area = 8.73 km^2), with a water volume of 5.21×10^8 m^3, is located in a closed-basin dammed at its northern end by the Anuchin Glacier (Faucher et al., 2019). Lake Untersee has two sub-basins: 1) a large well-mixed oxic basin at the northern and central section with a maximum depth of 169 m; and 2) a shallower basin at its southern section with a maximum depth of 100 m depth (Wand et al. 1997; Andersen et al., 2011). Formation of moats on its surface, which is expected with a local mean annual air temperature (MAAT) of 9.5±0.7°C (2008-2017 period) is restricted by high ablation rates (61±11 cm yr^{-1}) (Faucher et al., 2019) which significantly cools its ice cover (e.g., Hoffman et al., 2008). The lake is losing annually 4.90±0.8 x 10^6 m^3 of water (or 0.94±0.17% of total lake water volume) (Faucher et al., 2019). To maintain its water balance, Lake Untersee receives an equal volume of inflow sourced from the subaqueous terminus melting of the Anuchin Glacier (40-45% of annual contribution) and subglacial meltwater and/or from groundwater (55-60% of yearly input) (Faucher et al., 2019).

The δD-$\delta^{18}O$ composition of the oxic water column narrowly ranges from –288.4 to –287.3‰ and from –37.9 to –37.6‰, respectively (Fig. 3-5). With D-excess ranging from 12.8 to 14.7‰, the water samples are distributed above the GMWL in a δD-$\delta^{18}O$ plot (Fig. 3-5). The ice cover sampled in the central sector of Untersee (core #1) has δD-$\delta^{18}O$ values varying from –278.6 to –273.0‰ and from –35.5 to –34.2‰, respectively, with D-excess ranging from –1.3 to 6.9‰. The δD-$\delta^{18}O$ values in the ice cover at the southern section of the lake (core #2) showed a similar range (δD: –279.5 and –268.5‰; $\delta^{18}O$: –36.2 to –35.6‰; D-excess: –8.8 to 11.4‰). In a δD-$\delta^{18}O$ scatter plot, the ice cover data are distributed below the GMWL.

FREEZCH9 was used with input parameters defined as 1% annual mixing (Faucher et al., 2019), $\alpha_{i\text{-}w}$ of O'Neil's (1968) and Suzuoki and Kimura's (1973) corrected for initial isotope composition of water, and the δD-$\delta^{18}O$ of input water were adjusted to match the measurements in the oxic water column. The input water's initial chemistry was based on data from a nearby shallow firn core (Isaksson et al., 1996). The modeling indicates that the measured δD-$\delta^{18}O$ values in the water column is in isotopic equilibrium with initial lake water δD-$\delta^{18}O$ values of –275‰

and –35‰, respectively. With 1% annual mixing, the time to reach isotopic equilibrium in the water column is in the order of c. 300-500 years.

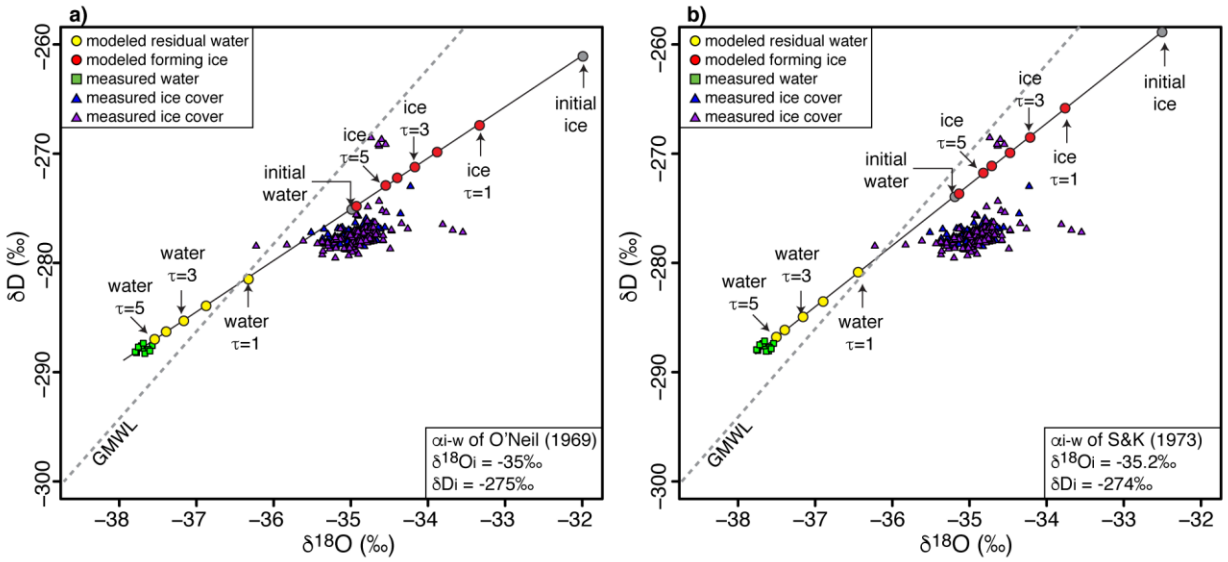

Figure 3-5: Modeled stable water isotope evolution of Lake Untersee's water and forming ice using (a) O'Neil's (1968) and (b) Suzuoki & Kimura's (1973) fractionation factors.

3.4 Discussion

3.4.1 δD-δ^{18}O composition of input waters to Lake Untersee

Based on a hydrological and energy mass balance, it was suggested that two sources recharge well-sealed perennially ice-covered Lake Untersee: subaqueous terminus melting of the Anuchin Glacier (40-45% of annual contribution) and from subglacial meltwater and/or from groundwater (55-60% of annual input) (Faucher et al., 2019). The *FREEZCH9* modeling using 1% annual mixing (or recharge) suggests that the δ^{18}O composition of Lake Untersee (–37.9 to –37.6‰) is in equilibrium with source waters having an average δ^{18}O composition of *c.* –35‰. The δ^{18}O composition of the contribution from the subaqueous melting of the Anuchin Glacier can be estimated from the thickness of the glacier at the lake-glacier interface (c. 160 m) and the age-depth relation from the Dome Fuji, Dome C, and Taylor Dome ice cores (Uemera et al., 2012; Lorius et al., 1979; Steig et al., 2000). The age of the ice in the uppermost c. 160 m at these three sites varies from 0 to 3000-4500 years (Fig. 3-6A); assuming a similar age-depth relation applies for the Dronning Maud Land region, the average age of the subaqueous meltwater recharging Lake Untersee is estimated at c.1800 years. The δ^{18}O composition of a series of shallow ice cores

(uppermost 50 cm) of a 3.2 km long transect on both sides of the medial moraine on the Anuchin Glacier ranged from –36.4 to –30.8‰ (average of –34.2±1‰). Given that over the past 3000-5000 years, the $\delta^{18}O$ time-series of deep ice cores showed only small fluctuations (in the order of 0.5‰; Fig. 3-6b), the average $\delta^{18}O$ of near-surface ice of the Anuchin Glacier likely reflects that of the subaqueous melting of the Anuchin Glacier over a 160 m thick section (or c. 1800 years). Therefore, the $\delta^{18}O$ of Lake Untersee water is in equilibrium with subaqueous melting of the Anuchin Glacier having an average $\delta^{18}O$ composition of –34.2±1‰ and a two-component mixing model indicates that the subglacial meltwater has an average $\delta^{18}O$ composition of–35.8±1‰ (δD: –280‰; D-excess: 6‰). Considering that the $\Delta\delta^{18}O$ of last glacial maximum to Holocene age glacial ice is in the order of 6-8‰, the subglacial meltwater recharging Lake Untersee is likely of similar age (late Holocene) to that of the Anuchin Glacier. It does not reflect subglacial meltwater sourced during the last glacial period or far in the Antarctic interior.

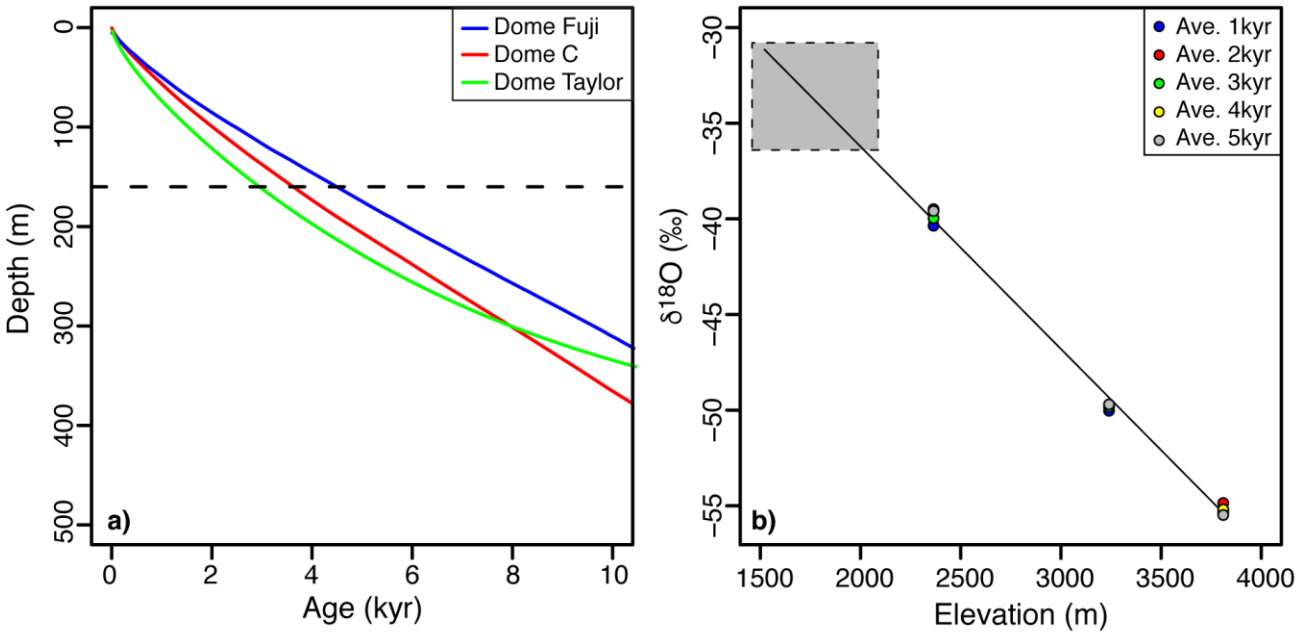

Figure 3-6: (a) Age-Depth relationship for the Dome Fuji (Uemera et al., 2012), Dome C (Lorius et al., 1979), and Taylor Dome ice cores (Steig et al., 2000). The dotted line indicates the thickness of the Anuchin Glacier at the lake glacier interface. (b) Elevation of the ice field feeding the Anuchin Glacier based on the average $\delta^{18}O$ ratios in the Dome Fuji (3810 m.a.s.l.), Dome C (3240 m.a.s.l.), and Taylor Dome (2365 m.a.s.l.) ice cores during the last 5,000 years.

The oxic water column of Lake Untersee is well-mixed due to buoyancy-driven convection, which allows for effective mixing within a time scale of one month (Steel et al., 2015). Based on the lake's water volume, its surface area, and ablation rate, the residence time of water in the lake was estimated at c. 100 years (Faucher et al., 2019), and $\delta^{18}O$ steady-state is achieved within 300-500 years. Considering that the waters in Lake Untersee plot above the GMWL in a δD-$\delta^{18}O$ plot with D-excess of 14‰, this suggests that for at least the past 500 years: 1) subaqueous melting of the Anuchin Glacier and subglacial meltwater were the only sources of recharge to the lake (i.e., no recharge from surface streams with an evaporated $\delta^{18}O$ signature); 2) the δD-$\delta^{18}O$ composition of the subglacial meltwater is likely distributed on the GMWL and does not reflect a subglacial meltwater that has evolved under cryo-freezing; and 3) the ice cover has remained well-sealed to atmospheric exchange for at least the past 500 years (i.e., no evaporative loss of the water column).

3.4.2 Application of *FREEZCH9*

This study developed an isotope-augmented version of *FREZCHEM* (*FREEZCH5*) and made it recursive (*FREEZCH9*) to predict the δD-$\delta^{18}O$ evolution of well-sealed perennially ice-covered lakes and subglacial lakes. The model accounts for changes in the ice-water isotope fractionation factor as freezing increases the salinity of the residual water and, to maintain the lake volume in equilibrium, mixes some input water of fixed chemistry and δD-$\delta^{18}O$ composition to the residual water in the lake. *FREEZCH9* allows prediction of the isotopic steady-state of the lake water and ice cover. Lerman (1979) suggested that the δD-$\delta^{18}O$ steady-state of freezing lakes is reached after more than three residence times. Although the modeling reaches the same condition, the δD-$\delta^{18}O$ composition of freezing lakes is not only determined by the residence time of water but also by volume of ice that freezes annually which determines the volume of water is added and mixes in the lake. For mixing scenarios < ~ 5%, the difference between $\delta^{18}O$ input and equilibrium in the lake water approaches $\ln(\alpha^{18}O_{i\text{-}w})$; however, as the amount of annual mixing approaches 99%, the $\delta^{18}O$ input and equilibrium approaches 0. In terms of deviation from the GMWL, the difference between D-excess of input and equilibrium in the lake water approaches 8‰, and is reduced to near 0 as the amount of annual mixing approaches 99% (Fig. 3-3d).

FREEZCH9 allows to test for the effects of input water with differing isotopic signatures (i.e., evaporated water, meteoric water, cryo-freezing water) on the distribution of lake water isotopic composition in δD-$\delta^{18}O$ space (Fig. 3-7). Horita (2009) suggested that lakes with δD-$\delta^{18}O$

composition plotting above the GMWL are reflective of being affected by the freezing process. The residual waters in well-sealed ice-covered lakes and subglacial lakes that are recharged by meteoric-like waters (i.e., plotting along the GMWL) should plot above the GMWL, regardless of their annual mixing rate. The extent to which the D-excess of these lakes will deviate from the GMWL (i.e., D-excess) will be a function of their annual mixing rate. This is the case for Lake Vostok (0.0037% annual mixing) where the $\delta^{18}O$ of recharge water (–56.7‰) approximates that in the accreted ice (–56.2‰) and the water column is depleted by c. 3‰ (–59.0±0.3‰) but with D-excess (17±1‰) *c.* 10 ‰ higher than the input water (7.2‰).

In the case of well-sealed perennially ice-covered lakes or subglacial lakes recharged by surface or soil waters (e.g., ephemeral streams) and whose δD-$\delta^{18}O$ composition is shifted below the GMWL due to evaporation, the δD-$\delta^{18}O$ of the water column may not be shifted above the GMWL following the freezing process (Fig. 3-7). The latter would be dependent on the extent of evaporation and mixing conditions in the lake.

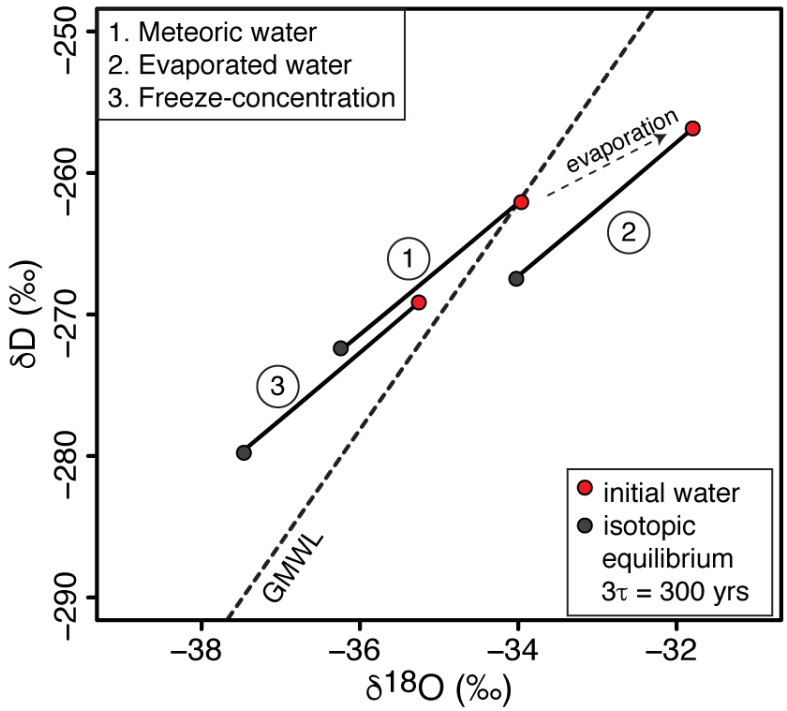

Figure 3-7: Effects of freeze concentration (i.e., $\delta^{18}O$ depletion of residual waters) and evaporation (i.e., kinetic $\delta^{18}O$ enrichment) on the location of initial (red) and steady-state (black) δD-$\delta^{18}O$ values of residual waters in well-sealed ice-covered lakes and their deviation above and below the GMWL. The mixing rate for this example is 1%; steady-state is reached within c. 300 years.

Finally, in the case of well-sealed perennially ice-covered lakes or subglacial lakes recharged by subglacial waters that have experienced freeze-concentration, the δD-δ^{18}O of these lakes will strongly deviate above the GMWL for any mixing scenarios. That is because the recharge waters will have δD-δ^{18}O composition plotting above the GMWL, and the freezing process taking place in the lake will shift the δD-δ^{18}O of the lake water further above the GMWL (but within limits shown in Fig. 3-3c,d). Such lakes may have D-excess that evolved to values greater than 17‰. There might be a regional groundwater system beneath the Antarctic Ice Sheet, as inferred for Lake Bonney in the McMurdo Dry Valleys from airborne transient electromagnetic sensor (i.e., Mikucki et al., 2015). If this regional groundwater system includes circulation through subglacial lakes, this isotopic signature could be used to infer the source of water (mainly from basal melting or multiple freeze-concentration).

3.5 Conclusion

In this study, we developed an isotope-augmented version of *FREZCHEM* (*FREEZCH5*). We made it recursive (*FREEZCH9*) to predict the δD-δ^{18}O evolution of two well-sealed perennially ice-covered lakes (Lake Untersee and Vostok). The following conclusions can be drawn from our results:

1) Unlike previous models, our modified recursive version of *FREEZCHEM* (*FREEZCH9*) takes into consideration the combined effects of residual water mixing with incoming waters and evolving geochemistry (i.e., soluble salt increases) on the stable water isotopic signal of sealed polar lacustrine environments; it is a reliable tool to estimate the time taken for residual waters to reach δD-δ^{18}O equilibrium.

2) When compared, the δ^{18}O composition of residual waters (modeled with *FREEZCH9*) and measured δ^{18}O of well-sealed ice-covered lake's input(s) can inform on the annual turnover rate of the latter.

3) Our stable water isotope evolution modeling of Lake Vostok suggest that the δD-δ^{18}O composition of its liquid water should be close to –453.5‰ and –59.1‰, respectively; this validates the isotopic calculations done by Ekaykin et al. (2016) for the lake's upper water column isotopic composition (estimated at -455‰ and -59‰ for δD-δ^{18}O, respectively).

4) The distribution of lake water isotopic composition in δD- δ^{18}O space depends on the

effects of input water (i.e., evaporated water, meteoric water, cryo-freezing water) having different D-excess signatures. Hence, *FREEZCH9* might prove to be useful in determining if subglacial lakes fully or partially recharge the hypothetical groundwater systems of the McMurdo Dry Valleys (i.e., Mikucki et al., 2015).

5) Lake Untersee's water inputs are partially derived from the subaqueous terminal melting of the Anuchin Glacier and subglacial meltwater and/or groundwater infiltrations. Our study shows that the lake's water inputs are of Holocene age. The δD-$\delta^{18}O$ of the subaqueous terminus melting of the Anuchin Glacier is estimated at -34.2 ‰, indicating that the isotopic composition of subglacial meltwater and/or groundwater infiltrations are very similar to the latter (δD-$\delta^{18}O$ values of c. -36 ‰). Stable water isotope from its well-mixed oxic water column also indicates that for the last 500 years, the lake has not been fed by surface waters (only by subaqueous terminus melting of the Anuchin Glacier and from subglacial and/or meltwater contributions). It has not been in direct contact with the atmosphere and was not fed by previously freeze-concentrated waters (i.e., from a subglacial lake).

3.6 References

Bell, R. E., Studinger, M., Tikku, A. A., Clarke, G. K., Gunter, M. M. & Meertens, C. (2002). Origin and fate of Lake Vostok water frozen to the base of the East Antarctic ice sheet. *Nature* 416, 307–310.

Bird, M. I., Chivas, A. R., Radnell, C. J. & Burton, H. R. (1991). Sedimentological and stable-isotope evolution of lakes in the Vestfold Hills, Antarctica. *Palaeogeogr. Palaeoclimatol. Palaeoecol.* 84(1–4), 109–130.

Burton, J. A., Prim, R. C., & Slichter, W. P. (1953). The Distribution of Solute in Crystals Grown from the Melt. Part I. Theoretical. *J. Chem. Phys*. 21(11), 1987–1991.

Dansgaard, W. (1964). Stable isotopes in precipitation. *Tellus* 16, 436-468.

Dugan, H. A., Doran, P. T., Wagner, B., Kenig, F., Fritsen, C. H., Arcone, S. A., Kuhn, E., Ostrom, N. E., Warnock, J. P. & Murray, A. E. (2015). Stratigraphy of Lake Vida, Antarctica: hydrologic implications of 27 m of ice. *The Cryosphere* 9, 439–450.

Ekaykin, A. A., Lipenkov, V. Y., Petit, J. R., Johnsen, S., Jouzel, J., & Masson-Delmotte, V. (2010). Insights into hydrological regime of Lake Vostok from differential behavior of deuterium and oxygen-18 in accreted ice, *J. Geophys. Res.*115, C05003.

Ekaykin, A. A., Lipenkov, V. Y., Kozachek, A. V. & Vladimirova, D. O. (2016). Stable water isotopic composition of the Antarctic subglacial Lake Vostok: Implications for understanding the lake's hydrology. *Isot. Environ. Health Stud. 52,* 1–9.

Fisher, D. A., Lacelle, D., Pollard, W. & Faucher, B. (2019). A model for stable isotopes of residual water and ice in permafrost using arbitrary water chemistries and soil specific empirical residual water functions; comparisons to field data. *Permafr. Periglac. Process* 32(2), 248-260.

Faucher, B., Lacelle, D., Fisher, D. A., Andersen, D. T., & McKay, C. P. (2019). Energy and water mass balance of Lake Untersee and its perennial ice cover, east Antarctica. *Antarctic Science* 31(5), 271-285.

Gibson, J. A. E. (1999). The meromictic lakes and stratified marine basins of the Vestfold Hills, East Antarctica. *Antarc Sci*. 11, 175–192.

Gooseff, M. N., Lyons, W. B., McKnight, D. M., Vaughn, B. H., Fountain, A. G. & Dowling, C. (2006). A stable isotopic investigation of a polar desert hydrologic system, McMurdo Dry Valleys, Antarctica. *Arct. Antarct. Alp. Res.* 38, 60–71.

Hoffman, M. J., Fountain, A. G. & Liston, G. E. (2008). Surface energy balance and melt thresholds over 11 years at Taylor Glacier, Antarctica. *JGR*. 113(F4).

Horita, J. (2009). Isotopic evolution of saline lakes in the low-latitude and polar regions. *Aquat. Geochem.* 15, 43–69.

Isaksson, E., Karlen, W., Gundestrup, N., Mayewski, P., Whitlow, S. & Twickler, M. (1996). A century of accumulation and temperature changes in Dronning Maud Land, Antarctica. *J. Geophys. Res.* 101(D3), 7085–7094.

Jeffries, M. O., Krouse, H. R., Shakur, M. A. & Harris, S. A. (1984). Isotope geochemistry of stratified Lake' A', Ellesmere Island, N.W.T., *Canada. Can. J. Earth Sci*. 21(9), 1008–1017.

Jouzel, J. & Souchez, R. A. (1982). Melting-refreezing at the glacier sole and the isotopic composition of the ice. *J. Glaciol.* 28(98), 35-42.

Killawee, J. A., Fairchild, I. J., Tison, J. L., Janssens, L. & Lorrain, R. (1998). Segregation of solutes and gases in experimental freezing of dilute solutions: implications for natural glacial systems. *Geochim. Cosmochim. Acta*. 62, 3637–3655.

Lacelle, D. (2011). On the $\delta^{18}O$, δD and D-excess relation in meteoric precipitation and during equilibrium freezing: theoretical approach and field examples. *Permafr. Periglac. Process.* 22, 13–25.

Legrand, M., Lorius, C., Barkov, N. I. & Petrov, V. N. (1988). Vostok (Antarctica) ice core: Atmospheric chemistry changes over the last climatic cycle (160,000 years), *Atmos. Environ.* 22(2), 317-331.

Lerman, A. (1979). *Geochemical processes: water and sediment environments*. New York, Wiley-Interscience.

Li, Y., Lu, Y., Zhang, Z. Z., Shi, H. & Xi, H. (2019). Characterizing three-dimensional features of Antarctic subglacial lakes from the inversion of hydraulic potential—Lake Vostok as a case study. *Adv. Polar Sci.* 30(1), 70-75.

Lipenkov, V. Y., Ekaykin, A. A., Polyakova, E. V. & Raynaud, D. (2016). Characterization of subglacial Lake Vostok as seen from physical and isotope properties of accreted ice. *Philos Trans A Math Phys. Eng. Sci*. 374(2059).

Lorius, C., Merlivat, L., Jouzel, J. & Pourchet, M. (1979). A 30,000 yr isotope climatic record from Antarctic ice. *Nature* 280, 644-648.

Lyons, W. B. & Finlay, J. C. (2008). Biogeochemical processes in high-latitude lakes and rivers. *In Polar Lakes and Rivers: Limnology of Arctic and Antarctic Aquatic Ecosystems*, Vincent WF, Laybourn-Parry J (eds). Oxford University Press: New York; 137–156.

Lyons, W. B., Welch, K. A., Welch, S. A., Camacho, A., Rochera, C., Michaud, L., de Wit, R. & Carey, A. E. (2013). Geochemistry of streams from Byers Peninsula, Livingston Island. *Antarc. Sci.* 25, 181-190.

Lyons, W. B., Welch, K. A., Priscu, J. C., Tranter, M. & Royston-Bishop, G. (2016): Source of Lake Vostok cations constrained with strontium isotopes. *Front. Earth Sci*. 4, 78.

Marion, G. M. & Kargel, J. S. (2008). Cold Aqueous Planetary Geochemistry with FREZCHEM: From Modeling to the Search for Life at the Limits. Springer, Heidelberg 251 pp.

Marion, G. M., Mironenko, M. V. & Roberts, M. W. (2010). FREZCHEM: A geochemical model for cold aqueous solutions. *Comput. Geosci.* 36, 10–15.

Matsubaya, O., Sakai, H., Torii, T., Burton, H. & Knowles, K. (1979). Antarctic saline lakes stable isotopic ratios, chemical compositions and evolution. *Geochim. Cosmochim. Acta*. 43, 7–25.

McKay, C. P., Clow, G., Wharton, R. A. Jr. & Squyres, S. W. (1985). Thickness of ice on perennially frozen lakes. *Nature* 313, 561-562.

Mikucki, G., Auken, E., Tulaczyk, S., Virginia, R. A., Schamper, C., Sørensen, K. I., Doran, P. T., Dugan, H. & Foley, N. (2015). Deep groundwater and potential subsurface habitats beneath an Antarctic Dry Valley. *Nat. Commun*. 6, 6831.

Miller, L. G. & Aiken, G. R. (1996). Effects of glacial meltwater inflows and moat freezing on mixing in an ice-covered Antarctic lake as interpreted from stable isotope and tritium distributions. *Limnol. Oceanogr*. 41(5), 966-976.

Morgan, F., Barker, G., Briggs, C., Price, R., & Keys, H. (2007). Environmental Domains Analysis for the Antarctic Continent: Version 2.0 Final report. Landcare Research Report LC0708/055 for Antarctica New Zealand and Department of Conservation. Lincoln, NZ. 89p.https://www.landcareresearch.co.nz/publications/researchpubs/eda_v2_final_report.pdf and https://www.ats.aq/documents/recatt/Att408_e.pdf

O'Neil, J. R. (1968). Hydrogen and oxygen isotope fractionation between ice and water. *J. Phys. Chem*. 72, 3683-3684.

Petrenko, V. F. & Whitworth, R. W. (1999). *Physics of Ice* (Oxford: Oxford University Press).

Priscu, J. C. (Ed.) (1998). Ecosystem dynamics in a Polar Desert: The McMurdo Dry Valleys, Antarctica. *Antarctic Research Series* 72, 369p. American Geophysical Union, Washington DC.

Priscu, J. C. & Foreman, C. M. (2009). *Lakes of Antarctica*. In: Gene E. Likens, (Editor) Encyclopedia of Inland Waters. 2, 555-566. Oxford: Elsevier.

Richter, W. & Strauch, G. (1983). Deuterium and O-18 variations in lakes of the Schirmacher Oasis (East-Antarctica). *Isotopenpraxis*. 19(5), 145–153.

Royston-Bishop, G., Tranter, M., Siegert, M. J., Lee, V. & Bates, P. D. (2004). Is Vostok lake in steady state? *Ann. Glaciol.* 39, 490–494.

Santibáñez, P. A., Michaud, A. B., Vick-Majors, T. J., D'Andrilli, J., Chiuchiolo, A., Hand, K. P. & Priscu, J. C. (2019). Differential incorporation of bacteria, organic matter, and inorganic ions into lake ice during ice formation. *JGR Biogeosciences* 124, 585– 600.

Siegert, M. J., Kwok, R., Mayer, C. & Hubbard, B. (2000). Water exchange between the subglacial Lake Vostok and the overlying ice sheet. *Nature* 403, 643–646.

Siegert, M. J., Popov, S. & Studinger, M. (2011). Vostok Subglacial Lake: a review of geophysical data regarding its discovery and topographic setting, in *Antarctic Subglacial Aquatic Environments*, eds M.J. Siegert, M.C. Kennicutt II and R.A. Bindschadler (Washington, DC: American Geophysical Union), 45–60.

Sofer, Z. & Gat, J. R. (1972). Activities and concentrations of oxygen-I8 in concentrated aqueous salt solutions: Analytical and geophysical implications. *Earth Planet. Sci. Letf.* 15, 232-238.

Sofer, Z. & Gat, J. R. (1975). The isotope composition of evaporating brines: Effect of the isotopic activity ratio in saline solutions. *Earth Planet. Sci. Lett.* 26, 179-186.

Souchez, R. A. & Jouzel, J. (1984). On the isotopic composition in delta D and delta18O of water and ice during freezing. *J. Glaciol*. 30, 369–372.

Souchez, R., Petit, J., Jouzel, J., de Angelis, M. & Tison, J. (2004). Reassesing Lake Vostok's behaviour from existing and new ice core data. *Earth Planet. Sci. Lett.* 217(1–2), 163–170.

Steel, H. C. B., McKay, C. P. & Andersen, D. T. (2015). Modeling circulation and seasonal fluctuations in perennially ice-covered and ice-walled Lake Untersee, Antarctica. *Limnol. Oceanogr*. 60, 1139–1155.

Steig, E. J., Morse, D. L., Waddington, E. D., Stuiver, M., Grootes, P. M., Mayewski, P. A., Twickler, M. S. & Whitlow, S. I. (2000). Wisconsinan and Holocene climate from an ice core at Taylor Dome, western Ross Embayment, *Antarctica. Geogr. Ann.* 82, 213-225.

Stewart, M. K. & Friedman, I. (1975). Deuterium fractionation between aqueous salt solutions and water vapor. *J. Geophys. Res.* 80, 3812-3818.

Studinger, M., Bell, R. E., Buck, R. W., Karner, G. D. & Blankenship, D. D. (2004). Sub-ice geology inland of the Transantarctic Mountains in light of new aerogeophysical data. *Earth Planet Sc. Lett.* 20(3), 391-408.

Suzuoki, T. & Kimura, T. (1973). D/H and 18O/16O fractionation in ice-water system. *Mass Spectrom*. 21, 229-233.

Terwilliger, K. P. & Dizio, S. F. (1970). Salt rejection phenomena in the freezing of saline solutions, *Chem. Engineering Sci.* 25, 1331-1349.

Touzeau, A., Landais, A., Stenni, B., Uemura, R., Fukui, K., Fujita, S., Guilbaud, S., Ekaykin, A., Casado, M., Barkan, E., Luz, B., Magand, O., Teste, G., Le Meur, E., Baroni, M., Savarino, J., Bourgeois, I. & Risi, C. (2016). Acquisition of isotopic composition for surface snow in East Antarctica and the links to climatic parameters, *The Cryosphere* 10, 837-852.

Uemura, R., Masson-Delmotte, V., Jouzel, J., Landais, A., Motoyama, H. & Stenni, B. (2012). Ranges of moisture-source temperature estimated from Antarctic ice cores stable isotope records over glacial–interglacial cycles, *Clim. Past.* 8, 1109–1125.

Vincent, W. F., Hobbie, J. E. & Laybourn-Parry, J. (2008). Introduction to the limnology of high-latitude lake and river ecosystems. In Vincent, W.F. and J. Laybourn-Parry, eds. *Polar lakes and rivers: limnology of Arctic and Antarctic aquatic ecosystems*. Oxford, UK, Oxford University Press, 1–23.

Wand, U., Schwarz, G., Brüggemann, E. & Bräuer, K. (1997). Evidence for physical and chemical stratification in Lake Untersee (central Dronning Maud Land, East Antarctica). *Antarctic Science*. 9(1), 43-45.

Wand, U., Samarkin, V. A., Nitzsche, H. M. & Hubberten, H. W. (2006). Biogeochemistry of methane in the permanently ice-covered Lake Untersee, central Dronning Maud Land, East Antarctica. *Limnol. Oceanogr.* 51, 1180–1194.

Wang, J. H., Robinson, C. B. & Edelman, I.S. (1953). Self-diffusion and structure of liquid water, III, Measurement of the self-diffusion of liquid water with ^{2}H, ^{3}H, and ^{18}O as tracers, *J. Am. Chern. Soc.* 75, 466-470.

Weisleitner, K., Perras, A., Moissl-Eichinger, C., Andersen, D. T. & Sattler, B. (2019). Source Environments of the Microbiome in Perennially Ice-covered Lake Untersee, Antarctica. *Front. Microbiol.* 10, 1019.

Wilson, A. T. & Wellman, H. W. (1962). Lake Vanda: An Antarctic Lake: Lake Vanda as a Solar Energy Trap. *Nature* 196: 1171–1173.

Wingham, D. J., Siegert, M. J., Shepherd, A. & Muir, A. S. (2006). Rapid discharge connects Antarctic subglacial lakes. *Nature* 440(7087), 1033–1036.

Wright, A. & Siegert, M. A. (2012). Fourth inventory of Antarctic subglacial lakes. *Antarctic Science* 24, 659–664.

CHAPTER 4: GLACIAL LAKE OUTBURST FLOODS SUSTAIN MICROBIAL ECOSYSTEM IN LAKE UNTERSEE, ANTARCTICA

Abstract

Antarctica hosts several oligotrophic ice-covered lakes with benthic phototrophic mats, often dominated by cyanobacteria, accounting for most of the biomass within the lake. Climate-driven changes to their ice cover and peripheral glacial systems impacts ecosystem structure and function within these lakes. Here, we show that periodic glacial lake outburst floods (GLOFs) can replenish CO_2-depleted lakes with carbon, helping to maintain primary production within the benthic microbial mats. Over the past several hundred years, Lake Untersee has been in a hydrological steady-state with poorly buffered, high pH water and inorganic and organic carbon, amongst the lowest reported for Antarctic lakes. However, in mid-January 2019, Untersee experienced a GLOF that increased the water level by 2 m (1.75×10^7 m^3), modifying its water chemistry and inorganic carbon load. High-resolution grain size and carbon isotope analyses of the microbial mats suggest that GLOFs occurred periodically over the Holocene, explaining the observed carbon balance within this ecosystem. This indicates that flooding events such as this may also provide a biological stimulus to other CO_2-depleted Antarctic lacustrine and coastal ecosystems around the continent.

4.1 Introduction

Perennially ice-covered lakes are found in many Antarctica regions, such as the McMurdo Dry Valleys (MDV), Bunger Hills, Vestfold Hills, Larsemann Hills, Schirmacher Oasis, and Soya Coast (Bormann, 1995; Matsumoto et al., 1992; Perriss & Laybourn-Parry, 1997). These lakes are typically recharged during the summer by the surface inflow of glacial meltwater from the surrounding catchment. Many of them support extensive benthic microbial communities, with primary productivity being limited by light attenuation through the perennial ice cover and by the availability of nutrients (Gibson et al., 2006; Jungblut et al., 2010; McKnight et al., 2004).

In remote Antarctica, GLOFs are rarely observed. Still, some have been described in recent years in the Larsemann Hills region, where ice-dammed perennially ice-covered lakes drained catastrophically (Pryakhina et al., 2020); however, their impacts on water chemistry and benthic microbial ecosystems were not described. Here, we provide evidence from Lake Untersee, a large ultra-oligotrophic, perennially ice-covered lake in East Antarctica, that periodic GLOFs can replenish nutrients and help maintain the long-term primary production of benthic phototrophic communities.

Lake Untersee is a perennially ice-covered lake in Dronning Maud Land that is characteristically different from other lakes in Antarctica. The closed-basin lake formed at c. 12-10 ka BP following the Anuchin Glacier retreat and arrived at its current configuration near 7-6 ka BP (Bormann, 1995; Schwab, 1998). The lake is in hydrological steady-state, recharged by subaqueous melting of glacial ice and subglacial meltwater (Faucher et al., 2019), and remains well-sealed to the atmosphere with no open water along the margin that would enhance gas exchanges or increase sunlight penetration (Andersen et al., 2015; Faucher et al., 2020). The lake has a Na(Ca)-SO_4 geochemical facies with high pH (10.6) that reflects a heritage of recharge from glacial meltwater, with minor contributions of Ca^{2+}-Na^{+} solutes from *in situ* weathering of plagioclase and aluminosilicate minerals (Marsh et al., 2020). The total inorganic carbon (TIC) concentration in the lake is one to three orders of magnitude lower than what has been reported for the ice-covered lakes in the MDV (Lyons et al., 2013; Neumann et al., 2004a). Unlike most other lakes in Antarctica, the TIC is sourced from the melting of glacial ice with the direct release of occluded CO_2 gases into the water column with no direct contribution from atmospheric CO_2. Despite the ultra-oligotrophic, low-light conditions, and lack of a seasonal moat, the lake hosts a

benthic microbial ecosystem composed of photosynthetic microbial mats, small cuspate pinnacles and large conical stromatolitic structures to depths of at least 130 m (Andersen et al., 2011; Hawes et al., 2019). Although there are many examples of modern microbialites and stromatolites with an abundance of morphological attributes, Untersee is the only known lake that hosts large conical stromatolites, up to 70 cm tall, analogous to those found in the fossil record dating back to the Archaean 3.45Gya (Allwood et al., 2006). The top layer of the microbial mats comprises a cyanobacteria community that shifts to a heterotrophic community in the underlying layers (Koo et al., 2017). Carbon isotope analyses show the microbial ecosystem in Lake Untersee to be CO_2-depleted, and as a result, the phototrophs growing in the upper-most layer of the mats are fixing carbon without the isotopic fractionation of HCO_3^- from the high pH water or the respired CO_2 from heterotrophs in the layers of the underlying mat (Marsh et al., 2020). This circular carbon budget results in lower gross photosynthesis and sequestration rates of organic carbon than the microbial mats in MDV lakes (Hawes et al., 2019).

Lake Untersee has been in a hydrological steady-state with no summer moating for at least the past several hundred years (Kaup et al., 1988; Faucher et al., 2019, 2020; Hermichen et al., 1985). However, field observations made in December 2019 showed that the lake water level increased by about 2 m with respect to the past decades. This study builds on our previous studies about the water balance and the characteristics and sources of carbon to Lake Untersee (i.e., Andersen et al., 2011; Faucher et al., 2020, 2019; Marsh et al., 2020). This study aims to evaluate the carbon mass balance of Lake Untersee's ecosystem and assess the effect of GLOFs on the CO_2-depleted benthic phototrophs. The objectives are to determine: 1) the amount of carbon stored in Lake Untersee; 2) the carbon balance under steady-state hydrological conditions; and 3) the effect of GLOFs on the chemistry (i.e., TIC, TOC, and $^{13}C_{TIC}$ and $^{14}C_{TIC}$) of the lake water column and how it may modify the carbon balance of the ecosystem. This carbon mass balance approach, coupled with carbon isotope analyses, provides essential insight into this lake's fate and other Antarctic lacustrine ecosystems impacted by glaciers' response to a warming climate.

4.2 Study area

The Untersee Oasis is located in the Gruber Mountains, approximately 150 km south of the Princess Astrid Coast. The local geology consists of plagioclase of the Precambrian Eliseev anorthosite-norite complex (Bormann, 1995) (Fig. 4-1). The Oasis contains two large perennially

ice-covered lakes (Hermichen et al., 1985). Lake Untersee is a 6.5 km long and 2.5 km wide ice-dammed lake (volume of 5.21×10^8 m^3) that lies adjacent to the Anuchin Glacier and reaches a maximum depth of 169 m in its northern basin. This is separated by a sill that cuts across the lake at 50 m depth from a smaller 100 m deep basin to the south. The northern basin is homo-thermal, well-oxygenated to the bottom, and well-mixed due to buoyancy-driven convection caused by melting of the ice-wall at the glacier-lake interface (Steel, McKay, & Andersen, 2015; Wand et al., 2007). In contrast, the southern basin is density stratified below the sill depth and is anoxic at its base; the higher density prevents mixing with the overlying oxic water column (Bevington et al., 2018; Wand et al., 2006; 2007). Except for a boulder field at the south end of the lake and other large boulders scattered across the ice cover, the ice cover's surface cover on Lake Untersee is smooth and free of any fine sediments. As a result, sedimentation rates based on four replicate passive traps at 20 m depth, deployed for two years, yield a much lower accumulation rate of 6 g m^{-2} compared to MDV lakes (i.e., 41 g m^{-2} for Lake Hoare; Wharton et al., 1989).

Lake Untersee has a local climate dominated by intense evaporation and sublimation with little melt due to southerly solid katabatic winds, low humidity, and mean annual air temperature of –10.6°C (Andersen et al., 2015). As a result of the hyper-arid climate, the lake loses c. 1% of its water annually from the sublimation of the 2–4 m thick ice cover and based on δD-$\delta^{18}O$ of the water column, it has not developed a moat for at least the past 300–500 years (Faucher et al., 2020). An equal inflow is recharging the lake to maintain its water balance, with subaqueous melting of terminus ice contributing 40–45% of the annual water budget and subglacial meltwater contributing the remainder (i.e., Faucher et al., 2019). Lake Obersee is a smaller ice-dammed lake (volume of 8.07×10^7 m^3) located c. 6 km NE of Untersee with a maximum depth of 83 m (Koo et al., 2017). This shallower lake has higher productivity in the water column than Lake Untersee, attributed in part to the availability of higher dissolved phosphate levels (Kaup et al., 1988; Haendel & Kaup, 1995).

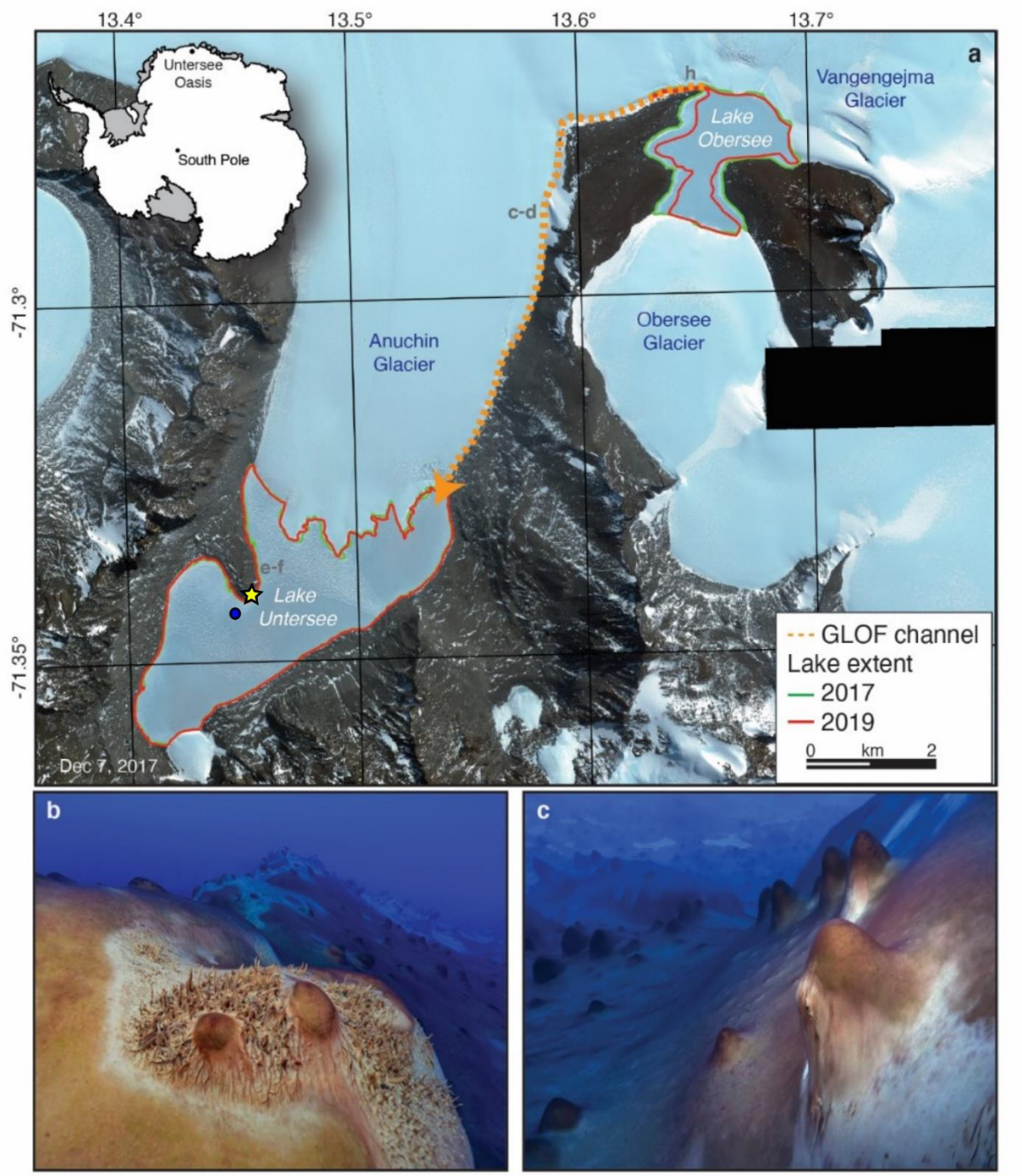

Figure 4-1: Lake Untersee and its benthic microbial ecosystem, Dronning Maud Land, Antarctica. (a) Location map showing 2017-2019 extents of Lake Untersee and Lake Obersee and flow direction of the 2019 glacial lake outburst flood. Background DigiGlobe satellite imagery, December 7, 2017; ©2020 Digital Globe NextView License (provided by NGA commercial imagery program). Map generated using QGIS 3.14. Letters indicate the location where photographs shown in figure 4-4 were taken. The yellow star indicates the location of the meteorological (and time-lapse camera) station, and the blue dot indicates the sampling location our collected microbial mat cores (b-c), Photographs of laminated microbial mats, cones, and pinnacles growing in Lake Untersee at 12-13 m and c. 20 m depths. Photos were taken near the sampling location of the mats. Note the clarity of the water column, a reflection of the CO_2-depleted water.

Measurements of the chemical composition of the oxic water column of Lake Untersee over the 1982-2018 period showed that it has a Na(Ca)-SO_4 geochemical facies with homogenous temperature (0.5°C), pH (10.5-10.8), specific conductivity (505-510 µS/cm^{-1}) and dissolved oxygen (DO; 145-150%) (Andersen et al., 2011; Hermichen et al., 1985; Wand et al., 2007). The TIC in the lake water ranged from 0.3-0.4 mg C L^{-1} (one to three orders of magnitude lower than ice-covered lakes in the MDV (Lyons et al., 2013; Neumann et al., 2004a), with $\delta^{13}C_{TIC}$ averaging –9.1±0.4‰ (Marsh et al., 2020). The total organic carbon (TOC) in the oxic water is also low (0.12±0.02 mg C L^{-1}), which is one order of magnitude lower than in other ice-covered lakes and deep subglacial lakes (Takacs et al., 2001; Vick-Majors et al., 2020), but closer to the average compiled for Antarctic glacial ice (Hood et al., 2015). Radiocarbon analysis of TIC in the oxic waters yielded $F^{14}C_{TIC}$ of 0.4143-0.4361, equivalent to apparent ages of 6666±98 to 7079±76 yrs BP (Marsh et al., 2020). The $F^{14}C_{TOC}$ yielded values of 0.4233±0.02 (6906±610 yrs BP) and 0.5547±0.02 (4734±606 yrs BP), respectively. Lake Obersee has a similar chemistry with pH of 9.9, conductivity c. 91 µS/cm^{-1} and DO c. 190% (Andersen, unpublished data).

The benthic environment of Lake Untersee is dominated by laminated microbial mats (Andersen et al., 2011; Hawes et al., 2019). Field observations suggest that the photosynthetic mats cover nearly 100% of the lake bottom to depths of 130 m, but coverage is patchy in the deeper sections; photosynthetic mats are absent from the anoxic regions of the southern basin. The phototrophic mats are growing in very low light conditions. Approximately 5% of incident irradiance is transmitted through the lake ice, with a vertical extinction coefficient for scalar photosynthetically active radiation (PAR) of 0.033 m^{-1}, resulting in a 0.1% surface irradiance at a depth of ~ 135 m (Andersen et al., 2011). Metagenomic16S rRNA sequencing showed that the top layer of the microbial mats is composed of cyanobacteria (Phormidium sp., Leptolyngbya sp., and Pseudanabaena sp) that progresses into a heterotrophic community (Actinobacteria, Verrucomicrobia, Proteobacteria, and Bacteroidetes) in the underlying layers (Koo et al., 2017). In 2017, Marsh et al. (2020) analyzed microbial mats sampled near the push moraine's eastern edge at depths of 18.5, 17, and 13 m. The mats were 6 to 10 cm thick and transitioned sharply to sediments. The individual mat laminae (0.2-1 mm) were composed of organic material intermixed with anorthite/kaolinite silt- and clay-sized particles with a few distinct layers having higher quart/tremolite sand grains. The organic C abundance of the mats ranged from 1.0-5.8 w.t.%, with the microbial mats' organic carbon density calculated at 793±264 g m^{-2}. The $\delta^{13}C_{org}$ of the

microbial mats averaged –10.6±1.9‰, with a few individual layers having much lower values (–18.1 to –15‰). Several individual mat laminae were radiocarbon dated: the top laminae yielded ages of 10,875±37 yrs BP to 9524±48 yrs BP; the bottom mat layers were dated between 16,208±65 yrs BP and 12,031±68 yrs BP. The underlying sediments consist of clay- to gravel-size particles with organic C abundance and $^{14}C_{org}$ much lower than in the microbial mats (≤1 w.t.% and 19,370 yrs BP, Core 3). Considering that Lake Untersee formed c. 12-10ka BP (Schwab, 1998), the heterogeneous particle size in the sediments and older ^{14}C age suggest that glaciogenic sediments were deposited in the basin before the formation of Lake Untersee.

4.3 Methods

4.3.1 Carbon mass balance

A carbon mass balance approach was used to assess if the amount of organic carbon stored in the microbial mats and the oxic water column of Lake Untersee is in equilibrium with carbon inputs into the lake. The carbon mass balance builds on the water mass balance model of Lake Untersee presented in Faucher et al. (2019):

$$[\mathbf{EQ.4-1}]\ \Delta S = P + Is + Ie + Ig - Os - Og$$

where:

ΔS = change in the volume of water;

P is total annual precipitation;

I_s, I_e and I_g are the inflows of surface water, subaqueous melting of terminus ice (originating from the melting of the submerged Anuchin Glacier at the ice–lake water interface) and groundwater (subglacial meltwater or other sources), respectively;

O_s and O_g are the outflows of surface water and groundwater, respectively.

The lake loses 0.6-1.2% of its water through sublimation of its ice cover, and groundwater outflows (O_g) are not likely occurring. Direct recharge from total precipitation (P) and surface water (I_s) is ruled out because the lake has been well-sealed for the past 300-500 years. Therefore, the lake is recharged by only two sources: subaqueous melting of the Anuchin Glacier and subglacial meltwater. Using an energy mass-balance approach, it was determined that the subaqueous meltwater contributes 40-45% of the annual recharge, and subglacial

meltwater/groundwater contributions accounts for the remaining 55-60%. The carbon mass balance model can therefore be simplified to:

$$\textbf{[EQ. 4-2]}\ \Delta carbon\ (g\ C) = Ia_{TIC} + Ia_{TOC} + Ig_{TIC} + Ig_{TOC} - Os_{TIC} - Os_{TOC}$$

where:

I_a and I_g are the annual inflows of subaqueous melting of the Anuchin Glacier's terminus (1.98–2.23 × 10^6 m^3) and subglacial meltwater/groundwater contributions (2.68–2.92 × 10^6 m^3);

O_s is outflow surface waters via ice cover ablation (3.22–6.43 × 10^6 m^3).

The carbon concentration (TIC and TOC) of the subaqueous and subglacial meltwaters inputs to Lake Untersee were determined by Marsh et al. (2020) to explain the $\delta^{13}C_{TIC}$ and $^{14}C_{TIC}$ composition of the lake water. Based on the annual inputs of carbon to the lake, the cumulative mass of carbon in the lake ecosystem, and the evolution of $F^{14}C_{TIC}$ in the oxic water column and ^{14}C in mats over the past 12ka (since the formation of the lake) were calculated for four different scenarios and compared to our measurements (Appendix C, Table C2): S1) the lake was always well-sealed and under hydrological steady-state, as observed presently; S2) during the early formative stage, the water column of the lake was exchanging with atmospheric CO_2 with no weathering, but then switched to a well-sealed ice cover and was under hydrological steady-state; S3) same as S2, but with additional TIC contribution from open system weathering of plagioclase minerals; S4) same as S3, but with additional TIC contribution from GLOFs. The cumulative mass of carbon was calculated in 500-year time-steps. The evolution of $F^{14}C_{TIC}$ follows the accumulation of carbon to the lake with $F^{14}C$ of 0.8 (estimated from the age of occluded CO_2 gases being released into the lake; Faucher et al., 2020) and its decay over time using the half-life = 5730 years. The ^{14}C profile in the mats assumes the mats are using the TIC solely in lake water as their carbon source, and ^{14}C of the mats reflects the evolution of $^{14}C_{TIC}$ in the water column. However, due to the significant carbon reservoir effect in the water column, the ^{14}C ages of the mats cannot be calibrated to calendar years, and an age-depth model cannot be performed.

4.3.2 Changes in elevation and water volume for Lakes Untersee and Obersee

Surface elevation changes of lakes Untersee and Obersee during the 2004-2020 period were assessed using ICESat & ICESat-2 (ATL06 products) datasets available on the *Open Altimetry* web-based application (Nandigam et al., 2018; Smith et al., 2020). ICESat and ICESat-

2 altimetry data have vertical precisions of ~ 14 and 0.4 ± 2-4 cm, respectively (Brenner, DiMarzio, & Zwally, 2007; Markus et al., 2017). Although the altimetry data represents elevation at discrete points, we assume in our temporal analysis that the ice cover's elevation is constant across the lakes' surface, which is corroborated with *in situ* dGPS elevation measurements of Untersee maide in 2016. Changes in lake water volume were subsequently determined from digitized, georeferenced, and enhanced (with our measurements) bathymetric maps of Lake Untersee and Lake Obersee (Schwab, 1998; Wand et al., 2006); volume and surface area calculations were made with the *Surface Volume* tool in the *ArcGIS pro 2.4* software.

4.3.3 Lake water analyses

During the field season at Lake Untersee in November 2019, measurements of pH, temperature, specific conductivity, total dissolved solids (TDS), dissolved oxygen (DO), and chlorophyll were made using a calibrated Hydrolab DS5 Water Quality Sonde through holes drilled in the ice cover at the North and South basins (Fig. 4-1). Lake water samples were collected at 5-10m intervals from the same locations as previous years using a clean 2.5 L Niskin bottle. The water samples were immediately transferred into sampling bottles unfiltered due to the ultra-clear and low-particulate content in the waters and the high pH waters' sensitivity to rapid absorption of atmospheric CO_2 that would affect pH and dissolved inorganic carbon (DIC) (i.e., Marsh et al., 2020). Water samples for TIC-TOC analyses were collected in 40 mL amber glass vials with a butyl septa cap. Radiocarbon samples were collected in pre-baked (500°C for 3 hours) 1 L amber glass bottles.

The TIC-TOC concentration and their stable isotope ratios ($\delta^{13}C_{TIC}$, $\delta^{13}C_{TOC}$) in lake waters were measured with a wet TOC analyzer interfaced with a Thermo DeltaPlus XP isotope-ratio mass spectrometer using methods described by St-Jean (2003) at the Ján Veizer Stable Isotope Laboratory, University Ottawa. The isotope ratios are presented as permil deviation relative to VPDB and expressed using the delta-notation. The 2σ analytical precision is ± 0.5 ppm for TIC and TOC concentrations and ± 0.2‰ for $\delta^{13}C_{TIC}$ and $\delta^{13}C_{TOC}$.

Radiocarbon analysis of TIC-TOC in waters was performed at the A.E. Lalonde Accelerator Mass Spectrometry Laboratory, University of Ottawa. Sample preparation, extraction of inorganic and organic carbon from waters, and graphitization are described by St-Jean et al. (2017). Graphitized samples were analyzed on a 3MV tandem mass spectrometer, and the $^{14}C/^{12}C$

ratios are expressed as fraction of Modern Carbon ($F^{14}C$) and corrected for spectrometer and preparation fractionation using the AMS measured $^{13}C/^{12}C$ ratio (Crann et al., 2017; Kieser et al., 2015). Radiocarbon ages are calculated as $-8033\ln(F^{14}C)$ and are reported in ^{14}C yr BP (BP=AD1950) (Stuiver & Polach, 1977). The 2σ errors are reported with the results and <0.013 $F^{14}C$ (or <190 years).

4.4 Results and Discussion

4.4.1 Carbon stored in Lake Untersee

Based on the 2017 TIC-TOC measurements in the oxic water column and organic carbon content in microbial mats, Lake Untersee stores 5.42 to 6.71 × 10^9 g C, with >95% of the carbon pool residing in the microbial mats (Table 4-1). The TIC and TOC pools in the lake waters are 1.81 ×10^8 g C and 6.19 ×10^7 g C, respectively, with the organic C reservoir in the microbial mats reaching 5.17 to 6.47 × 10^9 g C. The latter was calculated from the average organic C content (793 ± 264 g m^{-2}) of three cores collected nearby the push moraine, the surface area of the oxic lake bottom (8.15 km^2), and scaling to the three scenarios of mat coverage along the oxic lake bed: S1) 100%; S2) 90%; and S3) 80% mat coverage. Tiny carbonate spherules (few mm) are sometimes found within the mat layers; however, these are rare and excluded from the carbon reservoir.

Table 4-1: Amount of carbon stored in the oxic water column and microbial mats of Lake Untersee, Antarctica. The amount of carbon stored in mats was calculated using an organic carbon density of 793 ± 264 g m^2 and a surface area for the lake's oxic basin following three possible mat coverage scenarios. TIC = total inorganic carbon; TOC = total organic carbon.

Reservoirs	**Volume/surface area**	**Carbon (g C)**
Lake oxic water	5.16E+08 m^3	2.43E+08
TIC (0.35 mg C L^{-1})		1.81E+08
TOC (0.12 mg C L^{-1})		6.19E+07
Mats		
S1 (1x)	8.15E+06 m^2	6.47E+09
S2 (0.9x)	7.34E+06 m^2	5.82E+09
S3 (0.8x)	6.52E+06 m^2	5.17E+09
Total		5.42-6.71E+09

4.4.2 Carbon mass balance and hydrological steady-state

As an initial carbon mass balance scenario, the carbon input into Lake Untersee assumes the lake is in a hydrological steady-state, and each term is multiplied by its carbon concentration (Table 4-2). Subaqueous melting of the Anuchin Glacier at the lake-glacier interface releases occluded atmospheric CO_2 gas directly in the water column that contributes 0.0165 mg C L^{-1} as TIC. Oxidation of the TOC in the water column is not a significant contributor to the TIC pool directly released into the water column because $\delta^{13}C_{TIC}$ averages –9.1 ± 0.4‰, similar to the $\delta^{13}C_{CO2}$ of occluded gases (–7.3 to –6.3‰) (Eggleston et al., 2016; Schmitt et al., 2012; Marsh et al., 2020). The TOC of the Anuchin Glacier flowing over the crystalline bedrock is assumed to be similar to that measured in the Vostok ice core from the interior of the East Antarctic Ice Sheet (0.03 g C L^{-1}). The TIC-TOC concentrations in the subglacial meltwater recharging Lake Untersee (Ig_{TIC} and Ig_{TOC}) are similar to those calculated for the subaqueous meltwater with little to no carbonate dissolution or oxidation of organic material. A major contribution from subglacial carbonate dissolution or oxidation of organic carbon in the Precambrian crystalline bedrock (i.e., Wadham et al., 2010; Wynn et al., 2006) was ruled out by Marsh et al. (2020) since the carbonate and organics would have $\delta^{13}C$ values near 0 and c. –25‰, respectively (Clark, 2015), and would be ^{14}C dead, which would result in a very different $\delta^{13}C_{TIC}$ and $F^{14}C_{TIC}$ in the water column and older ^{14}C age in the bottom layer of mats. In Lake Untersee, there is a limited output of carbon (Os_{TIC}, Os_{TOC}): with the pH of the water column being 10.5, there is no CO_2 gas escaping through the sublimation of the ice cover, and the soluble ions are segregated in the water column during freezing at the ice-water interface (i.e., Marsh et al., 2020; Santibáñez et al., 2019). Therefore, taking the TIC and TOC concentrations of the subaqueous and subglacial meltwaters and their respective water volume added annually, these two water sources would contribute 2.28×10^5 g C yr^{-1} (Table 4-2). Lake Untersee formed 12-10 ka BP and has remained well-sealed and in a hydrological steady-state for at least the past 300-500 years (Faucher et al., 2020). Assuming these conditions were maintained throughout its existence, the lake is missing $3.11\text{-}4.21\times10^9$ g C (57-62%).

Table 4-2: Annual input volume of subaqueous (Ia) and subglacial meltwater (Is) recharging Lake Untersee with their estimated total inorganic carbon (TIC) and total organic carbon (TOC) concentration used in the carbon mass balance calculations. Under hydrological steady-state, the lake loses the same water volume by sublimation of the ice cover (Os). However, given the alkaline nature of the water, no CO_{2g} is lost. Also shown is the contribution from glacial lake outburst floods (GLOF) with a 2000 years recurrence interval.

	Volume (m^3)	**TIC (mg C L^{-1})**	**TOC (mg C L^{-1})**	**Total C (mg C L^{-1})**
Ia	2.09E+06	0.0165	0.03	9.72E+04
Is	2.81E+06	0.0165	0.03	1.31E+05
Os	4.90E+06	0	0	0
GLOFs	1.75E+07	8	0	1.40E+08

4.4.3 Carbon mass balance and moating

The δD-$\delta^{18}O$ composition of Lake Untersee indicates that the lake has been well-sealed with no summer moating for the past 300-500 years; however, a potential source for the missing carbon is uptake of atmospheric CO_2 in the water column during a period when the lake developed a summer moat along its margin. Paleo-temperature reconstructions show that Dronning Maud Land was 1-2°C warmer in the early Holocene than today (Ciais et al., 1994). The warmer temperature caused the rapid thinning of the EAIS (Mackintosh et al., 2014), and meltwater from the retreating glacier subsequently filled the closed-basin valley and produced Lake Untersee (Hiller et al., 1988). During the early formative stage of Untersee, the lake likely developed a summer moat, as evidenced from the ^{14}C ages of bottom microbial mat layers (13-12 ka) that correspond to the timing of lake formation. This indicates that, at the time of lake formation, the cyanobacteria were fixing DIC under an open system with respect to CO_2 ($F^{14}C_{DIC} \sim 1$). Following regional cooling, the lake developed its permanent ice cover. The water column became sealed to atmospheric CO_2 exchange, likely shortly after 12ka as evidenced by the scarcity of calcite observed in the mats (i.e., Andersen et al., 2011). The microbial mats consumed the DIC reservoir in the water column while receiving DIC-DOC contributions from subaqueous and subglacial meltwaters. Therefore, assuming the water column was in equilibrium with the atmosphere during the early formative stage of Lake Untersee, geochemical modeling predicts that the weathering of plagioclase minerals from glacial meltwater would generate pH near 10.5 with DIC reaching 1.3-1.5 mg C L^{-1} (Table 4-3). If the lake then became well-sealed shortly after it formed and was being recharged solely by the subaqueous and subglacial meltwaters, similar to hydrological conditions over the past few

hundred years, carbon mass balance calculations indicate the lake would have accumulated 3.51×10^9 g C, which is 3-3.6×10^9 g C lower than the estimated total carbon reservoir.

Table 4-3: Results of numerical simulations using PHREEQC hydrogeochemical software (Parkhurst & Appelo, 2013). Simulations were conducted using the average chemical composition of glacial meltwater (Core Epica, western Dronning Maud Land; Isaksson et al., 1996) as input and were equilibrated with atmospheric CO_2 (P_{CO2} = –3.43) or allowed weathering of plagioclase mineral under open-system (P_{CO2} = –3.43), which simulates Lake Untersee during early formative stage. Calcite was allowed to precipitate if saturation was reached.

Reactions	**pH initial**	**pH final**	**DIC ppm C**
Glacial water	5.6		0.00165
Equilibrium with atm CO_2	5.6	5.4	0.37
Weathering (pCO_2 = -3.43)			
albite, anorthite	5.6	7.0	1.20
albite, anorthite, kaolinite	5.6	10.3	1.52
anorthite, kaolinite	5.6	10.5	1.29
anorthite, kaolinite, plagioclase	5.6	10.4	1.39
Lake water			
Equilibrium with atm CO_2	10.6	7.1	1.50
Weathering (pCO_2 = -3.43)			
albite, anorthite	10.5	7.2	1.66
albite, anorthite, kaolinite	10.5	10.4	0.17
anorthite, kaolinite	10.5	10.6	0.12
anorthite, kaolinite, plagioclase	10.5	7.9	8.05

4.4.4 Glacial Lake Outburst Floods (GLOFs)

ICESat-1 and ICESat-2 laser altimetry data combined with field observations show that the elevation of the ice cover of Lake Untersee remained stable (~608 m a.s.l.) between October 22nd, 2003, and December 12th, 2018 (Fig. 4-2).

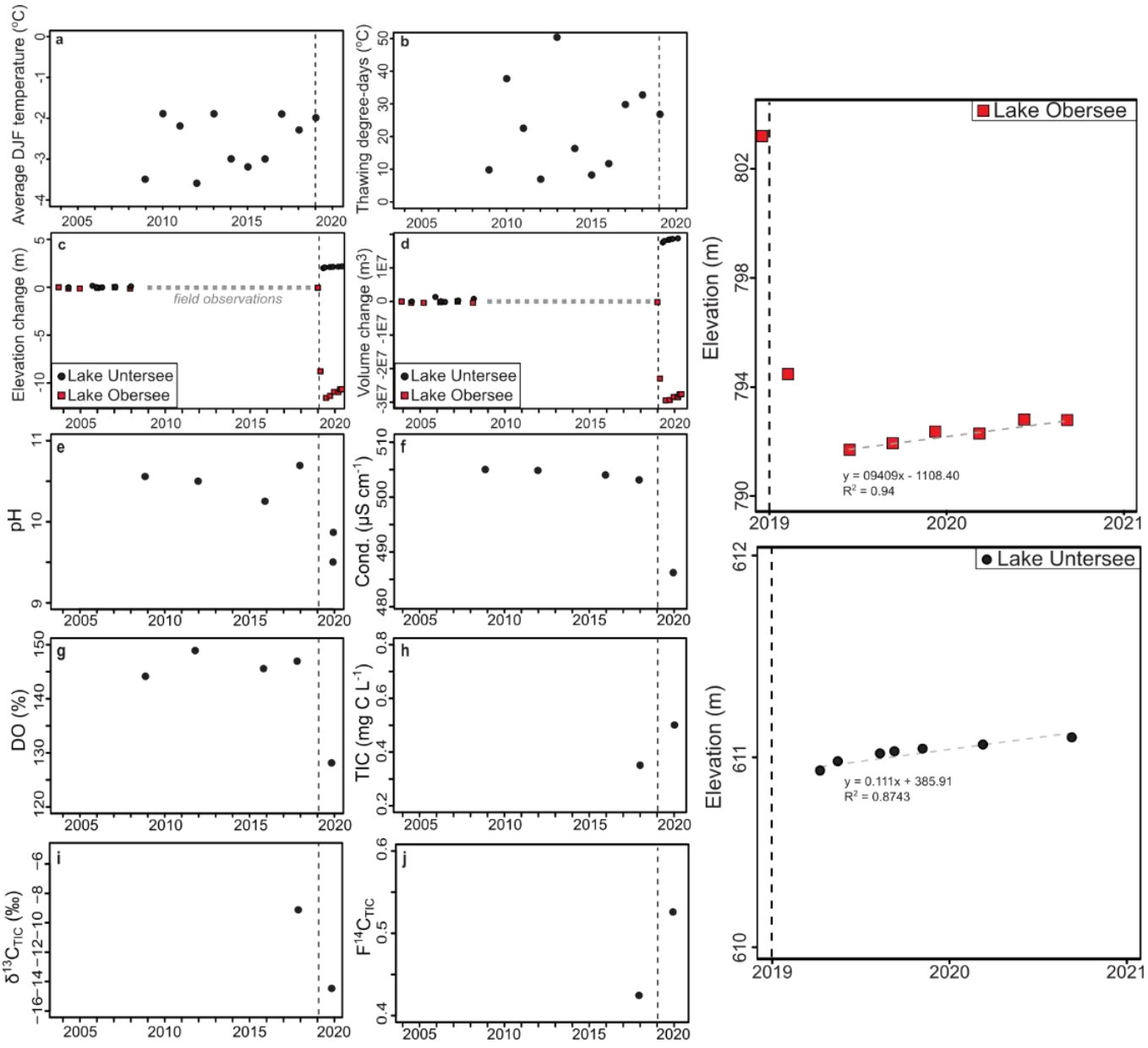

Figure 4-2: 2004-2020 variations in hydrochemical parameters of Lake Untersee, Antarctica.
(a) Average summer (DJF) air temperature at the Untersee Oasis. (b) Thawing degree-days at the Untersee Oasis. (c-d) Changes in elevation and volume for Lakes Untersee and Obersee (elevation data from ICESat and ICESat-2). (e-f) Mean values of pH, conductivity, dissolved oxygen (DO), total inorganic carbon (TIC), $\delta^{13}C_{TIC}$, and $F^{14}C_{TIC}$ in the oxic water column of Lake Untersee. The dashed vertical line represents the timing of the 2019 glacial lake outburst flood. The scatter plots on the right side of the figure show elevation data for Lake Untersee and Lake Obersee after the 2019 GLOF event.

However, between December 12^{th,} 2018, and February 7^{th,} 2019, altimetry data shows that Lake Untersee's elevation increased by 2.0 m, resulting in a volume change of $+1.75\times10^7$ m^3 (or +3% increase in volume). Time-lapse photography shows the sudden release of water through the ice cover on Jan 14-15^{th,} 2019 (Fig. 4-3). The change cannot be attributed to a surge or extensive surface melting of the Anuchin Glacier because its position was unchanged, and the number of thawing degree days only reached 26.8 (ranks 6 out of 11 years, since 2008; Andersen et al., 2015; Fig. 4-2b).

Figure 4-3: Time-lapse photography of glacial lake outburst flood in Lake Untersee, Antarctica. The glacial lake outburst flood started on January 13th-14th 2019, as evidenced by the sudden release of water through the ice cover and continued for many weeks. The abrupt increase in water level at Lake Untersee is linked to a GLOF from Lake Obersee, dammed by the Vangengejma and Obersee glaciers. Between December 12^{th,} 2018, and February 7^{th,} 2019, the elevation of Lake Obersee decreased by 11.3 m, a reduction in volume of 2.29×10^7 m^3, likely caused by a section of the Vangengejm Glacier that collapsed or shifted through a glacial tunnel or by fast-moving ice-streams surrounding the Untersee Oasis (Fig. 4-4). The sudden release of water from the NW sector of Lake Obersee flowed for 8.3 km in a narrow channel along the east lateral moraine into the NE corner of Lake Untersee. It resulted in the thermal erosion of the Anuchin Glacier's East lateral moraine (Fig. 4-4).

Figure 4-4: Glacial lake outburst flood-related features in the Untersee Oasis. (a) Extent of Lake Obersee (Dec. 7th 2017). ©2020 Digital Globe NextView. (b) Extent of Lake Obersee (March 20th 2020). ©2020 Digital Globe NextView. (c) Ancient outflow channel on the Anuchin Glacier's East lateral moraine (photo taken in Nov. 2011). (d) Thermally eroded outflow channel on the Anuchin Glacier's East lateral (photo taken in Nov. 2019). (e) Extent of two Kames on the NE side of Lake Untersee's push moraine before the GLOF event (Dec. 7th 2017). ©2020 Digital Globe NextView. (f) Extent of two Kames on the NE side of Lake Untersee's push moraine after the 2019 GLOF event (Dec. 13th 2019). ©2020 Digital Globe NextView. (g) Thermally eroded outflow channel at the NE extremity of the Anuchin Glacier (image taken on Dec. 1st 2019). (h) Outflow channel at the NW extremity of Lake Obersee (image taken on Dec. 1st 2019).

The sudden addition of water originating from Lake Obersee altered the hydrochemistry of the oxic water column of Lake Untersee from its stable composition measured since the early 1980s. The pH decreased from 10.6 to 9.5, specific conductivity decreased from 505-520 to 480 µS/cm^{-1}, and DO decreased from 150% to 120%. The TIC increased from 0.35±0.05 mg C L^{-1} to 0.5±0.02 mg C L^{-1} with $\delta^{13}C_{TIC}$ values decreasing from –9.1±0.4‰ to –14.5±1.9‰. The $F^{14}C_{TIC}$ increased from 0.4233±0.02 to 0.5107-0.5481 (Fig. 4-2). The water that entered the lake in mid-January 2019 was not sampled because we were not at the site; however, in late November 2019, a stream was still flowing in the GLOF channel into the NE corner of Lake Untersee; this small stream had pH=7.7, conductivity = 70 µS/cm^{-1}, TIC = 1.8 mg C L^{-1}, $\delta^{13}C_{TIC}$ = –18.5‰ and $F^{14}C_{TIC}$ = 0.5844 (4315±34 yrs BP).

Geochemical modeling using the *PHREEQC* hydrogeochemical software (Parkhurst & Appelo, 2013) suggests that the stream's geochemical composition was obtained following weathering of plagioclase minerals of Lake Obersee water in equilibrium with atmospheric CO_2 (Table 4-3). Therefore, the GLOF weathered plagioclase and biotite-bearing gneisses morainic material as it flowed into Lake Untersee. Considering that the GLOF contributed 3%vol of water to Lake Untersee, a two-component mixing of the stream water chemistry being added to the lake matches well the late 2019 conductivity of the lake (Appendix C, Table C1). However, parameters affected by exchanges with atmospheric gases, such as DO, TIC, and $F^{14}C_{TIC}$, have mixing values that differ from those measured in the lake, which suggests interaction with the atmosphere. The lower DO is attributed to partial degassing of the water column through the c. 50 m wide melt-out hole that developed in the NE corner of the lake in January 2019 or along fractures in the ice cover, whereas the higher TIC and $F^{14}C_{TIC}$ in the water column is attributed to some uptake of modern atmospheric CO_2 from the melt-out hole. Indeed, based on the 3% two-component mixing scenario (Appendix C, Table C1), the 2019 TIC concentration in the lake (LU 2019) is 21% lower than expected (i.e., missing 0.11 ppm C). This missing TIC could be derived from a modern atmospheric CO_2 (with $F^{14}C$ = 1) uptake through the melt-out hole: this would match the measured $F^{14}C_{TIC}$ of 0.5259, in 2019.

4.4.5 GLOFs and carbon mass balance

The 2019 GLOF from Lake Obersee added c. 1.75×10^{7} m^{-3} (3%vol) of water to Lake Untersee and replenished the oxic water column with c. 1.40×10^{8} g C (Table 4-2). The amount of carbon added by this single GLOF event is still too low to explain the total carbon stored in Lake Untersee. However, high-resolution analyses in the microbial mat cores revealed individual matching layers with higher sand fraction, lower $\delta^{13}C_{org}$ values, and younger ^{14}C ages (Fig. 4-5). We suggest that these shared characteristics in the mats are due to past GLOFs.

Unlike ice-covered lakes in the MDV (e.g., Jepsen et al., 2010; Squyres et al., 1991; Wharton et al., 1992), the surface ice cover of Lake Untersee is free of any fine sediments, and the main source of sediments is glacial flour from the subaqueous and subglacial meltwaters (Andersen et al., 2011). The 2019 GLOF, with an estimated discharge of 9-10 m^3 s^{-1}, had sufficient velocity to transport sand-sized sediments that would be deposited into the lake. A thin layer of sand was not observed on the mats' surface because the samples were collected in December 2017. Nonetheless, we did observe for the first time a thin layer of fine sediment covering light sensors that we retrieved in December 2019. The 2019 GLOF also increased the TIC in the oxic water column to 0.5±0.02 mg C L^{-1}, significantly decreased the $\delta^{13}C_{TIC}$, and increased the $F^{14}C_{TIC}$ (Fig. 4-2). After a GLOF of this magnitude, the cyanobacteria in the top mat layer would be fixing the HCO_3^- with this modified $\delta^{13}C_{TIC}$ and $F^{14}C_{TIC}$ signatures, and that would be recorded in the $\delta^{13}C_{org}$ and ^{14}C of the microbial mat since fixation of the HCO_3^- would still occur with no ^{13}C fractionation due to the high pH and still very low TIC (i.e., Marsh et al., 2020). As the microbial mats progressively sequester the DIC reservoir in the water column while continuing to receive DIC-DOC contribution from subaqueous and subglacial meltwaters with vastly different $\delta^{13}C_{TIC}$ and $F^{14}C_{TIC}$ compositions relative to the GLOF, the $\delta^{13}C_{TIC}$ in the water column will, over time, return to those measured before the 2019 GLOF while the $F^{14}C_{TIC}$ will evolve following its decay. As a result, the shift in grain size and carbon isotopes within a single mat layer can be used as proxies of GLOF occurrences and provide evidence that GLOFs sporadically recharged Lake Untersee over the Holocene (Fig. 4-5). It should also be noted, however, that a change in grain size and carbon isotopes is unlikely to be recorded the same way in the mats due to limnological factors (e.g., water circulation, topography) and variations in metabolism and carbon assimilation within the mats due to differences in other stressors (i.e., light attenuation with depth, availability of other

nutrients). A gradient in sediment deposition following a GLOF, with coarser material deposited in the northeast corner of the lake and fining with increasing distance, should also be observed.

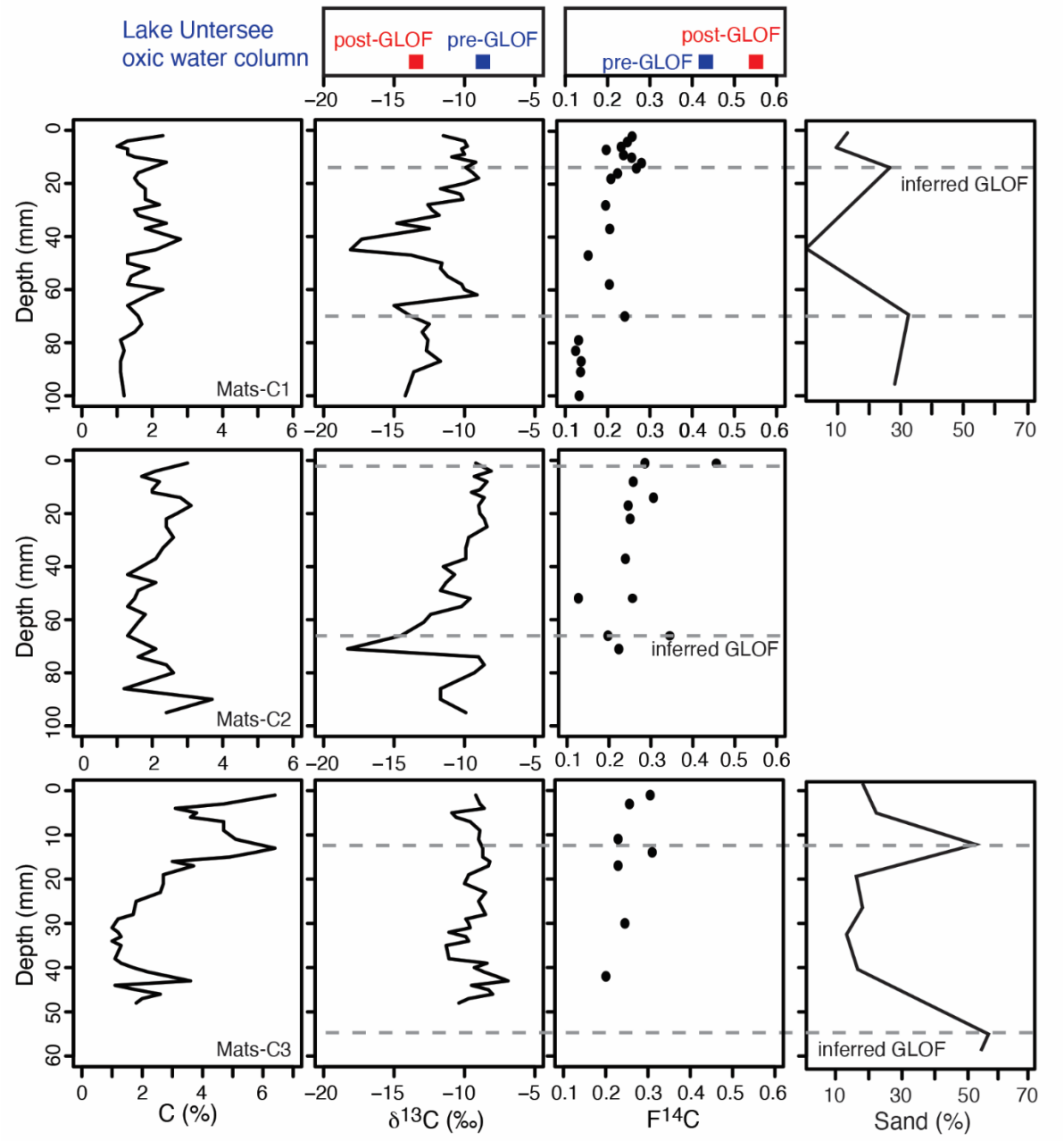

Figure 4-5: Organic carbon content, $\delta^{13}C$, $F^{14}C$, and sand-fraction of three microbial mat cores sampled in Lake Untersee, Antarctica. Cores were collected in proximity to photographs shown in Fig. 4-1b,c. Dashed lines associate increases in sand-size fraction within the mats with increases in $F^{14}C$ and decreases in $\delta^{13}C$. These particle size distribution changes and carbon isotopes in the mats are inferred to be related to GLOFs that transport sand and supply TIC into Lake Untersee with a lower $\delta^{13}C_{TIC}$ and higher $F^{14}C_{TIC}$ signature relative to the water column. Also shown for comparison are the $\delta^{13}C_{TIC}$ and $F^{14}C_{TIC}$ values in the water column of Lake Untersee before and after the 2019 GLOF.

Assuming GLOFs of similar magnitude and chemical composition occur every 2000 years, with the lake being recharged solely by subaqueous and subglacial meltwater all other years, we can reach the total carbon reservoir with the carbon balance calculation (Fig. 4-6a). Besides, numerical modeling of the evolution of $F^{14}C_{TIC}$ in the oxic water column and the ^{14}C age distribution in the microbial mats following the addition of younger carbon to the lake by the GLOF also agrees well with the measurements (Fig. 4-6b,c). Therefore, our findings demonstrate that GLOFs can sustain the long-term productivity of perennially ice-covered and CO_2-depleted lakes, like Lake Untersee, by sporadically supplying them with inorganic carbon.

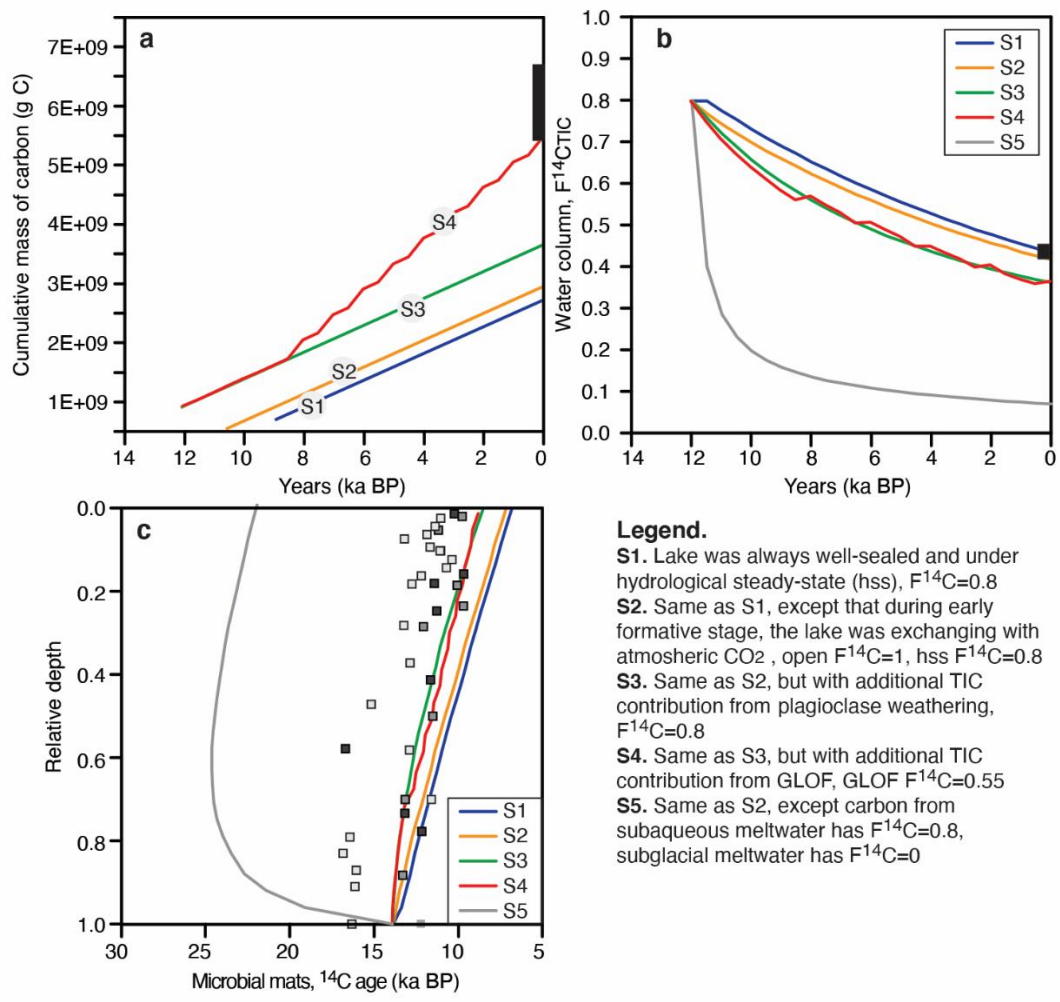

Figure 4-6: Carbon mass balance and numerical modeling of ^{14}C evolution in the water column and microbial mats of Lake Untersee, Antarctica. (a) The cumulative mass of carbon accumulating in Lake Untersee's oxic water column and microbial mats under four different scenarios. The black bar is the amount of carbon stored. (b) Evolution of $F^{14}C_{TIC}$ in Lake Untersee under four different scenarios. The black bar is the measured $F^{14}C_{TIC}$ in the lake. (c) Evolution of ^{14}C age of microbial mats. The ^{14}C profile in the mats assumes the mats solely use the TIC in lake water as their carbon source and ^{14}C ages reflect the evolution of $^{14}C_{TIC}$ in the water column. White, black, and grey boxes respectively indicate radiocarbon ages of microbial mat laminae in cores #1, #2, and #3.

4.5 Conclusion

In conclusion, the effects of GLOFs on nutrient loading and their impact on the functioning of aquatic ecosystems remain poorly studied (Meerhoff et al., 2019; Ross et al., 2020), and these events are just beginning to be observed in remote Antarctica (e.g., Pryakhina et al., 2020). Our findings from the well-sealed perennially ice-covered Lake Untersee show that GLOFs can replenish the CO_2-depleted lake with nutrients and maintain the long-term primary production of its unique microbial ecosystem. Antarctica also hosts several subglacial lakes that are hydrologically connected by outburst floods to carbon-deprived coastal waters (Siegert et al., 2016) with limited photosynthetic primary production (Rignot et al., 2013; Vick-Majors et al., 2020). Accordingly, Lake Untersee represents a microcosm of the biological stimulus potential of GLOFs for Antarctic lacustrine and coastal ecosystems.

4.6 References

Allwood, A. C., Walter, M. R., Kamber, B. S., Marshall, C. P. & Burch, I. W. (2006). Stromatolite reef from the Early Archaean era of Australia. *Nature* 441, 714–718.

Andersen, D. T., McKay, C. P. & Lagun, V. (2015). Climate Conditions at Perennially Ice-Covered Lake Untersee, East Antarctica. *J. Appl. Meteorol. Climatol.* 54, 1393–1412.

Andersen, D. T., Sumner, D. Y., Hawes, I., Webster-Brown, J. & McKay, C. P. (2011). Discovery of large conical stromatolites in Lake Untersee, Antarctica. *Geobiology* 9, 280–293.

Bastidas Navarro, M., Martyniuk, N., Balseiro, E. & Modenutti, B. (2018). Effect of glacial lake outburst floods on the light climate in an Andean Patagonian lake: implications for planktonic phototrophs. *Hydrobiologia.* 816, 39–48.

Bevington, J., McKay, C. P., Davila, A., Hawes, I., Tanabe, Y. & Andersen, D. T. (2018). The thermal structure of the anoxic trough in Lake Untersee, Antarctica. *Antarct. Sci.* 30, 333–344.

Bormann, P. (1995). The Schirmacher Oasis, Queen Maud Land, East Antarctica and its surroundings. *Polarforschung* 64, 151–153.

Brenner, A. C., DiMarzio, J. P. & Zwally, H. J. (2007). Precision and accuracy of satellite radar and laser altimeter data over the continental ice sheets. *IEEE Trans. Geosci. Remote Sens.* 45(2), 321-331.

Ciais, P., Jouzel, J., Petit, J. R., Lipenkov, V. & White, J. W. C. (1994). Holocene temperature variations inferred from six Antarctic ice cores. *Ann. Glaciol.* 20, 427–436.

Clark, I. (2015). Groundwater Geochemistry and Isotopes. CRC Press, Boca Raton.

Crann, C. A., Murseli, S., St-Jean, G., Zhao, X., Clark, I. D. & Kieser, W. E. (2017). First Status Report on Radiocarbon Sample Preparation Techniques at the A.E. Lalonde AMS Laboratory (Ottawa, Canada). *Radiocarbon* 59, 695–704.

Dore, J. E. & Priscu, J. C. (2001). Phytoplankton phosphorus deficiency and alkaline phosphatase activity in the McMurdo Dry Valley lakes, Antarctica. *Limnol. Oceanogr.* 46, 1331–1346.

Eggleston, S., Schmitt, J., Bereiter, B., Schneider, R. & Fischer, H. (2016). Evolution of the stable carbon isotope composition of atmospheric CO2 over the last glacial cycle. *Paleoceanography* 31, 434–452.

Faucher, B., Lacelle, D., Fisher, D. A., Andersen, D. T. & McKay, C. P. (2019). Energy and water mass balance of Lake Untersee and its perennial ice cover, East Antarctica. *Antarct. Sci*. 31, 271–285.

Faucher, B., Lacelle, D., Fisher, D. A., Weisleitner, K. & Andersen, D. T., (2020). Modeling δD-δ^{18}O Steady-State of Well-Sealed Perennially Ice-Covered Lakes and Their Recharge Source: Examples From Lake Untersee and Lake Vostok, Antarctica. *Front. Earth Sci.* 8, 220.

Gibson, J. A. E., Wilmotte, A., Taton, A., van de Vijver, B., Beyens, L. & Dartnall, H. J. G. (2006). Biogeographic Trends in Antarctic Lake Communities, in: Trends in Antarctic Terrestrial and Limnetic Ecosystems. Springer Netherlands, Dordrecht, pp. 71–99.

Haendel, D. & Kaup, E. (1995). Nutrients and primary production., in: Bormann, P., Fritzshe, D. (Eds.), The Schirmacher Oasis, Queen Maud Land, East Antarctica, and Its Surroundings. Justus Perthes Verlag.

Hawes, I., Sumner, D. & Jungblut, A. D., (2019). Complex Structure but Simple Function in Microbial Mats from Antarctic Lakes, in: Hurst, C. (Ed.), The Structure and Function of Aquatic Microbial Communities. *Adv. Environ. Microb.* Vol 7. Springer, Cham, pp. 91–120.

Hermichen, W. -D., Kowski, P. & Wand, U. (1985). Lake Untersee, a first isotope study of the largest freshwater lake in the interior of East Antarctica. *Nature* 315, 131–133.

Hiller, A., Wand, U., Kampf, H. & Stackebrandt, W. (1988). Occupation of the Antarctic continent by petrels during the past 35 000 years: Inferences from a 14C study of stomach oil deposits. *Polar Biol.* 9, 69–77.

Hood, E., Battin, T. J., Fellman, J., O'Neel, S. & Spencer, R. G. M. (2015). Storage and release of organic carbon from glaciers and ice sheets. *Nat. Geosci.* 8, 91–96.

Isaksson, E., Karlén, W., Gundestrup, N., Mayewski, P., Whitlow, S. & Twickler, M. (1996). A century of accumulation and temperature changes in Dronning Maud Land, Antarctica. J. *Geophys. Res. Atmos.* 101, 7085–7094.

Jepsen, S. M., Adams, E. E. & Priscu, J. C. (2010). Sediment melt-migration dynamics in perennial antarctic lake ice. *Arctic, Antarct. Alp. Res*. 42, 2010.

Jungblut, A. D., Lovejoy, C. & Vincent, W. F. (2010). Global distribution of cyanobacterial ecotypes in the cold biosphere. *ISME J*. 4, 191–202.

Kaup, E., Loopman, A., Klokov, V., Simonov, I. & Haendel, D. (1988). Limnological investigations in the Untersee Oasis, in: Martin, J. (Ed.), Limnological Studies in Queen Maud Land (East Antarctica). *Tallinn Valgus*, pp. 28–42.

Kieser, W. E., Zhao, X. L., Clark, I. D., Cornett, R. J., Litherland, A. E., Klein, M., Mous, D. J. W. & Alary, J. F. (2015). The André E. Lalonde AMS Laboratory - The new accelerator mass spectrometry facility at the University of Ottawa. *Nucl. Instruments Methods Phys. Res. Sect. B Beam Interact. with Mater. Atoms. 361, 110-114.*

Koo, H., Mojib, N., Hakim, J. A., Hawes, I., Tanabe, Y., Andersen, D. T. & Bej, A. K. (2017). Microbial communities and their predicted metabolic functions in growth laminae of a unique large conical mat from Lake Untersee, East Antarctica. *Front. Microbiol*. 8, 1347.

Lyons, W. B., Leslie, D. L., Harmon, R. S., Neumann, K., Welch, K. A., Bisson, K. M. & McKnight, D. M. (2013). The carbon stable isotope biogeochemistry of streams, Taylor Valley, Antarctica. *Appl. Geochemistry* 32, 26–36.

Mackintosh, A. N., Verleyen, E., O'Brien, P. E., White, D. A., Jones, R. S., McKay, R., Dunbar, R., Gore, D. B., Fink, D., Post, A. L., Miura, H., Leventer, A., Goodwin, I., Hodgson, D. A., Lilly, K., Crosta, X., Golledge, N. R., Wagner, B., Berg, S., van Ommen, T., Zwartz, D., Roberts, S. J., Vyverman, W. & Masse, G. (2014). Retreat history of the East Antarctic Ice Sheet since the Last Glacial Maximum. *Quat. Sci. Rev.* 100, 10–30.

Markus, T., Neumann, T., Martino, A., Abdalati, W., Brunt, K., Csatho, B., Farrell, S., Fricker,

H., Gardner, A., Harding, D., Jasinski, M., Kwok, R., Magruder, L., Lubin, D., Luthcke, S., Morison, J., Nelson, R., Neuenschwander, A., Palm, S., Popescu, S., Shum, C. K., Schutz, B.E., Smith, B., Yang, Y. & Zwally, J. (2017). The Ice, Cloud, and land Elevation Satellite-2 (ICESat-2): Science requirements, concept, and implementation. *Remote Sens. Environ.* 190, 260-273.

Marsh, N. B., Lacelle, D., Faucher, B., Cotroneo, S., Jasperse, L., Clark, I. D. & Andersen, D. T. (2020). Sources of solutes and carbon cycling in perennially ice-covered Lake Untersee, Antarctica. Sci. Rep. 10(1), 12290, 1–12.

Matsumoto, G. I., Nakaya, S., Murayama, H., Masuda, N., Kawano, T., Watanuki, K. & Torii, T. (1992). Geochemical characteristics of Antarctic lakes and ponds. *Proc. NIPR Symp. Polar Biol.* 5, 125–145.

McKnight, D. M., Runkel, R. L., Tate, C. M., Duff, J. H. & Moorhead, D. L. (2004). Inorganic N and P dynamics of Antarctic glacial meltwater streams as controlled by hyporheic exchange and benthic autotrophic communities. *J. North Am. Benthol. Soc.* 23, 171–188.

Meerhoff, E., Castro, L.R., Tapia, F. J. & Pérez-Santos, I. (2019). Hydrographic and Biological Impacts of a Glacial Lake Outburst Flood (GLOF) in a Patagonian Fjord. *Estuaries and Coasts*, 42, 132–143.

Nandigam, V., Lin, K., Phan, M., Borsa, A., Khalsa, S. J. S. & Crosby, C. (2018). Rapid access and visualization of spaceborne altimetry data from ICESAT and ICESAT-2, in: International *Geoscience and Remote Sensing Symposium* (IGARSS).

Neumann, K., Lyons, W. B., Priscu, J. C., Desmarais, D. J. & Welch, K. A. (2004). The carbon isotopic composition of dissolved inorganic carbon in perennially ice-covered Antarctic lakes: Searching for a biogenic signature. *Ann. Glaciol.* 39, 518–524.

Parkhurst, D. L. & Appelo, C. A. J. (2013). Description of Input and Examples for PHREEQC Version 3 — A Computer Program for Speciation , Batch-Reaction , One-Dimensional Transport , and Inverse Geochemical Calculations. U.S. Geol. Surv. Tech. Methods, B. 6, chapter A43.

Perriss, S. J. & Laybourn-Parry, J. (1997). Microbial communities in saline lakes of the Vestfold hills (eastern Antarctica). *Polar Biol.* 18, 135–144.

Pryakhina, G. V., Boronina, A. S., Popov, S. V. & Chetverova, A. A. (2020). Hydrological Studies of Lake Outbursts in the Antarctic Oases. *Russ. Meteorol. Hydrol.* 45(2), 118-123.

Rignot, E., Jacobs, S., Mouginot, J. & Scheuchl, B. (2013). Ice-shelf melting around antarctica. *Science*, 341(6143), 266-270.

Ross, L., Pérez-Santos, I., Parady, B., Castro, L., Valle-Levinson, A. & Schneider, W. (2020). Glacial lake outburst flood (GLOF) events and water response in a patagonian fjord. *Water*, 12(1), 248.

Santibáñez, P. A., Michaud, A. B., Vick-Majors, T. J., D'Andrilli, J., Chiuchiolo, A., Hand, K. P. & Priscu, J. C. (2019). Differential Incorporation of Bacteria, Organic Matter, and Inorganic Ions Into Lake Ice During Ice Formation. *J. Geophys. Res. Biogeosciences*, 124, 585–600.

Schmitt, J., Schneider, R., Elsig, J., Leuenberger, D., Lourantou, A., Chappellaz, J., Köhler, P., Joos, F., Stocker, T. F., Leuenberger, M. & Fischer, H. (2012). Carbon isotope constraints on the deglacial CO2 rise from ice cores. *Science*, 336(6082), 711-714.

Schwab, M. J. (1998). Rekonstruktion der spatquartaren Klima und Umweltgeschichte der Schirmacher Oase und des Wohlthat Massivs (Ostantarktika). Ber. Polarforschung 293, 1–128.

Siegert, M. J., Ross, N. & Le Brocq, A. M. (2016). Recent advances in understanding Antarctic subglacial lakes and hydrology. *Philos. Trans. R. Soc. A Math. Phys. Eng. Sci.*, 374(2059).

Smith, B., Fricker, H. A., Gardner, A., Siegfried, M. R., Adusumilli, S., Csatho, B. M., Holschuh, N., Nilsson, J. & Paolo, F. S., ICESat-2 Science team (2020). ATLAS/ICESat-2 L3A Land Ice Height, Version 3. [ATL06]. [WWW Document]. NASA Natl. Snow Ice Data Cent. Distrib. Act. Arch. Center.

Squyres, S. W., Andersen, D. W., Nedell, S. S. & Wharton, R. A. (1991). Lake Hoare, Antarctica: sedimentation through a thick perennial ice cover. *Sedimentology* 38, 363–379.

St-Jean, G. (2003). Automated quantitative and isotopic (13C) analysis of dissolved inorganic carbon and dissolved organic carbon in continuous-flow using a total organic carbon analyser. *Rapid Commun. Mass Spectrom.*, 17, 419–428.

St-Jean, G., Kieser, W. E., Crann, C. A. & Murseli, S. (2017). Semi-Automated Equipment for CO2 Purification and Graphitization at the A.E. Lalonde AMS Laboratory (Ottawa, Canada). *Radiocarbon* 59, 941–956.

Steel, H. C. B., McKay, C. P. & Andersen, D.T. (2015). Modeling circulation and seasonal fluctuations in perennially ice-covered and ice-walled Lake Untersee, Antarctica. *Limnol. Oceanogr*. 60, 1139–1155.

Stuiver, M. & Polach, H. A. (1977). Discussion Reporting of 14C data. Radiocarbon 19(3), 355-363.

Takacs, C. D., Priscu, J. C. & McKnight, D. M. (2001). Bacterial dissolved organic carbon demand in McMurdo Dry Valley lakes, Antarctica. *Limnol. Oceanogr.* 46, 1189–1194.

Vick-Majors, T. J., Michaud, A. B., Skidmore, M. L., Turetta, C., Barbante, C., Christner, B. C., Dore, J. E., Christianson, K., Mitchell, A. C., Achberger, A. M., Mikucki, J. A. & Priscu, J. C. (2020). Biogeochemical Connectivity Between Freshwater Ecosystems beneath the West Antarctic Ice Sheet and the Sub-Ice Marine Environment. *Global Biogeochem. Cycles* 34, e2019GB006446.

Wadham, J. L., Tranter, M., Skidmore, M., Hodson, A. J., Priscu, J., Lyons, W. B., Sharp, M., Wynn, P. & Jackson, M. (2010). Biogeochemical weathering under ice: Size matters. *Global Biogeochem. Cycles* 24.

Wand, U., Samarkin, V. A., Nitzsche, H. -M. & Hubberten, H. -W. (2006). Biogeochemistry of methane in the permanently ice-covered Lake Untersee, central Dronning Maud Land, East Antarctica. *Limnol. Oceanogr.* 51, 1180–1194.

Wand, U., Schwarz, G., Brüggemann, E. & Bräuer, K. (1997). Evidence for physical and chemical

stratification in Lake Untersee (central Dronning Maud Land, East Antarctica). *Antarct. Sci.* 9, 43–45.

Wharton, R. A., McKay, C. P., Clow, G. D., Andersen, D. T., Simmons, G. M. & Love, F. G. (1992). Changes in ice cover thickness and lake level of Lake Hoare, Antarctica: implications for local climatic change. *J. Geophys. Res*., 97(C3), 3503-3513.

Wharton, R. A., Simmons, G. M. & McKay, C. P. (1989). Perennially ice-covered Lake Hoare, Antarctica: physical environment, biology and sedimentation. *Hydrobiologia* 172, 305–320.

Wynn, P. M., Hodson, A. & Heaton, T. (2006). Chemical and Isotopic Switching within the Subglacial Environment of a High Arctic Glacier. *Biogeochemistry* 78, 173–193.

CHAPTER 5: ICE-COVERED PONDS IN THE UNTERSEE OASIS (EAST ANTARCTICA): DISTRIBUTION, HYDROCHEMISTRY, MICROBIAL ACTIVITY AND TRAJECTORY UNDER A WARMING CLIMATE

Abstract

This study investigates the distribution and hydrochemistry of ice-covered ponds in the Untersee Oasis, East Antarctica. A hierarchical cluster analysis showed that their hydrochemistry clusters were based on the amount of solar radiation reaching their surface during the summer. This influences ice cover stability: ponds that receive higher solar radiation develop moats or completely lose their ice cover during summer, whereas those that receive lower solar radiation retain their full ice cover and remain well-sealed to direct exchanges with the atmosphere. Tritium and $^{14}C_{TIC}$ measurements suggest that the ponds are recharged by modern snowmelt that has equilibrated with atmospheric CO_2. The geochemical facies of the ponds support snowmelt recharge. However, ice cover stability controls the solute load and $\delta^{18}O$ in the ponds along different trajectories. Moatless perennially ice-covered ponds have high pH, low TDS, and TIC and likely host a CO_2-depleted benthic microbial ecosystem. Moated perennially ice-covered ponds and those with seasonal ice cover have lower pH, higher TDS, and TIC and $\delta^{13}C_{TIC}$ that suggest availability of carbon is not limiting photosynthesis of the benthic microbial community. These findings can be used to assess the fate of ponds in the region under a warming climate where moatless ponds start developing moats or even become seasonally ice-covered.

5.1 Introduction

Antarctica's ice-free regions contain thousands of surface ice-covered lakes that host benthic microbial ecosystems (Doran et al., 2004; Greco et al., 2020; Matsumoto et al., 1992; Vincent et al., 2008). Studies on perennially ice-covered lakes in the McMurdo Dry Valleys (MDV) have suggested that the chemical and biological properties of the water column and the primary productivity of the benthic microbial ecosystem are strongly associated with the fate of their ice cover (Fountain et al., 2016; Gooseff et al., 2017; Obryk et al., 2016) and changes to recharge conditions (Badgeley et al., 2017; Lawrence et al., 2020; Lyons et al., 2012; Matsubaya et al., 1978; Mikucki et al., 2015). For example, thinning or removal of the ice cover during summer would alter light levels and initiate wind-driven mixing, resulting in the disruption of stratification regimes and circulation patterns. The introduction of additional surface meltwater could affect the water column's turbidity and ionic composition while delivering allochthonous carbon and other nutrients (Andersen et al., 2015; Dore & Priscu, 2001; Priscu, 1995). Numerical modeling predicts that some Antarctic ice-covered surface lakes (e.g., Lake Bonney, Crooked Lake) could undergo a shift from a perennial to seasonal ice coverage within the coming decades because of increases in air temperature and insolation (Echeverría et al., 2019; Obryk et al., 2019). However, the perennially ice-covered lakes in the MDV all form moats, such that predictions on how future ice cover losses (i.e., a shift to a seasonal ice coverage) will influence their hydrochemistry and microbial activity rely primarily on studies from the more coastal seasonally ice-covered lakes (e.g., Schirmacher Oasis, Bunger Hills, and Vestfold Hills), and high Arctic ice-covered lakes (e.g., Vincent et al., 2008; Mueller et al., 2009; Lehnherr et al., 2018).

The Untersee Oasis is a ~ 60 km^2 ice-free region in Dronning Maud Land (East Antarctica). The Oasis hosts two large perennially ice-covered lakes and multiple smaller ice-covered ponds (Kaup et al., 1988; Haendel et al., 2011; Priscu & Foreman, 2009). These lacustrine basins host benthic microbial ecosystems in the form of mats, pinnacles, and in Lake Untersee's case, large conical stromatolites (Andersen et al., 2011; Greco et al., 2020; Koo et al., 2017). Field observations revealed that Lake Untersee, Lake Obersee, and some of the ponds do not develop moats during the austral summer, whereas other ponds have seasonal ice coverage. Therefore, the lakes and ponds in the region present the full spectrum of ice cover types (i.e., perennially to seasonally ice-covered). Thus, the comparison of hydrochemical properties between basins with

different ice coverages can yield insight into their water column response and microbial activity to a warming climate.

This study aims to make an empirical prediction of the hydrochemical changes and microbial activity of the ice-covered ponds in the Untersee Oasis under a warming climate and changing ice cover regime. This objective is accomplished by first describing the ponds' distribution throughout the Oasis and by presenting their morphometric properties, including measurements made on ice cover blisters. We then determine the major solutes, δD-$\delta^{18}O$, total inorganic and organic carbon (TIC-TOC), and radiocarbon of TIC ($^{14}C_{TIC}$) to assess the source of solutes and water recharging the ponds. Geochemical modeling is also used to evaluate the effects of freezing and evaporation on solute load evolution. The ponds' microbial activity is assessed using $\delta^{13}C_{TIC}$-$\delta^{13}C_{TOC}$ in the ponds relative to the recharge water. Combined, the measurements are used to predict the trajectory of the Untersee Oasis ponds' hydrochemical properties under a warming climate as they transition from moatless perennially ice-covered to seasonally ice-covered.

5.2 Study area

The Untersee Oasis (71.3°S; 13.5°E) is located in the Gruber Mountains of Queen Maud Land, approximately 150 km from the Princess Astrid Coast and ~ 90 km southeast of the Schirmacher Oasis (Fig. 5-1). The Untersee Oasis, which the East Antarctic Ice Sheet surrounds, has two main ice-free valleys: 1) the Lake Untersee Valley, an ~ 11 km long and ~ 4 km wide north-south trending valley; and 2) the Aurkjosen Valley, a ~ 4 km long and ~ 3 km wide east-west trending valley. The local geology consists of Precambrian norite, anorthosite, and anorthosite-norite alternation of the Eliseev massif complex (Bormann et al., 1986; Kampf & Stakerbrandt, 1985; Paech & Stackebrandt, 1995). The East Antarctic Ice Sheet covered the region during the Late Pleistocene and based on ^{14}C ages of stomach oils from snow petrel nests, thinning of the ice sheet began at c. 35-30 ka (Hiller et al., 1988). This led to a reconfiguration of the local ice flow, and the Untersee Oasis came to its current configuration at c. 6-4ka. The surface sediments in the Oasis consist mainly of till and colluvium, often covered by a thin layer of eolian sediments (Schwab, 1998). The Lake Untersee Valley has a large terminal moraine with ice-cored lateral moraines.

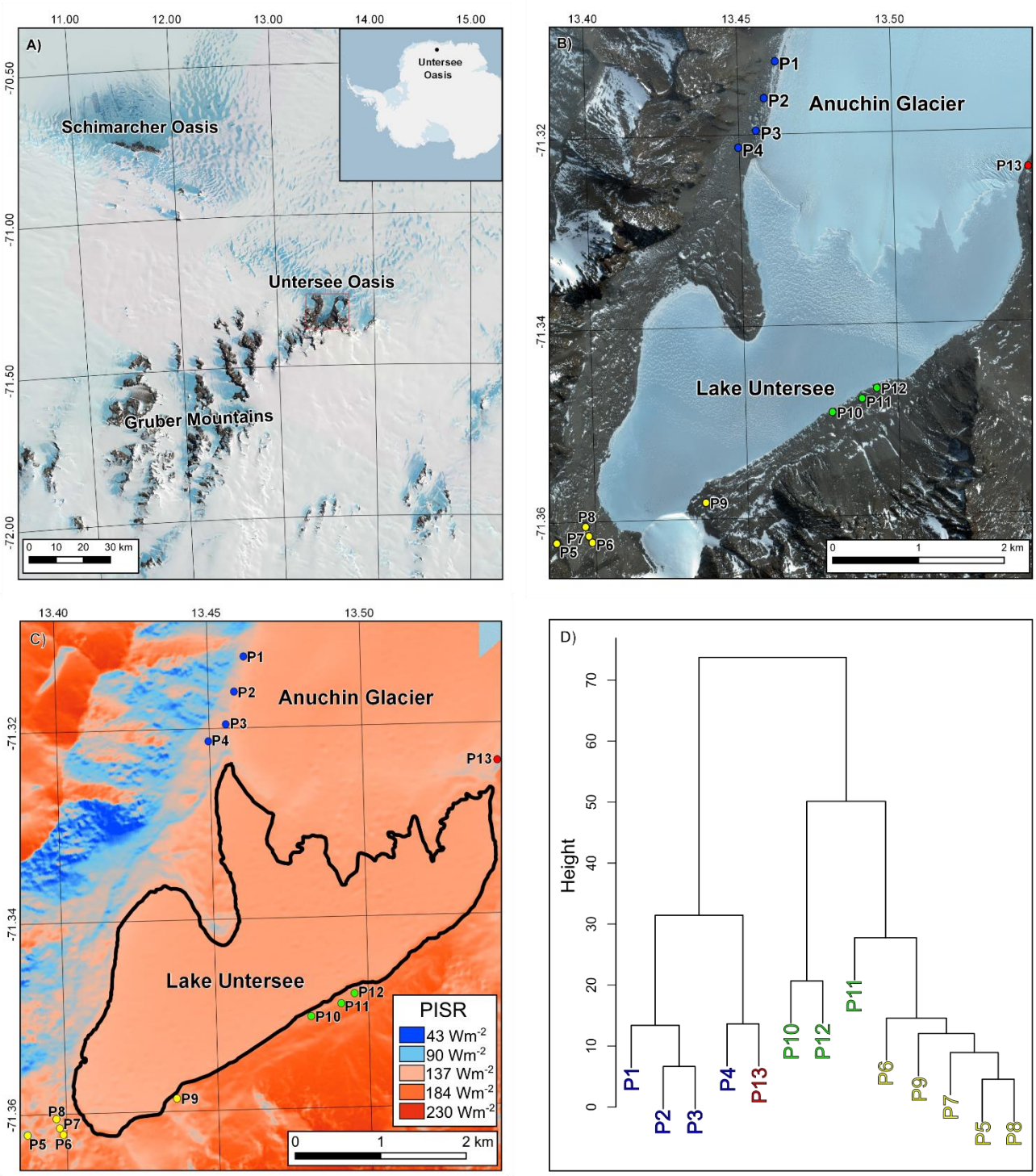

Figure 5-1: A) Location map of Dronning Maud Land's Untersee Oasis (overlaid on the LIMA Landsat high-resolution virtual mosaic; Bindschadler et al., 2008); B) Location map of sampled ponds (overlaid on a December 7th, 2017th WorldView satellite image); C) Potential Incoming Solar Radiation (PISR; Wm^{-2}) map for the Untersee Oasis, during the austral summer; D) Hierarchical cluster plot of the ponds (based on their pH, TIC, TOC, PISR, $\delta^{18}O$, and D-excess values).

The Untersee Oasis has a polar desert climatic regime. Data collected during the 2008-2017 period by an automated weather station along the shoreline of Lake Untersee (71.34°S, 13.45°E, 612 m a.s.l.) yielded a mean annual air temperature of –9.5±0.7°C with thawing degree-days ranging from 7 to 51, and a mean relative humidity of 42±5% (Dale T. Andersen et al., 2015; Faucher et al., 2019). Despite having a relatively warm mean annual air temperature for Antarctica, the Oasis climate is dominated by intense evaporation and sublimation, which limits surface melting due to cooling associated with the latent heat of sublimation (e.g., Hoffman, Fountain, & Liston, 2008). The snow in the region is characterized by Ca(Na)-SO_4 facies (Isaksson et al., 1996). The slope of the local meteoric water line (LMWL) in the Untersee Oasis is 7.8 ($\delta D = 7.8*\delta^{18}O + 5.2$; unpublished data), similar to the one at nearby Neumayer station ($\delta D = 7.9*\delta^{18}O + 7.6$; Fernandoy et al., 2010). In the Untersee Oasis, near-surface samples of the Anuchin Glacier and snow have $\delta^{18}O$ values ranging from –36.4 to –22.3‰ (Faucher et al., 2020). The tritium concentration of snow sampled at the nearby Schirmacher Oasis in the late 1990s was 5.8±0.5 TU (Sinha et al., 2000).

The Untersee Oasis's hydrology is characterized by standing water bodies with no supraglacial streams on the Anuchin Glacier. Lake Untersee (8.7 km^2) and Lake Obersee (3.4 km^2) are the two largest perennially ice-covered lakes, and neither develop a seasonal moat. In addition, numerous perennially ice-covered ponds are present along the lateral and terminal moraines of the Lake Untersee valley. The smallest water bodies are in the cryoconite holes on the Anuchin Glacier, and glacial ice patches on the ice cover Lake Untersee (Weisleitner et al., 2019; 2020). The Aurkjosen Valley has only one perennially ice-covered pond, and it is located at the head of the valley. Lakes Untersee, Obersee, and Burevestniksee (situated on the west lateral moraine; herein referred to as P3) are the only water bodies previously analyzed for their geochemical composition. All three lakes are characterized by high pH (9.5-11.4), high dissolved oxygen (120-280%), and low specific conductivities (90-480 $\mu S/cm^{-1}$). Snow petrels are one of the few wildlife inhabiting the oasis, and they often bathe in moated sections of ponds.

5.3 Methods

5.3.1 Distribution and morphology of ponds

The distribution and morphology of ponds in the Untersee Oasis was determined from photos acquired in December 2017 and November 2019 using a *DJI Phantom 4 Pro* unmanned air vehicle (UAV). The UAV was flown 30 m above the ground in a gridded survey with the *DJI Mission Planner* software, with 85% forward and 75% side overlap. The photos at 1 cm resolution were captured at 400 ISO, shutter speed of 1/1000 s, and with focus fixed at infinity. The accuracy of the GPS tags from the JPEG Exif metadata was optimized with ground control points surveyed using a Trimble R9s dGPS and a local base station. The *Agisoft Photoscan Pro v.1.4* software was used to generate point-cloud models of the ponds. The dense point-cloud models in .LAS data format (WGS 1984 UTM zone 33S projection) were used to create ortho-mosaics and digital surface models (DSMs). The ortho-mosaics and DSMs were used to determine each pond's elevation and surface area and the height and volume of ice blisters (if present) using the Surface Volume tool in *ArcGIS Pro 2.4.*

5.3.2 Field sampling

Out of the 39 ponds identified in Untersee Oasis, 13 were sampled to determine their geochemical composition. Water was collected near each pond's edge, and no attempt was made to determine if the ponds were stratified; the samples should be considered surface water. Due to the ponds' high pH, the samples were collected unfiltered and transferred immediately into sampling bottles with care to limit exchanges with atmospheric CO_2. Water samples for major ions and δD-$\delta^{18}O$ analyses were collected in sealed 20 ml HDPE bottles (samples for cations and anion were collected in separate bottles, with cation samples acidified using 2 µL of trace metal grade 10% nitric acid). Samples for pH, specific conductivity, total inorganic carbon (TIC), and $\delta^{13}C_{TIC}$ compositions were collected in 40 ml pre-baked glass amber bottles with care to limit atmospheric interactions. Samples for $^{14}C_{TIC}$ analyses were collected in 1L pre-baked glass amber bottles. Samples for tritium were collected in sealed 125- or 1000-ml HDPE bottles. All water samples were shipped in coolers and stored at 4°C until analyses at the University of Ottawa.

5.3.3 Laboratory analyses

The ponds' pH and specific conductivity were measured from samples collected in glass amber bottles with septum using a calibrated *Mettler Toledo* handheld meter. For measurements,

the septum was removed, and the probe was inserted in the cap to limit exchange with atmospheric CO_2. Major cations (Ca^{2+}, Na^{+}, $Mg^{2+,}$ and K^{+}) were measured acidified using an *Agilent 4200* inductively coupled plasma atomic emission spectrometer. Major anions (SO_4^{2-}, NO_3^{-} and Cl^{-}) were measured by ion–chromatography (IC) using a *DIONEX* ion-chromatograph. Analytical precision is ±5%. The average charge balance error was +12% using measured cations-anions and [OH^{-}] and [H^{+}] for average pH of 10.

The stable water isotopes of the ponds and melted ice samples were determined using a *Los Gatos Research* liquid water analyzer coupled to a CTC LC-PAL auto-sampler for simultaneous measurements of $^{18}O/^{16}O$ and D/H ratios. The results are presented using the δ-notation, where δ represents the parts per thousand differences for $^{18}O/^{16}O$ or D/H in a sample with respect to Vienna Standard Mean Ocean Water (VSMOW). Analytical reproducibility for $\delta^{18}O$ and δD was ±0.3‰ and ±1‰, respectively. Deuterium excess (*d*) was calculated according to (Dansgaard, 1964) ($d = \delta D - 8*\delta^{18}O$).

The total organic and inorganic carbon (TOC and TIC) and their stable isotope ratios ($^{13}C/^{12}C$) in the ponds were measured at the Jan Veizer Laboratory by a wet TOC analyzer interfaced with a Thermo DeltaPlus XP isotope ratio mass spectrometer using methods described by St-Jean (2003). The isotope ratios are presented using the δ-notation with respect to the Vienna Ped Dee Belemnite reference (VPDB). The 2σ analytical precision is ±0.5 ppm for TOC and TIC concentrations and ±0.2‰ for the isotopes. The detection limit of TIC and TOC analyses is <0.3 ppm.

Radiocarbon analysis of the TIC in the ponds was performed at the University of Ottawa's A.E. Lalonde Accelerator Mass Spectrometry laboratory. Sample preparation, extraction of inorganic and organic from waters, and graphitization is described by Murseli et al. (2019). Graphitized samples were analyzed on a 3MV tandem mass spectrometer. The $^{14}C/^{12}C$ ratios are expressed as fraction of modern carbon ($F^{14}C$) and corrected for spectrometer and preparation fractionation using the AMS measured $^{13}C/^{12}C$ ratio (Crann et al., 2017). Radiocarbon ages are calculated as $-8033\ln(F^{14}C)$ and reported in ^{14}C yr BP (BP=AD1950) as described by (Stuiver & Polach, 1977). The 2σ errors are less than 0.013 $F^{14}C$ (or <190 years).

Tritium (^{3}H) sample preparation and measurement were performed by the University of Ottawa's A.E. Lalonde Tritium and Radiohalide laboratory. The samples were enriched by

electrolytic and were then decay counted on a low–background Quantilus liquid scintillation counter. Results are reported in tritium units (TU), and the 2σ analytical precision is ±0.8 TU.

5.3.4 Modeling Potential Incoming Solar Radiation

The amount of potential incoming short wave radiation that reaches the ice-covered lakes has a significant impact on their heat and energy balance (Mckay et al., 1985; Petrov et al., 2005). The potential incoming solar radiation (PISR) in the Untersee Oasis was determined using the Area Solar Radiation tool in *ArcGIS Pro 2.4* and the 8 m spatial resolution Reference Elevation Model of Antarctica (REMA) (Howat et al., 2019). The PISR was computed at 1h interval for austral summer (December, January and February) with a sky size of 512 cells and cloud cover and transmissivity set at 30 and 80% (according to Andersen et al., 2015), respectively. The PISR is represented in WHm^{-2} and was converted to Wm^{-2} by dividing by the direct duration. The PISR raster output fits reasonably well with the incoming summer radiation measured at the meteorological station at Lake Untersee (measured = 100 Wm^{-2} (by Andersen et al., 2015) and modeled = 120 Wm^{-2}).

5.4 Results and Discussion

5.4.1 Distribution of ponds in the Untersee Oasis

We inventoried a total of 39 ponds in the Lake Untersee valley. The ponds are located in four regions: the west (n=24) and east (n=7) lateral moraines of the Anuchin Glacier, the terminal moraine (n=5), and the eastern shore of Lake Untersee (n=3); no ponds were observed along the west shoreline of the lake (Fig. 5-1B). The ponds' mean surface area is 2190±4536 m^2 (60 to 21,771 m^2), and based on Landsat and Digital Globe imagery, it appears that they have maintained a similar extent for the past two decades. Unlike ponds in the MDV (Berry Lyons et al., 2012), most of the sampled ponds in the Untersee Oasis do not show a relation between surface area and elevation except for the ponds situated along west lateral moraine (Fig. 5-2). Field and airborne observations suggest that channels interconnect these ponds; a spill-and-fill could explain why P3 (Lake Burevestniksee), located at a lower elevation, is the largest one along the western moraine. The ponds' interconnectivity was also noted for those on the east lateral moraine, but the elevation-surface area relation is weak. The PISR during the austral summer in the Untersee Oasis ranges from 119 to 162 Wm^{-2}, with ponds located along eastern sections received higher PISR (Fig. 5-1C). This spatial variation in the PISR affects the stability of the ice cover during austral summers.

In December 2019, some of the ponds along the east shoreline of Lake Untersee had developed moats (e.g., P5-P9, P11-P12), whereas others completely lost their ice cover (e.g., P10, seasonal ice cover). Conversely, the ponds along the western lateral moraine (i.e., P1-P4) did not develop moats, and their shorelines were still covered by snow.

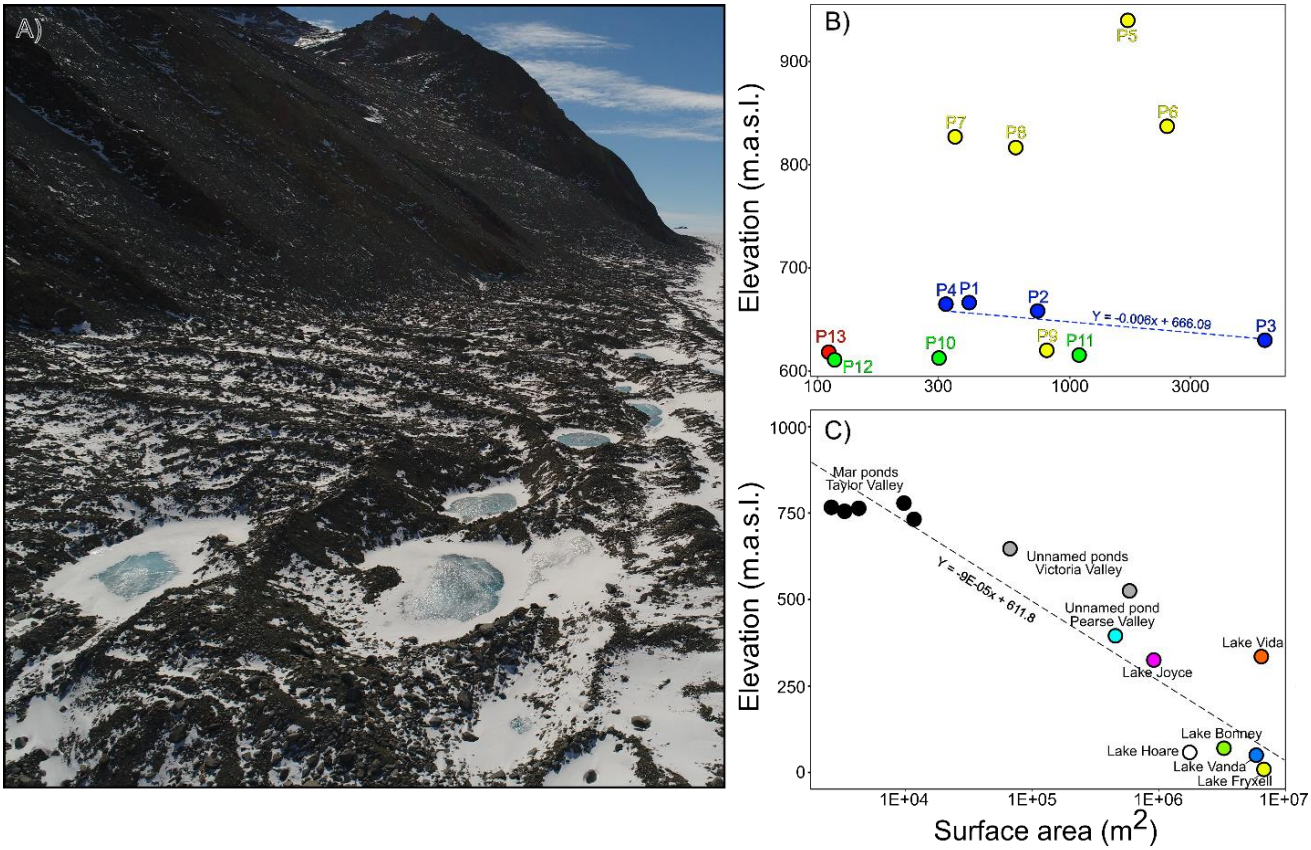

Figure 5-2: A) Aerial photo of some of the west lateral moraine ponds (photo taken above the P3 pond, in the NW direction). B) Scatter plot showing the surface area (m^2) and elevation of the Untersee Oasis ponds. Note the negative relationship between pond elevation and surface area for the west lateral moraine ponds. X axis has a logarithmic scale. C) Scatter plot showing the surface area (m^2) and elevation relation for lakes and ponds in the MDV (data from Lyons et al., 2012; Fountain et al., 2017).

Singular ice blisters were observed on six of the 13 sampled ponds. All six blisters were elliptical, with an average height, surface area, and volume of 0.48 m, 157 m^2, and 27.4 m^3 respectively (Appendix D, Table D1). Dilation cracks were observed on all ice blisters, and the cracks were typically oriented along the long axis of the blisters. The surface area of ponds with ice blisters was <1100 $m^{2,}$ and the volume of the ice blister showed a positive relationship with the surface area of the ponds (Fig. 5-3). The only other Antarctica location where ice blisters on

perennially ice-covered ponds have been observed is in Terra Nova Bay, in Northern Victoria Land (Guglielmin et al., 2009). The ice blisters in Terra Nova Bay have similar morphology to those in the Untersee Oasis, with a positive correlation between the ponds' surface area and the blister's volume. This positive relationship suggests that the ice blisters are likely formed by closed-system hydrostatic pressures developing during the ice cover accretion in winter and that their water column almost completely freezes to the bottom. The ponds that do not develop ice cover blisters likely have a water column that remains thick enough in the winter to prevent hydrostatic uplift of the overlying ice cover and are not fed by water flowing in supra or intra-permafrost taliks.

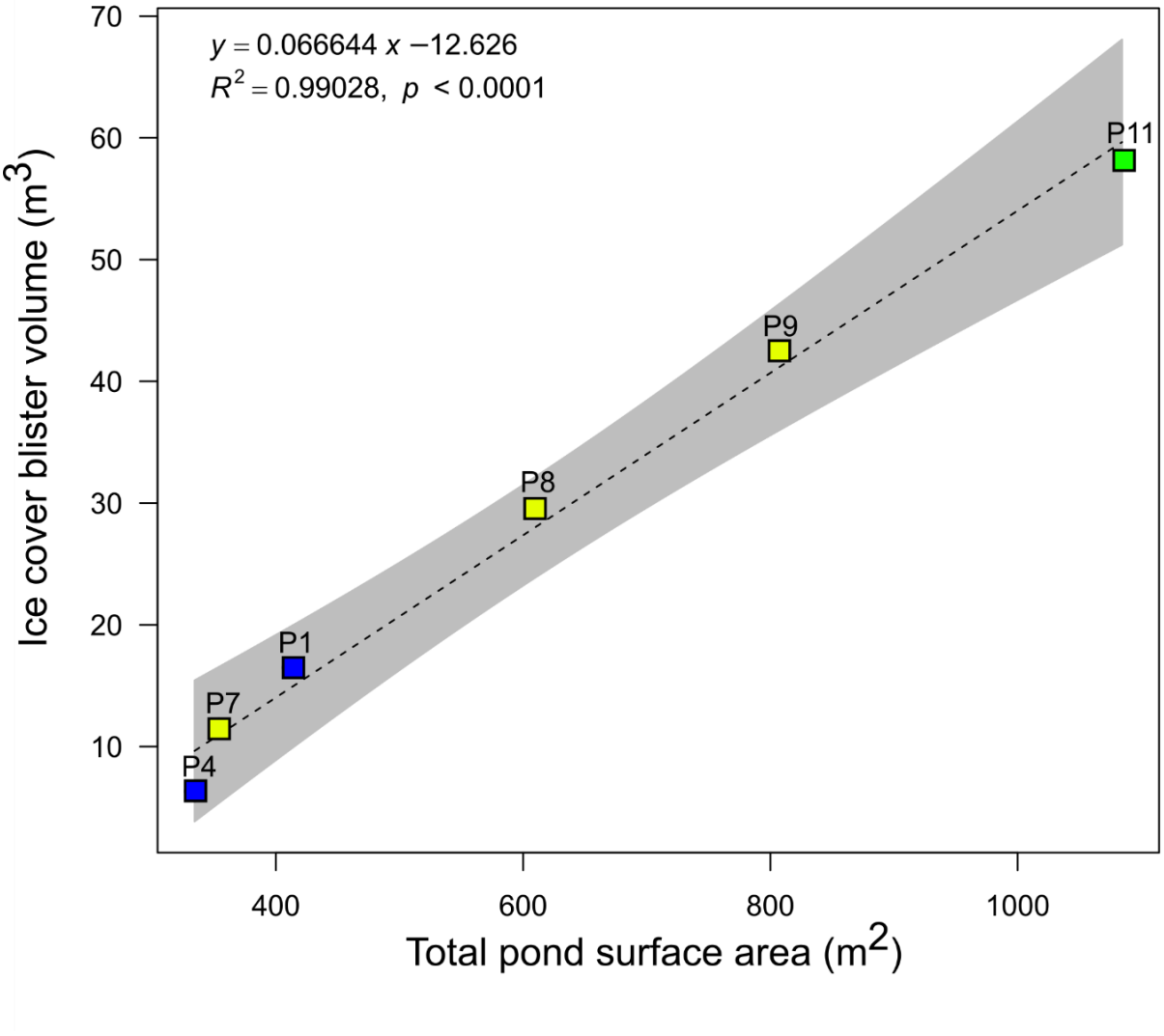

Figure 5-3: Scatter plot showing the relation between total pond surface area (m^2) and ice blister volume (m^3).

5.4.2 Geochemistry of ponds

A hierarchical cluster analysis was performed to summarize the measured physical and chemical variables of the 13 sampled ponds in Untersee Oasis. The hierarchical cluster analysis clustered the ponds into three groups based on their location and spatial variation in PISR (Fig. 5-1D). Group 1 consists of the ponds along the west and east lateral moraines (i.e., P1-P4, P13). These ponds receive low PISR (119 to 129 Wm^{-2}), they do not develop a moat, and their near-surface water is characterized by a neutral to high pH (7.4 to 11.8) (Appendix D, Table D2). Further, they have a wide range in specific conductivity (84 to 900 $\mu S/cm^{-1}$), a Na-Cl facies (exception is P3 that has a Ca-SO_4 facies) and $\delta^{18}O$ values that are the most depleted (–41.9 to –30.3‰) and negatively correlated with [Cl^-]; this group of ponds shares the most characteristics with Lake Untersee (i.e., Marsh et al., 2020). Group 2 consists of the ponds located along the east shoreline of Lake Untersee. These ponds receive the highest PISR (154 to 162 Wm^{-2}), and most develop moats during the summer (i.e., P11-P12), while others have a seasonal ice cover (i.e., P10). The near-surface waters have the lowest pH (6.9 to 7.8) with high specific conductivity (162 to 2380 $\mu S/cm^{-1}$) and high $\delta^{18}O$ values (–24.3 to –20.9‰) that are positively correlated with [Cl^-]. Their δD-$\delta^{18}O$ values plot well below the LMWL. Group 3 includes the ponds situated on the terminal moraine (i.e., P5-P9), at the south of the Lake Untersee Valley. These ponds receive intermediate PISR (134 to 144 Wm^{-2}), and some develop ephemeral moats. They are characterised by a Na-SO_4 geochemical facies, have neutral to high pH (7.1 to 9.7), low specific conductivity (59 to 232 $\mu S/cm^{-1}$), and their $\delta^{18}O$ values show no relation with [Cl^-]. In the following sections, we discuss the source of solutes, the effect of PISR on moating and evolution of the water chemistry, and the trajectory of hydrochemistry of ponds under a warming climate.

5.4.3 Source of recharge and solutes to the ponds

The source of water recharging the ponds in the Untersee Oasis can be constrained by the tritium and $F^{14}C_{TIC}$ measurements. Tritium is a radionuclide (12.5-year half-life) produced naturally in the upper atmosphere with enhanced anthropogenic production during the early 1960s from nuclear testing (Clark, 2015). Tritium was detected in five of the six ponds sampled for this analysis (1.5 to 11.8 TU; Appendix D, Table D3); these concentrations are in the range of modern levels measured in nearby snow and ice cores (5-7 TU range) (Naik et al., 2010; Sinha et al., 2000). These ponds also have $F^{14}C_{TIC}$ in the 0.97 to 1.0 range (Appendix D, Table D3), suggesting that the waters have been in contact and equilibrated with contemporary atmospheric CO_2. Together,

the tritium and $F^{14}C_{TIC}$ measurements indicate that the ponds are recharged by modern snowmelt. This snowmelt runoff likely recharges the ponds via summer moats (for those that develop one) and/or along the edge of the lake basin (for those that maintain full summer ice coverage). However, P2 had a tritium concentration below detection limit (<0.8 TU) but had $F^{14}C_{TIC}$ of 0.99. P2 is located along the western lateral moraine, and it is likely recharged by surface melting of tritium-free snow (i.e., residual snow along the shoreline or at higher elevation) that have dissolved modern atmospheric CO_2.

The geochemistry of the ponds supports recharge from snowmelt. The ponds have low TDS and Ca(Na)-SO_4 or Na-Cl facies (Fig. 5-4). Normalizing solute concentrations to Cl^- (a conservative tracer) allows the effects of cryo- or evapo-concentration of solutes in the ponds to be removed and comparisons to be made with the values in snow and other possible sources of solutes (e.g., Marsh et al., 2020). Snow in the Untersee Oasis was not analyzed for chemistry, but it should be similar to the geochemical record of shallow firn cores from the EPICA Dronning Maud Land (Isaksson et al., 1996). The ponds have Na/Cl and Ca/Cl molar ratios (1.36±0.81; 0.75±0.31, respectively) that are higher than those in the nearby EPICA DML core (0.49±0.21; 0.034±0.036, respectively), suggesting that weathering of local silicate minerals might contribute Na^+ and Ca^+ ions (Kaup et al., 1988; Hermichen et al., 1985; Marsh et al., 2020). Plagioclase weathering simulations under closed- and open-system scenarios (for moatless and moated ponds) with PHREEQC yield much higher Na/Cl and Ca/Cl ratios than those measured for the ponds, regardless of the plagioclase mineral assemblage used for the simulations (Marsh et al., 2020). This suggests that, as for Lake Untersee, weathering of plagioclase is a minor contributor of Ca^+ and Na^+ (< 1% in the ponds). Given the absence of local sulfate evaporites, the SO_4 in the ponds is sourced from marine and/or terrestrial aerosols contributing to snowmelt (Alexander et al., 2003; Marsh et al., 2020). This is confirmed by the $\delta^{34}S_{SO4}$ in P2 and P3 (11.4 and 11.1‰) that are within the range of the non-sea-salt sulfate component (7.5–15.1‰; Alexander et al., 2003; Jonsell et al., 2005).

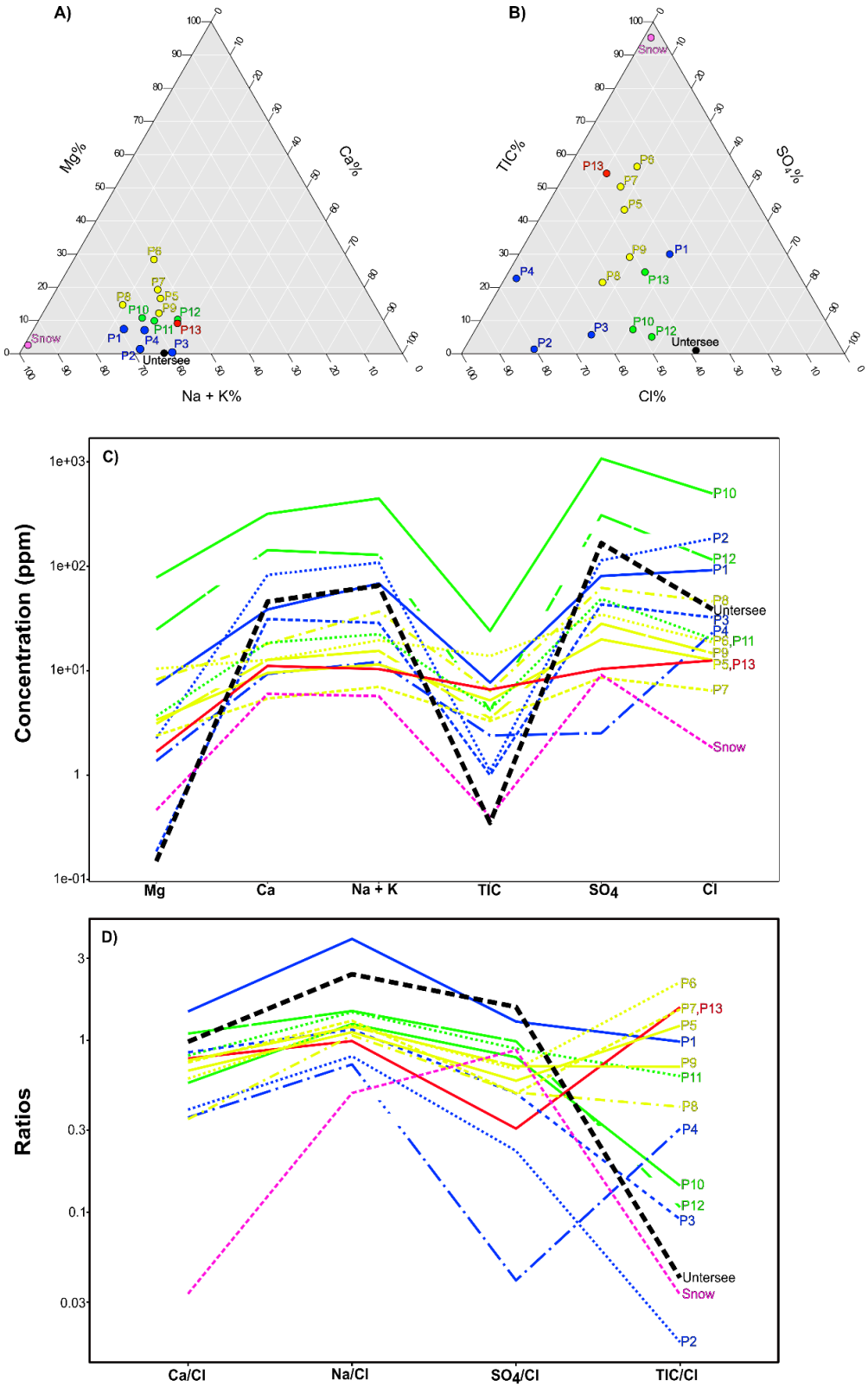

Figure 5-4: A) Cations ternary plot; B) Anions ternary plot; C) major cations concentration line chart; and D) Cl^- normalized ratios line chart for Ca, Na, SO_4 and TIC in the Untersee Oasis ponds. Values from Lake Untersee's oxic water column (2017) and from nearby snow/firn samples (Isaksson et al., 1996) have been added for comparisons.

5.4.4 Fate of ice cover and evolution of $\delta^{18}O$ and solutes

Despite all 13 sampled ponds being recharged by snowmelt and solutes sourced from snow and plagioclase weathering, the $\delta^{18}O$ and solutes evolved differently within the ponds (i.e., Horita, 2009). Ponds situated in regions that receive higher PISR (group 2) develop moats or completely lose their ice cover during the summer. This allows for evaporation of open water and leads to an enrichment of δD-$\delta^{18}O$ and solutes and a positive relation between $\delta^{18}O$ and $[Cl^-]$, as observed for the ponds along the east shoreline of Lake Untersee (Fig. 5-5C). Conversely, ponds situated in regions with lower PISR (group 1) do not develop moats. The δD-$\delta^{18}O$ composition and solute load are affected mainly by the freezing at the bottom of the ice cover. This process leads to a depletion in δD-$\delta^{18}O$ and enrichment of solutes and a negative relation between $\delta^{18}O$ and $[Cl^-]$; as the ponds along the western lateral moraine display (Fig. 5-5C).

Here, we model the evolution of $\delta^{18}O$ and $[Cl^-]$ in the ponds in a freezing system (group 1) and an evaporative system (group 2) (Fig. 5-5C). The modeling exercise is not meant to reproduce the values measured in the ponds as we do not have sufficient control on key input variables for each pond, but to shed light on the extent freezing and evaporation are affecting the isotopic chemistry of the ponds. For the freezing simulation, we used the recursive *FREEZCH9* model developed by Faucher et al. (2020) and Fisher et al. (2020) for moatless perennially ice-covered lakes. *FREEZCH9* takes into account the changing salinity in the water column as a result of freezing and mixes the recharge water to the residual water. Under hydrological steady-state, the evolution of δD-$\delta^{18}O$ and solutes in the water column are controlled by the rate of recharge that is determined by the sublimation rate of the surface of the ice cover (which equals the freezing rate at the bottom of the ice cover (i.e., Mckay et al., 1985). For the ponds, freezing was simulated, assuming the ponds are under hydrological steady-state with mixing rates of 5 and 50%, $\delta^{18}O$ of the recharge water of –32‰ and Cl^- of 2 and 10 ppm (similar to the nearby EPICA DML core; Isaksson *et al.,* 1996). Modeling shows that isotopic equilibrium is reached after three or more residence times. The difference between initial and equilibrium $\delta^{18}O$ values is determined by mixing, but $[Cl^-]$ would continue to increase progressively. The $\delta^{18}O$-Cl^- composition of P1 and P4 have a good fit with that predicted under a steady-state freezing system. However, P2 and P3 plot below the steady-state $\delta^{18}O$-Cl^- curve, either because 1) they have not yet received summer recharge at the time of sampling or 2) they are recharged by meltwater with lower $\delta^{18}O$ composition. The latter is the most likely scenario considering that the distribution of P2 and P3

along the freezing line only suggests that these ponds would nearly wholly freeze, but no ice blisters were observed.

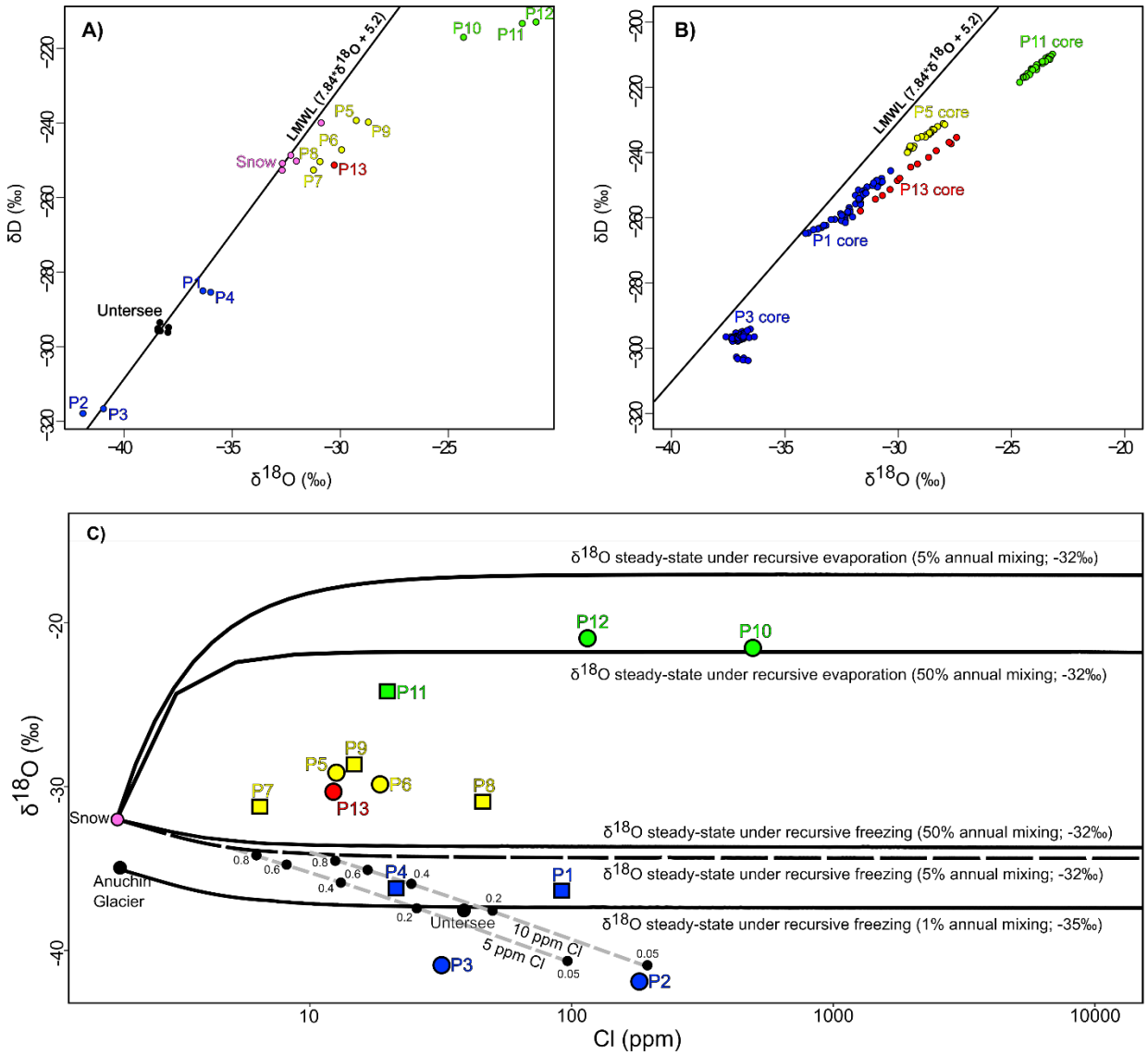

Figure 5-5: Scatter plots of A) δD-$\delta^{18}O$ of near-surface water and B) ice cover samples. C) Evolution modeling of $\delta^{18}O$ and Cl^- in the water column of the ponds under steady-state freezing (group 1) and evaporation (group 2). Grey dotted lines indicate the predicted evolution of $\delta^{18}O$-Cl^- values under ice cover freezing for well-sealed ponds with an annual mixing rate of 5% that have reached $\delta^{18}O$ steady-state. In both freezing simulations, the initial $\delta^{18}O$ is set to -32‰, and the initial Cl^- values are set to 5 and 10 ppm (similar to that of the nearby DML firn core; Isaksson et al., 1996). Squares and circles each respectively indicate ponds with and without ice cover blisters. Black dots accompanied by decimal numbers show the fraction of residual water left in each of the six simulations.

To model the effect of evaporation on the $\delta^{18}O$ and Cl^- of ponds that develop moats (group 2), we used a recursive model similar to *FREZCHEM5* to simulate evaporation. Still, we did not include the effect of seasonal freezing at the bottom of the ice cover. The latter is not critical given that the water-vapor fractionation factor ($\alpha^{18}O$-w-v = 1.0116 at 0°C; Majzoub, 1971) is ~ 4 times larger than the water-ice fractionation factors ($\alpha^{18}O$-i-w = 1.0031; O'Neil, 1968). For the ponds, evaporation was simulated for temperature and relative humidity in the boundary layer of 0°C and 80%, respectively, and the same conditions used for freezing: hydrological steady-state, mixing rates of 5 and 50%, $\delta^{18}O$ of the recharge water of –32‰, with Cl^- of 2 and 10 ppm. The $\delta^{18}O$-Cl^- composition of P10-P12 has a good fit with that predicted under a steady-state evaporative system (Fig. 5-5C). Under an evaporative system, the evolution of δD-$\delta^{18}O$ and solutes in the water column progressively increases, with isotopic equilibrium being reached after three or more residence times and the difference between initial and equilibrium $\delta^{18}O$ ratios determined by the mixing rate. Our simulations demonstrate that the group 2 ponds are affected by evaporation and that this is a consequence of the higher PISR that they receive during the summer months.

5.4.5 Benthic microbial activity in the ponds

The TIC and $\delta^{13}C_{TIC}$ in the water column of perennially ice-covered lakes has been used to assess the carbon cycling of their benthic microbial ecosystem (e.g., Wharton et al., 1993; Lawson et al., 2004; Neumann et al., 2004). For example, in near-neutral pH benthic lacustrine ecosystems where abundant CO_2 is available for carbon fixation by the Rubisco enzyme, photosynthetic activity preferentially utilizes ^{12}C, producing microbial mats with depleted $\delta^{13}C$ and leaving the residual TIC enriched in ^{13}C (Hage et al., 2007; Hayes, 1993; Lawson et al., 2004). However, in high pH CO_2-depleted ecosystems, the cyanobacteria transport HCO_3^- and CO_3^{2-} to their cells where carbonic anhydrase subsequently catalyzes the production of dissolved CO_2 used for carbon fixation (Badger, 1987; Hayes, 1993). This process is non-fractionating since all the TIC is used; Lake Untersee is an example of such a CO_2-depleted ecosystem, and the $\delta^{13}C$ values of englacial meltwater, TIC in the water column, and top layer of mats are equal (Marsh et al., 2020).

The TIC and $\delta^{13}C_{TIC}$ of the snowmelt that recharges the ice-covered ponds has not been determined because snowmelt was absent during our field campaigns. Snowmelt flowing over plagioclase material should have TIC and $\delta^{13}C_{TIC}$ in near-equilibrium with atmospheric CO_2: [TIC] of 1.2-1.5 ppm C and $\delta^{13}C_{TIC}$ ~ –6.8‰ (assuming a pH of 5.6 for atmospherically equilibrated

waters, $\delta^{13}C_{CO2}$ of –8‰, and a CO_2(gas)-CO_2(aqueous) fractionation factor of 1.0012 at 0°C (Clark, 2015). However, the ponds have higher pH (7-10), [TIC] (>1.5 ppm C), and lower $\delta^{13}C$ (–18.0 to –1.9‰) (Fig. 5-6). Although the soils around the ponds are largely deprived of organic matter (Shamilishvili et al., 2020), the ponds, especially those that develop moat, are frequently visited by snow petrels that leave organic material. The TOC in the ponds is in the 1.2 to 12.6 ppm C range and is much higher than in Lake Untersee (~ 0.3 ppm C), with low $\delta^{13}C_{TOC}$ values (<–15‰, except P2 and P3; Fig. 5-6). Steele (2005) found that the $\delta^{13}C$ of the snow petrels' humeri bone collagen ranged between –24.7 to –22.9‰, and this is in the range of the $\delta^{13}C_{TOC}$ in most ponds. The decomposition of TOC would provide additional TIC and produce $\delta^{13}C_{TIC}$ with a value similar to the $\delta^{13}C_{TOC}$ (e.g., Lawson et al., 2004). Assuming that the TIC in the ponds is sourced mostly from the oxidation of TOC, the higher $\delta^{13}C_{TIC}$ over $\delta^{13}C_{TOC}$ suggests that, unlike Lake Untersee, the benthic microbial mats of most ponds are not CO_2-depleted (Fig. 5-6). The maximum carbon fractionation factor of cyanobacteria ranges between 1.018 and 1.023 (Calder & Parker, 1973; Pardue et al., 1976), which is slightly higher than the difference between $\delta^{13}C_{TIC}$ over $\delta^{13}C_{TOC}$ (5-15‰ higher). P2 and P3 have well-sealed ice covers with pH, [TIC], [TOC], and TIC/Cl similar to Lake Untersee, but with higher $\delta^{13}C_{TIC}$ and $\delta^{13}C_{TOC}$ values (Fig. 5-6). These two ponds are recharged by snowmelt likely with [TIC] near 1.5 ppm C and $\delta^{13}C_{TIC}$ near –6.8‰ and photosynthesis uptake of CO_2 could decrease the TIC and increase $\delta^{13}C_{TIC}$; if that is the case, photosynthesis activity appears to be restricted compared to the other ponds given the more negligible difference between the predicted input and measured pond water columns' $\delta^{13}C_{TIC}$.

Overall, it appears that most ponds host a benthic microbial ecosystem that is not CO_2-depleted. The range in TIC/Cl in the ponds is similar to that of perennially ice-covered lakes in the MDV. However, the $\delta^{13}C_{TIC}$ values are much lower in the ponds in the Untersee Oasis. This would suggest that the source of TIC is different, mainly sourced from the oxidation of TOC in the ponds. In the MDV, the lakes are recharged by glacial meltwater rivers where it can source TIC from the dissolution of atmospheric CO_2, and carbonate dissolution with $\delta^{13}C$ near 0‰ is also a source of TIC to these lakes. Conversely, the Untersee Oasis lacks rivers and snowmelt channels directly entering the ponds.

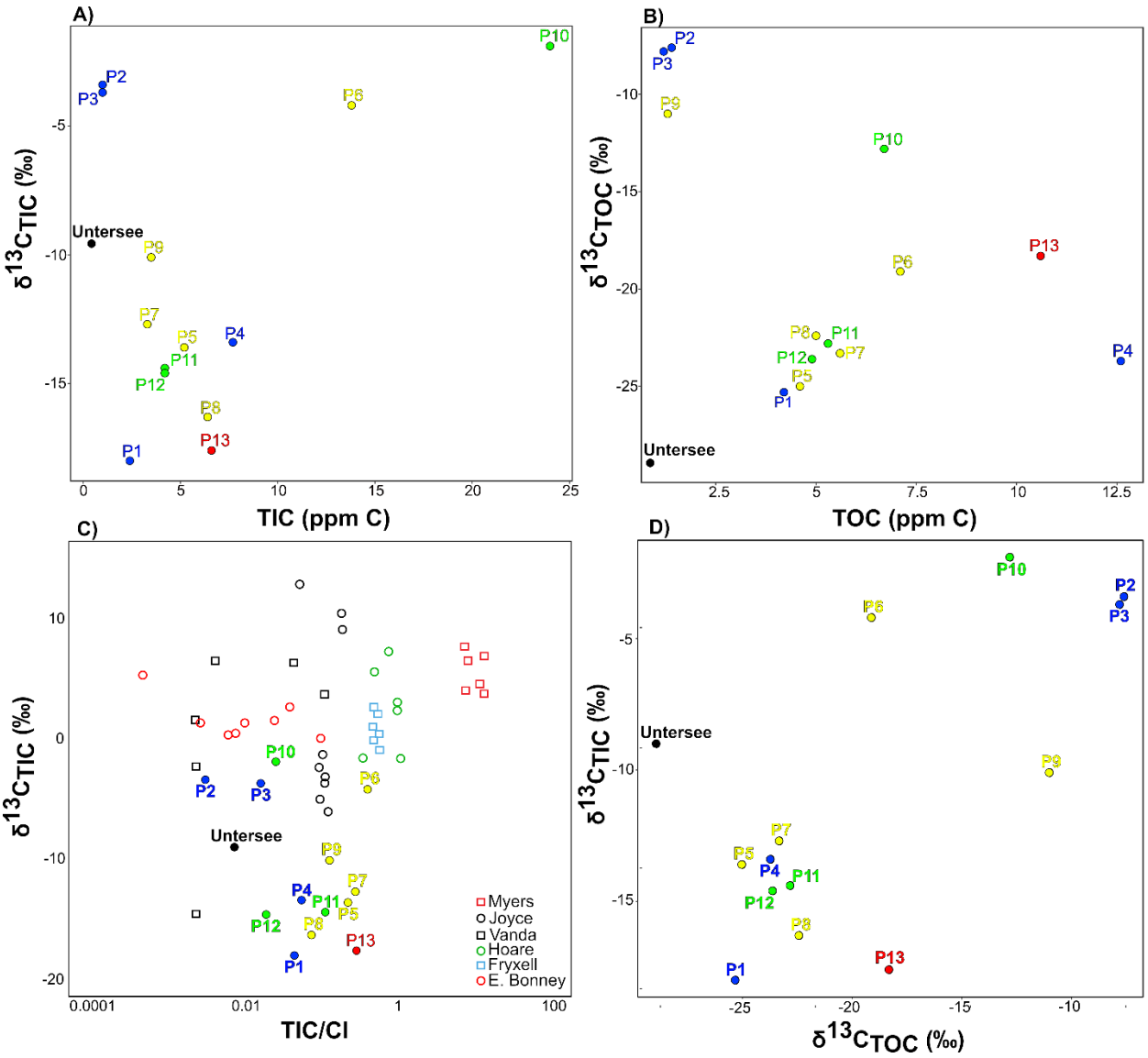

Figure 5-6: Scatter plots showing: relation between A) TIC (ppm C) and $\delta^{13}C_{TIC}$; B) TOC (ppm C) and $\delta^{13}C_{TOC}$; C) TIC/Cl and $\delta^{13}C_{TIC}$, including data from MDV lakes (Neumann et al., 2004b); and D) $\delta^{13}C_{TOC}$ and $\delta^{13}C_{TIC}$.

5.4.6 Climate change and trajectory of ponds

The MAAT in Antarctica's Queen Maud Land region has increased at a rate of 1.1±0.7°C per decade between 1998 and 2016 (Medley et al., 2018), but it has remained stable in the Untersee Oasis since the early 1960s (Andersen et al., 2015; Turner et al., 2004). However, the MAAT in the Oasis is likely to increase in the coming decades due to polar amplification of climate change. This should result in ice cover phenology shifts (e.g., Obryk et al., 2019). The Untersee Oasis hosts the full range of ice-covered ponds, ranging from moatless perennially ice-covered (e.g., Lake Untersee, Lake Obersee, and ponds situated along the west lateral moraine), to perennially ice-covered forming moats (e.g., terminal and east lateral moraine ponds), and some seasonally ice-covered ponds (e.g., Lake Untersee's east shoreline). Therefore, the findings derived from this study can be used to make an empirical prediction of the trajectory of the Untersee Oasis ponds' hydrochemical properties under a warming climate and a shift in ice cover phenology.

A shift from moatless perennially ice-covered ponds to seasonally ice-covered ponds may not cause a change in the source of recharge, unless supraglacial streams start to form on the Anuchin Glacier; the radiocarbon and tritium levels in all the ponds have similar values since they are all recharged by atmospheric CO_2 equilibrated snowmelt. However, a decrease ice cover extent would cause an increase in TDS and $\delta^{18}O$ composition as both parameters are negatively correlated with the persistence of ice cover (Fig. 5-7). This is expected since TDS, and $\delta^{18}O$ values of the water should increase as evaporation concentrates the ions in the pond and enriches $\delta^{18}O$ (Fig. 5-5C). Finally, a shift from moatless perennially ice-covered ponds to seasonally ice-covered ponds may cause a decrease in pH but an increase in TIC and TOC load, a consequence of increased interactions with the atmosphere (i.e., uptake of CO_2) and input of allochthonous organics likely derived from the snow petrels, and local soil/rock microbiota. This would shift the CO_2-depleted benthic microbial ecosystem of moatless perennially ice-covered lakes to one where carbon is not limiting photosynthesis.

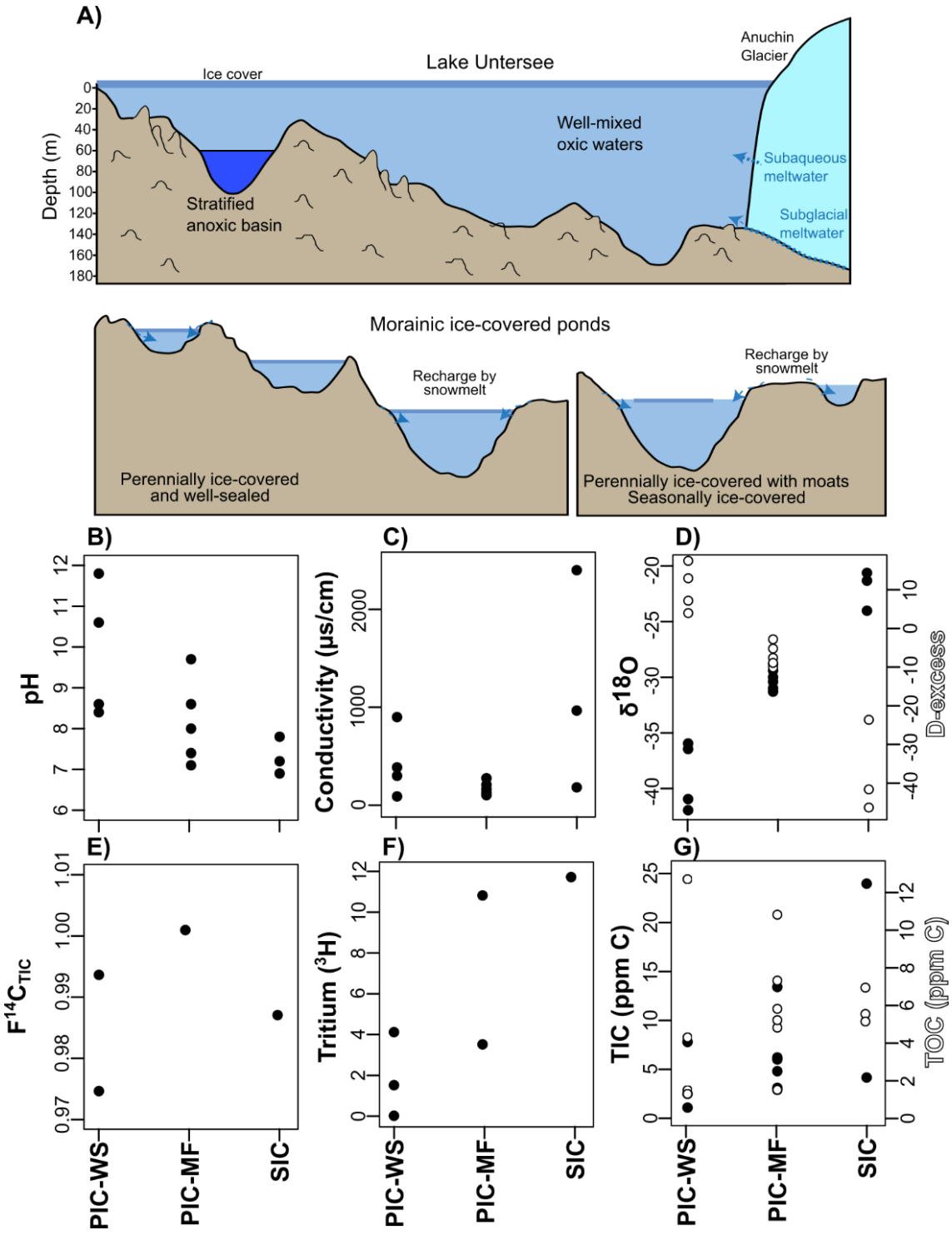

Figure 5-7: A) Cross-sectional view of the well perennially sealed Lake Untersee (including its oxic and anoxic basins) and the Untersee Oasis ponds with varied ice cover types (i.e., from perennially ice-covered and well sealed to seasonally ice-covered). Scatter plots showing variations between the ponds' empirically measured hydrochemical properties with regards to their ice-coverage type are also presented (PIC-WS, PIC-MF, and SIC respectively indicate perennially ice-covered and well-sealed, perennially ice-covered and moat-forming, and seasonally ice-covered). Those can be used to determine the trajectory of the hydrochemistry and microbial activity properties of ponds in the Oasis as they evolve in a changing climate.

5.5 Conclusion

The Untersee Oasis lacks surface streams but currently hosts 39 freshwater lacustrine basins with moatless perennial ice covers to seasonal ice covers. Our findings suggest that an increase in insolation (or air temperatures) would result in a shift in ice cover phenology. A reduction in ice coverage would lead to enhanced interactions between the ponds' water column and the atmosphere and increased inputs of allochthonous carbon (likely from snow petrels); however, unless supraglacial streams begin to form, the source of water recharging the ponds would remain essentially unchanged. Therefore, the empirical data allows to determine the trajectory of the hydrochemistry and microbial activity properties of ponds in the Oasis as they evolve in a changing climate.

5.6 References

Alexander, B., Thiemens, M. H., Farquhar, J., Kaufman, A. J., Savarino, J. & Delmas, R. J. (2003). East Antarctic ice core sulfur isotope measurements over a complete glacial–interglacial cycle. *JGR: Atmospheres 108*(D24).

Andersen, D. T., Sumner, D. Y., Hawes, I., Webster-Brown, J. & Mckay, C. P. (2011). Discovery of large conical stromatolites in Lake Untersee, Antarctica. *Geobiology*, *9*(3), 280–293.

Andersen, Dale T., McKay, C. P. & Lagun, V. (2015). Climate conditions at perennially ice-covered lake Untersee, East Antarctica. *JAMC 54*(7), 1393–1412.

Badgeley, J. A., Pettit, E. C., Carr, C. G., Tulaczyk, S., Mikucki, J. A. & Lyons, W. B. (2017). An englacial hydrologic system of brine within a cold glacier: Blood Falls, McMurdo Dry Valleys, Antarctica. *J. Glaciol. 63*(239), 387–400.

Badger, M. R. (1987). The CO2 concentrating mechanism in aquatic phototrophs. In M. D. Hatch & N. K. Boardman (Eds.), *The biochemistry of Plants: A comprehensive Treatise.* New York, NY.: Academic Press.

Bindschadler, R., Vornberger, P., Fleming, A., Fox, A., Mullins, J., Binnie, D., Paulsen, S. J., Granneman, B. & Gorodetzky. D. (2008). The Landsat image mosaic of Antarctica, *Rem. Sens. Environ.* 112, 4214-4226.

Bormann, P., Bankwitz, P., Bankwitz, E., Damn, V., Hurtig, E., Kampf, H., … Stakerbrandt, W. (1986). Structure and development of the passive continental marging across the Princess Astrid Coast, East Antarctica. *J. Geodyn. 373*(1449), 347–373.

Calder, J. A. & Parker, P. L. (1973). Geochemical implications of induced changes in C13 fractionation by blue-green algae. *Geochim. Cosmochim. Acta 37*, 133–140.

Clark, I. (2015). Groundwater geochemistry and isotopes. In *Groundwater Geochemistry and Isotopes*.

Crann, C. A., Murseli, S., St-Jean, G., Zhao, X., Clark, I. D. & Kieser, W. E. (2017). First Status Report on Radiocarbon Sample Preparation Techniques at the A.E. Lalonde AMS Laboratory (Ottawa, Canada). *Radiocarbon 59*(3), 695–704.

Dansgaard, W. (1964). Stable isotopes in precipitation. *Tellus 16*, 436–468.

Doran, P. T., Priscu, J. C., Berry Lyons, W., Powell, R. D., Andersen, D. T., & Poreda, R. J. (2004). Paleolimnology of extremely cold terrestrial and extraterrestrial environments. In R. Pienitz, M. S. V. Douglas, & J. . Smol (Eds.), *Long-Term Environmental Change in Arctic and Antarctic Lakes* (pp. 475–508). Dordrecht, The Netherlands.: Kluwer Academic Publishers,.

Dore, J. E. & Priscu, J. C. (2001). Phytoplankton phosphorus deficiency and alkaline phosphatase activity in the McMurdo Dry Valley lakes, Antarctica. *Limnol. Oceanogr. 46*(6), 1331–1346.

Kaup, E., Loopmann, A., Klokov, V., Simonov, I. & Haendel D. (1988). Limnological investigations in the Untersee Oasis. In *Martin, J. (Ed.), Limnological Studies in Queen Maud Land (East Antarctica).* (pp. 28–42).

Echeverría, S., Hausner, M. B., Bambach, N., Vicuña, S. & Suárez, F. (2019). Modeling present and future ice covers in two Antarctic lakes. *Journal of Glaciology 66*(255), 11–24.

Faucher, B., Lacelle, D., Fisher, D. A., Andersen, D. T. & McKay, C. P. (2019). Energy and water mass balance of Lake Untersee and its perennial ice cover, East Antarctica. *Antarc. Sci. 31*(5), 271–285.

Faucher, B., Lacelle, D., Fisher, D. A., Weisleitner, K. & Andersen, D. T. (2020). Modeling δD-δ18O Steady-State of Well-Sealed Perennially Ice-Covered Lakes and Their Recharge Source: Examples From Lake Untersee and Lake Vostok, Antarctica. *Front. Earth Sci. 8*, 220.

Fernandoy, F., Meyer, H., Oerter, H., Wilhelms, F., Graf, W. & Schwander, J. (2010). Temporal and spatial variation of stable-isotope ratios and accumulation rates in the hinterland of Neumayer station, East Antarctica. *J. Glaciol. 56*(198), 673–687.

Fisher, D. A., Lacelle, D., Pollard, W. & Faucher, B. (2020). A model for stable isotopes of residual liquid water and ground ice in permafrost soils using arbitrary water chemistries and soil-specific empirical residual water functions. *Perm. Perigl. Processes* 32(2) 248-260.

Fountain, A. G., Gooseff, M., Obryk, M., Fernandez-Diaz, J. C., Morin, P., Van Horn, D. J., … Shrestha, R. (2017). High-resolution elevation mapping of the McMurdo Dry Valleys, Antarctica, and surrounding regions. *Earth Syst. Sci. Data 9*(2), 435–443.

Fountain, A. G., Saba, G., Adams, B., Doran, P., Fraser, W., Gooseff, M., … Virginia, R. A. (2016). The Impact of a Large-Scale Climate Event on Antarctic Ecosystem Processes. *BioScience 66*(10), 848–863.

Gooseff, M. N., Barrett, J. E., Adams, B. J., Doran, P. T., Fountain, A. G., Lyons, W. B., … Wall, D. H. (2017). Decadal ecosystem response to an anomalous melt season in a polar desert in Antarctica. *Ecol. Evol. 1*(9), 1334–1338.

Greco, C., Andersen, D. T., Hawes, I., Bowles, A. M. C., Yallop, M. L., Barker, G. & Jungblut, A. D. (2020). Microbial Diversity of Pinnacle and Conical Microbial Mats in the Perennially Ice-Covered Lake Untersee, East Antarctica. *Front. Microbiol. 11*, 3173.

Guglielmin, M., Lewkowicz, A. G., French, H. M. & Strini, A. (2009). Lake-ice blisters, terra nova bay area, Northern Victoria Land, antarctica. *Geografiska Annaler, Series A: Physical Geography 91*(2), 99–111.

Haendel, D., Hermichen, W. D., Höfling, R. & Kowski, P. (2011). Hydrology of the lakes in Central Wohlthat Massif, East Antarctica: new results. *Isot. Environ. Health Stud. 47*(4), 402–406.

Hage, M. M., Uhle, M. E. & Macko, S. (2007). Biomarker and stable isotope characterization of coastal pond-derived organic matter, McMurdo Dry Valleys, Antarctica. *Astrobiology 7*, 645–661.

Hayes, J. M. (1993). Factors controlling 13C contents of sedimentary organic compounds: principles and evidence. *Mar. Geol. 113*, 111–125.

Hermichen, W. D., Kowski, P. & Wand, U. (1985). Lake Untersee, a first isotope study of the

largest freshwater lake in the interior of East Antarctica. *Nature 315*(6015), 131–133.

Hiller, A., Wand, U., Kämpf, H. & Stackebrandt, W. (1988). Occupation of the Antarctic continent by petrels during the past 35 000 years: Inferences from a 14C study of stomach oil deposits. *Polar Biol. 9*(2), 69–77.

Hoffman, M. J., Fountain, A. G. & Liston, G. E. (2008). Surface energy balance and melt thresholds over 11 years at Taylor Glacier, Antarctica. *JGR: Earth Surface 113*(4), 1–12.

Horita, J. (2009). Isotopic Evolution of Saline Lakes in the Low-Latitude and Polar Regions. *Aquat. Geochem.* 15, 43–69.

Howat, I. M., Porter, C., Smith, B. E., Noh, M. -J. & Morin, P. (2019). The Reference Elevation Model of Antarctica, *The Cryosphere* 13, 665-674.

Isaksson, E., Karlen, W., Gundestrup, N., Mayewski, P., Whitlow, S. & Twickler, M. (1996). A century of accumulation and temperature changes in Dronning Maud Land, Antarctica. *JGR 101*(95), 7085–7094.

Jonsell, U., Hansson, M. E., Morth, C. M. & Torssander, P. (2005). Sulfur isotopic signals in two shallow ice cores from Dronning Maud Land, Antarctica. *Tellus Ser. B Chem. Phys. Meteorol. 57*, 341–350.

Kampf, H. & Stakerbrandt, W. (1985). Geological investigation in the Eliseev anorthosite massif, central Dronning Maud Land, East Antarctica. *Zeitschrift Fur. Geologische Wissenschaften 13*(3), 32–60.

Koo, H., Mojib, N., Hakim, J. A., Hawes, I., Tanabe, Y., Andersen, D. T. & Bej, A. K. (2017). Microbial communities and their predicted metabolic functions in growth laminae of a unique large conical mat from Lake Untersee, East Antarctica. Front. Microbiol. 8, 1347.

Lawrence, J. P., Doran, P. T., Winslow, L. A. & Priscu, J. C. (2020). Subglacial brine flow and wind-induced internal waves in Lake Bonney, Antarctica. *Antarc. Sci. 32*(3), 223–237.

Lawson, J., Doran, P. T., Kenig, F., Des Marais, D. J. & Priscu, J. C. (2004). Stable Carbon and Nitrogen Isotopic Composition of Benthic and Pelagic Organic Matter in Lakes of the McMurdo Dry Valleys, Antarctica. *Aquat. Geochem. 10*, 269–301.

Lehnherr, I., St Louis, V. L., Sharp, M., Gardner, A. S., Smol, J. P., Schiff, S. L., … Talbot, C. H. (2018). The world's largest High Arctic lake responds rapidly to climate warming. *Nat. Commun. 9*(1), 1–9.

Lyons, W. B., Welch, K. A., Gardner, C. B., Jaros, C., Moorhead, D. L., Knoepfle, J. L. & Doran, P. T. (2012). The geochemistry of upland ponds, Taylor Valley, Antarctica. *Antarc. Sci. 24*(1), 3–14.

Majzoub, M. (1971). Fractionnement en oxygen-18 et deuterium entre l'eau et sa vapeu. *Journal de Chimie Physique, 68*, 563–568.

Marsh, N. B., Lacelle, D., Faucher, B., Cotroneo, S., Jasperse, L., Clark, I. D. & Andersen, D. T. (2020). Sources of solutes and carbon cycling in perennially ice-covered Lake Untersee, Antarctica. *Sci. Rep.* 10(1), 12290, 1–12.

Matsubaya, O., Sakai, H., Tori, T., Burton, H. & Kerry, K. (1978). Antarctic saline lakes-stable isotopic ratios , chemical compositions and evolution. *Geochim. Cosmochim. Acta 43*, 7–25.

Matsumoto, G. I., Nakaya, S., Murayama, H., Masuda, N., Kawan, T., Watanuki, K. & Torii, T. (1992). Geochemical characteristics of Antarctic lakes and ponds. *Proceedings of the NIPR Symposium on Polar Biology*, *5*, 125–145.

Mckay, C. P., Clow, G. D., Wharton, R. A. & Squyres, S. W. (1985). Thickness of ice on perennially frozen lakes. *Nature*, *313*, 561–562.

Medley, B., McConnell, J. R., Neumann, T. A., Reijmer, C. H., Chellman, N. & Sigl, M. (2018). Temperature and snowfall in western Queen Maud Land increasing faster than climate model projections. *Geophys. Res. Lett. 45*, 1472–1480.

Mikucki, J. A., Auken, E., Tulaczyk, S., Virginia, R. A., Schamper, C., Sorensen, K. I., … Foley, N. (2015). Deep groundwater and potential subsurface habitats beneath an Antarctic dry valley. *Nat. Commun.* 6, 6831.

Mueller, D. R., Hove, P. Van, Antoniades, D., Jeffries, M. O. & Vincent, W. F. (2009). High Arctic lakes as sentinel ecosystems : Cascading regime shifts in climate, ice cover, and mixing. *Limnol. Oceanogr. 54*(2009), 2371–2385.

Murseli, S., Middlestead, P., St-Jean, G., Zhao, X., Jean, C., Crann, C. A., … Clark, I. D. (2019). The Preparation of Water (DIC, DOC) and Gas (CO2, CH4) Samples for Radiocarbon Analysis at AEL-AMS, Ottawa, Canada. *Radiocarbon*, *61*, 1563–1571.

Naik, S. S., Thamban, M., Laluraj, C. M., Redkar, B. L. & Chaturvedi, A. (2010). A century of climate variability in central Dronning Maud Land, East Antarctica, and its relation to Southern Annular Mode and El Nio-Southern Oscillation. *JGR Atmospheres*, *115*(16), 1–12.

Neumann, K., Lyons, W. B., Priscu, J. C., Desmarais, D. J. & Welch, K. A. (2004). The carbon isotopic composition of dissolved inorganic carbon in perennially ice-covered Antarctic lakes: Searching for a biogenic signature. *Ann. Glaciol. 39*, 518–524.

O'Neil, J. R. (1968). Hydrogen and oxygen isotope fractionation between ice and water. *J. Phys. Chem. 72*(10), 3683–3684.

Obryk, M.K., Doran, P. T., & Priscu, J. C. (2019). Prediction of Ice-Free Conditions for a Perennially Ice-Covered Antarctic Lake. *JGR: Earth Surface* 686–694.

Obryk, Maciej K., Doran, P. T., Friedlaender, A. S., Gooseff, M. N., Li, W., Morgan-Kiss, R. M., … Ducklow, H. W. (2016). Responses of Antarctic Marine and Freshwater Ecosystems to Changing Ice Conditions. *BioScience 66*(10), 864–879.

Paech, H.-J. & Stackebrandt, W. (1995). Geology. In P. Bormann & D. Fritzsche (Eds.), *The Schirmacher Oasis, Queen Maud Land, East Antarctica and its surroundings* (pp. 59–159).

Pardue, J. W., Scalan, R. S., Van Baalen, C. & Parker, P. L. (1976). Maximum carbon isotope fractionation in photosynthesis by blue-green algae and a green alga. *Geochim. Cosmochim. Acta 40*, 309–312.

Petrov, M. P., Terzhevik, A. Y., Palshin, N. I., Zdorovennov, R. E. & Zdorovennova, G. E. (2005).

Absorption of Solar Radiation by Snow-and-Ice Cover of Lakes. *Hydrol Process 32*, 496-504.

Priscu, J .C. & Foreman, C. M. (2009). Lakes of Antarctica. *Encyclopedia of Inland Waters*, *2*, 555–566.

Priscu, John C. (1995). Phytoplankton nutrient deficiency in lakes of the McMurdo dry valleys, Antarctica. *Freshw. Biol. 34*(2), 215–227.

Schwab, M. J. (1998). Rekonstruktion der spatquartaren Klima und Umweltgeschichte der Schirmacher Oase und des Wohlthat Massivs (Ostantarktika). Ber. Polarforschung 293, 1–128.

Shamilishvili, G., Abakumov, E. V. & Andersen, D. T. (2020). Biogenic-abiogenic interactions and soil formation in extreme conditions of untersee oasis, surroundings of lake Untersee, central Queen Maud land, East Antarctica. *LNESS 1*, 457–479.

Sinha, R., Navada, S. V., Chatterjee, A., Kumar, S., Mitra, A. & Nair, A. R. (2000). Hydrogen and Oxygen isotopes analysis of Antarctic Lake waters, Schirmacher Oasis, East Antarctica. *Curr. Sci. 78*(8), 992–995.

St-Jean, G. (2003). Automated quantitative and isotopic (13C) analysis of dissolved inorganic carbon and dissolved organic carbon in continuous-flow using a total organic carbon analyser. *Rapid Commun. Mass Spectrom*. 17, 419–428.

Steele, W. K. (2005). Stable isotope ratios of Antarctic petrel (Thalassoica antarctica) and snow petrel (Pagodroma nivea) bone collagen. *Polar Biol. 28*(9), 672–679.

Stuiver, M. & Polach, H. A. (1977). Discussion Reporting of 14C data. *Radiocarbon* 19(3), 355-363.

Turner, J., Colwell, S. R., Marshall, G. J., Lachlan-Cope, T. A., Carleton, A. M., Jones, P. D., … Iagovkina, S. (2004). The SCAR READER project: Toward a high-quality database of mean Antarctic meteorological observations. *J. Clim. 17*(14), 2890–2898.

Vincent, A. C., Mueller, D. R. & Vincent, W. F. (2008). Simulated heat storage in a perennially ice-covered high Arctic lake: Sensitivity to climate change. *JGR: Oceans 113*(4), 1–11.

Vincent, W. F., Hobbie, J. E. & Laybourn-Parry, J. (2008). Introduction to the limnology of high-latitude lake and river ecosystems. In W. F. Vincent & J. Laybourn-parry (Eds.), *Polar Lakes and Rivers: Limnology of Arctic and Antarctic Aquatic Ecosystems* (pp. 1–23). Oxford, UK: Oxford University Press.

Weisleitner, K., Perras, A. K., Unterberger, S. H., Moissl-Eichinger, C., Andersen, D. T. & Sattler, B. (2020). Cryoconite Hole Location in East-Antarctic Untersee Oasis Shapes Physical and Biological Diversity. *Front. Microbiol.* 11, 1165.

Weisleitner, K., Perras, A., Moissl-Eichinger, C., Andersen, D. T. & Sattler, B. (2019). Source Environments of the Microbiome in Perennially Ice-Covered Lake Untersee, Antarctica. *Front. Microbiol.* 10, 1019.

Wharton, R. A., Lyons, W. B. & Des Marais, D. J. (1993). Stable isotopic biogeochemistry of

carbon and nitrogen in a perennially ice-covered Antarctic lake. *Chem. Geol.* 107, 159–172.

CHAPTER 6: CONCLUSIONS

6.1 Summary and conclusions

The Antarctic continent encompasses thousands of surface ice-covered lakes with contrasting ice cover regimes, water column properties, and ecosystem characteristics. Much of the current paradigms about ice-covered Antarctic limnology have been established by studying lakes situated in Victoria Land's McMurdo Dry Valley. However, there is a potential to learn much more on the subject by gathering data on other ice-covered Antarctic lakes that have not received attention during the past century. One of those poorly studied Antarctic regions hosting ice-covered lakes is Queen Maud Land's Untersee Oasis. To date, studies at Untersee had mainly focused on describing their physical and chemical limnology (e.g., Hermichen et al., 1985; Wand et al., 1997, 2006; Steel et al., 2015; Bevington et al., 2018) and microbial ecology (e.g., Wand et al., 2006; Andersen et al., 2011; Koo et al., 2017; Greco et al., 2021). However, very little work has been done to constrain the chemical properties (including input source) and water/energy mass balance of ice-covered lentic bodies in this polar oasis. This is detrimental to understanding how their ice cover, water-column, and benthic ecosystem will evolve under the polar amplification of climate warming. Thus, this thesis's primary goal was to conduct laboratory and numerical modeling analyses of samples gathered during the 2016-2019 Untersee Oasis field expeditions to fill these knowledge gaps.

It is initially concluded, through mass balance calculations, that the largest ice-covered lake in the region (i.e., Lake Untersee) and its ice cover were respectively in hydrological and energetic steady-states (Chapter 2) before a catastrophic GLOF event affected Untersee in late 2018-early 2019 (Chapter 5). Those mass balance calculations also indicate that the lake is typically exclusively fed by subglacial meltwaters (55-60%) and by the subaqueous melting of the Anuchin Glacier (40-45%). Also, it is demonstrated via the interpolation of ice cover thickness measurements that variations in wind speed throughout Lake Untersee's surface area (i.e., variations in turbulent heat fluxes), in conjunction with solar radiation, are responsible for local fluctuations in surface ice cover ablation rates (and associated water freezing rates at the bottom of the ice cover). A new method for estimating ice cover ablation (and underwater freezing rate) for perennially ice-covered lakes relying upon the extraction of ice cover δD-$\delta^{18}O$ and bubble content from ice cores is also presented in Chapter 2. The latter is a time-efficient method that

eliminates the need to re-visit sites yearly to measure the classically used ablation stakes' extraction rate.

Data on the thermodynamics of Lake Untersee (presented in Chapter 2) provide insights on the partitioning of effective energy and mass transfer units [EEMT; Wm^{-2}] between the lake surface radiative and water column energies, using a critical zone approach (e.g., Rasmussen et al., 2012; Minor et al., 2020) (Fig. 6-1). Assuming a biomass enthalpy of ~ 22 MJ/Kg, an average value for organic materials (Rasmussen, 2012), we can estimate the energy associated with reduced carbon from primary productivity (EBIO) to be ~ 0.95 Wm^{-2}.

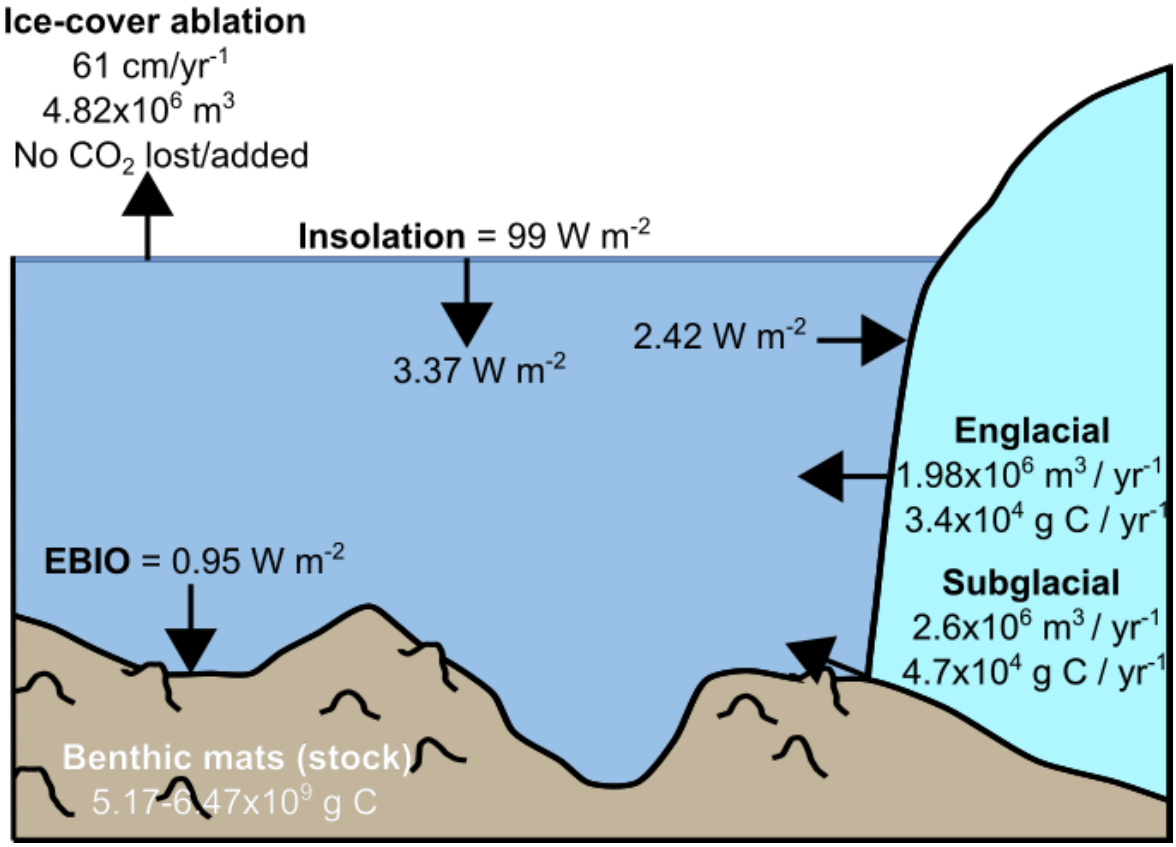

Figure 6-1: Partitioning of energy and water-carbon fluxes in Lake Untersee. The mean ice cover surface insolation was measured at 99 Wm^{-2} during the 2008-2017 period, and with a PAR transmissivity of (4.9±1%) and the range of the thickness of the ice cover (1.96 to 3.96 m), 3.37±0.84 Wm^{-2} enters the water column (Faucher et al., 2019). The amount of sunlight energy needed to sustain the englacial melting of the Anuchin Glacier (for a glacial velocity of 8-9 m yr^{-1}) is 2.42 Wm^{-2}. Assuming a biomass enthalpy of ~ 22 MJ/Kg, an average value for organic materials (Rasmussen, 2012), we can estimate the energy associated with reduced carbon from primary productivity (EBIO) to be ~ 0.95 Wm^{-2}.

The δD-$\delta^{18}O$ steady-state of Lake Untersee was studied using a newly developed recursive hydrochemical model (*FREEZCH9*) that considers salinity-induced modifications of the ice-water D/H and $^{18}O/^{16}O$ water-ice fractionation factors in well-sealed lake waters (Chapter 3). This was done by modifying the isotope-augmented *FREEZCH5* model (Fisher et al., 2020) and making it recursive and sensitive to solute load concentration. It is shown that the lake was in an isotopic steady-state and that its water column had not been interacting with the atmosphere for at least 500 years (i.e., a well-sealed ice cover) before the 2019 GLOF event. Simulations also suggest that the isotopic compositions of subglacial meltwater and/or groundwater infiltrations feeding the lake are very similar (δD-$\delta^{18}O$ values of ~ -36‰) and are slightly depleted compared to the average $\delta^{18}O$ composition of the Anuchin Glacier (~ -34.2‰). The validity of the model's outputs was tested by conducting runs with a Lake Vostok ice cover hydrochemistry dataset. Our simulations support the findings highlighted in previous studies (e.g., Ekaykin et al., 2016) that suggest that Lake Vostok should be in an isotopic steady-state. Further, our *FREEZCH9* model can be used to constrain the various fractionation mechanisms (e.g., freezing, evaporation) that input water may have undergone before its incorporation into a lake's water column. As such, *FREEZCH9* could be used to determine if some Antarctic surface lakes are fed by regional groundwater systems circulating through subglacial lakes that have undergone cryo-freezing.

A GLOF event lasting between December 2018 and February 2019 increased Lake Untersee's water column's depth by 2.0 m (corresponding to a volume increase of 1.75×10^7 m^3) (Chapter 4). The water originated from the nearby Lake Obersee. The latter lost 2.29×10^7 m^{-3} during this catastrophic flooding event and saw its elevation reduced by 11.3 m. The GLOF cannot be attributed to a surge or extensive surface melting of the Anuchin Glacier because its position remained at the same location, and the number of thawing degree days (i.e., 26.8) was not exceptionally high during that summer. Instead, it was likely caused by a section of the Vangengejm Glacier that collapsed or shifted through a glacial tunnel or by fast-moving ice-streams surrounding the Untersee Oasis. The sensible heat brought in by the GLOF waters melted a 50 x 50 m moat at the NE of Lake Untersee. This led to increased interactions between the surface waters and the atmosphere, thereby modifying Lake Untersee's water chemistry and inorganic carbon load. Through high-resolution grain size and carbon isotope analyses of benthic microbial cores, it is proposed that GLOFs periodically affected Lake Untersee throughout the Holocene. Carbon mass balance calculations support this hypothesis. Overall, our findings show that GLOFs

can increase the primary productivity of benthic ecosystems in CO_2-depleted ice-covered lakes by sporadically supplying them with inorganic carbon.

The distribution and hydrochemistry of smaller ice-covered water bodies in the Untersee Oasis (n=39) were also studied during this PhD research. We found that those offer the full spectrum of ice-coverage type (i.e., seasonally to perennially ice-covered) and that they were distributed: 1) on the Anuchin Glacier's west and east lateral moraines; 2) on the Lake Untersee Valley's terminal moraine; and 3) on the eastern edge of Lake Untersee. Those sub-regions receive varying amounts of incoming solar radiation during the Austral summer, which controls their ice cover stability: ponds that receive higher solar radiation develop moats or completely lose their ice cover during summer, whereas those that receive lower solar radiation retain their full ice cover and remain well-sealed to direct exchanges with the atmosphere. It is concluded that the Untersee Oasis ponds are fed by modern snowmelt that has equilibrated with atmospheric CO_2, and that their ice cover type controls the evolution of their solute load and stable water isotope ratios. We predict that climate change will likely progressively reduce their ice coverage and that this will lead to enhanced interactions between the water column of the ponds and the atmosphere. Unless supraglacial streams begin to form on the Anuchin Glacier, the source of water recharging the ponds will remain essentially unchanged. Overall, the empirical data collected during the investigation can be used to determine how their hydrochemistry and benthic microbial primary productivity will be modified as they evolve in a changing climate.

6.2 Key contributions

The main research goals of this PhD research project (outlined in section 1.4) were met. Further, the findings presented in this dissertation are novel scientific contributions to the study of hydrochemistry and mass balance of ice-covered lakes and ponds in Queen Maud Land's Untersee Oasis:

1. Hydrological and energy mass balance assessment of one of the largest ice-covered freshwater lakes in the interior of East Antarctica (Lake Untersee).
2. Determination of Lake Untersee's input sources, including relative contributions.
3. Development of a time-efficient method for estimating the ice-cover ablation and freezing rates of perennially ice-covered lakes.

4. Development of a recursive hydrological model that can be used to properly assess the isotopic steady-state and input source(s) of well-sealed ice-covered lakes.
5. Characterization of Glacial Lake Outburst Floods (GLOFs) effects on the water chemistry and benthic mat primary productivity of CO_2-depleted ice-covered lakes.
6. Identification and mapping of ice-covered lentic bodies in the Untersee Oasis.
7. Assessment of the Untersee Oasis ponds' input source.
8. Use of empirical data to assess the possible modifications that lentic basins in the Untersee Oasis will undergo as their ice coverage is progressively reduced under climate warming.

6.3 Limitations and future research directions

This PhD dissertation provides novel information on ice-covered lakes' hydrochemistry in the poorly studied ice-free Untersee Oasis. Nonetheless, the studies presented in Chapters 2-5, including their outcomes, are subject to several limitations. These are discussed in the section below:

The findings that have emerged from the thermodynamics and hydrological balance study of Lake Untersee (Chapter 2) rely on several assumptions. First, it is assumed that the lake is an endorheic basin. However, given the lake's surface area and depth, it can be hypothesized that a through talik should be present beneath it (i.e., Mackay, 1963). This permeable unit would allow groundwater to recharge the lake and could simultaneously be a drainage passage for the lake waters. Yet, the lake water volume annually lost via groundwater discharges was not considered when calculating the lake's hydrological mass balance. Instead, calculations of annual outflow volume were solely based on the lake's averaged ice cover ablation rate. For this reason, we may have overestimated the yearly discharge rate of subglacial and/or groundwater into Lake Untersee (assuming that calculations related to the annual input contributions of subaqueous melting of the Anuchin Glacier are correct). Hopefully, subglacial meltwater discharges will be measured in the coming field season via a remotely operated underwater vehicle (ROV).

Further, presupposing that Lake Untersee's inflows and outflow(s) have returned to "baseline" (i.e., pre-GLOF), one should expect its lake ice cover elevation to remain stable in the coming years. Conversely, the ice cover of Lake Obersee, from which the GLOF waters originated, should slowly return to its pre-GLOF elevation. Those hypotheses should be tested in future studies.

Based on hydrochemical model simulations with *FREEZCH9*, it is suggested that Lake Untersee was in an isotopic steady-state until the early 2019 GLOF (Chapter 3 & Chapter 4). The newly developed recursive model showcased in Chapter 3 was also tested with a dataset from Lake Vostok. Our results match reasonably well with those obtained via the use of other hydrological models (e.g., Royston-Bishop, 2004; Souchez et al., 2004). However, our model was designed to work especially well for estimating the isotopic steady-state of highly saline well-sealed ice-covered lakes. However, Lake Untersee's water column has a low solute load, and it is hypothesized that this is also the case for Lake Vostok's upper water column (e.g., Siegert et al., 2001; 2003) are both freshwater basins. As a result, the *FREEZCH9* model still needs to be tested to its full capacity. This could be done, for example, by running simulations with accreted ice and water column samples taken from the newly discovered Devon Ice Cap subglacial lakes in the Canadian High Arctic (i.e., Rutishauser et al., 2018). In the future, *FREEZCH9* could also be used for the isotopic steady-state modeling of salty oceanic waters hidden below the thick ice cover of Enceladus and other icy planetary bodies in our solar system.

This thesis showcases the first study to assess the impacts of GLOFs on the hydrochemistry and benthic microbial activity of perennially ice-covered CO_2-depleted lakes (Chapter 4). Calculations employed to derived Lake Untersee's current water column and benthic microbial mat carbon load rely on the lake's energy and mass balance study (Chapter 2). Although we are fairly confident in our hydrological mass balance calculations and results, uncertainties regarding how much DIC (subsequently used for photosynthesis) were brought in Untersee's water column by the subaqueous melting of the Anuchin Glacier and subglacial/groundwater contributions throughout the existence of the lake remain. It is also unclear how much of the lake's benthic zone is covered by benthic microbial mats; divers have only observed the lake floor to depths of ~ 20-50m and do not have access to its deepest portions due to safety reasons. However, we did use a plausible range of benthic microbial mat coverage scenarios in our study. Nonetheless, this should certainly be looked into, and there are plans to use an ROV during the next field season to shed some light on the matter. Further, the amount of carbon stored in mats was calculated using the organic carbon density of three cores taken near the Oasis's push moraine: this is where the collection of benthic microbial mat cores is the safest for divers. Hence, the lake's floor's organic carbon density in other locations was not considered in our study. Still, cores could have been taken in other areas of Lake Untersee using a gravity core, but this equipment was not accessible

to us during the 2016-2019 field seasons. Our study also suggests that grain size, $\delta^{13}C$, and ^{14}C in microbial mat cores can be used as markers to detect past GLOF events. Those could be supplemented by additional markers such as Beryllium (^{9}Be & ^{10}Be) isotopes (e.g., Sproson et al., 2021) or ^{222}Rn (in interstitial microbial mat layer waters) (e.g., Linhoff et al., 2017) in future studies.

Empirical data is used to determine the trajectory of the hydrochemistry and microbial activity properties of ponds in the Oasis as they evolve in a changing climate (Chapter 5). This study's main limitation is that the pond water sampling was restricted to their water column's near-surface. Further, depth profiling was also not undertaken on most of the ponds. Those small lentic basins were usually challenging to reach (i.e., required scrambling), meaning that carrying heavy coring and multiparameter sondes alone was often not the safest option. Still, depth profile measurements were made for two of the ponds (on the Anuchin Glacier's west lateral moraine; P2 & P3) and revealed that their bottom portion was more solute-rich than the overlying water column. However, it remains unclear if this trend also applies to other ponds in the Oasis, especially in other sectors. If logistically possible, the resampling and depth profiling of those ponds are needed to determine if the findings presented in Chapter 5 only apply to their near-surface waters.

The second-largest perenially ice-covered lake in the Untersee Oasis (Lake Obersee) was not investigated during this PhD research project. Plans were made to perform an energy and mass balance study on Lake Obersee (e.g., Chapter 2) during the 2019 field season, but access to the lake, which was safe in previous years, became too dangerous after the 2019 GLOF event due to a shift/collapse of the Vangengejm Glacier. Its lake level should be monitored in the coming years; a water column replenishment rate could then be measured and used in subsequent mass balance calculations. It would also be worthwhile to evaluate if a decrease in water column depth shortly after the 2019 GLOF increased the amount of solar radiation received by the benthic mats, thereby increasing their primary productivity and/or if this also reduced the amount of underwater habitat for the mats.

Overall, this dissertation is a stepping stone for the contemporary hydrochemical study of ice-covered lakes in Antarctica's Queen Maud Land Untersee Oasis. It is shown through field measurements, laboratory analyses, and hydrochemical modeling that those lentic bodies are complex thermodynamic, hydrologic, and biological systems. However, their paleolimnological

characteristics (e.g., Doran et al., 2002; Wilson, 1964; Lyons et al., 1985) remain mostly unexplored; unraveling valuable paleoenvironmental information (e.g., the timing of formation, filling, and desiccating events) about those water bodies should be the main focus of future studies. Those could inform on the potential hydrochemical modifications they have undergone in the past under colder (e.g., ~ 2 kyr BP) or warmer (e.g., ~ 11-9 kyr BP) periods than today. A synergy between the results of such investigations and the predictions about the Untersee Oasis ice-covered lentic basin's fate under a warming climate (Chapter 5) could then be established.

6.4 References

Andersen, D. T., Sumner, D. Y., Hawes, I., Webster-Brown, J. & McKay, C. P. (2011). Discovery of large conical stromatolites in Lake Untersee, Antarctica. *Geobiology,* 9: 280–293.

Bevington, J., McKay, C. P., Davila, A., Hawes, I., Tanabe, Y. & Andersen, D. T. (2018). The thermal structure of the anoxic trough in Lake Untersee, Antarctica. *Antarc. Sci. 30*(6), 333–344.

Doran, P. T., Priscu, J. C., Lyons, W. B., Walsh, J. E., Fountain, A. G., McKnight, D. M., Moorhead, D. L., Virginia, R. A., Wall, D. H., Clow, G. D., Fritsen, C. H., McKay, C. P. & Parsons, A. N. (2002). Antarctic climate cooling and terrestrial ecosystem response. *Nature* 415(6871): 517–520.

Ekaykin, A. A., Lipenkov, V. Y., Kozachek, A. V. & Vladimirova, D. O. (2016). Stable water isotopic composition of the Antarctic subglacial Lake Vostok: Implications for understanding the lake's hydrology. *Isot. Environ. Health Stud. 52*, 1–9.

Fisher, D. A., Lacelle, D., Pollard, W. & Faucher, B. (2020). A model for stable isotopes of residual liquid water and ground ice in permafrost soils using arbitrary water chemistries and soil-specific empirical residual water functions. *Perm. Perigl. Processes* 32(2) 248-260.

Greco, C., Andersen, D. T., Hawes, I., Bowles, A. M. C., Yallop, M. L., Barker, G. & Jungblut, A. D. (2020). Microbial Diversity of Pinnacle and Conical Microbial Mats in the Perennially Ice-Covered Lake Untersee, East Antarctica. *Front. Microbiol.* 11, 3173.

Hermichen, W. D., Kowski, P. & Wand, U. (1985). Lake Untersee, a first isotope study of the largest freshwater lake in the interior of East Antarctica. *Nature 315*(6015), 131–133.

Koo, H., Mojib, N., Hakim, J. A., Hawes, I., Tanabe, Y., Andersen, D. T. & Bej, A. K. (2017). Microbial communities and their predicted metabolic functions in growth laminae of a unique large conical mat from Lake Untersee, East Antarctica. *Front. Microbiol*. 8, 1347.

Linhoff, B. S., Charette, M. A., Nienow, P. W., Wadham, J. L., Tedstone, A. J. & Cowton, T. (2017). Utility of 222Rn as a passive tracer of subglacial distributed system drainage. *Earth Planet. Sci. Lett.* 462, 180–188.

Lyons, W. B., Mayewski, P. A., Donahue, P. & Cassidy, D. (1985). A preliminary study of the sedimentary history of Lake Vanda, Antarctica: climatic implications. N.Z. *J. Mar. Freshwat. Res.* 19, 253-260.

MacKay, R. (1963). The Mackenzie delta area N.WT.: Canada Dept. of Mines and Tech. Services, Geographical Branch, Memoir 8.

Minor, J., Pearl, J.K., Barnes, M.L., Colella, T.R., Murphy, P.C., Mann, S. & Barron-Gafford, G.A. (2020): Critical zone science in the Anthropocene: Opportunities for biogeographic and ecological theory and praxis to drive earth science integration. *Prog. Phys. Geogr.* 44(1), 50–69

Rasmussen, C. (2012). Thermodynamic constraints on effective energy and mass transfer and catchment function, *Hydrol. Earth Syst. Sci.* 16, 725–739.

Royston-Bishop, G., Tranter, M., Siegert, M. J., Lee, V. & Bates, P. D. (2004). Is Vostok lake in steady state? *Ann. Glaciol.* 39, 490–494.

Rutishauser, A., Blankenship, D. D., Sharp, M., Skidmore, M. L., Greenbaum, J. S., Grima, C., … Young, D. A. (2018). Discovery of a hypersaline subglacial lake complex beneath Devon Ice Cap, Canadian Arctic. *Sci. Adv.* 4(4), eaar4353.

Siegert, M. J., Ellis-Evans, J. C., Tranter, M., Mayer, C., Petit, J.-R., Salamatin, A. & Priscu, J. C. (2001). Physical, chemical and biological processes in Lake Vostok and other Antarctic subglacial lakes. *Nature* 414(6864), 603–609.

Siegert, M. J., Tranter, M., Ellis-Evans, J. C., Priscu, J. C. & Lyons, W. B. (2003). The hydrochemistry of Lake Vostok and the potential for life in Antarctic subglacial lakes. *Hydrol.Process.* 17, 795–814.

Souchez, R., Petit, J., Jouzel, J., de Angelis, M. & Tison, J. (2004). Reassesing Lake Vostok's behaviour from existing and new ice core data. *Earth Planet. Sci. Lett.* 217(1–2), 163–170.

Sproson, A. D., Takano, Y., Miyairi, Y., Aze, T., Matsuzaki, H., Ohkouchi, N. & Yokoyama, Y. (2021). Beryllium isotopes in sediments from Lake Maruwan Oike and Lake Skallen, East Antarctica, reveal substantial glacial discharge during the late Holocene. *Quat. Sci. Rev.* 256, 106841.

Steel, H. C. B., McKay, C. P. & Andersen, D. T. (2015). Modeling circulation and seasonal fluctuations in perennially ice-covered and ice-walled Lake Untersee, Antarctica. *Limnol. Oceanogr. 60*(4), 1139–1155.

Wand, U, Samarkin, V. A., Nitzsche, H.-M. & Hubberten, H.-W. (2006). Biogeochemistry of methane in the permanently ice-covered Lake Untersee, central Dronning Maud Land, East Antarctica. *Limnol. Oceanogr. 51*(2), 1180–1194.

Wand, U., Schwarz, G., Brüggemann, E. & Bräuer, K. (2007). Evidence for physical and chemical stratification in Lake Untersee (central Dronning Maud Land, East Antarctica). *Antarc. Sci. 9*(01), 43–45.

Wilson, A. T. (1964): Evidence from chemical diffusion of a climatic change in the McMurdo Dry Valleys 1200 years ago. *Nature* 201, 176-177.

APPENDIX A: SUPPLEMENTAL INFORMATION FOR CHAPTER 2

Table A1: Coordinates and yearly horizontal displacement of a target placed on the Anuchin Glacier's surface.

Date	Latitude (°S)	Longitude (°E)	Elevation	Displacement from 2008 (m)
16-Dec-08	71.29477	13.52183	754 m	0
3-Dec-11	71.29501	13.52177	734 m	27
22-Nov-12	71.29506	13.52180	750 m	32
29-Nov-13	71.29516	13.52168	-	44
16-Dec-14	71.29520	13.52167	-	48
21-Dec-15	71.29531	13.52170	-	60
17-Dec-16	71.29541	13.52172	741 m	72
6-Dec-17	71.295448	13.521693	-	76

Table A2: Summary of ice cover thickness and freeboard measurements made on Lake Untersee (including hole coordinates) between 2008 and 2018.

Year	Hole ID	Latitude (°south)	Longitude (°east)	Freeboard (cm)	Ice thickness (cm)
2008	CampHole2	71.34266	13.45007	47	240
2008	CampHole3	71.34222	13.44875	48	248
2008	CampHole2' Ablation3	71.34266	13.45007	39	231
2008	CampHole4	71.34019	13.44051	20	272
2008	WaterLevelHole	71.34708	13.41513	28	257
2008	AnoxicHoleD8 Ablation2	71.35603	13.42762	23	231
2008	MatSurvey	71.34491	13.45737	28	287
2008	GlacialHoleG3	71.33696	13.47434	33	351
2008	5MfromGlacialhole Ablation1	71.33696	13.47434	33	345
2008	Ablation5	71.34821	13.44766	24	268
2008	Ablation6	71.35094	13.43929	30	249
2008	Ablation9	71.32919	13.45729	33	358
2008	Ablation10	71.34140	13.47218	28	316
2008	Ablation11	71.34106	13.48648	29	321
2008	Ablation8 East Bay 2008	71.32808	13.53856	25	259
2011	11 Dive Hole 2008	71.34252	13.44942	24	240
2011	11 Camp 1	71.33275	13.45390	27	348
2011	11 Camp 2	71.33252	13.45537	56	383
2011	11 Camp 3	71.33253	13.45603	42	369
2011	11 Camp 4 Dive Hole 2011	71.33233	13.45678	42	374
2011	11 Anox	71.35606	13.42751	22	240
2011	11 Oxic hole a	71.33691	13.47471	33	367
2011	11 Oxic hole b	71.33695	13.47465	33	361

2011	11 Glacial Bay #3	71.32928	13.45705	34	396
2011	11 Glacial Bay #2	71.32952	13.46100	30	372
2011	11 Glacial Bay #1	71.33152	13.46285	48	393
2011	11 SW Hole #1	71.34835	13.42777	29	258
2011	11 SW Hole #2	71.35177	13.41843	23	245
2011	11 SW Hole #3	71.34797	13.41778	34	260
2011	11 SW Hole #4	71.34436	13.42488	29	268
2011	11 South #1	71.34727	13.47460	29	315
2011	11 Abation 6	71.35106	13.43907	25	253
2011	11 Dawn Camera	71.34322	13.44954	40	290
2011	11East Bay 1	71.32803	13.53840	28	260
2011	11East Bay 2	71.32982	13.53595	27	240
2011	11East Bay 3	71.33438	13.53307	22	238
2011	11East Bay 4	71.33630	13.52190	22	232
2011	11East Bay 5	71.33734	13.51986	20	237
2011	11East Bay 5b	71.33734	13.51986	19	233
2011	11East Bay 6	71.33762	13.51407	23	263
2011	11East Bay 6b	71.33762	13.51407	25	265
2011	11East Bay 7	71.33514	13.51573	23	248
2011	11East Bay 8	71.33432	13.50412	30	301
2011	11 East Bay 9	71.33708	13.49141	35	326
2012	Oxic hole	71.33690	13.47478	42	368
2012	Anoxic hole East	71.35606	13.42752	25	244
2012	Anoxic hole West	71.35606	13.42751	21	244
2012	Drinking water hole	71.33252	13.45537	45	384
2014	Drinking water	71.33213	13.45538	40	382
2016	Water hole	71.33222	13.45558	43	377
2016	Dive Hole 1	71.34206	13.45428	45	266
2016	Oxic basin hole	71.33697	13.47497	38	364
2016	Anoxic basin hole	71.35608	13.42689	26	250
2016	ROV hole near Glacier at Anoicx Basin	71.33111	13.48400	30	250
2017	Water Hole	71.33244	13.45471	37	368
2017	Anoxic Basin Hole	71.35609	13.42688	29	248
2017	Oxic Basin Hole	71.33682	13.47571	35	358
2017	Dive Hole	71.34197	13.45458	31	281
2017	Ablation Rope 1	71.33657	13.49087	30	320
2017	Ablation Rope 2	71.34747	13.45975	25	302
2018	AB1	71.35588	13.42738	26	220
2018	AB3	71.35737	13.42468	28	206
2018	AB4	71.35561	13.42493	26	216
2018	AB5	71.35505	13.42824	29	217

2018	AB6	71.35556	13.43047	24	220
2018	AB7	71.35713	13.43301	24	218
2018	AB8	71.35596	13.42137	27	210
2018	AB9	71.35548	13.42354	26	216
2018	AB10	71.35536	13.42241	23	219
2018	AB11	71.35551	13.42027	28	218
2018	AB12	71.35516	13.4203	27	215
2018	AB13	71.35552	13.41828	22	221
2018	AB14	71.35573	13.41628	28	217
2018	AB15	71.35489	13.41723	33	219
2018	AB16	71.35667	13.421	27	220
2018	AB17	71.35771	13.4194	27	215
2018	AB18	71.35667	13.42327	27	214
2018	AB19	71.33965	13.43898	25	216
2018	AB20	71.34137	13.44458	59	250
2018	AB21	71.35883	13.41277	48	262
2018	AB22	71.35842	13.40967	32	209
2018	AB23	71.34198	13.45457	30	210
2018	2017 Dive Hole	71.34197	13.45458	23	333

APPENDIX B: SUPPLEMENTAL INFORMATION FOR CHAPTER 3

The *FREEZCH9* model presented in Chapter 3 should be used when evolving ice-covered lakes lose liquid water by freezing and have it replaced by new inflow water of fixed chemistry and isotopic composition. The program is called FREEZCH9.FOR which is virtually identical to FREEZCH8.FOR.

This program takes the water isotope-enhanced *FREZCHEM*(v15) and makes it into a subroutine that accepts a time-varying input file called INPUT5B.TXT that changes each loop. The main chemistry part of *FREZCHEM*(v15) has not been changed at all. All that is needed for the additional calculations is taken from the PPRINT subroutine in *FREZCHEM*(v15) by saving the new array names' required results.

The main two new subroutines specific to this lake mixing looping program are:

1) **FREEZCHLP**: this is the "subroutinized" version of *FREZCHEM*(v15). *FREZCHEM*(v15) gets solved for each loop using the newly mixed waters that are defined in the INPUT5B file, which is defined in the "Mixing" subroutine called "**LOOPIN**".

Argument for FREEZCHLP is (ITKOUNT,KOUNT,SITKOUNT,XCXIM,UTEKWDTH,GRFACT,DELTEM).

2) **LOOPIN:** This routine takes the state of the lake's chemistry, and isotopes after an amount of freezing DICE ≥ XXIM has occurred and then mixes the same amount (DICE) of new glacier water into the lake to produce the input chemistry and isotopes for the next loop. This is all stored in the dynamic input file INPUT5B. The hydrated precipitates are accumulated from loop to loop, and it is assumed that the ice formed is pure and that all the soluble chemistry is left behind in the lake (liquid) water.

The main summary output file FRUDLOOP.TXT is also populated by LOOPIN. The quantities in FRUDLOOP for the various loops are all post mixing for that loop.

Argument for LOOPIN is (PATH,NEQFR,XIM,AMOLAR,SL,FINTEM,UTEKWDTH,ITKOUNT,DELTEM,FINWAT,DELWAT,FINPRE,DELPRE,TEMPI,ALK,JDAF,XXIM,KOUNT,SITKOUNT,TEUCT).

Table B1: File names and numbers in the *FREEZCH9* model.

File number	File name (all "TXT" file types)	Function
9	INPUT5 (if kount=1) INPUT5B (if kount≠1)	INPUT5 is input for initial state of lake & INPUT5B is mixed water input file for each subsequent loop
11	FRUDLOOP	Main summary file for post loop results for chem. and isotopes
2	FRout	Main output file for chemistry produced for each loop, but only last loops' is saved
8	TEST8	Generated temperature scan results for chem. and isotopes each loop. Only last loops' is saved.

NB A few small files are needed to run *FREZCHEM* ("NUANCES", SOLIDMASS" and "SOLIDPHASE").

Table B2: Keyboard Inputs in the *FREEZCH9* program.

Name of variable	Function
GRFACT	For each loop some amount of new glacier water is added to the lake. GRFACT is the fraction of that additions chemistry to assume.
XXIM	The lake water slug followed, starts each loop as 1000 gms of liquid water and ends up nominally with (1000-XXIM) gms. So XXIM is the replacement rate in parts per thousand; ie 1 % = 10 ppt.
ITKOUNT	The total number of loops or additions to the lake. (Loop counter is KOUNT).
SITKOUNT	The fraction of loop output to store in FRUDLOOP, a "10" means $1/10^{th}$ is saved.
UTEKWDTH	The temperature scan width in number of temperature steps (DELTEM) to run *FREZCHEM* over each loop. It starts just above the last melting Temperature (TL) and goes below the temperature at which XXIM gms has been frozen out each loop. For strong chemistry this input can be ~ 10 and for weak chemistry ~ 40. Experiment sometimes required and the file TEST8.TXT shows if the scan width is large enough.

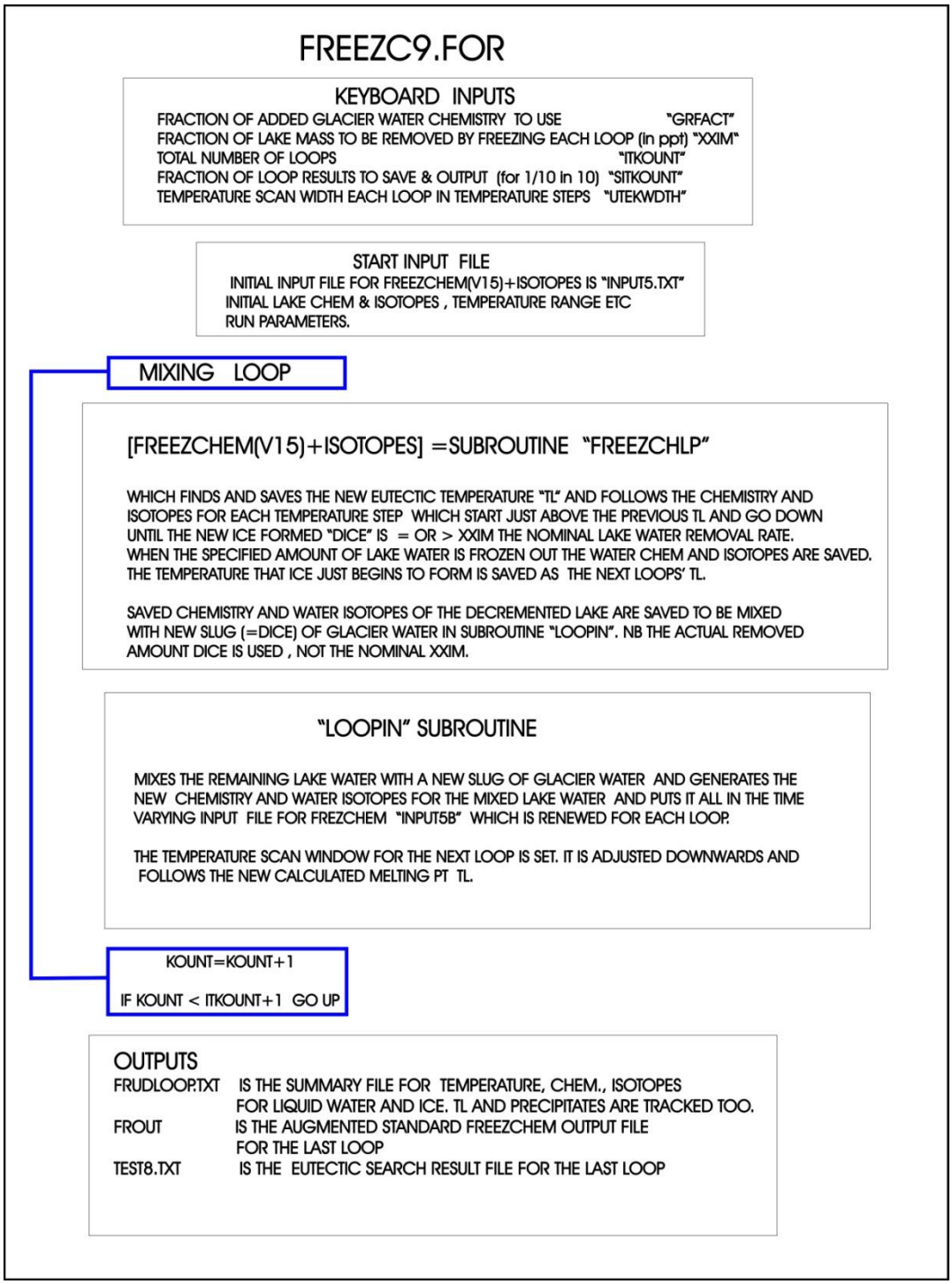

Figure B1: Flow chart for the *FREEZCH9* program.

Table B3: Stable water isotope data for Lake Untersee's oxic water column (sampling location = 71.337°S, 13.475°E).

Sample ID	Depth	δD (‰)	$\delta^{18}O$ (‰)
Untersee OH - 10 m	10 m	-287.5	-37.8
Untersee OH - 20 m	20 m	-287.5	-37.7
Untersee OH - 30 m	30 m	-288	-37.8
Untersee OH - 40 m	40 m	-287.8	-37.8
Untersee OH - 50 m	50 m	-287.9	-37.8
Untersee OH - 60 m	60 m	-287.9	-37.8
Untersee OH - 70 m	70 m	-288	-37.8
Untersee OH - 80 m	80 m	-288.4	-37.8
Untersee OH - 90 m	90 m	-287.3	-37.7
Untersee OH - 100 m	100 m	-288.3	-37.9
Untersee OH - 110 m	110 m	-288.4	-37.9
Untersee OH - 120 m	120 m	-287.5	-37.6
Untersee OH - 130 m	130 m	-287.9	-37.6
Untersee OH - 140 m	140 m	-288.2	-37.7
Untersee OH - 150 m	150 m	-288	-37.6

Table B4: Stable water isotope data for Lake Untersee's ice cover (Core #1 taken at 71.349°S, 13.429°E; Core #2 taken at 71.356°S, 13.429°E).

Sample ID	Depth	δD (‰)	$\delta^{18}O$ (‰)
Core #1 - 2 cm	2 cm	-276.2	-34.8
Core #1 - 4 cm	4 cm	-276.7	-34.8
Core #1 - 6 cm	6 cm	-277.2	-35
Core #1 - 8 cm	8 cm	-277.7	-35.1
Core #1 - 10 cm	10 cm	-277.8	-35.1
Core #1 - 12 cm	12 cm	-276.3	-34.7
Core #1 - 14 cm	14 cm	-277.3	-34.9
Core #1 - 16 cm	16 cm	-277.6	-34.8
Core #1 - 18 cm	18 cm	-277.5	-34.7
Core #1 - 20 cm	20 cm	-278.1	-34.7
Core #1 - 22 cm	22 cm	-277	-34.5
Core #1 - 24 cm	24 cm	-276.9	-34.3
Core #1 - 26 cm	26 cm	-276.5	-33.8
Core #1 - 28 cm	28 cm	-277	-33.7
Core #1 - 30 cm	30 cm	-277.2	-33.5
Core #1 - 32 cm	32 cm	-277.5	-34.9
Core #1 - 34 cm	34 cm	-277.4	-34.8
Core #1 - 36 cm	36 cm	-277.9	-34.7
Core #1 - 38 cm	38 cm	-278.8	-34.9

Core #1 - 40 cm	40 cm	-278	-34.7
Core #1 - 42 cm	42 cm	-277	-34.9
Core #1 - 44 cm	44 cm	-278.2	-35.3
Core #1 - 46 cm	46 cm	-278	-35.6
Core #1 - 48 cm	48 cm	-278.4	-35.8
Core #1 - 50 cm	50 cm	-278.5	-36.2
Core #1 - 52 cm	52 cm	-277	-34.7
Core #1 - 54 cm	54 cm	-277.7	-34.9
Core #1 - 56 cm	56 cm	-278.2	-35.3
Core #1 - 58 cm	58 cm	-277.8	-35.1
Core #1 - 60 cm	60 cm	-277.5	-35.2
Core #1 - 62 cm	62 cm	-277.6	-34.9
Core #1 - 64 cm	64 cm	-278.7	-35.1
Core #1 - 66 cm	66 cm	-278.6	-35
Core #1 - 68 cm	68 cm	-277.5	-34.9
Core #1 - 70 cm	70 cm	-278	-35
Core #1 - 72 cm	72 cm	-274.3	-34.6
Core #1 - 74 cm	74 cm	-275.7	-34.9
Core #1 - 76 cm	76 cm	-274.9	-34.8
Core #1 - 78 cm	78 cm	-275.6	-34.9
Core #1 - 80 cm	80 cm	-278.1	-34.9
Core #1 - 82 cm	82 cm	-278.4	-35
Core #1 - 84 cm	84 cm	-279.5	-35.2
Core #1 - 86 cm	86 cm	-278.8	-35.1
Core #1 - 88 cm	88 cm	-279.2	-35.4
Core #1 - 90 cm	90 cm	-277.4	-35
Core #1 - 92 cm	92 cm	-277.5	-35
Core #1 - 94 cm	94 cm	-278.7	-35.3
Core #1 - 96 cm	96 cm	-278.2	-35.2
Core #1 - 98 cm	98 cm	-278.5	-35.3
Core #1 - 100 cm	100 cm	-277.2	-34.8
Core #1 - 102 cm	102 cm	-277.6	-34.8
Core #1 - 104 cm	104 cm	-278	-34.9
Core #1 - 106 cm	106 cm	-278.3	-34.9
Core #1 - 108 cm	108 cm	-278.8	-35.1
Core #1 - 110 cm	110 cm	-277	-34.8
Core #1 - 112 cm	112 cm	-277.9	-34.7
Core #1 - 114 cm	114 cm	-277.9	-34.9
Core #1 - 116 cm	116 cm	-278.6	-35
Core #1 - 118 cm	118 cm	-278.1	-34.8
Core #1 - 120 cm	120 cm	-277.2	-35
Core #1 - 122 cm	122 cm	-277.2	-34.7
Core #1 - 124 cm	124 cm	-277.7	-34.9
Core #1 - 126 cm	126 cm	-277.9	-34.8

Core #1 - 128 cm	128 cm	-278.1	-34.9
Core #1 - 130 cm	130 cm	-277.4	-34.9
Core #1 - 132 cm	132 cm	-278.1	-34.9
Core #1 - 134 cm	134 cm	-278.7	-35
Core #1 - 136 cm	136 cm	-277.9	-34.9
Core #1 - 138 cm	138 cm	-277.7	-34.9
Core #1 - 140 cm	140 cm	-277	-34.9
Core #1 - 142 cm	142 cm	-277.2	-34.7
Core #1 - 144 cm	144 cm	-278	-34.6
Core #1 - 146 cm	146 cm	-277.9	-34.6
Core #1 - 148 cm	148 cm	-276.4	-34.3
Core #1 - 150 cm	150 cm	-275.2	-34.6
Core #1 - 152 cm	152 cm	-275.4	-34.5
Core #1 - 154 cm	154 cm	-277.4	-34.9
Core #1 - 156 cm	156 cm	-278.7	-35.2
Core #1 - 158 cm	158 cm	-277.9	-35.2
Core #1 - 160 cm	160 cm	-277.7	-34.9
Core #1 - 162 cm	162 cm	-277.4	-34.7
Core #1 - 164 cm	164 cm	-277.1	-34.8
Core #1 - 166 cm	166 cm	-277.9	-34.8
Core #1 - 168 cm	168 cm	-277.3	-34.8
Core #1 - 170 cm	170 cm	-277.1	-34.9
Core #1 - 172 cm	172 cm	-276.8	-34.7
Core #1 - 174 cm	174 cm	-277.7	-34.9
Core #1 - 176 cm	176 cm	-277.9	-34.9
Core #1 - 178 cm	178 cm	-268.5	-34.7
Core #1 - 180 cm	180 cm	-268.7	-34.6
Core #1 - 182 cm	182 cm	-269.1	-34.5
Core #1 - 184 cm	184 cm	-269.3	-34.6
Core #1 - 186 cm	186 cm	-269.1	-34.6
Core #1 - 188 cm	188 cm	-277.7	-35
Core #1 - 190 cm	190 cm	-278.8	-35
Core #1 - 192 cm	192 cm	-278.7	-35.1
Core #1 - 194 cm	194 cm	-279	-35
Core #1 - 196 cm	196 cm	-278.4	-34.9
Core #1 - 198 cm	198 cm	-277.5	-35
Core #1 - 200 cm	200 cm	-278.2	-35.3
Core #1 - 202 cm	202 cm	-278.9	-35.4
Core #1 - 204 cm	204 cm	-276.9	-35.1
Core #1 - 206 cm	206 cm	-277.9	-35.2
Core #1 - 208 cm	208 cm	-277.7	-35.2
Core #1 - 210 cm	210 cm	-278.1	-35.4
Core #1 - 212 cm	212 cm	-278.2	-35.4
Core #1 - 214 cm	214 cm	-278.3	-35
Core #1 - 216 cm	216 cm	-278.6	-35

Core #1 - 218 cm	218 cm	-279.3	-35
Core #1 - 220 cm	220 cm	-279.2	-34.9
Core #1 - 222 cm	222 cm	-278.7	-34.5
Core #1 - 224 cm	224 cm	-277.1	-34.9
Core #1 - 226 cm	226 cm	-278	-34.9
Core #1 - 228 cm	228 cm	-277.8	-34.8
Core #1 - 230 cm	230 cm	-278	-34.8
Core #1 - 232 cm	232 cm	-277.5	-34.6
Core #1 - 234 cm	234 cm	-276.7	-34.7
Core #1 - 236 cm	236 cm	-278	-34.9
Core #2 - 2 cm	2 cm	-273	-34.2
Core #2 - 4 cm	4 cm	-275.5	-34.4
Core #2 - 6 cm	6 cm	-276.7	-34.6
Core #2 - 8 cm	8 cm	-277.1	-34.5
Core #2 - 10 cm	10 cm	-276.9	-34.6
Core #2 - 12 cm	12 cm	-276.9	-34.7
Core #2 - 14 cm	14 cm	-277.5	-34.8
Core #2 - 16 cm	16 cm	-277.8	-34.8
Core #2 - 18 cm	18 cm	-277.4	-34.8
Core #2 - 20 cm	20 cm	-277.4	-34.8
Core #2 - 22 cm	22 cm	-277.2	-35
Core #2 - 24 cm	24 cm	-277.9	-35.1
Core #2 - 26 cm	26 cm	-277.8	-35.1
Core #2 - 28 cm	28 cm	-277.9	-35.2
Core #2 - 30 cm	30 cm	-277.8	-35.4
Core #2 - 32 cm	32 cm	-276.3	-34.7
Core #2 - 34 cm	34 cm	-277.5	-34.9
Core #2 - 36 cm	36 cm	-277.7	-34.9
Core #2 - 38 cm	38 cm	-277.6	-34.7
Core #2 - 40 cm	40 cm	-277.3	-34.7
Core #2 - 42 cm	42 cm	-276.5	-34.8
Core #2 - 44 cm	44 cm	-277.8	-34.8
Core #2 - 46 cm	46 cm	-277.6	-34.7
Core #2 - 48 cm	48 cm	-277.7	-34.8
Core #2 - 50 cm	50 cm	-278.3	-34.9
Core #2 - 52 cm	52 cm	-276.7	-35.1
Core #2 - 54 cm	54 cm	-276.8	-35.2
Core #2 - 56 cm	56 cm	-276.8	-35.1
Core #2 - 58 cm	58 cm	-276.9	-35.3
Core #2 - 60 cm	60 cm	-277.8	-35.3
Core #2 - 62 cm	62 cm	-275.9	-34.8
Core #2 - 64 cm	64 cm	-278.6	-35.2
Core #2 - 66 cm	66 cm	-278.4	-35.2
Core #2 - 68 cm	68 cm	-278.2	-35.2
Core #2 - 70 cm	70 cm	-278.3	-35.3

Core #2 - 72 cm	72 cm	-276.5	-34.8
Core #2 - 74 cm	74 cm	-277.8	-35
Core #2 - 76 cm	76 cm	-278	-35
Core #2 - 78 cm	78 cm	-277.9	-35.2
Core #2 - 80 cm	80 cm	-278.3	-35.3
Core #2 - 82 cm	82 cm	-276.3	-34.9
Core #2 - 84 cm	84 cm	-277.2	-35
Core #2 - 86 cm	86 cm	-277.1	-35.1
Core #2 - 88 cm	88 cm	-277.4	-35.3
Core #2 - 90 cm	90 cm	-277.2	-35.5
Core #2 - 92 cm	92 cm	-276.8	-34.8
Core #2 - 94 cm	94 cm	-278	-35
Core #2 - 96 cm	96 cm	-278.1	-34.9
Core #2 - 98 cm	98 cm	-278.3	-35
Core #2 - 100 cm	100 cm	-278.3	-35
Core #2 - 102 cm	102 cm	-276.9	-34.7
Core #2 - 104 cm	104 cm	-277.4	-34.9
Core #2 - 106 cm	106 cm	-277.8	-34.8
Core #2 - 108 cm	108 cm	-277.5	-34.7
Core #2 - 110 cm	110 cm	-277.7	-34.7
Core #2 - 112 cm	112 cm	-277.7	-35
Core #2 - 114 cm	114 cm	-278	-34.8
Core #2 - 116 cm	116 cm	-278.5	-34.8
Core #2 - 118 cm	118 cm	-277.9	-34.7
Core #2 - 120 cm	120 cm	-277.7	-34.7
Core #2 - 122 cm	122 cm	-276.3	-34.8
Core #2 - 124 cm	124 cm	-277	-34.9
Core #2 - 126 cm	126 cm	-277	-35
Core #2 - 128 cm	128 cm	-277.7	-35
Core #2 - 130 cm	130 cm	-277.8	-35
Core #2 - 132 cm	132 cm	-277.1	-35
Core #2 - 134 cm	134 cm	-277.2	-34.9
Core #2 - 136 cm	136 cm	-277.6	-35.1
Core #2 - 138 cm	138 cm	-277.6	-34.9
Core #2 - 140 cm	140 cm	-276.9	-34.8
Core #2 - 142 cm	142 cm	-277.9	-34.8
Core #2 - 144 cm	144 cm	-276.7	-34.6
Core #2 - 146 cm	146 cm	-277.5	-34.9
Core #2 - 148 cm	148 cm	-277.8	-34.9
Core #2 - 150 cm	150 cm	-278.3	-34.9
Core #2 - 152 cm	152 cm	-277.5	-35
Core #2 - 154 cm	154 cm	-277.2	-34.9
Core #2 - 156 cm	156 cm	-277.2	-35
Core #2 - 158 cm	158 cm	-277.8	-34.9
Core #2 - 160 cm	160 cm	-277.9	-34.9

Core #2 - 162 cm	162 cm	-277	-34.9
Core #2 - 164 cm	164 cm	-277.3	-35.1
Core #2 - 166 cm	166 cm	-277.5	-34.8
Core #2 - 168 cm	168 cm	-276.4	-34.7
Core #2 - 170 cm	170 cm	-277.4	-34.9
Core #2 - 172 cm	172 cm	-277.5	-35
Core #2 - 174 cm	174 cm	-278.1	-35
Core #2 - 176 cm	176 cm	-278.3	-35.1
Core #2 - 178 cm	178 cm	-277.7	-35
Core #2 - 180 cm	180 cm	-278.3	-35.2
Core #2 - 182 cm	182 cm	-277	-35
Core #2 - 184 cm	184 cm	-277.8	-35.2
Core #2 - 186 cm	186 cm	-277.5	-35.1
Core #2 - 188 cm	188 cm	-277.2	-35
Core #2 - 190 cm	190 cm	-277.7	-35.1

APPENDIX C: SUPPLEMENTAL INFORMATION FOR CHAPTER 4

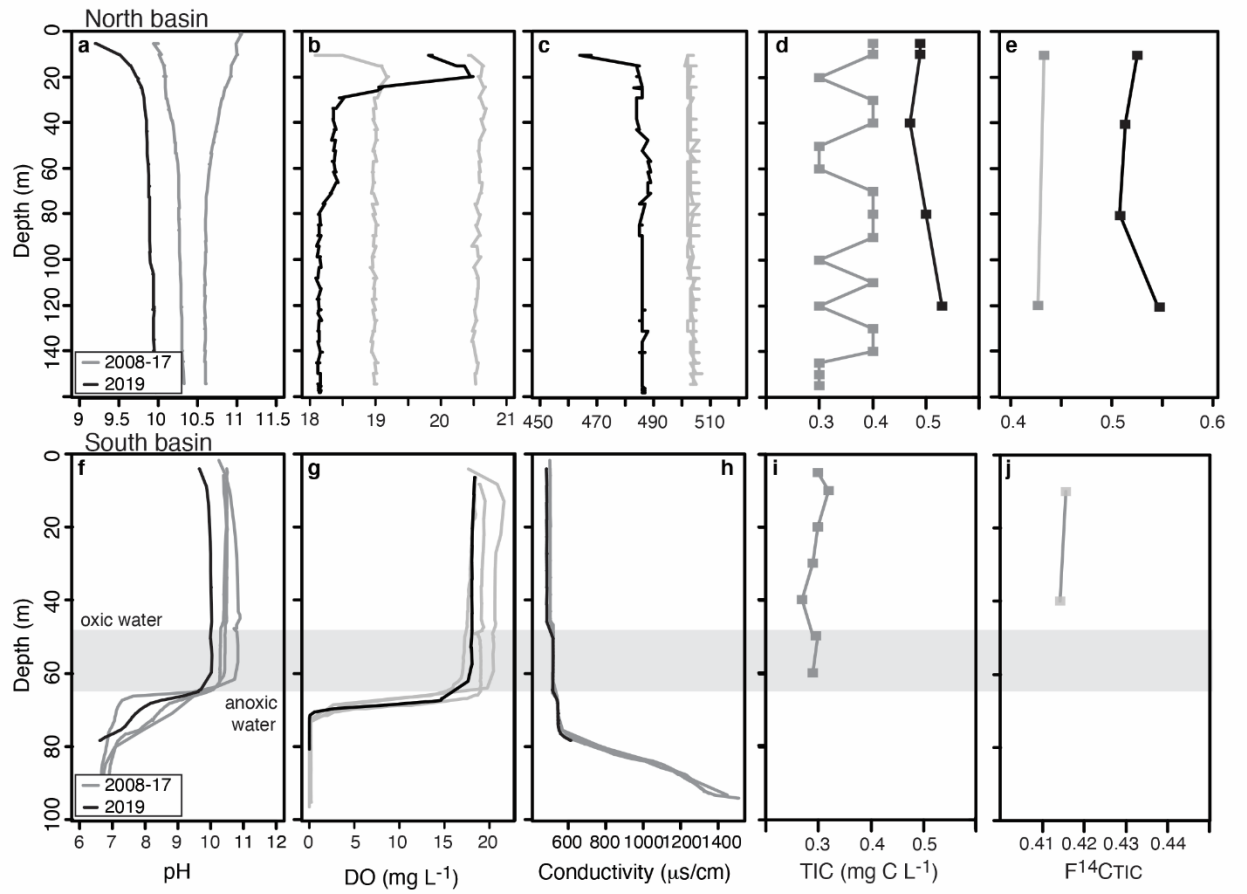

Figure C1: Depth profile measurements of pH, dissolved oxygen (DO), conductivity (µS/cm^{-1}), total inorganic carbon (TIC), and $F^{14}C_{TIC}$ within the oxic and anoxic water columns of Lake Untersee, Antarctica. Measurements of pH, DO, and conductivity were made in 2008, 2011, 2015, 2017, and 2019.

Table C1: Hydrochemical parameters of Lake Untersee (2011-2017 and 2019) and the GLOF stream (2019). Two-component mixing models between Lake Untersee and the 2019 stream, with varying water additions from the GLOF, are included.

	pH	DO (%)	Conductivity (µS/cm^{-1})	TIC (mg C L^{-1})	$\delta^{13}C_{TIC}$ (‰)	$F^{14}C_{TIC}$
LU 2011-17	10.5±0.3	146±1	515±3	0.35±0.02	–9.1±0.4	0.4241± 0.011
LU 2019	9.5	128	485	0.5	–14.5	0.5259
Stream 2019	7.7	100*	70.1	1.8	–18	0.5844
Two-component mixing (Lake Untersee and 2019 stream)						
Mixing, 3%	9.2	144.6	502	0.35	–9.4	0.4289
Mixing, 5%	9.0	143.7	493	0.38	–9.5	0.4321
Mixing, 10%	8.7	141.4	471	0.45	–10.0	0.4401

Note * estimated value.

Table C2: Hydrological and carbon values used to determine the carbon mass balance and evolution of $F^{14}C_{TIC}$ and ^{14}C in mats over the past 12ka shown in Fig. 4-6. The initial conditions represent the volume of water in the oxic water column; TIC for S1 represents that estimated from subaqueous melting of the Anuchin Glacier and direct release of occluded gas bubbles into the water column; TIC for S2 represents lake water in equilibrium with atmospheric CO_2, as calculated using PHREECQ hydrogeochemical software. TIC for S3 and S4 represents lake water in equilibrium with atmospheric CO_2 with additional weathering of plagioclase minerals, as computed using PHREECQ hydrological software.

	Initial conditions					Input			
Scenario	Volume (m^3)	TIC (mg C L^{-1})	TOC (mg C L^{-1})	Total C (g C)	$F^{14}C$	Volume (m^3)	Total C (g C)	$F^{14}C_{TIC}$	$F^{14}C_{TOC}$
S1	5.16E+08	0.0165	0.03	2.40E+07	0.80	4.9E+06	2.28E+05	0.80	0.80
S2	5.16E+08	0.4	0.03	2.22E+08	0.80	4.9E+06	2.28E+05	0.80	0.80
S3	5.16E+08	1.5	0.03	7.89E+08	0.80	4.9E+06	2.28E+05	0.80	0.80
S4	5.16E+08	1.5	0.03	7.89E+08	0.80	4.9E+06	2.28E+05	0.80	0.80
S5	5.16E+08	1.5	0.03	7.89E+08	0.80	4.9E+06	2.28E+05	0.80	0.00
GLOF	n/a	n/a	n/a	n/a	n/a	2.0E+07	2.00E+08	0.95	n/a

Table C3: Radiocarbon results of total inorganic carbon (TIC) and total organic carbon (TOC) in Lake Untersee, Antarctica.

Sample ID	Depth (m)	$F^{14}C_{TIC}$ (±2σ)	^{14}C yr BP (±2σ)	Lab ID	Reference
North Basin, 2017					
NB-10	10	0.4361 (0.0054)	6666 (98)	UOC-6214	Marsh et al., 2020
NB-40	40	0.5989 (0.0132)	4119 (176)	UOC-6215	Marsh et al., 2020
NB-120	120	0.4307 (0.004)	6766 (76)	UOC-6217	Marsh et al., 2020
South Basin, 2017					
SB-10	10	0.4156 (0.0046)	7054 (88)	UOC-6219	Marsh et al., 2020
SB-40	40	0.4143 (0.0038)	7079 (76)	UOC-6220	Marsh et al., 2020
North Basin, 2019					
NB-10	10	0.5283 (0.0037)	5125 (56)	UOC-12637	This study
NB-40	40	0.5165 (0.0035)	5307 (54)	UOC-12638	This study
NB-80	80	0.5107 (0.0034)	5397 (53	UOC-12639	This study
NB-120	120	0.5481 (0.0035)	4830 (51)	UOC-12640	This study
Stream, 2019					
ELMP-1	0	0.5844 (0.0025)	4315 (34)	UOC-12645	This study
North Basin, 2017	**$F^{14}C_{TOC}$**	**^{14}C yr BP (±2σ)**			
NB-10-40	10-40	0.4233 (0.0322)a	6906 (610)a	UOC-6540	Marsh et al., 2020
NB-80-120	80-120	0.5547 (0.0418)b	4734 (610)b	UOC-6541	Marsh et al., 2020

$F^{14}C$ = fraction modern carbon; ^{14}C yr BP = years before 1950; a = samples NB-10 and NB-40, b = samples NB-80 and NB-120 were combined to yield sufficient carbon for analysis.

APPENDIX D: SUPPLEMENTAL INFORMATION FOR CHAPTER 5

Table D1: Physicochemical characteristics of Untersee Oasis pond waters and morphometric properties of ice cover blisters.

				Ice blister		
Pond ID	**Elevation (m.a.s.l.)**	**Surface area (m^2)**	**Avg. PISR (Wm^{-2})**	**Height (m)**	**Area (m^2)**	**Volume (m^3)**
P1	666.5	413	128	0.45	112	16.5
P2	657.5	751	129	-	-	-
P3	631.0	5879	126	-	-	-
P4	665.0	334	119	0.48	46	6.3
P5	939.5	1707	134	-	-	-
P6	837.9	2422	136	-	-	-
P7	827.2	354	142	0.38	73	11.5
P8	816.7	611	136	0.54	153	29.7
P9	620.3	810	144	0.42	277	42.3
P10	612.4	303	162	-	-	-
P11	615.1	1085	154	0.61	278	58.3
P12	610.9	116	159	-	-	-
P13	615.9	114	123	-	-	-

Table D2: pH, conductivity, and major ions in the Untersee Oasis ponds.

Pond ID	**pH**	**Conductivity ($\mu S/cm^{-1}$)**	**Ca ($mg\ L^{-1}$)**	**K ($mg\ L^{-1}$)**	**Mg ($mg\ L^{-1}$)**	**Na ($mg\ L^{-1}$)**	**NO_3 ($mg\ L^{-1}$)**	**SO_4 ($mg\ L^{-1}$)**	**Cl ($mg\ L^{-1}$)**
P1	8.6	387	38.51	10.07	7.29	58.37	10.81	80.67	91.80
P2	10.4–10.6	850–900	31.18	4.43	0.19	24.25	0.18	43.10	32.40
P3	10.4–11.8	291–300	82.53	11.72	2.25	96.69	8.32	113.90	184.50
P4	8.4	90	9.31	1.28	1.37	10.87	8.02	2.52	23.15
P5	7.1	232	9.52	2.33	3.37	9.14	1.70	19.94	12.63
P6	8.6	93	12.68	4.62	10.43	14.89	0.21	34.48	18.73
P7	8	166	5.40	1.57	2.38	5.43	0.04	8.58	6.43
P8	9.7	59	18.08	4.91	8.23	31.86	1.78	61.98	45.97
P9	9.7	120	12.70	4.03	3.10	11.45	0.06	28.16	14.70
P10	6.9	2380	317.36	44.64	77.71	400.65	163.56	1072.79	496.43
P11	7.2	162	18.50	3.41	3.67	18.97	4.41	48.68	20.06
P12	7.8	946	142.56	17.67	24.67	110.69	239.22	308.09	115.19
P13	7.4	84	11.10	2.32	1.67	8.03	4.02	10.40	12.51

Table D3: Stable water isotope (δD-$\delta^{18}O$), TIC, TOC, $\delta^{13}C_{TIC}$, $F^{14}C_{TIC}$, and ^{3}H composition of pond waters in the vicinity of the Untersee Oasis.

Pond ID	$\delta^{18}O$ (‰)	δD (‰)	D-excess (‰)	TIC	TOC	$\delta^{13}C_{TIC}$	$\delta^{13}C_{TOC}$	$F^{14}C_{TIC}$	^{3}H
P1	-36.4	-285.0	5.7	2.4	4.2	-18.0	-26.1	-	4.1±0.8
P2	-41.9	-317.9	17.3	1.0	1.4	-3.4	-7.6	0.9947±0.0058	<0.8
P3	-40.9	-315.9	11.5	1.0	1.2	-3.7	-7.8	0.9757±0.006	1.5±0.8
P4	-35.9	-285.4	2.5	7.7	12.6	-13.4	-23.7	-	-
P5	-29.3	-239.3	-5.3	5.2	4.6	-13.6	-25.0	1.0011±0.0036	3.5±0.8
P6	-29.9	-247.2	-7.7	13.8	7.1	-4.2	-19.1	-	-
P7	-31.2	-252.6	-2.7	3.3	5.6	-12.7	-23.3	-	-
P8	-30.9	-250.4	-2.9	6.4	5.0	-16.3	-22.4	-	-
P9	-28.7	-239.8	-10.2	3.5	1.3	-10.1	-11.0	-	-
P10	-21.6	-213.3	-40.7	24.0	6.7	-1.9	-12.8	-	-
P11	-24.3	-217.0	-22.7	4.2	5.3	-14.4	-22.8	0.9872±0.0033	11.7±0.8
P12	-20.9	-212.9	-45.4	4.2	4.9	-14.6	-23.6	-	-
P13	-30.3	-251.3	-9.0	6.6	10.6	-17.6	-18.3	-	10.8±0.8